ABSTRACT

THOMAS, AJIMON. Using a Multi-Resolution Approach to Improve the Accuracy and Efficiency of Flooding Predictions. (Under the direction of Dr. Joel Casey Dietrich.)

This research describes a method to improve the accuracy and efficiency of coastal flooding predictions. First, an existing model is used to explore the effect of storm forward speed and timing on tides and storm surge during Hurricane Matthew (2016). It is hypothesized that the spatial variability of Matthew's effects on total water levels is due to the surge interacting nonlinearly with tides. If the storm occurred a few hours earlier or later, then the largest surges would have been shifted to other regions of the U.S. southeast coast. A change in forward speed of the storm also should alter its associated flooding due to differences in the duration over which the storm impacts the coastal waters. If the storm had moved faster, then the peak water levels would have increased along the coast, but the overall volume of inundation would have decreased.

Then this research explores ways to increase the model's accuracy and efficiency. To better represent Matthew's effects, a mesh with detailed coverage of the coastal regions from Florida to North Carolina was developed by combining regional meshes originally developed for floodplain mapping. Compared to predictions using the earlier model, the new mesh allows for simulations of inundation that better match to observations especially inland.

Then, to best utilize this new mesh, a multi-resolution approach is implemented to use meshes of varying resolution when and where it is required. It is hypothesized that, by 'switching' from coarse- to fine-resolution meshes, with the resolution in the fine mesh concentrated only at specific coastal regions influenced by the storm at that point in time, both accuracy and computational gains can be achieved. As the storm approaches the coastline and the landfall location becomes more certain, the simulation will switch to a fine-resolution mesh that describes the coastal features in that region. Application of the approach during Hurricanes Matthew and Florence revealed the predictions to improve in both accuracy and efficiency, as compared to that from single simulations on coarse- and fine-resolution meshes, respectively.

Finally, the efficiency of the approach is further improved in the case of Hurricane Matthew, by using multiple smaller fine-resolution meshes instead of a single high-resolution mesh for the entire U.S. southeast coast. Simulations are performed utilizing

predicted values of water levels, wind speeds and wave heights, as triggers to switch from one mesh to another. Results indicate how to achieve an optimum balance between accuracy and efficiency, by using the above mentioned triggers, and through a careful selection of the combination meshes to be used in the approach.

This research has the potential to improve the storm surge forecasting process. These gains in efficiency are directly a savings in wall-clock time, which can translate into more time to invest in better models and/or more time for the stakeholders to consider the forecast guidance.

Using a Multi-Resolution Approach to Improve the Accuracy and Efficiency of Flooding Predictions

by
Ajimon Thomas

A dissertation submitted to the Graduate Faculty of
North Carolina State University
in partial fulfillment of the
requirements for the Degree of
Doctor of Philosophy

Civil Engineering

Raleigh, North Carolina

2020

APPROVED BY:

John Baugh

Elizabeth Sciaudone

Rick Luettich

Joel Casey Dietrich
Chair of Advisory Committee

DEDICATION

To my parents Elcy Abraham and K.T. Thomas

For their unconditional love, and for raising me to be the person I am today

&

To all my teachers

For their sincere guidance, and in showing me the right path

BIOGRAPHY

Ajimon Thomas was born in Thiruvananthapuram, India, in 1987 to Elcy Abraham and K.T. Thomas. He grew up there, where he attended Loyola School. After graduating high school, Ajimon pursued an undergraduate degree in Civil Engineering at College of Engineering, Trivandrum, where he learned the basics of fluid behaviour, and was introduced to the importance of numerical methods in Civil Engineering. He then started graduate studies in Offshore Structures at National Institute of Technology, Calicut. Through the Masters thesis aimed at finding the response of semi-submersible under multi-directional seas, he developed a taste for programming and modelling of the ocean environment. After receiving his Masters degree, Ajimon spent the next two years working as an Assistant Professor in the Department of Civil Engineering at Mar Baselios College of Engineering and Technology, Thiruvananthapuram. He then made the long trip to the United States to pursue his doctoral studies under the direction of Dr. Casey Dietrich in the Department of Civil, Construction, and Environmental Engineering at North Carolina State University. Beyond academics, Ajimon enjoys playing and watching soccer, travelling and hiking, keeping aquariums, pencil sketching, and playing counter-strike.

ACKNOWLEDGEMENTS

It is a pleasure to thank the many people who have helped me build, and build toward this dissertation over the last six years.

First and foremost, I would like to thank my advisor Dr. Casey Dietrich for the encouragement and advice he has provided at every stage of my PhD. Casey's passion, guidance, moral support, and discipline have been indispensable to my growth as a researcher and as a person over these past six years. I could not have imagined having a better advisor and mentor for my PhD study. There have been numerous occasions where I remember feeling disheartened about the direction of my research, but inevitably, a meeting with Casey would reinvigorate my enthusiasm and raise my spirits immeasurably.

I am also thankful to my thesis committee for for their time, interest, encouragement, and insightful comments. Dr. Rick Luettich for sharing his deep knowledge in coastal modeling, Dr. John Baugh for teaching me the basics of Python programming which has helped me greatly throughout my research, and Dr. Elizabeth Sciaudone for being really friendly, helpful and encouraging whenever I had a question for her. This thesis would not be nearly as good without their help. I am also thankful to members of the ADCIRC community, especially Dr. Clint Dawson, Dr. Jason Fleming, Taylor Asher, Ashley Kauppila and Mark Loveland for their active collaboration, and contribution to my work over the years.

I gratefully acknowledge the funding sources that made my PhD work possible - North Carolina Sea Grant and the Department of Homeland Security. I am also grateful to the high performance computing clusters at NC State University (Henry2) and the University of Texas (Stampede2), that allowed me in running countless simulations. Without these supercomputers, my research would not be possible. I also want to thank the support staff of these centers for helping me when issues arose. Special thanks goes out to my Masters advisor, Dr. V. Mustafa, for introducing me to the world of ocean modeling.

The members of the coastal engineering team has contributed significantly to my personal and professional time at NC State. I am indebted to my many student colleagues in Mann 428 for providing a stimulating and fun environment in which to learn and grow. The group has been a source of friendships as well as good advice and collaboration. I would like to thank Dr. Margery Overton, Dr. Billy Edge and Dr. Alejandra Ortiz, for their support, and for everything they have taught me during the course of my PhD.

My thanks also goes out to former and current team members: Ayse Karanci, Rosemary Cyriac, Liliana Velásquez Montoya, Alireza Gharagozlou and Nelson Tull. In particular, I want to thank two people. Liliana for being my best friend for many years, for our lunches together to talk about anything and everything, and for being a source of great emotional support. Rosemary for the coffee-breaks and advice – you were always there with a word of encouragement or listening ear. I would like to also thank my other friends in Mann 428 who made my graduate school life more colourful. It's amazing to be able to go to work and know that you'll get to see a bunch of friends throughout the day. I am also thankful to the support given by my undergraduate researchers, Jenna Choi and Chloe Stokes. Chloe's contribution has been immense in getting work done, especially towards the end of my PhD.

My time at NC State was made enjoyable in large part due to the many friends and groups outside the coastal team, that became a part of my life. I am grateful for the time spent with them, our memorable trips into the mountains and beaches, and for many other memories. I want to thank all my roommates over the years, especially Kripaharan Ganesan and Abhilash Kusam, for the friendship, and interesting conversations we have had together. I would not be the same person without the friendships of Arpit Sardana, Poepoe Khaing, Josin Tom, Chelsea Armitage, and Sudharshana Mukhopadhyay. My time here was also enriched by Raleigh Coed Soccer Group, NC Soccer Group, and the Raleigh Aquarium Society. To my many friends back home in India, thank you for your thoughts, well-wishes, phone calls, and being there whenever I needed a friend.

Lastly, I am deeply thankful to my family for their love, support, and sacrifices. My sister, Ajimol Elcy Thomas, and her husband Nebu Jacob, deserve special thanks for their continued support and encouragement. My two nephews have been an endless source of joy and happiness, and have always enlivened my spirits. Most importantly, I wish to thank my parents, Elcy Abraham and K.T. Thomas, for supporting me in all my pursuits, and for giving me all the tools and opportunity I needed to succeed. To them I dedicate this dissertation.

TABLE OF CONTENTS

LIST OF TABLES

LIST OF FIGURES

Chapter 1

Introduction

Coastal regions are under a constant threat of property damage and casualties from hurricanes, tsunamis, Nor'easters, and winter storms. Sustained winds and heavy rainfall are not the only deadly factors during these natural hazards. The greatest threat to life comes in the form of storm surge, measured as the height of the water above the normal predicted astronomical tide. In flat regions, this may lead to intrusion of the salt water 10 to 20 miles inland (Conner et al., 1957). This flooding can also be accompanied by erosion processes due to wave action, including breaching of barrier islands. Large-scale features that would influence this surge include: the intensity, size, speed, and path of the storm; the general configuration of the coastline; bottom topography near the coast; and the stage of the astronomical tide (Harris, 1956; Reid et al., 1954). There can be also small-scale features that affect the surge locally, such as convergence or divergence in bays and estuaries, local wind-setup, seiching, etc.

The coastal populations on every continent exploded as global trade flowed through international ports, creating jobs and economic growth. In 2001, more than 50 percent of the world population lived within 200 km of the coastline (Tibbetts, 2002; Creel, 2003). Presently, 44 percent of the world's population lives within 150 km of the coast (UN Atlas of the Oceans, 2018). In the U.S., more than 39 percent (123.3 million people) of the population lived in coastal shoreline counties in 2010 (NOAA et al., 2013). These locations also had the highest population density of 446 persons per square miles, compared to the average U.S. density of 105 persons per square miles. With this ever-increasing growth and development of coastal areas, greater damage to property and loss of life from storms will continue to occur.

The development and implementation of numerical models allows in the prediction of these natural hazards so their potential effects can be understood and lives and property can be protected from future storms.

Storm surge forecasting begin as early as the 1950s when the central pressure of cyclones was used to estimate the maximum surge height (Hoover, 1957; Conner et al., 1957). Improvements to these methods included using wave heights and stratifying the cyclones according to their wind direction (Tancreto, 1958), employing multistation surge models (Pore, 1964) and using approach paths (Chan et al., 1979). Recognizing the complexity of surge forecasting, Harris (1963) developed a computer-aided empirical model that included pressure effect, direct wind effect, Coriolis force, waves and rainfall as processes affecting storm surge. His first approximation showed that the effects of the Coriolis force, waves, and wind set-up at sea are all proportional to the wind stress, and that the wind stress is proportional to the pressure gradient. Also in general, rainfall was observed to be correlated with below-normal pressures, resulting in all five factors being directly related to pressure gradients.

Advances in computing power allowed the inclusion of more parameters and usage of more complex equations, leading to development of the Special Program to List Amplitude of Surge from Hurricanes (SPLASH) (Jelesnianski, 1972). This approach computed peak surge via nomograms that used maximum wind, radius of the maximum wind, direction of landing, bathymetry, and central pressure data. The Federal Emergency Management Agency (FEMA) SURGE Model (Dresser et al., 1985) was first introduced in 1976 as the TTSURGE Model, and uses an explicit, two-dimensional, space-averaged, finite-difference scheme to simulate the surges caused by hurricanes. Inputs to the model include the bathymetry, coastline configuration, boundary conditions, bottom friction, and other flow resistance coefficients. Also required are the surface wind stress and atmospheric pressure distributions of a hurricane. The model uses a rectangular grid to represent the area of interest and usually employs a nested grid system so that greater detail can be added along the coastline. Hurricane Audrey of 1957 was successfully simulated using the model and the results showed good agreement with the flood records (Suhayda et al., 1988).

The Sea, Land, Overland Surge from Hurricane (SLOSH) model (Jelesnianski et al., 1992) was later designed by the National Weather Service to estimate storm surge heights resulting from historical, hypothetical, or predicted hurricanes by taking into account the atmospheric pressure, size, forward speed, and track data. During a hurricane, the potential surge for an area is calculated by running the model with hypothetical hurricanes with various landfall directions and locations, Saffir-Simpson categories, forward speeds, sizes, and tide levels. The envelope of high water from each such run is then combined to create worst case scenario to aid in hurricane evacuation plans. Although useful in forecasting and computationally fast, the spatial coverage of each SLOSH grid only ranges from an area the size of a few counties to a few states. But larger domains are needed for capturing large-scale processes and improved accuracy (Blain et al., 1994; Westerink et al., 1994). Also the use of a structured mesh can limit the ability for localized resolution and therefore potentially hampers accuracy in SLOSH (Kerr et al., 2013).

Coastal morphological features like inlets, lagoons, barrier islands and shoreline configuration have a great influence on inundation. The accuracy of flooding predictions thus depends on whether the model has sufficient resolution to resolve these features. Because it is difficult for finite difference models with structured grids to represent such fine features, finite element models using unstructured grids are employed in accurate storm surge forecasting. ADvanced CIRCulation (ADCIRC) (Luettich et al., 1992; Luettich et al., 2004; Westerink et al., 2008) is a depth-integrated, shallow-water, finite-element model capable of simulating tidal circulation and storm-surge propagation over large computational domains. ADCIRC is used by FEMA in the development of flood insurance rate maps and by the U.S. Army Corps of Engineers (USACE) for navigation and storm protection projects. The National Oceanic and Atmospheric Administration (NOAA) also uses ADCIRC for tidal calibrations and incorporation into its vertical datum transformation software VDatum. The use of unstructured meshes in ADCIRC allows the usage of triangular finite elements of varying sizes to represent complex coastal features, barrier islands and internal barriers. This also permits for gradation of the mesh that increases feature detail when moving from the deeper ocean, onto the continental shelf, into estuaries and marshes, and over low-lying coastal floodplains. More details of the model are given in Chapter 2.

These unstructured meshes can be still be large, composing of millions of elements. For example, the SL18TX33 mesh (Hope et al., 2013) uses 9 M vertices and 18 M elements to provide a detailed description of coastal floodplains of Alabama, Mississippi, Louisiana, and Texas. Element sizes varies from 20 km or larger in the Atlantic Ocean and Caribbean Sea, to as small as 20 m in channels and other similarly sized hydraulic features. Thus, although these models provide reliable and accurate results by virtue of their high-resolution description of coastal features, simulations can be computationally expensive, requiring several hours even on thousands of computational cores (Dietrich et al., 2012). This is a challenge in storm surge modeling, especially in forecasting applications where model predictions are required on the order of 1 hr or so, to aid emergency mangers in decision-making during a hurricane.

The present study describes a multi-resolution approach to cut down the total computational cost of running unstructured-mesh, storm surge models. The study begins with an application of the state-of-the-art in storm surge modeling to predict coastal flooding along the the U.S. southeast coast during Hurricane Matthew (2016). In the later chapters, I apply a multi-resolution method that permits the use of higher-resolution meshes to increase the accuracy of flooding predictions. This method will also help in decreasing the simulation time by using high-resolution only when required. This is attained by using multiple meshes with different levels of resolution at different times in the simulation. Higher-resolution meshes will be used to resolve coastal inundation only when necessary rather than during the entire simulation. An overview of each of the individual chapters of this dissertation is provided below.

Storm surge and flooding due to hurricanes can cause significant damage to property, loss of life, and long-term damage to coastal landscapes. Hurricane Matthew (2016) was a Category-5 storm that impacted the southeastern U.S. during October 2016, moving mostly parallel to the coastline from Florida through North Carolina. In Chapter 2, the tightly-coupled ADCIRC+SWAN storm surge forecasting model is used to simulate Matthew's effects on this long coastline, and then validated against extensive observations of surface pressures, wind speeds, waves, and water levels. Data-assimilated wind products was found to better represent Matthew's effects as compared to the parametric vortex model, which is based on best-track information from the National Hurricane Center. A relatively-coarse unstructured mesh having an average coastal resolution of 500 m, and having a coverage that included the coastal floodplains impacted by Matthew was then used to predict Matthew's impact on the U.S. southeast coast. Even with this relatively-coarse mesh, the modeled results showed good agreement to observations for waves, water levels and high water marks, thus proving the capability of the coupled ADCIRC+SWAN model to provide accurate coastal flooding predictions.

Although the overall error statistics from the Matthew hindcasts using the above-mentioned coarse-resolution mesh were comparable to that using meshes with much higher-resolution, there were localized regions like rivers along the South Atlantic Bight, sound-side of barrier islands in North Carolina, etc., where the errors where larger. This was attributed to its larger coastal resolution, which is insufficient to represent smaller features like channels, tidal inlets and dune crests. Therefore a mesh with detailed coverage of floodplains on the U.S. southeast coast is developed and validated in Chapter 3. This mesh will then be also used in later chapters for a coarse-grain mesh adaptivity, by including the floodplains only when required.

This high-resolution mesh was created from existing regional meshes, which were developed by FEMA for flood risk mapping. It has a resolution of less than 100 m in most places along the southeastern U.S. coastline with the element spacing going down to less than 10 m in some of the smaller channels in South Florida. This mesh was then tested by running ADCIRC+SWAN simulations of two storms that impacted the U.S. southeast coast in different ways. For both these storms, the predictions of water levels were either better or comparable to predictions using the coarse-resolution mesh mentioned above, meanwhile flooding a larger number of observed-stations. The main differences occurred inland away from the coastline, where it better captured the tidal impacts and/or had a better match to the peak water levels, due to its detailed representation of topography and bathymetry. Thus although this mesh has roughly three times the number of elements as that of the coarse-resolution mesh, its predictions were a better match to observations, especially inland.

In Chapter 4, a method to reduce the computational workload of storm surge models is proposed. Although different methods to increase resolution in storm surge models can be seen in literature, the proposed approach is a first of its kind. Rather than using a high-resolution mesh throughout the simulation, resolution can be turned on depending on where the storm is located at a particular point in time. A coarse-resolution mesh without extensive coastal detail is used when the storm is far away. As the storm approaches the region of interest, results are mapped on to a high-resolution mesh. The simulation then continues on the fine mesh providing high-accurate results for that coastline. A save is tine is also achieved as the use of a highly-refined mesh is avoided when the storm is far away. The approach was tested in the case of two storms with different parameters like track, intensity, etc, and results indicated a gain in accuracy and efficiency as compared to single simulations on coarse and fine meshes respectively.

In Chapter 5, the multi-resolution approach described in Chapter 4 is again applied to hindcasts of Hurricane Matthew along the U.S. southeast coast. But rather than using a single switch between the coarse and the full fine-resolution mesh, multiple smaller fine-resolution meshes will be used depending on the storm's impact area at different points in time. Questions about how best to apply the approach given information about the storm and predicted values of water levels, wind speeds, and wave heights will be explored using three simulations, each targeting a different level of accuracy and efficiency. Results from these simulations indicate how to achieve an optimum balance between accuracy and efficiency using the approach, and the best ways to choose combinations of meshes for representing the storm's impact region. Thus, an efficient use of the proposed method during forecasting can allow for a more accurate and timelier guidance. Finally, the importance on this study, and suggestions for future work are presented in Chapter 6.

Chapter 2

Influence of Storm Timing and Forward Speed on Tides and Storm Surge during Hurricane Matthew

2.1 Overview

In this chapter, the sensitivity of surge predictions to timing and forward speed of a storm are analyzed in the context of Hurricane Matthew (2016). First, the effects of Matthew on the southeastern U.S. coastline are explored by performing hindcasts of a coupled hydrodynamic-wave model, using three sources of atmospheric forcing and an unstructured mesh with a widespread coverage that includes the areas impacted by the storm. Then, the contribution of nonlinear interactions between surge and tides to the spatial variability of Matthew's effects on total water levels is analyzed. Finally, the influence of storm timing and forward speed on tides and surge during Matthew are separately analyzed. This chapter has been published in *Ocean Modelling* as Thomas et al. (2019).

2.2 Introduction

Matthew was a tropical cyclone that reached Category-5 hurricane status on the Saffir-Simpson hurricane wind scale during 2016. Matthew affected about 1900 km of coastline in the United States, caused 34 direct deaths and forced evacuations by 3 million people

(Stewart, 2017). Between 1900 UTC 06 October when the storm was located offshore of Miami, Florida, and 0600 UTC 09 October when it was located offshore of Cape Hatteras, North Carolina, Matthew remained close to the coast and moved along a shore-parallel track (Figure 2.1) with a relatively-slow forward speed of 5 to 7 m/s. Observations indicate large variations in peak water levels all along the U.S. Atlantic coast, and we hypothesize that this was caused by the storm's slower forward speed and shore-parallel track, which allowed it to interact with different stages in the tidal cycle at different locations and over several days.

Several studies have examined the interactions between tides and surge. In the 1950s, Proudman developed theoretical solutions for the propagation of an externally forced tide and surge into an estuary of uniform section (Proudman, 1955; Proudman, 1957) and also identified the tendency of peak surge to most often occur on high tides, which was later confirmed (Rossiter, 1961; Prandle et al., 1978). Tides and surge can also interact nonlinearly, thus causing the water levels to be even higher or lower than their individual contributions would suggest, due to feedbacks through bottom friction, shallow-water effects, and advection (Wolf, 1978). Nonlinear parameterization of bottom stress was found to the primary contributor to nonlinear tide-surge interactions along the Queensland coast of Australia (Tang et al., 1996), on the east coast of Canada and northeastern United States (Bernier et al., 2007), and along the Fujian coast (W. Zhang et al., 2010). Along the southeast coast of the United States, Coriolis acceleration was found to be a significant contributing factor to these perturbations (Valle–Levinson et al., 2013; Feng et al., 2016). The magnitude of these interactions can be large, reaching as high as 70% of the tidal amplitudes (Rego et al., 2010) along the Louisiana-Texas coast during Hurricane Rita, and 74 cm (Idier et al., 2012) for storms in the English channel. The tide-surge nonlinearities were also large with a mean absolute value of 60% of the tide magnitude (Lin et al., 2012) for synthetic surge events in New York Harbor, and at least $15 - 20\%$ for idealized cyclone tracks and straight coastlines representing the west coast of India (Poulose et al., 2017).

It can be challenging to include these nonlinear interactions in surge predictions. Flood risk studies typically represent the hurricane climate by using the Joint Probability Method (JPM) with synthetic storms to determine the flooding at various return periods. The effect of tides can be a crucial factor in these studies. For studies looking at smaller regions with small and in-phase tidal amplitudes, tides were introduced as a constant addition to the JPM integral error term (Niedoroda et al., 2010). Other studies included tides into the JPM analysis by randomly adding tidal heights to the surge response (Ho et al., 1975; Blanton et al., 2012; U.S. Army Corps of Engineers, 2018). However, these additions do not incorporate the often-large effect of the nonlinear interactions between the surge and tides. The present study quantifies these interactions along the entire U.S. southeast coast during Matthew, including their variation from the continental shelf into the estuaries. The representation of coastal floodplains is larger than in previous studies and can allow the flooding from the shore-parallel storm to interact with multiple phases of the tides.

The effects of storm parameters like size, landfall location, wind speeds, and direction of approach on surge have also been studied previously ((Weisburg et al., 2006; Irish et al., 2008; Sebastian et al., 2014)). The effect of storm forward speed can vary. The surge can be greater for a faster storm, e.g., for a standard hurricane on a representative shelf (Jelesnianski, 1972). Along the Louisiana-Texas shelf for Hurricane Rita, increasing the forward speed of the storm caused higher surges but smaller total flooded volumes (Rego et al., 2009). But the surge and inundation areas can also be greater for a slower storm, e.g., for the estuaries of North Carolina (Peng et al., 2004), and for the Dutch coast (N. J. Berg, 2013). For the Charleston Harbor in South Carolina, although a slower storm can produce larger inundation areas, whether or not it can produce larger surge depends on the faster storm's speed and the distance of the track from the harbor (Peng et al., 2006). While these studies have identified the vulnerability of the coastline to hurricane storm surge under different scenarios, they considered small regions or idealized coastlines, and storms that moved perpendicular to the coastline. The present study uses Hurricane Matthew's track along the coast from Florida to North Carolina to examine how the forward speed of a shore-parallel storm affects the surge and inundation along a complex estuarine coastline and coastal floodplain.

This study uses the coupled ADCIRC+SWAN model, which has proven to be accurate in flood predictions in many coastal systems (Hope et al., 2013; Suh et al., 2015; Dietrich et al., 2018). The model utilizes an unstructured, finite-element mesh developed for surge and tide predictions for the U.S. Atlantic and Gulf coasts (Riverside Technology et al., 2015). The unstructured mesh can represent a large domain, while using sufficient resolution to represent the complex shoreline. This combination allows for comprehensive validation and scenario testing. The goals of this study are to better understand the influence of storm timing and forward speed on flooding for a shore-parallel storm in a large domain. The goals are addressed by (a) validating model predictions of winds, and water levels during Matthew on a mesh with floodplain coverage over a large extent, (b) quantifying the contributions of nonlinear interactions to the total water levels, and (c) quantifying the differences in flooding due to differences in the storm's forward speed and time relative to the tidal cycle.

2.3 Hurricane Matthew

2.3.1 Synoptic History

Matthew began as a tropical wave off the west coast of Africa on 23 September 2016 (Stewart, 2017), and by 1200 UTC 28 September, measurements indicated a tropical storm formation about 27 km west-northwest of Barbados. Moving into the Caribbean Sea, Matthew attained hurricane status on 1800 UTC 29 September about 300 km northeast of Curaçao. Matthew then turned west-southwest and intensified to an estimated peak intensity of 75 m/s (Category-5) on 0000 UTC 1 October. Over the next few days, the storm weakened to a category 4 status as it moved northward and made landfall with peak wind speeds of 66 m/s over Haiti (1100 UTC 4 October) and 59 m/s over Cuba (0000 UTC 5 October). By 1200 UTC 6 October, the storm brought hurricane-force winds and flooding rains to most of the central and northwestern Bahamas with a peak wind speed of 64 m/s. The category 4 hurricane made landfall near West End, Grand Bahama Island, around 0000 UTC 7 October (Stewart, 2017).

A broad eastward-moving mid-latitude trough located over the central United States then caused Matthew to turn toward the north-northwest (Stewart, 2017) and impact much of the southeastern U.S. (Figure 2.1). The storm weakened to a category 3 hurricane around 0600 UTC 7 October about 64 km east of Vero Beach, Florida, and to a category 2 hurricane by 0000 UTC 8 October about 92 km east-northeast of Jacksonville Beach, Florida. As the storm moved northward, its wind field expanded causing hurricane-force wind gusts across the coastal regions of southeastern Georgia and southern South Carolina. The mid-latitude trough then caused the storm to weaken to a category 1 status (Stewart, 2017). Moving nearly parallel to the coast of South Carolina, Matthew made landfall around 1500 UTC 8 October just south of McClellanville, South Carolina.

The center of the hurricane then traveled offshore of the coast of South Carolina and remained just offshore of the coast of North Carolina through 9 October. Contributions from Matthew's tropical moisture, the ongoing extratropical transition and an increasing pressure gradient from an approaching cold front caused sustained hurricane-force winds over the Outer Banks and significant sound-side storm-surge flooding during the early hours of 9 October. Matthew lost its tropical characteristics by 1200 UTC 9 October, as it moved away from the U.S (Stewart, 2017).

2.3.2 Extensive Observations along U.S. East Coast

Matthew's effects on surface pressures and wind speeds, offshore and nearshore waves, and coastal water levels are well-described by observational data. Along the southeastern U.S. coast from Florida through North Carolina (Figure 2.1), the National Oceanic and Atmospheric Administration (NOAA), the U.S. Geological Survey (USGS), and other agencies collected information at hundreds of buoys, permanent and rapidly deployed gauges and stations, and real-time sensors. Along the storm's path, surface pressures were observed at 283 locations, wind speeds and directions were observed at 66 locations, and significant wave heights were observed at 16 locations (Table 2.1). Time series observations at buoys and stations operated by the NOAA National Data Buoy Center (NDBC) and the NOAA National Ocean Service (NOS) show how the peak, 10-minute-averaged wind speeds evolved during the course of the storm. Wave parameters were also observed at many of these same locations.

These winds and waves caused setup and storm surge along the southeastern U.S. coastline. NOS and USGS permanent and rapidly-deployed gauges collected observations; time series of water levels at 501 locations and 612 high-water marks (HWMs) were identified within the model extent. For the analyses herein, observations were omitted that did not operate during the storm peak or that showed elevated water levels after the storm due to freshwater run-off or wave run-up, thus leaving 289 time series and 464 HWMs to describe storm surge (Table 2.1). These observations are used to validate our predictive models for winds, and storm surge.

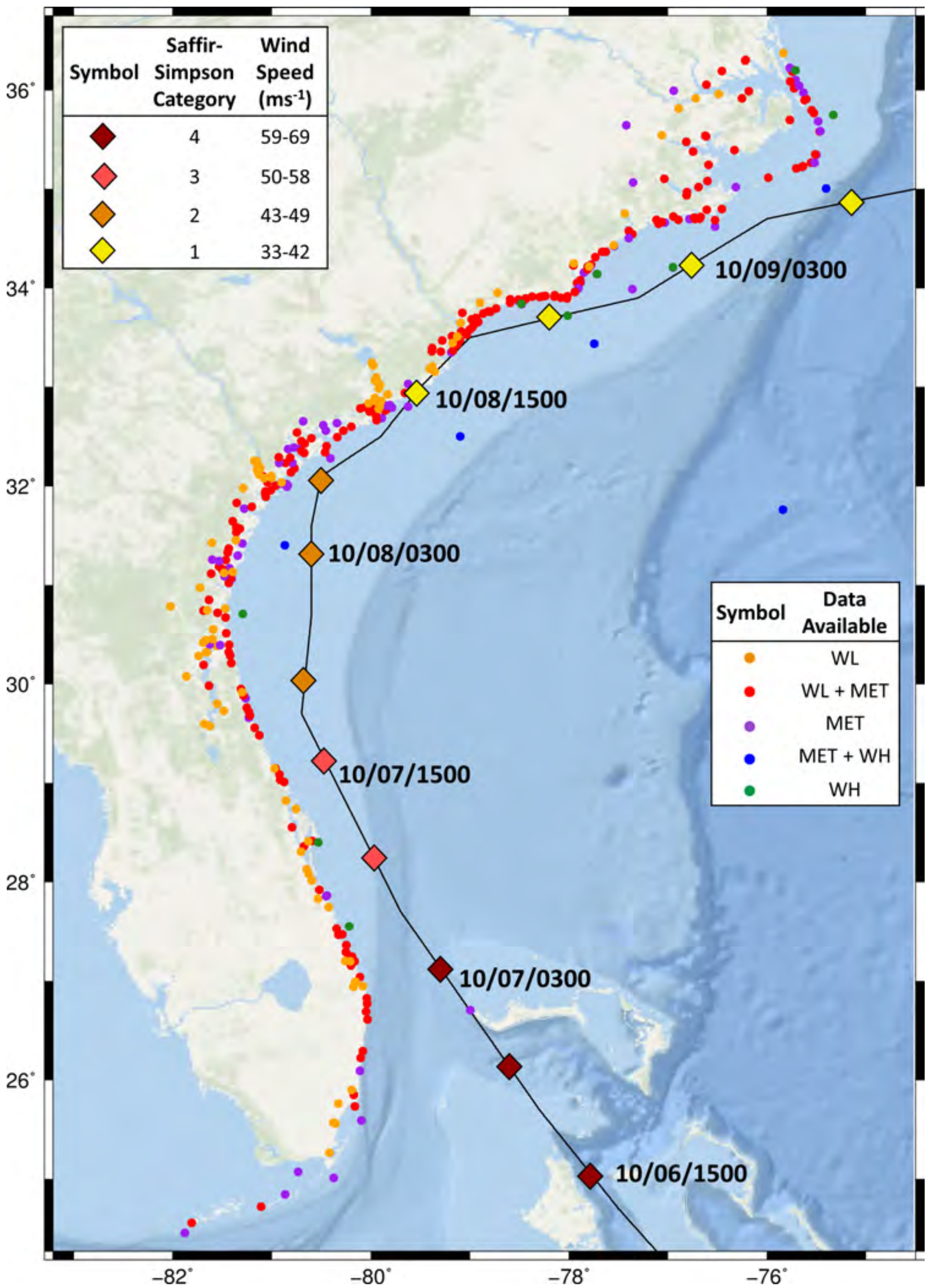

Figure 2.1 NHC best track for Matthew (black line and diamonds), along with observation locations (circles) on the U.S. southeast coast. High-water marks are not shown. The storm center positions are shown every 6 hr and color-coded to categories on the Saffir-Simpson scale. The storm positions are labeled in dates/times relative to UTC. The observation locations are color-coded to indicate whether they have data for meteorology (MET), waves (WH), and/or water levels (WL).

Table 2.1 Numbers of available observations for atmospheric, wave, and water-level responses to Matthew.

Data Source	Reference	Surface Pressure	Wind Speed	Wind Direction	Significant Wave Height	Water Levels	High Water Marks
NOS	NOAA (2018a)	19	19	19		21	
NDBC	NOAA (2017)	15	15	15	7		
CORMP	UNCW (2018)	6	6	6	3		
NERRS	NERRS (2018)	5	5	5			
USACE	USACE (2018)				1		
UNC CSI	UNC (2018)				1		
CDIP	SCO (2018)				4		
ICON	NOAA (2018b)	3	3	3			
ENP	NPS (2018)		1	1			
FIT	FIT (2018)	1	1	1			
USGS-PERM	USGS (2018)					77	
USGS-DEPL	USGS (2018)	8	6	7		17	464
USGS-STS	USGS (2018)	210				168	
NCEM	NCEM (2018)	10	10	10		6	
TOTAL		277	66	67	16	289	464

2.4 Methods

Predictions of waves and storm surge are sensitive to the atmospheric conditions used as forcing to the model simulations. In this study, we evaluate forcings from three sources: a vortex model based on storm parameters like the track, forward speed, and isotach radii; and two data-assimilated products available after the storm. Then the most-accurate atmospheric forcing is used for a detailed hindcast of Matthew's effects on water levels throughout the southeastern U.S., via comparison with extensive observations. This study uses the depth-averaged, barotropic version of ADCIRC, because the strong surface stresses during storms causes the water column to be well-mixed in shallow nearshore and coastal regions. This hindcast is then used as the basis for studies of the nonlinear interactions between tides and surge, and of the effects of storm timing and forward speed. In this section, details are provided about the three sources for surface pressure and wind fields that were evaluated for hindcasts of Matthew, as well as the input settings for the coupled ADCIRC+SWAN model.

2.4.1 Surface Pressure and Wind Fields

Hydrodynamic predictions are analyzed with three sources of atmospheric forcing: a parameterized vortex model based on storm parameters from the National Hurricane Center (NHC), and two data-assimilated products. For all three sources, the surface pressures and wind velocities are developed (either by the parametric model or by interpolation from the data-assimilated products) at the computational points in the model domain. ADCIRC accounts for canopy cover and applies a surface roughness reduction factor increases to full marine winds as overland regions are inundated (Kerr et al., 2013).

2.4.1.1 Parametric Vortex Model

It is common to use parametric vortex models to represent storm wind fields based on limited input information (Xie et al., 2006; Hu et al., 2012; Hu et al., 2015). These models assume a hyperbolic radial pressure field that depends on the ambient and cyclone central surface pressures, the radius to maximum winds, and the hurricane-shape parameter (Schloemer, 1954; Holland, 1980). Several parametric vortex models have been used within ADCIRC to generate wind and pressure fields in forecasting applications

(Mattocks et al., 2006; Mattocks et al., 2008; Dietrich et al., 2013a). The most complete is the Generalized Asymmetric Holland Model (GAHM),which has been shown to be a better representation than earlier versions (Gao et al., 2017), and to compare well with observation-based analysis products and full-physics numerical models (Dietrich et al., 2018; Cyriac et al., 2018). In this study, GAHM is used with the NHC Best Track storm parameters for Matthew (Stewart, 2017) to generate surface pressures and wind speeds at every computational point in the ADCIRC domain. Unlike the two atmospheric forcings described below, GAHM is not data-assimilated and only represents the vortex, with no far-field meteorological representation.

2.4.1.2 Data-Assimilated Atmospheric Products

Surface pressure and wind velocities from WeatherFlow Inc. (WF) were developed using the Weather Research and Forecasting (WRF) model (Skamarock et al., 2008), which can simulate weather processes at synoptic scales down to large eddy simulations at microscales. During Matthew, 52 stations measured sustained wind speeds greater than 22 m/s, with 32 stations measuring gusts of at least 33 m/s. These observations were assimilated into fields of surface pressures and wind velocities.These fields cover a period from 2000 UTC 06 October 2016 until 2000 UTC 09 October 2016, at 10-min intervals. The fields cover from latitude 24.15°N to 38.67°N and from longitude 83.55°W to 72.02°W with square elements of 96.12 arc-seconds (approximately 3 km north-south by 3 km east-west). The surface pressures and wind velocities are interpolated in space and time to the ADCIRC computational points within the WF domain (Figure 2.2).

The second source for data-assimilated products was Oceanweather Inc. (OWI), whose fields are based on observations from anemometers, airborne and land-based Doppler radar, airborne stepped-frequency microwave radiometer, buoys, ships, aircraft, coastal stations and satellite measurements (Bunya et al., 2010). For Matthew, the Tropical PBL (TropPBL) model (Cardone et al., 1994; Thompson et al., 1996) was applied in the core during the entire storm, with hand analysis overlay from 2100 UTC 06 October 2016 until 1500 UTC 09 October 2016, to better represent the interaction of the storm with the coast. The resultant wind and pressure fields are then subject to manual kinematic analysis using the IOKA system to add features that are not well-resolved by the TropPBL model, as well as in-situ, satellite, and aircraft data, into the final fields. These fields represent 30-min sustained wind velocities at a reference height of 10 m

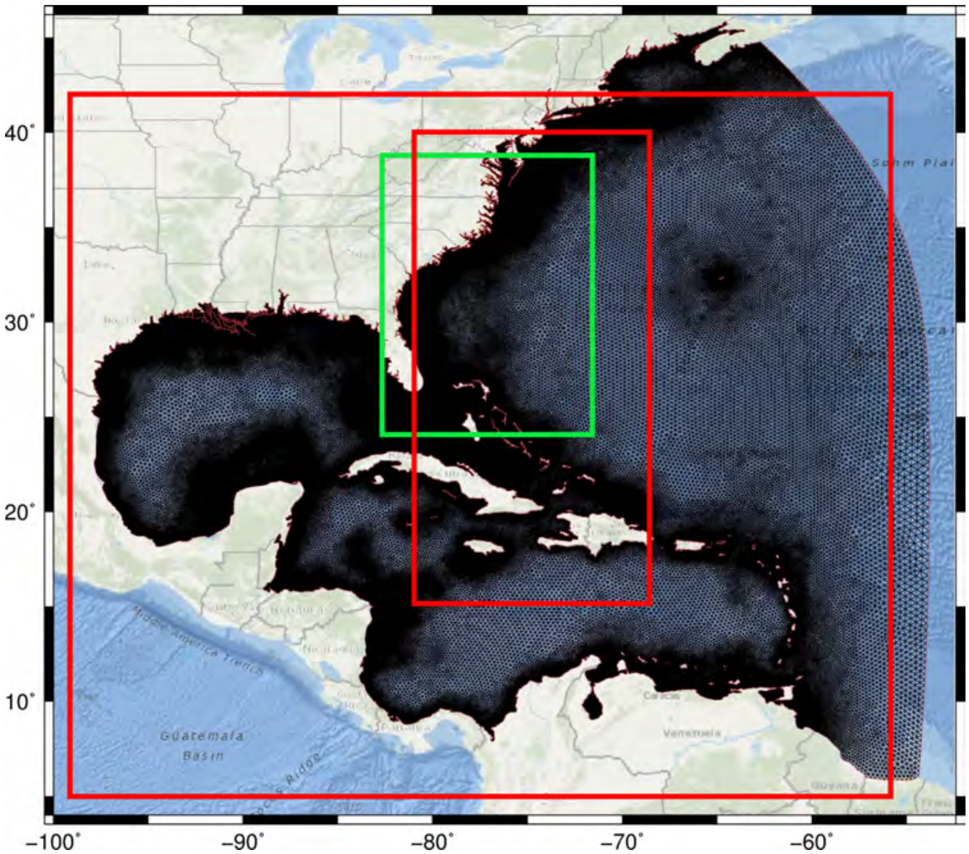

Figure 2.2 Coverage area of the WF (green) and OWI (red) wind grids over the HSOFS unstructured mesh (black).

above the ground/sea level with consideration to marine exposure. Lagrangian-based interpolation is then used to produce fields at 15 min intervals. For use as atmospheric forcing to hydrodynamic models, the surface pressure and wind fields are represented with a lower-resolution basin grid and a higher-resolution region grid (Figure 2.2). The basin grid covers from latitude 5°N to 42°N and from longitude 99°W to 55°W with a spatial resolution of 0.25°, whereas the higher-resolution region field covers from latitude 15°N to 40°N and from longitude 82°W to 68°W with a spatial resolution of 0.05°, both covering a period from 0000 UTC 01 October 2016 until 0000 UTC 11 October 2016, at 15 min intervals.

2.4.2 Coupled Models for Nearshore Waves and Circulation

The storm-induced waves and circulation during Matthew must be predicted by models that can represent their interactions over a wide range of temporal and spatial scales, including coastal flooding into overland regions. We use the coupled SWAN+ADCIRC models (Dietrich et al., 2011b; Dietrich et al., 2012), which have been validated extensively for flooding during tropical cyclones (Bhaskaran et al., 2013; Hope et al., 2013; Suh et al., 2015; Dietrich et al., 2018).z

The unstructured-mesh version of SWAN uses a sweeping Gauss-Seidel method to propagate efficiently the wave action density (Booij et al., 1999; Zijlema, 2010). The action balance equation is used to incorporate source/sink terms for nearshore wave physics, such as triad nonlinear interactions, bottom friction and depth-limited breaking, in addition to deep-water physics of quadruplet nonlinear interactions and whitecapping. The simulations in this study use SWAN version 41.01 with a time step of 600 s. The spectral space is discretized using 36 directional bins with directional resolution of 10° and 40 frequency bins with a logarithmic resolution over the range 0.031 to 1.42 Hz. This logarithmic discretization of frequencies is based on the ratio of $\Delta f/f = 0.1$ for the discrete interaction approximation of the quadruplet interactions (Hasselmann et al., 1985). This spectral discretization and other physical and numerical settings are the same as used in previous hindcast studies by the authors (Dietrich et al., 2011a; Dietrich et al., 2013b). To prevent excessive directional turning or frequency shifting at a single vertex due to steep gradients in bathymetry or ambient currents, the spectral velocities in SWAN are limited using a CFL restriction (Dietrich et al., 2013b) with an upper limit of 0.25.

ADCIRC uses the continuous-Galerkin finite element method to solve the shallow water equations on unstructured meshes (Luettich et al., 1992; Kolar et al., 1994; Luettich et al., 2004; Dawson et al., 2006; Westerink et al., 2008). Water levels are calculated using the Generalized Wave Continuity Equation (GWCE), which is a combined and differentiated form of the continuity and momentum equations (Kinnmark, 1986), whereas depth-averaged current velocities are determined from the vertically-integrated momentum equations. For the simulations in this study, ADCIRC version 52.30.13 is used in explicit mode with the lumped mass matrix form of the GWCE (Tanaka et al., 2011). The bottom drag is applied using a depth-dependent quadratic friction law, with a drag coefficient set by the Manning's n value specified for every vertex (Luettich et al., 1992; Luettich et al., 2004). These Manning's n values are also used by SWAN to compute roughness lengths based on the updated ADCIRC water levels at each mesh vertex (Bretschneider et al., 1986; Madsen et al., 1988; Dietrich et al., 2011a). The minimum bathymetric height and friction-surface velocity required for wetting are 0.10 m and 0.01 m/s, respectively. The spatially-constant horizontal eddy viscosity for the momentum equations was set to 50 $m^2\ s^{-1}$, and an ADCIRC time step of 1 s was used. The wind drag coefficients on the water surface are calculated using the Garratt formulation (Garratt, 1977; Westerink et al., 2008) with an upper limit of $C_D = 0.002$, similar to previous studies (Dietrich et al., 2011a; Dietrich et al., 2012). The advective transport terms were enabled to account for nonlinear interactions between surge and tides.

The unstructured-mesh spectral wave model SWAN and the shallow water circulation model ADCIRC were integrated into a coupled SWAN+ADCIRC model so they share the same computational cores and the same unstructured mesh (Dietrich et al., 2011b; Dietrich et al., 2012). ADCIRC interpolates the wind velocities and computes water levels and velocities, and then supplies them to SWAN, which uses them in its computations for evolution of spectral action density. At the end of each SWAN time step, wave radiation stresses and their gradients are computed by SWAN, and then passed on to ADCIRC, which applies them as surface stresses in its momentum equations. The coupling interval is taken to be the same as the SWAN time step of 10 min.

2.4.3 Unstructured Mesh to Describe the Southeast U.S. Coast

This study uses the Hurricane Surge On-Demand Forecasting System (HSOFS) mesh, which provides coverage of nearshore regions and coastal floodplains along the entire U.S. coast from Texas through Maine (Riverside Technology et al., 2015). The widespread coverage of the HSOFS mesh is possible because its local mesh resolution is typically coarser than meshes for specific coastal regions. The mesh has an average resolution of 500 m along the coast with some areas decreasing to a resolution of 150 m. At most locations, the mesh extends inland to a smoothed version of the 10-m topographic contour (Figure 2.3). It has a total of $1,813,443$ vertices and $3,564,104$ elements. Two primary data sources were used to provide bathymetry/topography: the USGS 1/9 arc second National Elevation Dataset (NED) Digital Elevation Model (DEM) (U.S. Geological Survey, 2018) supplied overland topography and the NOAA East Coast 2012 (EC2012) tidal constituent database mesh (Szpilka et al., 2016) supplied bathymetry. The mesh has been validated for 10 major tropical and extra-tropical storms covering a spectrum of landfalls across the U.S. coast including Isabel, Katrina, Ike, and Sandy (Riverside Technology et al., 2015). The HSOFS mesh is ideal for this study because its widespread coverage includes the nearshore regions and floodplains impacted by Matthew along the southeast U.S. coast.

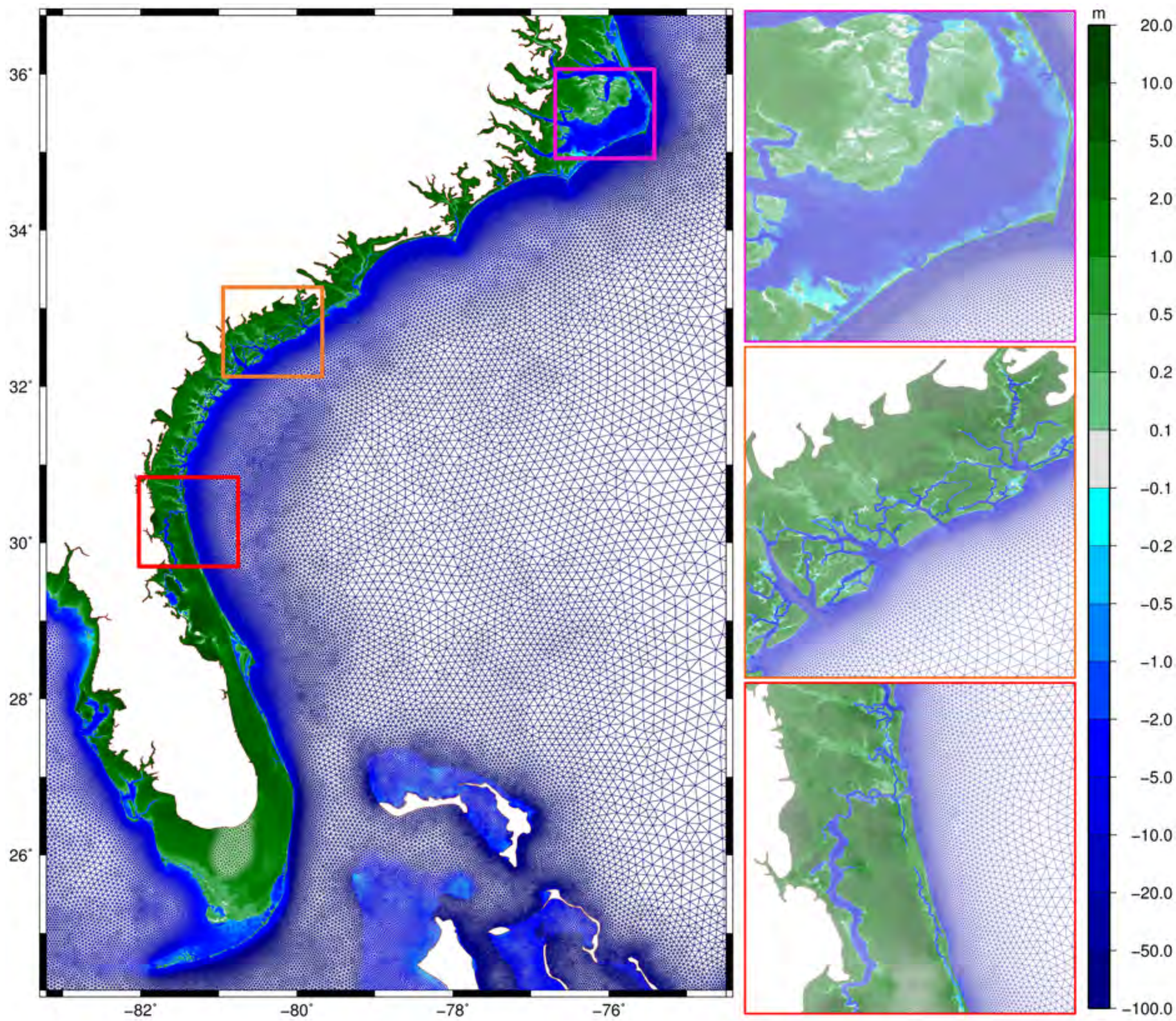

Figure 2.3 The HSOFS mesh topography and bathymetry (m relative to LMSL), contoured on the mesh elements (left figure). Colored boxes indicate specific regions as shown on the right: The Pamlico Sound, North Carolina (pink), the Cooper and Savannah Rivers along the South Carolina-Georgia coast (orange) and Upper Florida showing the Fernandina Beach and St. Johns River (red).

2.4.4 Adjustments for Water Level Processes on Longer Time Scales

To represent baroclinic and longer-term processes, water levels were adjusted *a priori* to account for local sea level rise and intra-annual mean sea surface variability. These adjustments are provided as a spatially-varying offset surface, and are thus an improvement over the spatially-constant adjustments used in previous studies (e.g., (Bunya et al., 2010; Dietrich et al., 2011a; Dietrich et al., 2018)). They provide a correction to the mean water levels before the storm, without the expense of running a three-dimensional, baroclinic model from the open ocean into the floodplains.

The ground elevations in the HSOFS mesh are referenced to local mean sea level based on the National Tidal Data Epoch from 1983 through 2001, and thus the sea level must be adjusted to conditions during Matthew in 2016. Sea level trends were computed at 29 NOAA tidal stations extending from Florida through Maine, using relationships provided by the NOAA Center for Operational and Oceanographic Products and Services (CO-OPS) (National Oceanic and Atmospheric Administration, 2018a) for a 15-year period from 2001 to 2016, to account for local increases in mean sea level relative to the datum used by the HSOFS mesh. This increase ranges from 3 to 5 cm for much of Florida through South Carolina, but increases to 7 to 8 cm in northeast North Carolina and Virginia (Figure 2.4).

The water levels were also adjusted to account for steric effects due to to thermal expansion of the ocean waters (Levitus et al., 2000; Willis et al., 2004; Antonov et al., 2005) and baroclinic interactions with the Gulf Stream (Ezer et al., 2013) using the regional long-term sea level station data at the time of landfall (Bunya et al., 2010). For Matthew, the steric adjustment resulted in a maximum water level increase of about 19 cm along the Georgia coast, but decreases to about 10 cm to the south in Florida and to the north in North Carolina and Virginia (Figure 2.4).

The total vertical reference level adjustment at each station was calculated as the sum of the local sea level rise and steric increase. This increase was then applied as an offset surface, which varies spatially along the coast, and transitions offshore to zero. This offset surface was provided to ADCIRC at the start of the simulation using a 1-day ramp and is implemented as a pseudo barometric pressure term in ADCIRC (Asher et al., 2018).

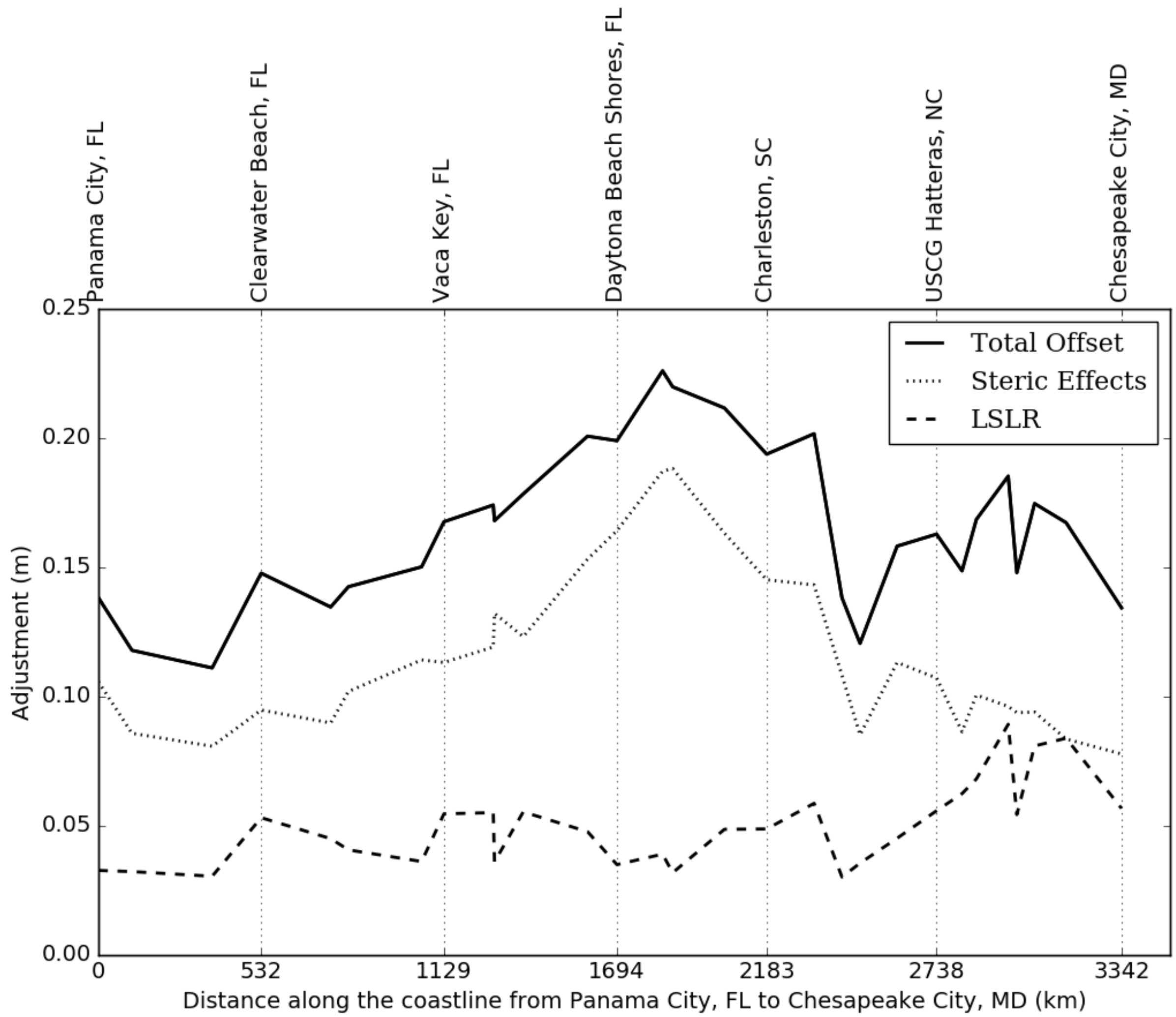

Figure 2.4 Variation of offset values (m) along the U.S. southeast coast. Adjustments are shown for local sea level rise (dashed), steric effects (dotted), and total offset (solid).

2.5 Model Validation

Hindcasts of Matthew were simulated with SWAN+ADCIRC and atmospheric forcing from the three sources: GAHM, WF, and OWI. To establish the ambient water level condition prior to the storm, the tides were spun-up in a 15-day simulation from 0000 UTC 17 September to 0000 UTC 02 October. Then the storm was simulated over a 9-day period from 0000 UTC 02 October to 0000 UTC 11 October.

2.5.1 Atmospheric Forcings

2.5.1.1 Evolution of Surface Pressures and Wind Speeds

The observed and predicted surface pressures and wind speeds are compared at selected locations ranging from Florida through North Carolina (Figure 2.5) and throughout the storm's evolution (Figures 2.6-2.7). Surface pressures are analyzed as pressure deficits, where an ambient pressure of 1013.25 hPa is subtracted from observed and predicted pressures. On 0800 UTC 07 October, when the storm was located offshore of Melbourne, Florida (Figure 2.6, first row), north-northeasterly winds were observed at the NDBC station TRDF1 at Trident Pier, Florida, with a maximum wind speed of 22.9 m/s and a pressure deficit of about 40 hPa (Figure 2.7, first row). GAHM over-predicts the peak wind speeds by about 10 m/s and under-predicts the pressure deficit by 20 hPa.

On 2000 UTC 07 October (about 10 hours later, and 19 hours before landfall), when the storm was located 35 mi east of St. Augustine, Florida (Figure 2.6, second row), the wind speeds decreased in all three fields. Close to the eye, the winds interact with the coast, with peak wind speeds of 25 to 30 m/s for both GAHM and OWI, and 20 m/s for WF. At this time, the NOS station MYPFI located at the entrance of the St. Johns River, Florida, received north-northeasterly winds with a maximum wind speed of 22.7 m/s and pressure deficit of about 28 hPa (Figure 2.7, second row). As Matthew moved northward, it brought hurricane-strength wind gusts to the coasts of southeastern Georgia and southern South Carolina. On 0615 UTC 08 October (about 9 hours before landfall), the USGS station 311941081265201 near Brunswick, Georgia, recorded a maximum wind speed of 16.1 m/s and a pressure deficit of about 29 hPa (Figure 2.7, third row), with all the three atmospheric forcings having similar results.

When the storm reached offshore of Charleston, South Carolina, it had weakened to Category-1 status. On 1350 UTC 08 October (about 1 hour before landfall), the offshore NDBC buoy 41004 observed southwesterly winds with a maximum speed of 23.5 m/s and a pressure deficit of 31.55 hPa (Figure 2.7, fourth row). At the peak, all three models gave similar results, except for GAHM under-predicting the pressure deficit by about 20 hPa. On 1500 UTC 08 October, the Category-1 storm made landfall in McClellanville, South Carolina (Figure 2.6, third row) with observed wind speeds of 39 m/s (Stewart, 2017). Near landfall, there is a difference in the storm track, with both GAHM and OWI predicting a slight inland trajectory for the storm compared to WF. After landfall, the

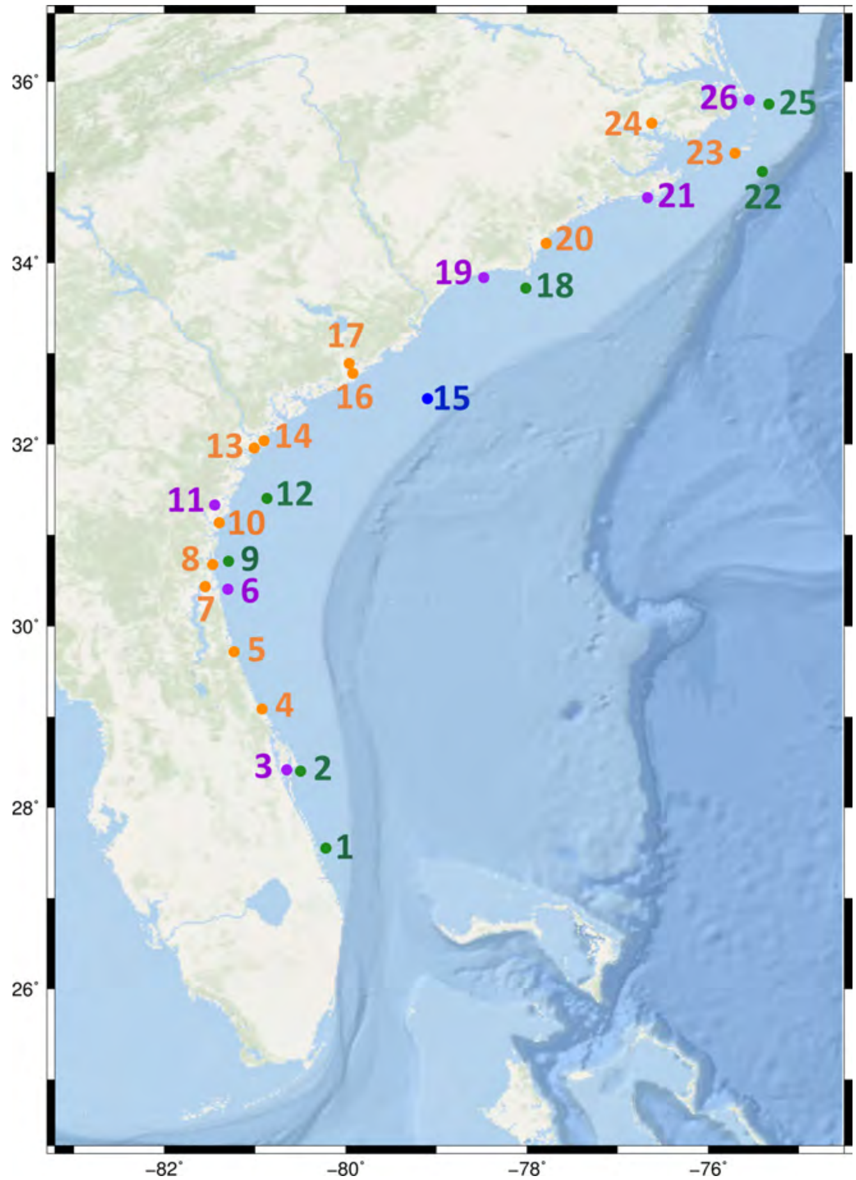

Figure 2.5 Locations of selected stations for comparison of surface pressures, wind speeds, significant wave heights and water levels. The points are color coded as in Figure 2.1 and numbered from south to north.

storm moved offshore in an east-northeastward direction.

By 0600 UTC 09 October, the storm was located 45 km offshore of Cape Hatteras, North Carolina (Figure 2.6, bottom row). The eye of the storm is similar for GAHM and OWI with a large eye surrounded by a small 10 to 15 m/s wind field, although

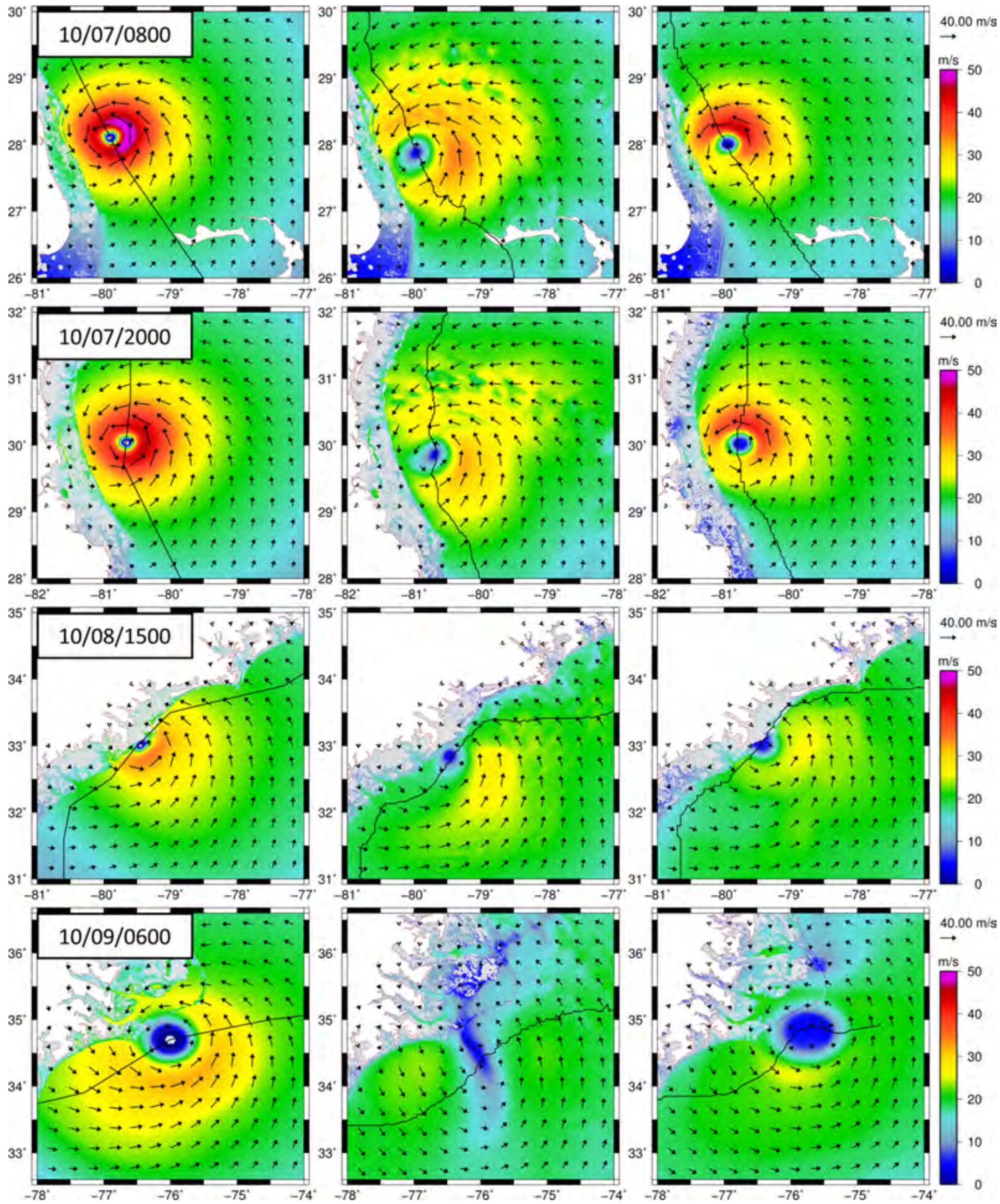

Figure 2.6 Hindcasts of wind speeds (m/s) during Matthew along the U.S. southeast coast. Rows correspond to: (top) 0800 UTC 07 October, approximately 31 hours before landfall; (second from top) 2000 UTC 07 October, approximately 19 hours before landfall; (second from bottom) 1500 UTC 08 October, approximately at landfall; and (bottom) 0600 UTC 09 October, approximately 15 hours after landfall. Columns correspond to: (left) GAHM; (center) WF; and (right) OWI. Black lines represent the storm track for each source.

GAHM has a much larger 25 to 30 m/s field offshore. At the NDBC buoy 41025 at Diamond Shoals, wind speeds at this time were 18 m/s, which matches for WF and OWI. The eye for WF has become disorganized and extends into Pamlico Sound. There are significant differences inside the sound, with modeled winds in the ranges of 20 to 30 m/s, 5 to 15 m/s, and 10 to 20 m/s for GAHM, WF, and OWI, respectively. The effects of Matthew's wind field were observed even at the NOS station 8652587 located north at the Oregon Inlet Marina, North Carolina, where a maximum wind speed of 20.56 m/s and a pressure deficit of about 20 hPa was recorded on 1006 UTC 9 October (Figure2.7, last row). The storm weakened to a tropical depression by 1200 UTC 9 October, when it was located 45 km southeast of Cape Hatteras.

Overall, for the surface pressures (Figure 2.7, left column), GAHM tends to under-predict the pressure deficits during the storm by more than 10 hPa. But the central pressure comes from the best-track file and represents an input to the GAHM, which is then used to produce the surface barometric field. Thus these under-predictions are almost entirely a result of errors in the central pressure coming from the best-track file. The data-assimilated WF and OWI products show a good match to the surface pressures at most locations, with exceptions of: WF before and after the storm, due to its relatively shorter time period; and OWI at NOS station BFTN7 at Beaufort, North Carolina, where it under-predicted the pressure deficit during the storm. The peak wind speeds are also matched well between observations and predictions (Figure 2.7, right column). The parametric GAHM has zero wind speeds before and after the storm, and it also tends to over-predict the peaks at locations in Florida (TRDF1) and into the Carolinas (41024, BFTN7). The data-assimilated WF and OWI products capture the large-scale synoptic wind patterns as well as the storm winds.

2.5.1.2 Error Statistics

The agreement between observations and predictions is quantified (Table 2.2) through the use of the root-mean-squared error E_{RMS}:

$$E_{RMS} = \sqrt{\frac{1}{N}\sum_{i=1}^{N} E_i^2}$$

and the mean normalized bias B_{MN}:

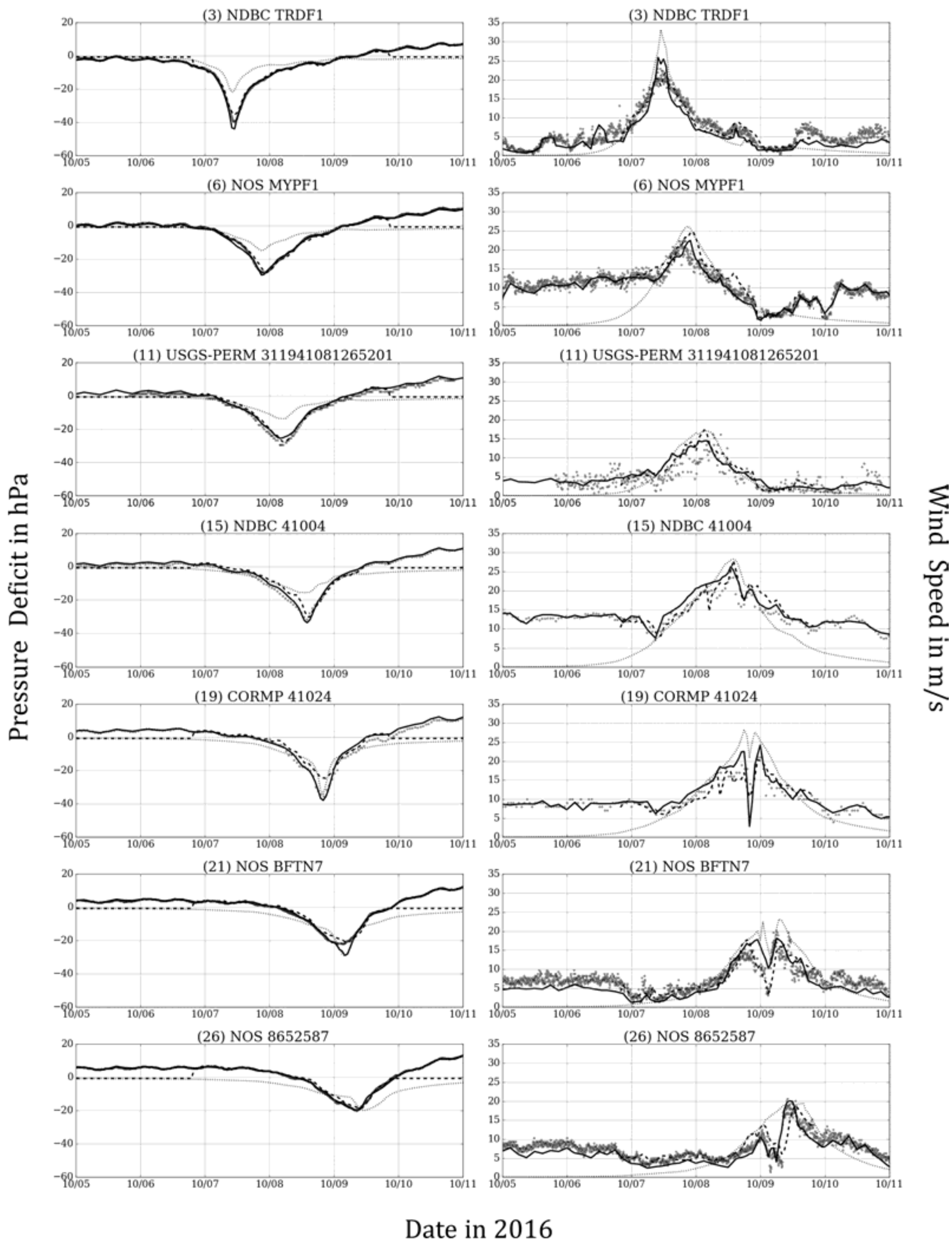

Figure 2.7 Time series of pressure deficits in hPa (left column) and wind speeds in m/s (right column) at seven locations (rows) shown in Figure 2.5. Observed values are shown with gray circles and predicted results using lines: GAHM (dotted), WF (dashed) and OWI (solid).

$$B_{MN} = \frac{\frac{1}{N}\sum_{i=1}^{N} E_i}{\frac{1}{N}\sum_{i=1}^{N} |O_i|}$$

where N is the number of observations and E_i is the difference between predicted and observed values. The E_{RMS} is an indication of the magnitude of error and has an ideal value of zero. The B_{MN} indicates the model's magnitude of over-prediction or under-prediction normalized to the observed value and also has an ideal value of zero. For surface pressures and wind speeds, as well as for water levels in the upcoming sections, these error statistics are calculated for a period ranging from 0000 UTC 05 October to 0000 UTC 11 October.

GAHM has the largest E_{RMS} and magnitude of B_{MN}, thus showing the benefits of the data-assimilated WF and OWI products. Both GAHM and WF under-predict the surface pressure deficits with negative B_{MN} values of -0.16 and -0.02, respectively, whereas OWI over-predicts the surface pressure deficit with a positive B_{MN} of 0.06. Although the peak wind fields in GAHM were the strongest (Figure 2.6), the negative B_{MN} reflects GAHM's lack of ambient winds before and after the storm. WF and OWI have positive B_{MN} for wind speeds of 0.16 and 0.06, respectively, thus indicating over-prediction. For both surface pressure deficits and wind speeds, OWI has smaller errors overall, and thus it is the best match to the observations.

Thus, OWI is a better representation of the atmospheric forcing during Matthew. It is a better match to the observed time series of surface pressures and wind speeds, at locations throughout the region (Table 2.2). Its fields also show the most-realistic representation of the storm's evolution near landfall and afterward (Figure 2.6). In the following sections, the authors will use OWI as the best approximation of the true behavior of Matthew as it moved offshore of the U.S. southeast coast. Although error statistics will be computed for water levels as forced with all three atmospheric sources, only OWI will be used in the analyses of spatial and temporal variability of storm surge, and only OWI will be used in the analyses of nonlinear interactions, storm timing and forward speed.

Table 2.2 Error statistics for surface pressure deficits, wind speeds, water levels, and high water marks.

		Model		
Parameter	Error	GAHM	WF	OWI
Surface Pressure Deficit	Stations	283	283	283
	E_{RMS} (hPa)	6.72	4.23	2.14
	B_{MN}	-0.16	-0.02	0.06
Wind Speed	Stations	66	61	66
	E_{RMS} (m/s)	5.60	2.98	2.29
	B_{MN}	-0.29	0.16	0.06
Water Level	Stations	233	238	241
	E_{RMS} (m)	0.42	0.37	0.28
	B_{MN}	-0.32	-0.27	0.04
High Water Marks	Stations	613	612	622
	E_{RMS} (m)	0.58	0.48	0.28
	B_{MN}	-0.21	-0.19	-0.03
	R^2	0.51	0.65	0.78
	Best-Fit Slope	0.78	0.80	0.96

2.5.2 Water Levels

2.5.2.1 Evolution of Water Levels

As Matthew tracked along the southeast coastline of the United States, heavy winds and rainfall elevated water levels at several locations to historic levels. Although Matthew brought northerly and north-easterly hurricane peak winds of 20 to 25 m/s along the Florida coast from Lake Worth to Port Canaveral, it resulted in very little storm tide with a maximum of 0.5 to 1 m (Figure 2.8, top left). As the storm moved northward, there was an increase in the water levels along the coastline. On 1700 UTC 07 October (Figure 2.8, top right), winds blowing from the northeast pushed water against the coastline with peaks of 1.5 to 2.5 m. The USGS-STS stations FLVOL03143 and FLSTJ03126 located between Orlando Beach and St. Augustine Beach, Florida, recorded peak water levels of 2.1 m and 2.56 m, respectively (Figure 2.9, top row) . The winds decreased as the storm moved northward and weakened from Category-3 to Category-2 status. The station NOS 8720218 at Mayport, Florida and located at the entrance of the St. Johns River, received peak winds of 20 to 25 m/s, causing a maximum water level of 1.59 m, the highest ever recorded at this site (Stewart, 2017) (Figure 2.9).

Along the St. Johns River, inundation occurred well inland from the coast (Figure 2.8, top right). The NOS 8720625 station at Racy Point observed a record peak of 1.58 m on 2236 UTC 07 October (Stewart, 2017), about 3.5 hr after a maximum was observed at the river entrance. North of the St. Johns River along the Florida Coast, Matthew caused storm tides of 2 to 2.3 m. On 0200 UTC 08 October (Figure 2.8, center left), the storm now centered offshore of Georgia, caused shore-parallel winds to drive water levels of 1 to 1.5 m into the relatively deep tidal inlets and sounds that separate the barrier islands stretching 160 km between the St. Marys and Savannah Rivers. Stations along the rivers that extend from these sounds recorded even higher peaks. The USGS-PERM 02226180 and USGS-STS GACHA17861 measured peak water levels of 1.87 m and 2.30 m, respectively (Figure 2.9, third row).

On 0800 UTC 08 October (Figure 2.8, center right), approximately 7 hours before landfall, easterly and north-easterly winds pushed water into the Savannah River, causing water levels larger than 2.5 m. The maximum storm surge recorded by a tide gauge in the United States during Matthew was at NOS 8670870 (Figure 2.9), located at the entrance of the Savannah River, where peak surge occurred during high-tide and caused maximum water levels of 2.59 m. As Matthew moved northward, a combination of wind and storm surge caused extensive damage along the South Carolina coastline. The USGS-STS sites on the islands south and east of Beaufort County, South Carolina, recorded peaks of 2 to 2.5 m. The highest peak of all observations collected during Matthew was at the USGS-STS SCBEA14284 at Bluffton, southwest of Beaufort, where a maximum of 2.66 m was recorded. As a Category-1 storm, Matthew caused extensive flooding in Charleston, South Carolina. At the tidal gauge NOS 8665530 (Figure 2.9) located at the Cooper River Entrance, a peak surge occurred during a low-tide resulting in a storm tide maximum of 1.87 m. On 1500 UTC 08 October at landfall (Figure 2.8, bottom left), south-easterly winds pushed water levels of 1.5 to 2 m against the coastline from Bulls Bay to Myrtle Beach.

The maximum water levels in North Carolina varied significantly by location. For the Atlantic coastline south of Oak Island, the maximum water levels were mostly in the range of 2 to 2.5 m. This decreased to 1.5 to 2 m from Oak Island to Masonboro Inlet and 1 to 1.5 m for the coastline from Wrightsville Beach to Cape Hatteras. On 0600 UTC 09 October (Figure 2.8, bottom right), northerly and northeasterly winds pushed

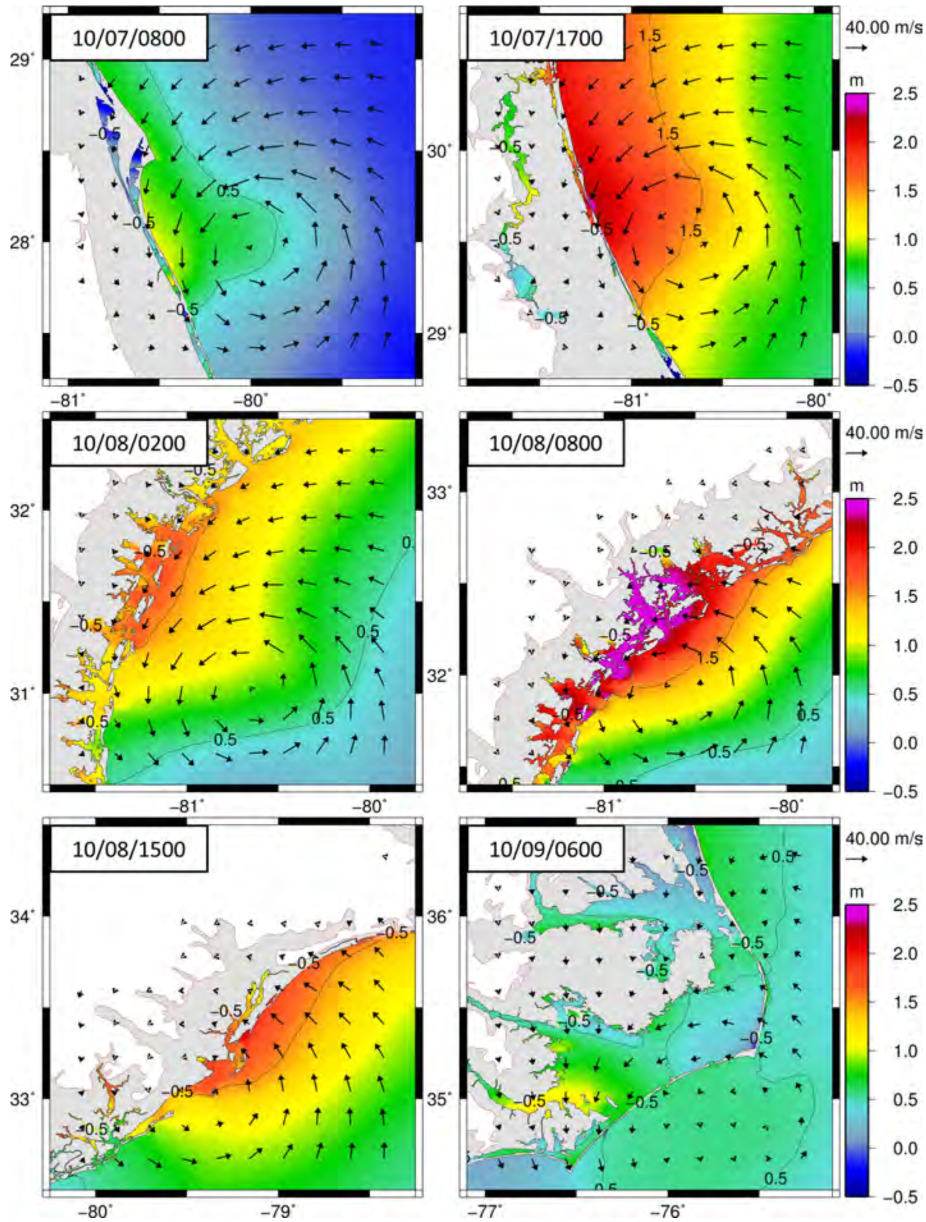

Figure 2.8 Contours of water levels (m relative to NAVD88) and vectors of OWI wind speeds (m/s) during Matthew along the U.S. southeast coast. Times correspond to: (top left) 0800 UTC 07 October, approximately 31 hours before landfall; (top right) 1700 UTC 07 October, approximately 22 hours before landfall; (center left) 0200 UTC 08 October, approximately 13 hours before landfall; (center right) 0800 UTC 08 October, approximately 7 hours before landfall; (bottom left) 1500 UTC 08 October, approximately during landfall; and (bottom right) 0600 UTC 09 October, approximately 15 hours after landfall.

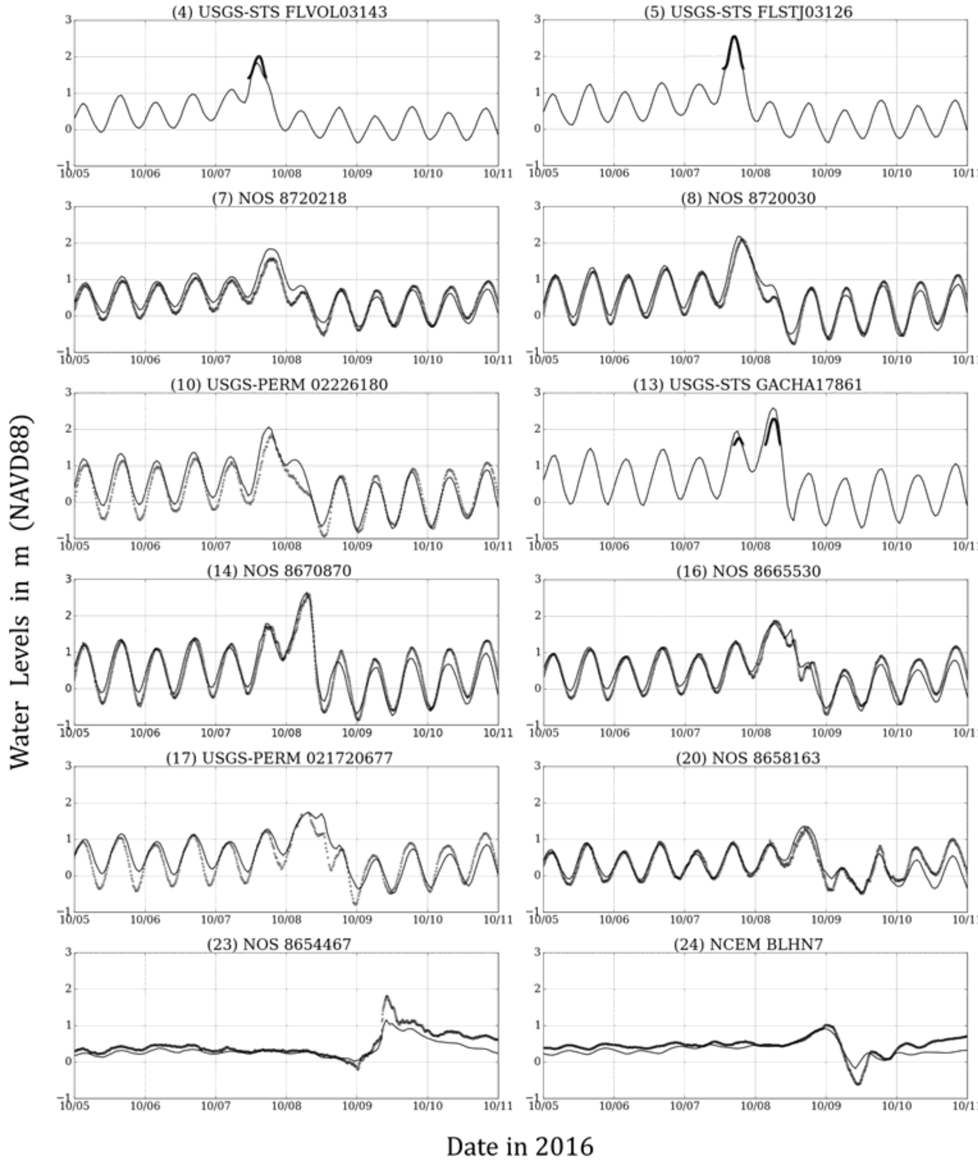

Figure 2.9 Time series of water levels (m relative to NAVD88) at 12 locations shown in Figure 2.5. Observed values are shown with gray circles, and predicted values using OWI (solid).

water levels of 0.5 to 1 m toward the western Pamlico Sound. The NOS 8654467 gauge at the United States Coast Guard station on Hatteras Island, received record water levels (Stewart, 2017) with a peak of 1.85 m (Figure 2.9, bottom left). On the rivers that drain into the Sound, the maximum water levels varied in the range of 0.5 to 1 m in the Neuse River, and 0.75 to 1.25 m in the Pamlico and Pungo Rivers (e.g., NCEM BLHN7 in Figure 2.9, bottom right). As the storm moved offshore, the winds decreased along the coast, and the water levels returned to normal tide levels at most locations.

2.5.2.2 Error Statistics

At most locations, the SWAN+ADCIRC predictions (with OWI atmospheric forcing) show good agreement with the observations (e.g., the 12 stations shown in Figure 2.5 with time series in Figure 2.9). One exception was NOS 8654467, where the model underestimated the peak by more than 0.5 m. There was an over-prediction of the peak at some stations (USGS-STS FLVOL03143, NOS 8720218, USGS-PERM02226180 and USGS-STS GACHA17861), but within 0.3 m. Otherwise, the model was able to closely predict variations in both the tides and surge levels. To quantify the model performance with regard to water level predictions, error statistics were computed (Table 2.2) only at locations wetted by the model. For 241 locations on the U.S. southeast coast, the overall E_{RMS} was 0.28 m and the B_{MN} was very close to zero. The largest errors occurred on the gauges upstream of the Savannah River, where E_{RMS} of about 0.58 to 1.27 m and B_{MN} of 0.83 to 1.56 were obtained. Large E_{RMS} of 0.41 to 0.94 m and B_{MN} of -0.56 to -0.87 were also observed at stations on the Sound side of the Outer Banks in North Carolina. These over-predictions in the Savannah River and under-predictions in the North Carolina Sounds can likely be attributed to the relatively-coarse representation of the channels and tidal inlets that lead to these locations. Comparing the overall statistics for water levels, simulations with GAHM had the highest E_{RMS} of 0.42 m and B_{MN} of -0.32, while simulations with OWI had the smallest E_{RMS} of 0.28 m and B_{MN} of 0.04. Simulations with GAHM and WF had negative B_{MN} and thus under-predicted the water levels.

A total of 464 USGS-observed HWMs inside the model domain were found to be suitable for analysis. When combined with the 289 hydrograph-derived peak water levels, a total of 753 locations were used to evaluate model performance during Matthew along the U.S. southeast coast. In Figure 2.10, the points are color-coded based on error (predicted less observed) expressed as percentage of the observed value. Warm colors indicate regions of over-prediction by ADCIRC, whereas cooler colors indicate regions of under-prediction. For the simulation forced by OWI, the errors in modeled peaks were within 10 percent at 322 (52 percent) of the 622 total stations wetted by ADCIRC and within 25 percent at 538 (87 percent) stations. For the scatter plots, the R^2 value was 0.78 and the slope of the best-fit line was 0.96 (Table 2.2). The E_{RMS} were largest on the Sound side of the Outer Banks in North Carolina. The model under-predicted the peaks by more than 25 percent at most locations in this region. In other regions, the errors were lesser especially along the coast from Florida to South Carolina, where the errors were usually less than 25 percent. A negative value of B_{MN} indicated an under-prediction of the peaks overall by all the three models. As seen for water levels, the observation-based OWI and WF fields led to better error statistics than GAHM for the predicted water levels. The best correlation between modeled and observed peaks were given by OWI with its better values of E_{RMS}, B_{MN}, R^2 and best-fit slope.

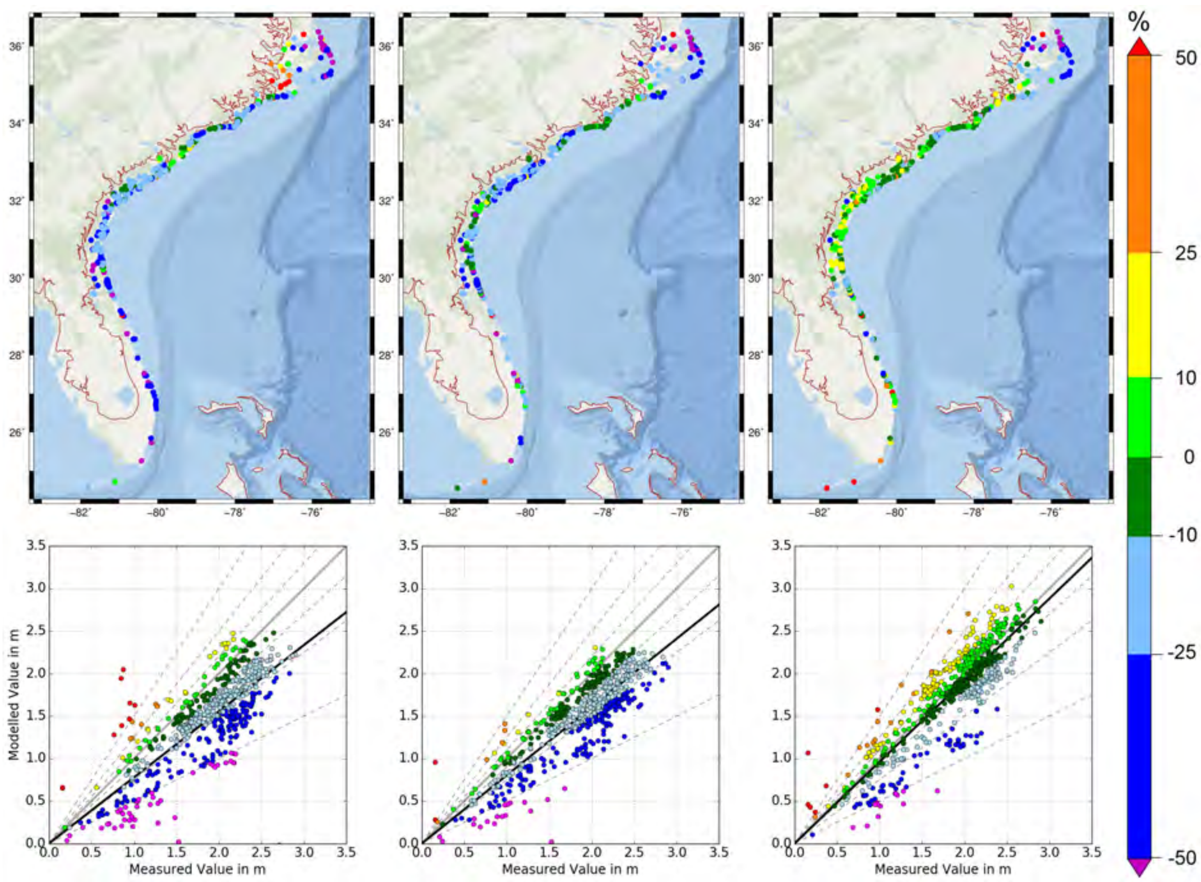

Figure 2.10 Locations (top row) and scatter plots (bottom row) of HWMs and peak hydrograph values during Matthew. Columns correspond to: (left) GAHM; (center) WF; and (right) OWI. Colors indicate error expressed as a percentage of observed value. Green points indicate errors within 10%; yellow and light blue indicate errors between 10% and 25%; orange and dark blue indicate errors between 25% and 50%; and red and purple indicate errors over 50%. The thick gray and black lines represent $y = x$ and best-fit lines, respectively. Statistical metrics are shown in Table 2.2.

Thus, the SWAN+ADCIRC simulation on the HSOFS mesh with OWI atmospheric forcing is the best prediction of the surface pressures, wind speeds, and water levels along Matthew's track from Florida through North Carolina. The water levels are a good match at both open-coast and inland locations, and the error statistics are comparable to other recent studies with SWAN+ADCIRC on higher-resolution meshes (e.g., (Hope et al., 2013)). It is noted that the simulation was not tuned to achieve this performance; the mesh and other input settings are similar to other studies, including real-time forecasting with ADCIRC. Using this well-validated simulation, we can now quantify the contributions of the nonlinear terms in ADCIRC, and then investigate the effects of storm timing and forward speed on the peak water levels.

2.6 Surge Interactions with Tides, Storm Timing and Forward Speed

2.6.1 Nonlinear Tide-Surge Interaction

The total storm tide should include contributions from both surge and tides. However, instead of a linear superposition, there are physical processes that causes their interaction to be a nonlinear phenomenon (Prandle et al., 1978; Wolf, 1981; Tang et al., 1996; Bernier et al., 2007; Horsburgh et al., 2007; Poulose et al., 2017). These processes are represented in the governing equations in ADCIRC as: (a) momentum advection on the surge due to the presence of the tide; (b) the nonlinear effects of bottom friction due to the quadratic parametrization; (c) the Coriolis acceleration (Valle–Levinson et al., 2013; Feng et al., 2016); and (d) the shallow water effect (Prandle et al., 1978; W. Zhang et al., 2010; Idier et al., 2012), which arises due to nonlinearities related to $H = h + \zeta$ terms in the mass and momentum equations. The importance of these terms varies from case to case and is associated with water depth, tidal ranges, and storm strength at specific locations. These nonlinear terms influence the distribution of energy between tide and surge and thus can be a crucial factor in the accurate prediction of total water levels during a hurricane. The goal of the present study is not to re-investigate the possible causes of these nonlinear interactions, but rather to quantify their behavior during a shore-parallel storm affecting a long coastline. In contrast to earlier studies in this region (Valle–Levinson et al., 2013; Feng et al., 2016), which used a typical resolution between 1 to 5 km along the coastline, this study includes sufficient resolution to represent the behavior of the interactions into the estuaries and coastal water bodies.

To separate the nonlinear interaction term from the storm tide, the nonlinear term can be computed as $(\eta_I) = (\eta_{T+W})$ - $(\eta_W + \eta_T)$, where each η represents water levels from a simulation with some combination of winds (W) and/or tides (T) (Bernier et al., 2007; W. Zhang et al., 2010; Rego et al., 2010). Therefore, the offset surface was disabled only for this subsection, to exclude the effects of relative sea level rise and steric effects on the nonlinear interaction between tide and surge. It is noted that, because we are using the depth-averaged, barotropic version of ADCIRC, this study may not represent all of the dynamics on the deeper shelf. However, it is a reasonable assumption that the storm's effects were distributed well into the water column, and the computational efficiency of the depth-averaged version allows for additional resolution to explore the interactions into the estuaries and coastal regions.

During Matthew, it was seen that the nonlinear interactions were large especially in regions with broader-shelf areas (Figure 2.11). In the estuaries along the South Atlantic Bight, the peak magnitudes of the nonlinear interactions were larger than 1 m. Farther offshore from the estuaries, the maximum values decreased to about 0.1 to 0.4 m along the coastline and to zero in the open-ocean. The tide-surge interaction significantly affected the total water levels only when they were large enough to interact. Our results show that with respect to Local Mean Sea Level (LMSL), the nonlinearities are destructive ($\eta_I < 0$) to the storm tide heights during a rising or high tide, and constructive ($\eta_I > 0$) during a low or falling tide. These results are similar to previous studies (Rego et al., 2010; Lin et al., 2012). At locations along Blackbeard Creek to the south of Savannah, Georgia (Figure 2.12), the interaction terms were small with a maximum of 0.27 m at station 1 located offshore. Moving inland, the magnitudes increased to a maximum of 0.48 m at station 2 near the coast and 1.04 m at station 3 in the estuary. At station 3, the nonlinear terms were as large as the tidal amplitudes. These values are large enough to be of practical importance during storm surge forecasting. There is also a phase shift in the peak of the nonlinear terms as compared to that to the surge, as has been recognized previously (Horsburgh et al., 2007). At station 3, this phase shift was 5 hr.

Thus, the tide-surge nonlinear interactions during Matthew occurred on the shallow and wider-shelf regions of the domain and varied in sign based on the tidal cycles. Although similar trends have been seen in the literature, this is the first study to represent

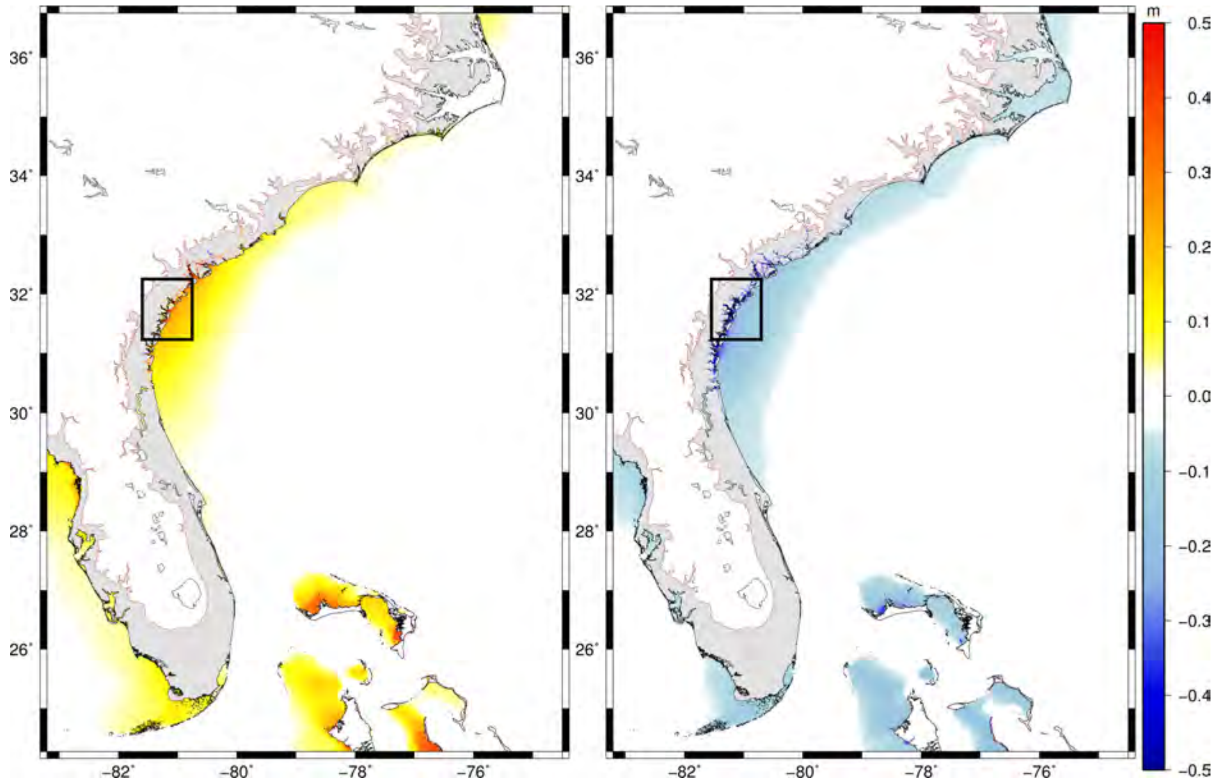

Figure 2.11 Nonlinear interactions on the U.S. southeast coast during Matthew. Columns correspond to: (left) positive maximum values and (right) negative maximum values. OWI was used as the source of meteorological forcing for the simulations with only winds, and winds and tides together. Boxes indicate the location of the region shown in Figure 2.12.

the interactions into the estuaries and floodplains over a long coastline for a shore-parallel storm, and with representation of these features at appropriate resolution. The magnitudes of these nonlinear terms were largest in the estuaries along the southeastern U.S. coast and are larger than in any of the previous studies. The nonlinear tide-surge interactions can have a significant effect in controlling the total water levels during a hurricane.

2.6.2 Storm Timing

The total water levels caused by Matthew as it moved along the U.S. coastline were affected by both variations in tidal amplitudes and by its coincidence with different parts of the tidal cycle at different locations. To understand how Matthew's time of occurrence would have influenced the total water levels along the coast, scenarios were simulated

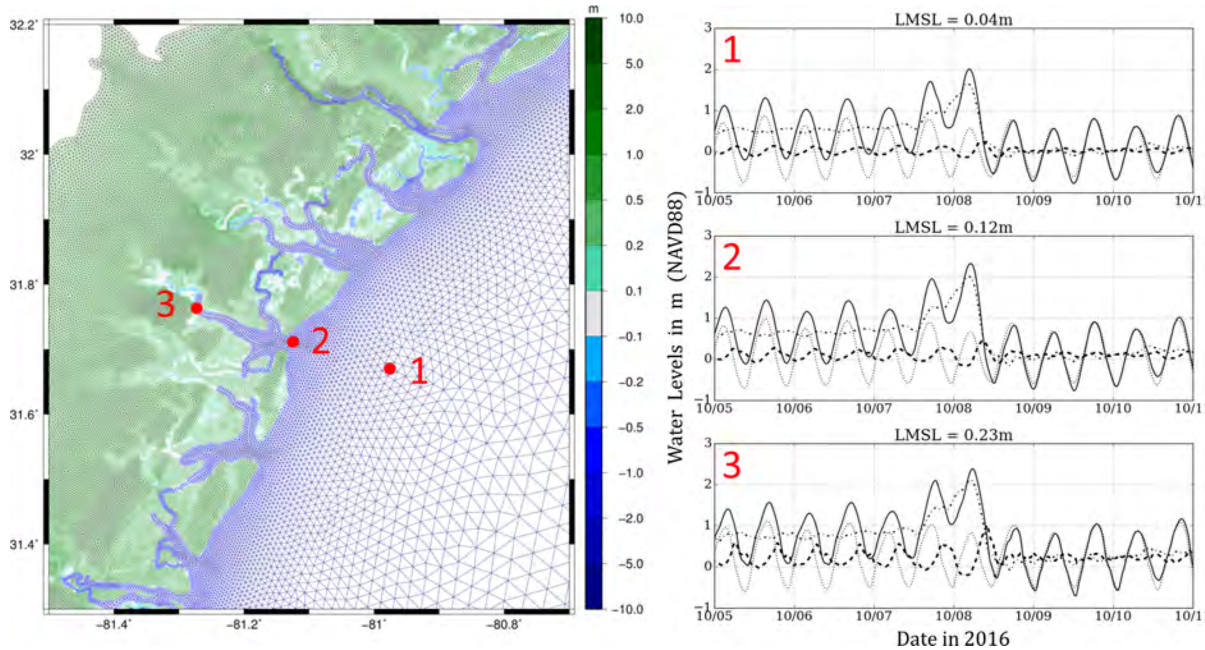

Figure 2.12 Nonlinear interaction terms during Matthew at three locations along the Blackbeard Creek, south of Savannah, Georgia. Columns correspond to: (left) location of stations and (right) time-series of water levels (m relative to NAVD88) with line types corresponding to: (solid) total water levels, (dashed-dotted) surge only, (dotted) tides-only, and (dashed) nonlinear terms. OWI was used as the source of meteorological forcing for the simulations with only winds, and winds and tides together.

to alter the storm's timing relative to the tidal cycle. For the U.S. southeast coast, the dominant tidal constituent is the principal lunar semi-diurnal M_2 tidal constituent. Thus simulations were conducted by delaying the storm by 3.11 hr, 6.21 hr, 9.32 hr and 12.42 hr, corresponding to one-fourth, half, three-fourth and full M_2 tidal periods, respectively. The storm forward speed was unchanged during these simulations.

These scenarios resulted in water levels that varied from that during the storm, with the greatest changes occurring during the +6.21 hr simulation and least changes happening during the +12.42 hr simulation. These variations are shown in Figure 2.13, where warm colors indicate an increase in water level and cool colors indicate a decrease in water levels. In regions like the Pamlico Sound where tides are small, there were no variations in the scenarios. In regions along the coastline where tides are dominant, the changes were larger and extended into the estuaries along the South Atlantic Bight. These plots indicate how the inundation along the U.S. southeast coastline would have varied if Matthew occurred at a different time.

To understand the changes in flooding at specific locations along the coastline, the maximum water levels during Matthew and the two scenarios above were plotted along the U.S. Atlantic coast (Figure 2.14). Near Trident Pier, Florida, where the surge occurred during a falling stage in the tidal cycle during Matthew, all scenarios caused increased flooding, especially the +6.21 hr simulation, which produced an increase of about 0.7 m. Near Fort Pulaski, Georgia, where maximum inundation was observed during Matthew, the surge coincided with a lower high tide. If the storm had been delayed by 12.42 hr, then the surge peak would have coincided with a higher high tide, thus further increasing the peak by about 0.20 m. Near Wrightsville Beach, North Carolina, where the surge occurred during a rising stage of the tide cycle, the peak would have increased by about 0.20 m if the surge had occurred 3.11 hr later. Thus for a shore-parallel storm like Matthew that interacted with tides over a large extent of the coastline, timing can significantly influence the flooding at locations along the coast.

2.6.3 Forward Speed

The impact of a hurricane's forward speed on coastal flooding has been recognized previously ((Jelesnianski, 1972; Peng et al., 2004; Peng et al., 2006; Rego et al., 2009; N. J. Berg, 2013)) and has been shown to have significant effects on peak surge heights and inundation volumes. Slower storms are generally considered to be more dangerous as they have considerably more time to impact the coastal waters and thus cause more flooding. Matthew had a forward speed of about 5 m/s as it passed North Carolina. In three scenario simulations, the forward speeds were 50% slower, 50% faster and 100% faster, which represent storm speeds of about 2.5 m/s, 7.5 m/s and 10 m/s, respectively, in North Carolina. These speeds are representative of the historical record (Blanton et al., 2008b). Tides were disabled in these simulations, in order to quantify the sole effect of forward speed on surge along this coastline.

The differences in maximum water levels between these scenarios and the base Matthew simulation (Figure 2.15) demonstrate how the flooding is affected by the forward speed of the storm. The 50% slower simulation had a decrease in flooding along the open coast. However, with more time to push water into inland areas, the slower storm caused an increase in flooding in the rivers (0.2 to 0.4 m in the St. Johns River, Florida, and Alligator River, North Carolina) and sounds (0.1 to 0.4 m in Pamlico Sound) along

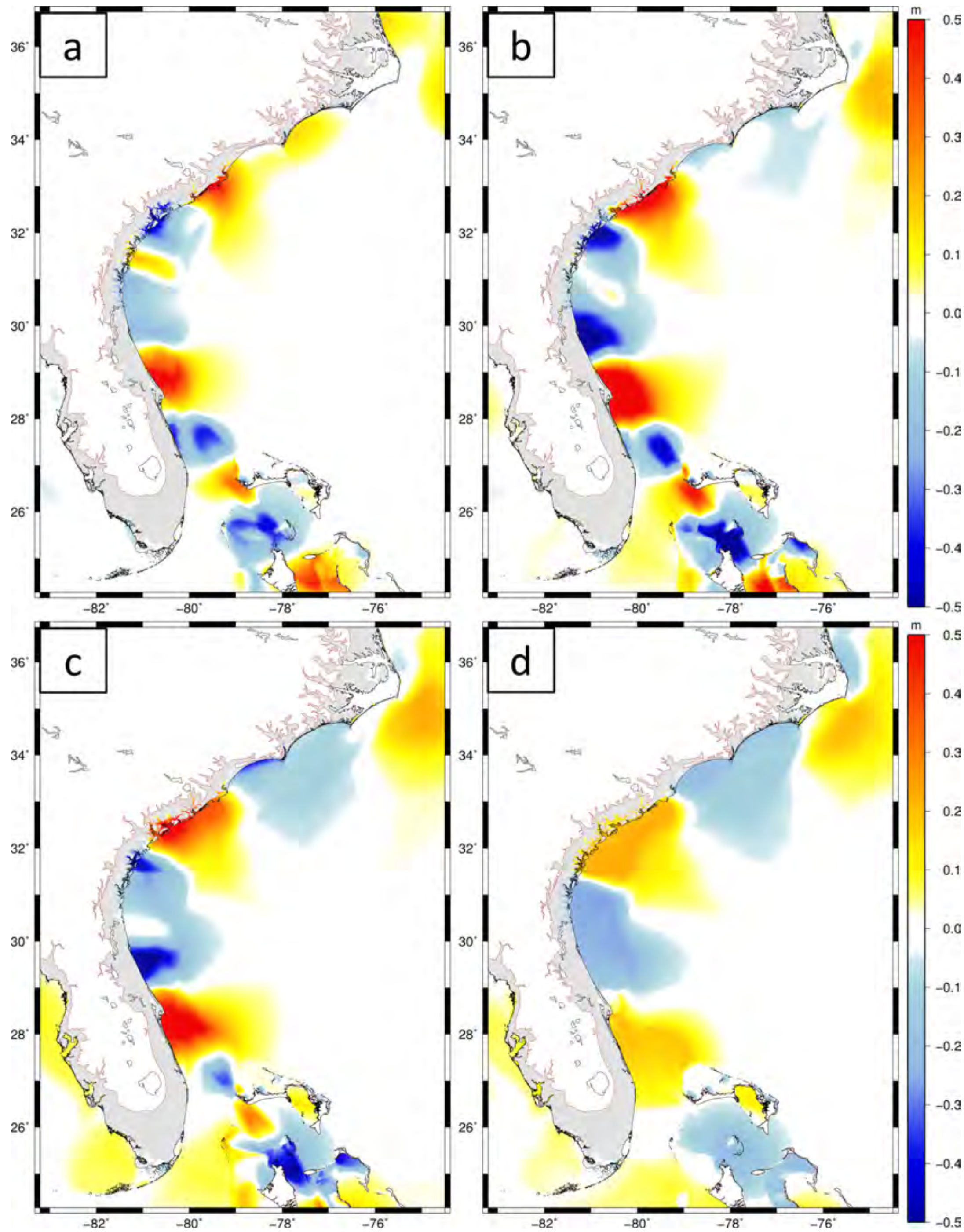

Figure 2.13 Change in maximum water levels on delaying the storm by: (a) 3.11 hr; (b) 6.21 hr; (c) 9.32 hr; and (d) 12.42 hr. OWI was used as the source of wind forcing for all these simulations. The coastline is shown in black and the mesh boundary in brown.

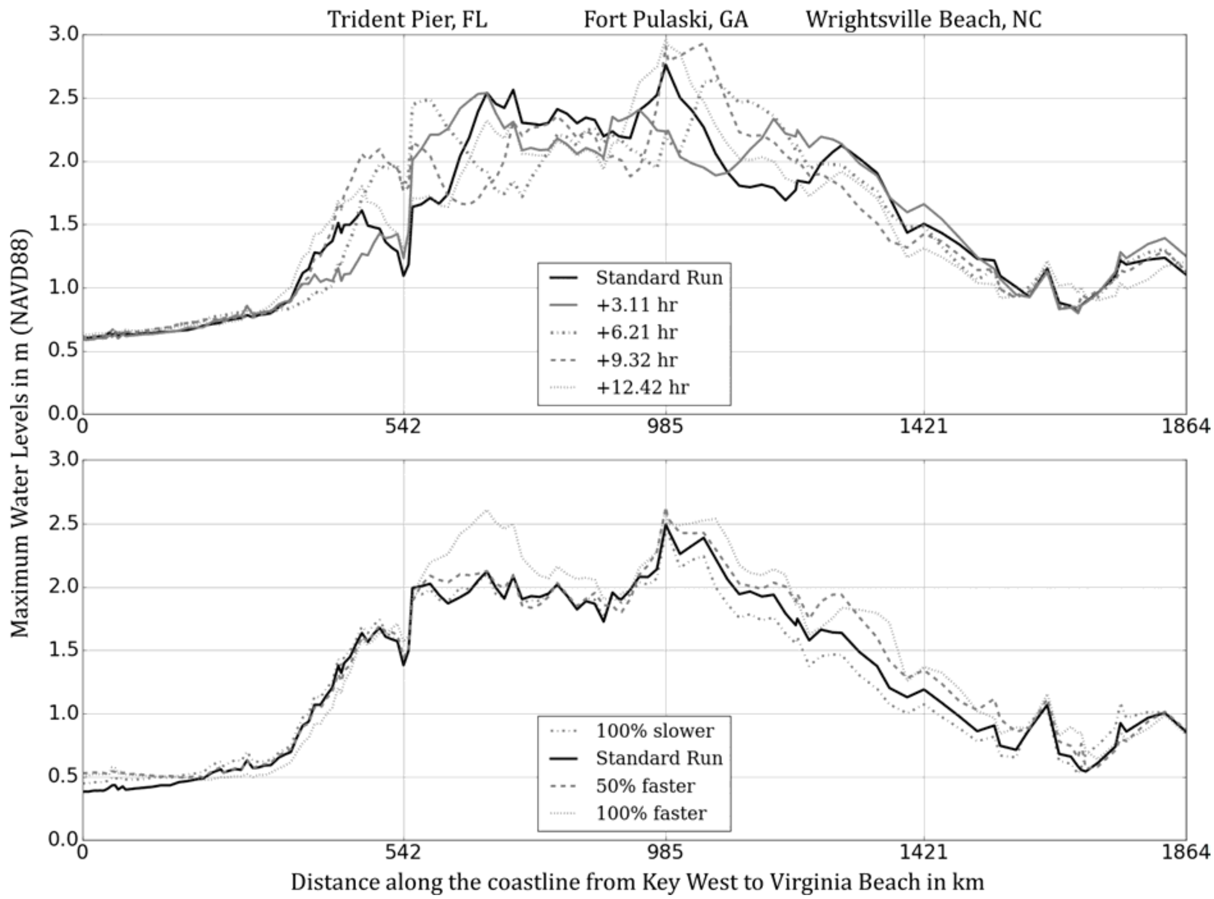

Figure 2.14 Variation in maximum water levels along the coastline on altering the storm timing (top) and forward speed (bottom). Water levels during the standard Matthew run are indicated by black solid lines and those from perturbations are shown using grey color with line types (solid, dashed, dotted or dashed-dotted) as indicated in the figure legends. OWI was used as the source of wind forcing for all these simulations.

the coast. The surge was also higher and pushed further inland in the estuaries and floodplains along the South Atlantic Bight. Near Savannah, Georgia, the water levels increased by about 0.9 m. As the speed of the storm was increased, the trends in water levels were seen to reverse. Water levels were increased on the open coast, but water levels were decreased in the bays and estuaries. The coastline between Daytona Beach and St. Augustine, Florida, had increased flooding of about 0.5 m. Along the coastline of southeast North Carolina, the water levels were also increased by 0.5 m. The increase in water levels along the South Atlantic Bight coastline was lesser and this may be due to the extensive lowlands in the region that absorb more surge. Reduced flooding was observed in the estuaries along the Bight. Near Savannah, Georgia this decrease was as much as 0.7 m.

These trends can be further quantified by examining the maximum water levels along the open coastline (Figure 2.14). The faster simulations produced larger water levels along the coastline as compared to the base Matthew simulation and the 50% slower scenario. About 260 km of coastline had water levels of 2 m or higher during Matthew. The 50% slower scenario caused a 6% decrease in this distance, whereas the 50% faster and 100% faster scenarios caused increases of 57% and 120%, respectively. Thus the faster storms would have pushed water levels of 2 m or higher against a longer stretch of coastline. But the inundation areas followed the opposite trends. Considering only the land regions that became wetted during the storm, Matthew had a total inundation volume of 5.5 km^3. For the 50% slower scenario, this volume was increased by 17%, while for the 50% and 100% faster scenarios, the volumes were decreased by about 6% and 16%, respectively. The faster storms increased the hazard at the open coast, while the slower storms pushed more flooding into overland regions. Thus although slower storms can produce more widespread flooding, faster storms can be dangerous as well, producing higher surges, especially at the coast.

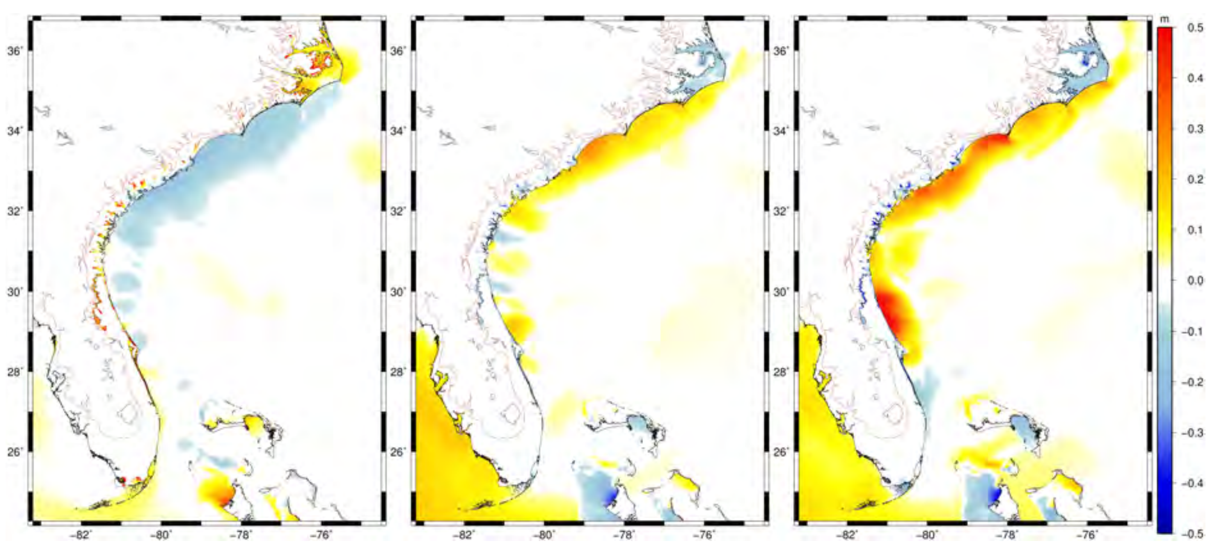

Figure 2.15 Change in maximum water levels on changing the forward speed of the storm: (left) decreasing by 50%, (center) increasing by 50%, and (right) increasing by 100%. OWI was used as the source of wind forcing for all these simulations. The coastline is shown in black and the mesh boundary in brown.

Proudman (Proudman, 1953) showed that the largest storm surges occurs when speed of the storm is close to the propagation speed of the long wave ($\sqrt{gh}$). For the 100% faster scenario, the storm forward speeds near the U.S. southeast coast were about 10 to 14 m/s which corresponds to a long wave for depths of 10 to 20 m. These isobaths vary in distances offshore along the U.S. southeast coast, but are within the region where the increased peaks were observed. Although the storm eye moved from south to north along the U.S. Atlantic coast, its anticlockwise winds caused the dominant direction of water velocities to be from north to south, with the coastline on its right side. Thus it is plausible that a faster storm would energize a shelf wave.

Increasing the forward speed of the storm caused an increase in peak water levels along the coastline but a decrease in overall volume of inundation. Regarding peak water levels, these results agree with Jelesnianski (Jelesnianski, 1972) and Rego (Rego et al., 2009), whereas they contradict Peng (Peng et al., 2004) and Berg (N. J. Berg, 2013). A slower storm causes lesser flooding on the open coast but pushes more water into the estuaries and bays. It also results in a larger total volume of inundation (Rego et al., 2009; Peng et al., 2004; Peng et al., 2006). However, none of these studies looked at shore-parallel storm effects on a large extent of complex shoreline. Although Matthew had varying effects along the southeast U.S. coastline from Florida through North Carolina, the maximum water levels and overland flooding would have changed as expected if the storm's forward speed had been faster.

2.7 Conclusions

Matthew caused devastating floods, strong winds, and moderate storm surge along the southeast coast of the United States, and made landfall as a Category-2 hurricane along the central South Carolina coast during early October 2016. From east-central Florida to North Carolina, the storm moved slowly along a shore-parallel track and causing widespread impacts that lasted for several days. The SWAN+ADCIRC modeling system was used to perform high-resolution modeling of water levels during the storm, and predictions were validated using the extensive network of observations throughout the region. Scenarios then quantified the effects of storm timing and forward speed on the surge and inundation. Our findings can be summarized as follows:

1. *Observation-based wind fields like WF and OWI provide better meteorological forc-*

ing for hindcasting, as compared to parametric models like GAHM. This is evident from their lower values of E_{RMS} and B_{MN} for both surface pressure deficits and wind speeds. OWI had the lowest error metrics, thus making it the most accurate wind and pressure fields during Matthew.

2. *SWAN+ADCIRC represents well the effects of Matthew along the U.S. Atlantic coast, even when applied on the relatively-coarse HSOFS mesh.* The model results using OWI forcing showed good agreement to observations for water levels and HWMs. Water level comparisons at 241 locations on the U.S. southeast coast resulted in an overall E_{RMS} of less than 30 cm and a B_{MN} very close to zero. There was also good correlation between modeled and measured peak water levels. For a total of 622 HWMs, the R^2 value was 0.78 and the slope of the best-fit line was 0.96. These values are comparable to results from studies using meshes with much higher resolution.

3. *The nonlinear interactions between tides and surge on the southeast U.S. Atlantic coast during Matthew had a constructive effect on the total water levels during a low or falling tide and a destructive effect during a high or rising tide.* This study is the first to consider these interactions for a long coastline during a shore-parallel storm. The magnitudes of these interactions varied at different regions with respect to the coast, with small values on the ocean side and large values on the estuary side. In the estuaries, these interactions were larger than 1 m, larger than in previous studies.

4. *Altering the timing of the storm caused locations along the coast to have increased or decreased water levels depending on how the storm coincided with various stages in the tidal cycle.* This is especially true for shore-parallel storms that travel along a large extent of the coastline over several tidal cycles.

5. *The storm's forward speed also had large effects on water levels.* This study is the first to consider these interactions for a long coastline during a shore-parallel storm. Slower storms with more time to impact the coastal waters cause more flooding in the bays and estuaries, and lesser values on the open coast. Faster storms moving quickly across the coastline cause high surges on the open coast, especially along straight coastlines and lower surges in the bays and estuaries.

Although this study is specific to Hurricane Matthew, it demonstrates the importance of considering the nonlinear tide-surge interactions in flood risk studies. It also shows that storm timing and forward speed can be two crucial factors that can significantly alter the surge during a hurricane.

Chapter 3

Benefits of a Higher-Resolution Mesh for Inland Flood Predictions

3.1 Overview

The prediction of storm surge and flooding will require models with high resolution of coastal regions, to describe the fine-scale bathymetric and topographic variations, natural and man-made channels, flow features and barriers. In the previous chapter, it was shown that the storm surge and flooding during Hurricane Matthew (2016) can be predicted with a model of the U.S. southeast coast. However, this model (specifically the HSOFS mesh) is relatively coarse, with a minimum mesh spacing of about 500 m, and thus it does not represent fully the surge propagation into inland regions.

In this chapter, we develop and validate a mesh with detailed coverage of floodplains on the U.S. southeast coast. This mesh will then be used in later chapters for a coarse-grain mesh adaptivity, by including the floodplains only when they will be affected by the storm.

The high-resolution mesh will be created from existing component meshes, which have been developed by FEMA and are well-validated for flood risk mapping. First, we share details about the different component meshes, including their coverage, resolution, and data sources. Then we discuss the process of mesh development, including decisions made in merging the individual meshes and creating a single nodal attribute file for the entire mesh. Finally, we evaluate the performance of the mesh by validating it for two storms that impacted the U.S. southeast coast.

3.2 Motivation

There has always been a delicate balance between resolution and efficiency in coastal ocean models that use unstructured meshes. Finite elements and unstructured meshes has been used in the field of ocean modeling as early as the 1970s and 1980s (Fix, 1975; Lynch et al., 1979; Platzman, 1981; Provost et al., 1986). Subsequent works dealt mainly with diagnostic models (P. G. Myers et al., 1995; Nechaev et al., 2003) and models based upon shallow water systems (Iskandarani et al., 1995; Lynch et al., 1987). Models that employ three-dimensional, hydrostatic (Lynch et al., 1996; Danilov et al., 2004) and non-hydrostatic (Labeur et al., 2005) dynamics were later developed. Some examples of ocean circulation models using unstructured meshes include ADvanced CIRCulation (ADCIRC) (Luettich et al., 1992), Finite Volume Community Ocean Model (FVCOM) (Chen et al., 2003), Stanford Unstructured Nonhydrostatic Terrain-following Adaptive Navier–Stokes Simulator (SUNTANS) (Fringer et al., 2006), Eulerian-Lagrangian CIRCulation (ELCIRC) (Y. Zhang et al., 2004), Second-generation Louvain-la-Neuve Ice-ocean Model (SLIM) (White et al., 2008), Semi-Implicit Eulerian–Lagrangian Finite Element (SELFE) (Y. Zhang et al., 2008) and Semi-implicit Cross-scale Hydroscience Integrated System Model (SCHISM) (Y. Zhang et al., 2016).

The use of unstructured meshes in ocean models allows for various advantages. Firstly, the spurious stresses on model boundary currents caused by the staircase representation of bathymetry and coastlines in structured meshes is avoided (Adcroft et al., 1998). Although it is possible to build structured meshes based on boundary fitted coordinate systems, these models work only for regional simulations (Dupont et al., 2004). Secondly, the use of an unstructured mesh on the sphere may remove pole and coordinate singularity problems (Williamson, 2007). Thirdly, the unstructured meshes enable the use of greater resolution in the direction normal to the coastline than tangentially. This is exactly what is required to resolve boundary layers, e.g. the western boundary layers (Haidvogel et al., 1999) or surface/bottom Ekman layers. Finally, unstructured meshes help in locally refining relatively small topological and dynamical features while maintaining coarser resolution elsewhere in a large domain, thereby cutting down computational costs (Danilov, 2013).

Higher levels of resolution are required in ocean circulation models to represent steep gradients in bathymetry like the continental shelf break (Westerink et al., 1992; Luettich et al., 1995; Blain et al., 1998; Hagen et al., 2000), represent wave propagation in shallow water regions (Hagen et al., 2001), and represent complex topography in overland regions (Westerink et al., 2008). Recent, state-of-the-art meshes contain millions of triangular elements with sizes ranging from 4 to 6 km in the deeper ocean, 500 to 1000 m on the continental shelf, 200 m within the coastal floodplains, and downward to 10 to 20 m within the fine-scale natural and man-made channels and barriers (e.g., (Dietrich et al., 2011a; Hope et al., 2013; Roberts et al., 2019)).

However, the resolution can vary between meshes, depending on their purposes. The HSOFS unstructured mesh (as described in Chapter 2), was developed for tide and surge predictions for the entire U.S. coast from Texas to Maine. To reduce its computational coast, the average resolution along the shoreline was limited to about 500 m, which is lesser than what is provided in meshes for specific regions. For example, a high-resolution mesh for the North Carolina region is the NC9 mesh, which was developed as a part of the FEMA Flood Mapping Study that involved running hundreds of simulations for hypothetical storms (Blanton et al., 2008a). It has sufficient resolution to properly represent the inlets on the North Carolina barrier islands, the back barrier sounds and the U.S. Intercoastal Waterway that runs north-south through the North Carolina sounds. The resolution in the HSOFS and NC9 meshes for the North Carolina region is compared in Figure 3.1. The HSOFS mesh has a fairly uniform spacing of about 500 m, whereas the NC9 mesh has a much higher resolution to represent finer features like dune crests, inlets, rivers and floodplains. In regions like the Oregon Inlet, the element spacing goes smaller than 50 m to represent the finer channels that drive flow into the Pamlico Sound.

Higher resolution of coastal features has been shown to improve the model representation of the underlying physical processes. In the South Atlantic Bight, the extensive Estuarine/Tidal Inlet Complex (ETIC) is highly dissipative and affects the regional energy balance for the semidiurnal tides (Blanton et al., 2004). Simulations of shelf tides with varying geometries indicated the inclusion of the ETIC to improve model skill and increase the tidal amplitude 5 to 10 % well out onto the shelf. Recently (Bacopoulos et al., 2017), the local and regional influence of the inter-tidal zones of the South Atlantic Bight on tidal propagation were studied using a four-mesh scheme including/excluding well-defined geophysical features like marsh, Atlantic Intercoastal Waterway and inlets/fully wetted estuarine zones. The estuarine and intertidal definition of the South Atlantic Bight coastline was found to modify the mode of tidal propagation, and associated reso-

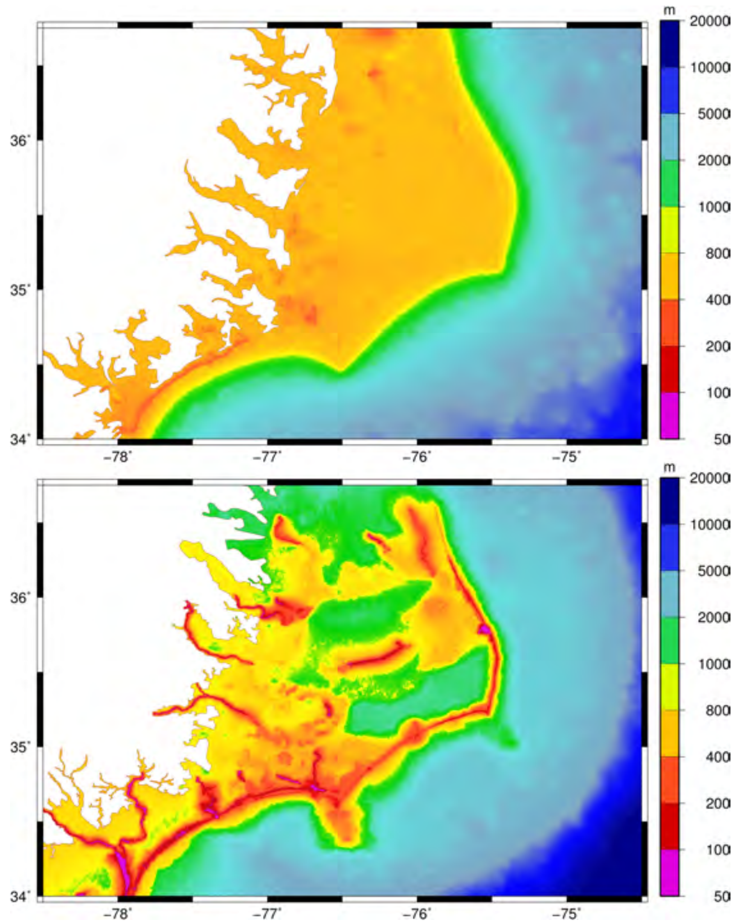

Figure 3.1 Resolution (m) in the North Carolina in the HSOFS (top) and NC9 (bottom) meshes.

nant properties, over the continental shelf. The tidal inlets and estuarine rivers positively impacted the M_2 resonance because of extended effective shelf width, and the floodplains and marshes negatively impacted the M_2 tidal circulation because of bottom friction and energy dissipation.

These studies demonstrate the necessity of a complete geometric and dynamic description of the domain/physics, which is only possible through the use of a high-resolution model. In the following subsections, we further motivate the requirement of adequate resolution in ADCIRC, via three examples.

3.2.1 Idealized Channel Test Case

Coastal regions often contain complex geometries, steep bathymetric gradients, small-scale islands and channels, etc., which require high levels of resolution. An idealized channel test case is used here to examine the influence of model resolution on flow in a channel. In this problem, tides are allowed to propagate from an ocean boundary in the south to a mainland boundary in the north, through a channel that runs along the center of the domain. How far the tides can propagate to the north boundary will depend on the channel representation in the model.

A scatter dataset at a resolution of 10 m provided the ground surface for the meshes in this study. In this dataset, the channel has a width of 10 km at the open ocean boundary in the south (y = 0), decreases to 800 m in width as it goes up to the coastline (y = 7.5 km) and to 150 m at the mainland boundary on the north (y = 11 km). Two meshes at varying levels of resolution are created using the Surface-water Modelling System (SMS) software (Figure 3.2). The first mesh has 64,415 vertices, with a resolution varying from 80 m at the ocean boundary to 20 m at the top boundary. This spacing is adequate to represent the channel throughout the domain. The second mesh has 2,755 vertices at a larger spacing of about 200 m everywhere. The coarser resolution has a poor representation of the channel bathymetry especially above the coastline.

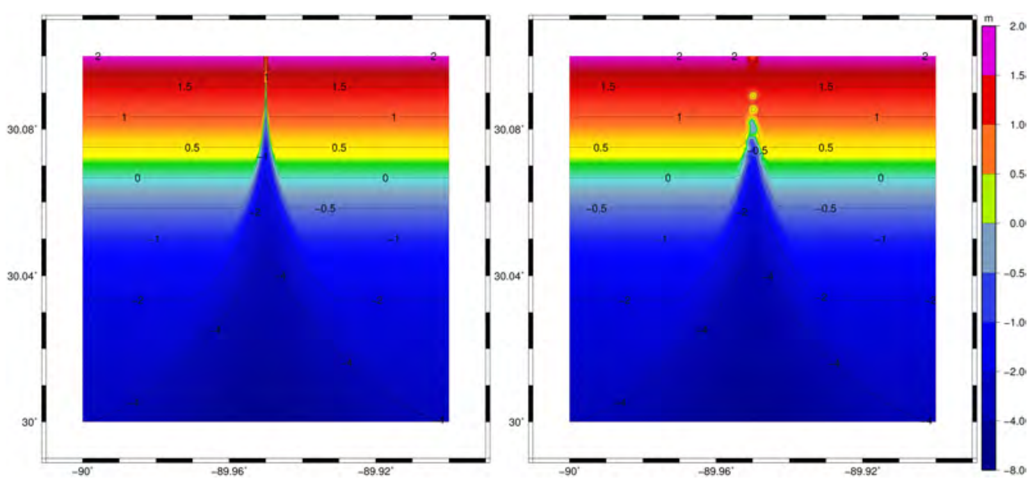

Figure 3.2 Differences in bathymetry and topography (m) between the higher resolution (left) and the coarser resolution (right) meshes used in the idealized channel test case. Blue contours indicate bathymetry and the zero contour represents the coastline.

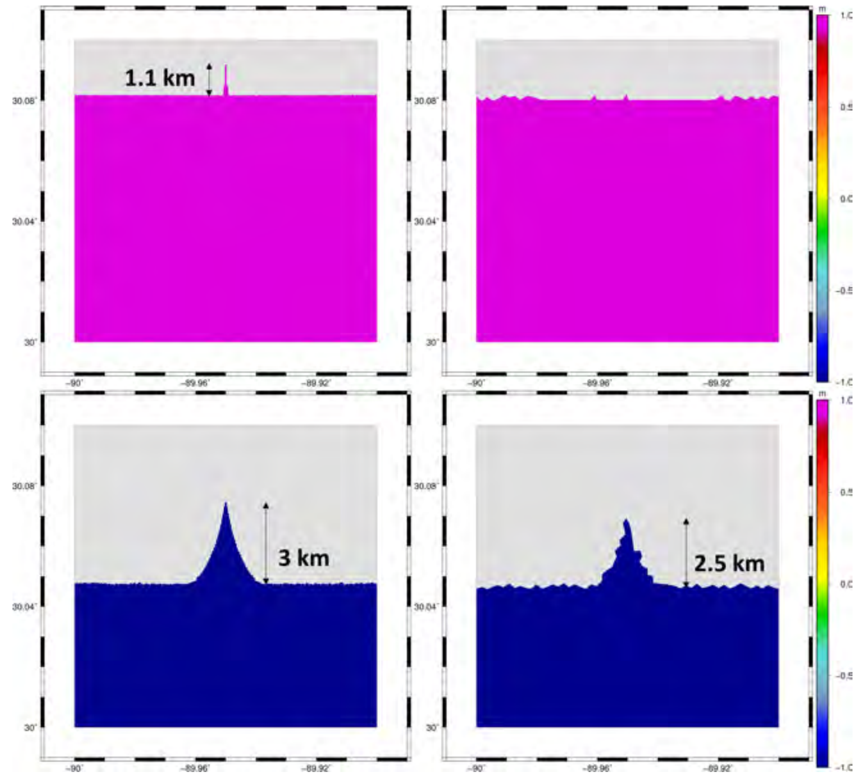

Figure 3.3 Water levels (m) in the two meshes. Columns correspond to: (left) finer and (right) coarser meshes. Rows correspond to water levels at the (top) peak flood stage and (bottom) peak ebb stage of the tides.

A diurnal tidal signal with a single constituent of amplitude 1 m is forced at the bottom ocean boundary. The other three boundaries are closed, with flow allowed to slip tangentially along the boundary but not allowed to flow across. Both meshes are forced for a total of 4 days. As the simulation proceeds, water floods and recedes in the channel, depending on the stage in the tidal cycle. At 21 hr into the simulation, the channel is at its peak flood stage (Figure 3.3, top). The higher-resolution mesh permits the flow to extend farther into the channel by more than a kilometer. Six hours later at the peak ebb stage (Figure 3.3, bottom), the higher-resolution mesh still has increased flooding. By virtue of its better channel description, the flow into the channel exceeds that in the low resolution mesh by about half a kilometer.

The simulations on the higher- and lower-resolution meshes take a total of 4 min and 1 min respectively, both running on 95 computational cores. Although the run-time is larger for the fine-resolution mesh, it clearly captures the flow along the channel better, on account of its added resolution. These differences in flooding can be crucial during forecasting and thus motivate the need for high-resolution models.

3.2.2 Hindcasts of Hurricane Matthew

As described in Chapter 2, hindcasts of Hurricane Matthew were simulated on the HSOFS mesh due to its widespread coverage along the storm's track. Although the overall error statistics were good, there were locations (especially inland) where the predictions were unsatisfactory. These can be attributed to the coarser resolution of the HSOFS mesh as compared to other region-specific meshes. Thus even with a high-resolution raster, features will be poorly represented upon interpolation of topography and bathymetry onto the mesh. For example, a channel represented at 10 m resolution in the raster, will not be properly represented in the model if its element spacing at that location is 100 m.

Along the Savannah River on the Georgia-South Carolina Border, there are numerous locations (Figure 3.4) where the HSOFS storm tide predictions (Figure 3.5) did not match well with observations. This is attributed to the poor representation of bathymetry on account of the coarser resolution in the mesh. For example, station 1 occurs in the Wilmington River where the channel is 150 m wide, but the element spacing in this region in the HSOFS mesh is 500 m. The channel is therefore not represented in the mesh, and the model remains dry throughout the simulation (Figure 3.5 top-left). At other locations, peak flooding is captured (not accurately) by the model, but the tidal cycles are not. At stations 4, 5 and 6 located in the 75 to 100 m wide Little Black River, the spacing in the mesh is 350 to 400 m. This coarser spacing again prevents representation of the finer features necessary to propagate tides in to these locations.

3.2.3 Forecasting during Hurricane Florence

The ADCIRC Surge Guidance System (ASGS) provides forecast guidance for winds, waves and storm surge during a hurricane. For the North Carolina coast, ADCIRC is run twice daily during normal conditions and four times daily during severe storms. When a storm is far from the North Carolina coast, simulations are run using the HSOFS mesh due to its extensive coverage along the U.S. coastline. Once the track is more certain and the storm approaches the NC coast, the guidance system switches over to the NC9 mesh due to its higher resolution in the region. This approach was used during Matthew in

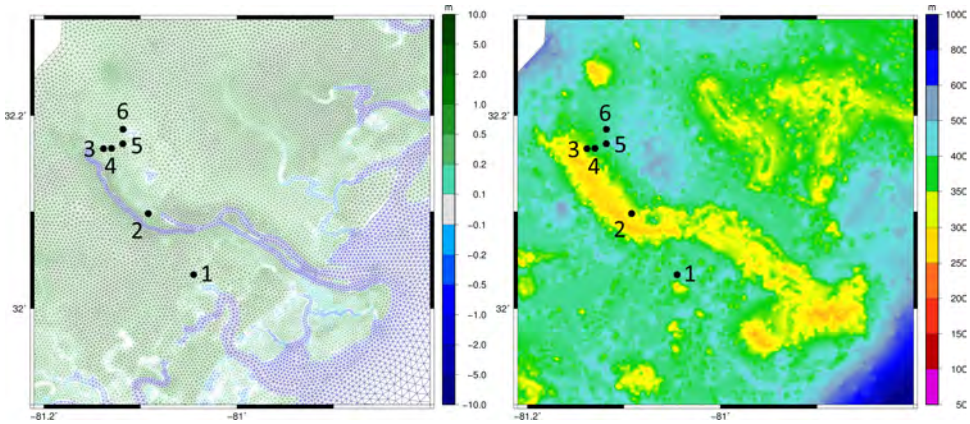

Figure 3.4 Bathy-topo (left) and resolution (right) in metres, along the Savannah River in the HSOFS mesh. The points indicate locations where time series of water levels are shown in Figure 3.5.

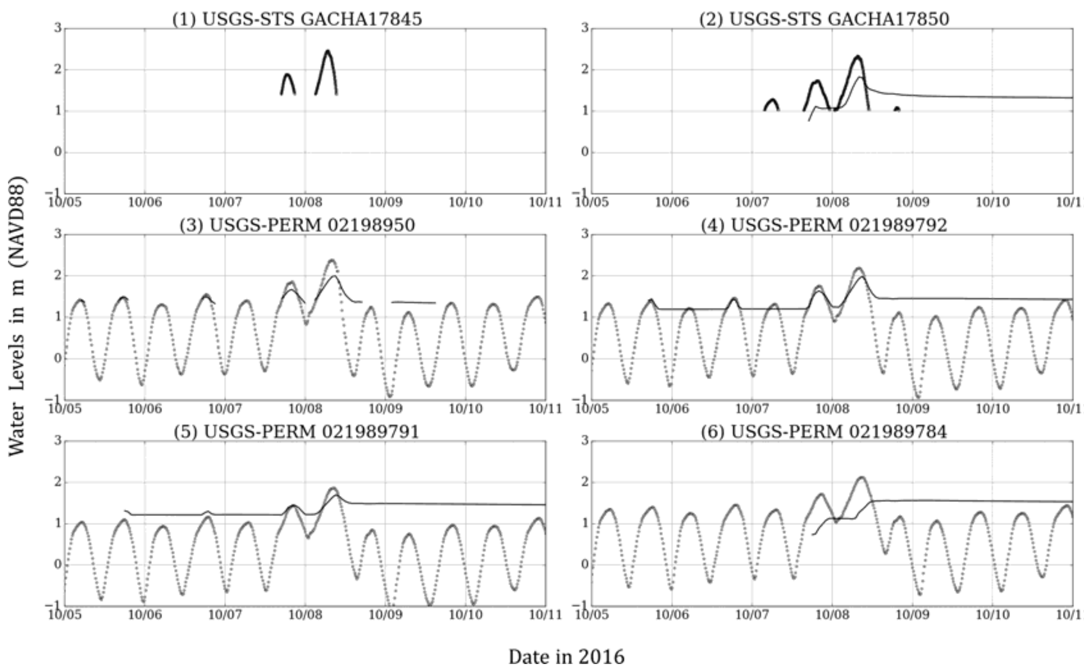

Figure 3.5 Time series of water levels (m relative to NAVD88) at 6 locations shown in Figure 3.4. Observed values are shown with gray circles, and predicted values using black lines.

2016. When the eye of the storm was away from the NC coast (until Advisory 41), the HSOFS mesh was used for the forecasts. As the storm-eye approached the NC border (starting from Advisory 42), the NC9 mesh was employed.

Florence was a powerful Category 4 hurricane that caused severe damage in the Carolinas and made landfall as a Category 1 hurricane in Wrightsville Beach, North Carolina, on 14 September 2018. Contrary to Matthew which had a shore-parallel track, Florence had a shore-normal track. Starting from Advisory 52 (0900 UTC 12 September), when the eye of the storm was located in the Atlantic and the storm track was directed toward Myrtle Beach, South Carolina, the ASGS ran simulations on both the HSOFS and NC9 meshes. On 2100 UTC 13 September, as the storm eye approached the NC9 coastline, Advisory 58 predicted the storm center to move near Wilmington, North Carolina.

The predicted maximum water levels varied between predictions on the HSOFS and NC9 meshes for the North Carolina region (Figure 3.6). Warmer and cooler colors indicate larger flooding in the HSOFS and NC9 meshes, respectively. The HSOFS mesh predicts higher water levels along the Outer Banks, away from the storm track. Increased water levels are also seen inside the Neuse and Pamlico Rivers that empty into the Pamlico Sound. The NC9 mesh has higher water levels in the New River and along the Outer Banks close to the storm track, and in the Albemarle and Currituck Sounds away from the storm. Inside the Pamlico Sound, the differences are close to zero. Although there are differences in the physics settings between these two simulations, majority of these variations in the predicted water levels are caused by the difference in mesh geometry.

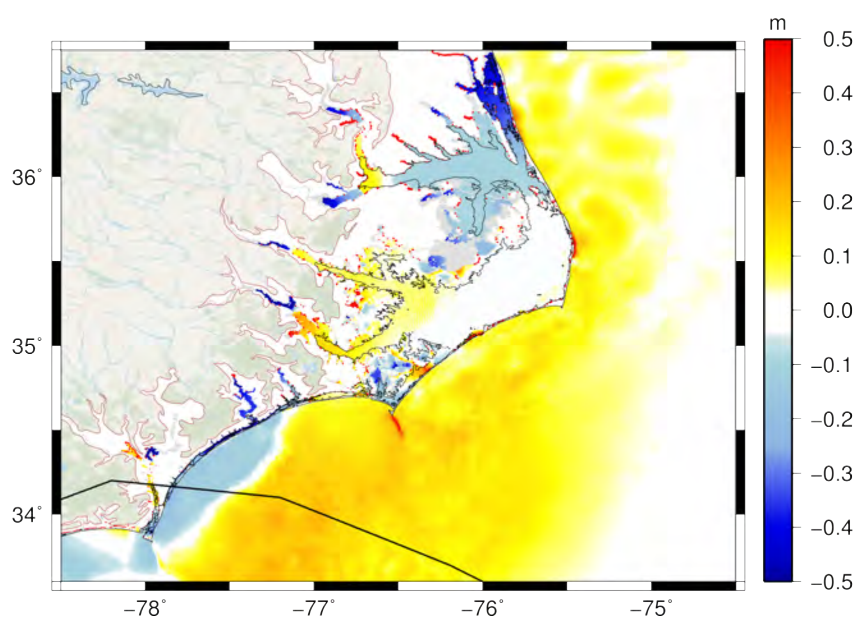

Figure 3.6 Difference in maximum water levels (m) between the HSOFS and NC9 meshes corresponding to the 58th advisory. The hurricane track is shown in black.

Close to the hurricane track, the maximum water levels varied along the coastline extent between the Cape Fear River and New River, for both the NC9 and HSOFS meshes (Figure 3.7). The higher resolution in the NC9 mesh allows ADCIRC to push more water into the rivers, and the flooding extends further into the river branches. The higher-resolution mesh also predicts over-topping of the dunes along the Outer Banks leading to higher water levels in the bays. These differences in water levels can be crucial, as these predictions aid emergency managers in taking necessary precautions during a hurricane. The model results are also used between storms for design and to establish insurance rates for local homeowners.

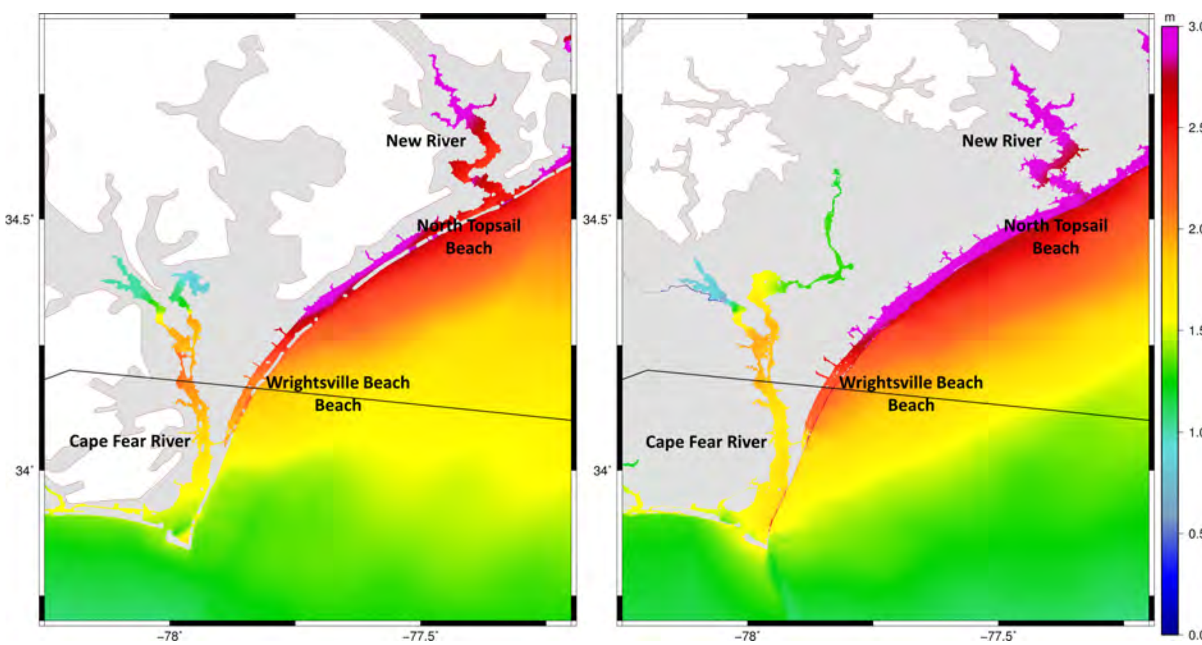

Figure 3.7 Maximum water levels (m) predicted using the HSOFS (left) and NC9 (right) meshes, corresponding to the 58th advisory. The hurricane track is shown in black.

Thus, a higher resolution mesh can represent finer features affecting the flow behavior, and thereby improve the accuracy of flooding predictions. Moreover, running Matthew for 9 days on the HSOFS mesh on the Stampede2 computing cluster at the Texas Advanced Computing Center, on a total of 532 cores (including 10 writer cores) takes only 57 min. While this shorter run time is an advantage for forecasting applications, the multi-resolution approach described in Chapters 4 and 5, will require a much higher simulation time to highlight its gain in performance. A high-resolution mesh with detailed description of the floodplains from FL to NC is therefore developed with the aim of providing a significant improvement in accuracy, as well a much larger run-time.

3.3 Component Meshes

The goal is to create a single mesh with high resolution of floodplains along the U.S. southeast coast from FL to NC. This will be done by merging five FEMA regional meshes: North Carolina (NC), South Carolina (SC), Georgia and Northeast Florida (GANEFL), East Coast Central Florida (ECCFL), and South Florida (SFL), on to an open-water mesh. These high-resolution meshes were developed originally for flood risk mapping for the next generation of Flood Insurance Rate Maps (FIRMs). Each regional mesh was used for simulations of hundreds of historical and synthetic storms, and thus each mesh has been tested extensively for predictions of coastal flooding (Blanton et al., 2008a; United Research Services, 2009; Bender, 2013; Bender, 2014; Bender, 2015). The details of the individual meshes are given herein.

3.3.1 North Carolina (NC)

The high-resolution mesh for North Carolina is the NC9 mesh. This mesh was built by appending a high-resolution mesh of the NC region to a previously-developed mesh (Blanton et al., 2004) of the western North Atlantic, the Gulf of Mexico and the Caribbean Sea. In NC, the mesh extends inland to the 15 m topographic contour to allow for storm surge flooding. In this region, the mesh has been designed to describe bathymetric and topographic features such as inlets, dunes and rivers as identifiable on satellite images, NOAA charts, and numerous DEMs and shoreline datasets (Blanton et al., 2008a). There is enough resolution to realistically represent the inlets through the NC barrier islands, the back barrier sounds and the Atlantic Intracoastal Waterway that runs north-south through the NC sounds. The version 9.99 of this mesh has 624,782 vertices and 1,234,231 elements. More than 90 percent of this resolution is applied within coastal NC.

Larger element sizes of 50 to 100 km occur in the Gulf of Mexico and open Atlantic, but the elements decrease in size as the bathymetry transitions to near-shore conditions (Figure 3.8). Mesh spacing along the NC coastline varies from 3 to 4 km on the continental shelf to about 100 m near the Outer Banks (Figure 3.1). Resolution in Pamlico

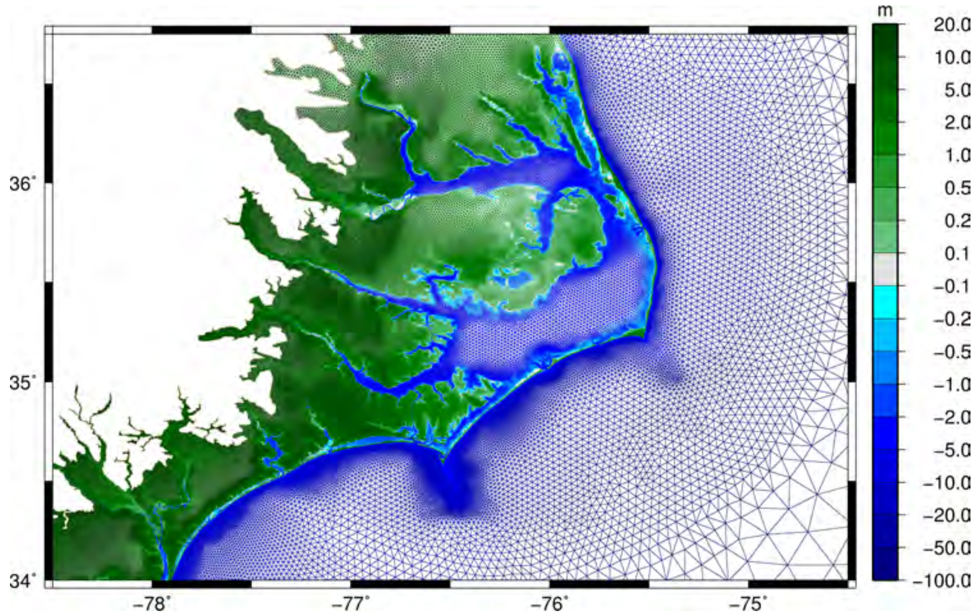

Figure 3.8 Bathymetry and topography (m) in the NC9 mesh.

and Albemarle Sounds varies from 1500 to 1800 m in the deeper regions to 100 to 300 m at the entrance of the rivers and shallower regions bordering the sounds (Cyriac et al., 2018). The resolution goes below 50 m in the narrow river channels that extend inland from the sounds and elsewhere along the NC coastline. This mesh has been optimized to maximize resolution throughout NC while minimizing the total computational cost by minimizing the number of vertices (Blanton et al., 2010).

3.3.2 South Carolina (SC)

The SC mesh was built by combining a higher resolution mesh of the SC coastal zone with a coarser large-domain model of the the Western North Atlantic (Westerink et al., 1993; Scheffner et al., 2001). Within SC, the mesh extends inland to about the 9 m topographic contour, which extends beyond the inundation level of the 0.2-percent annual-chance (500-year return period) still-water elevation (Figure 3.9, top)(United Research Services, 2009). Where LiDAR data were not available to interpolate bathymetry and topography, the model incorporated the best available data from USGS, NOAA, and sources with the state of South Carolina. It has 542,809 vertices and 1,073,925 elements.

The high-resolution portion of the mesh consists of approximately 440,000 vertices

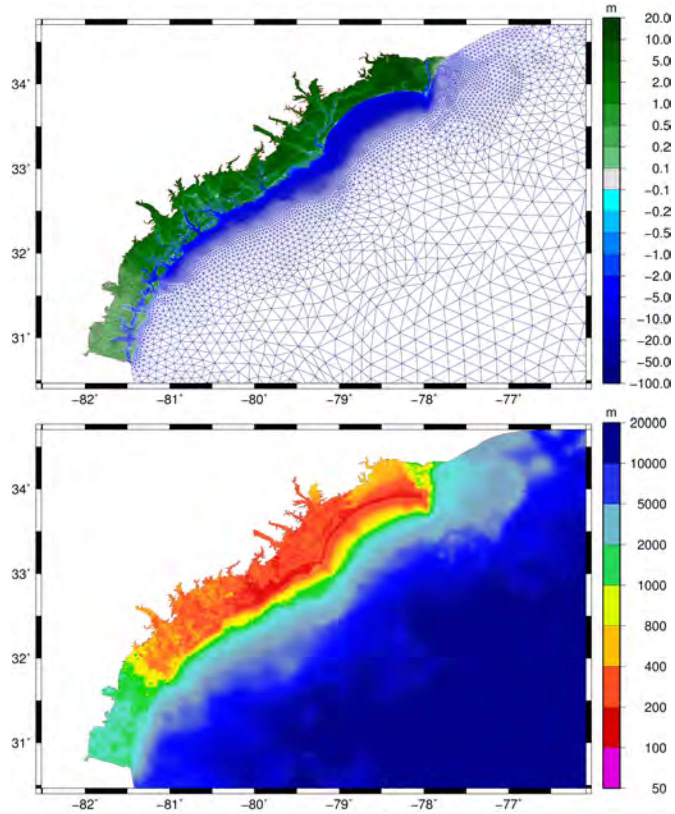

Figure 3.9 Bathymetry and topography in m (top), and resolution in m (bottom) in the SC mesh.

with a minimum resolution of 100 m (Water Environment Consultants, 2016). The mesh covers the coast of SC and extends approximately 50 km north and south beyond the SC borders into NC and GA. The resolution varies from 2 to 3 km on the continental shelf to 100 m along the coast including regions like the Charleston Harbor (Figure 3.9, bottom). Like in the NC mesh, higher resolution (element spacing below 100 m) is provided to properly describe smaller channels that originate from the sounds and inlets. The element spacing increases from the SC coasts, with a resolution of 200 to 500 m along the SC-GA border to 3000 m at the GA-FL border. The SC mesh has the coarsest coastal resolution among all the component meshes.

3.3.3 Georgia and Northeast Florida (GANEFL)

The Georgia and Northeast Florida (GANEFL) mesh was developed by combining a high-resolution mesh of the region with the coarser EC2001 mesh (Mukai et al., 2002) covering the Gulf of Mexico, Caribbean Sea and Western North Atlantic Ocean. The mesh extends into the 12.2 m topographic contour line to conservatively account for inundation by extreme storms, and covers the entire GA coast and FL counties north of Brevard (Figure 3.10, left). The mesh further extends 50 km northward into SC and 145 km south of the Volusia-Brevard county line in FL. The elevation data came from a variety of sources including inshore bathymetry from University of Florida, LiDAR data for Georgia and Florida coastlines, USGS DEMs, NOAA bathymetric data, and field reconnaissance data from 142 locations (Bender, 2013). The version 12 of this mesh has 2,968,735 vertices and 5,910,443 elements. About 90 percent of the vertices lie in the GANEFL region (Naimaster et al., 2013). The mesh has an element spacing of 50 to 100 m along the coastline, with the spacing going down as a low as 25 to 30 m in the smaller channels (Figure 3.10, right). Element sizes of 80 to 200 m extend 4.8 km offshore, with a 4 km resolution at the eastern shelf edge.

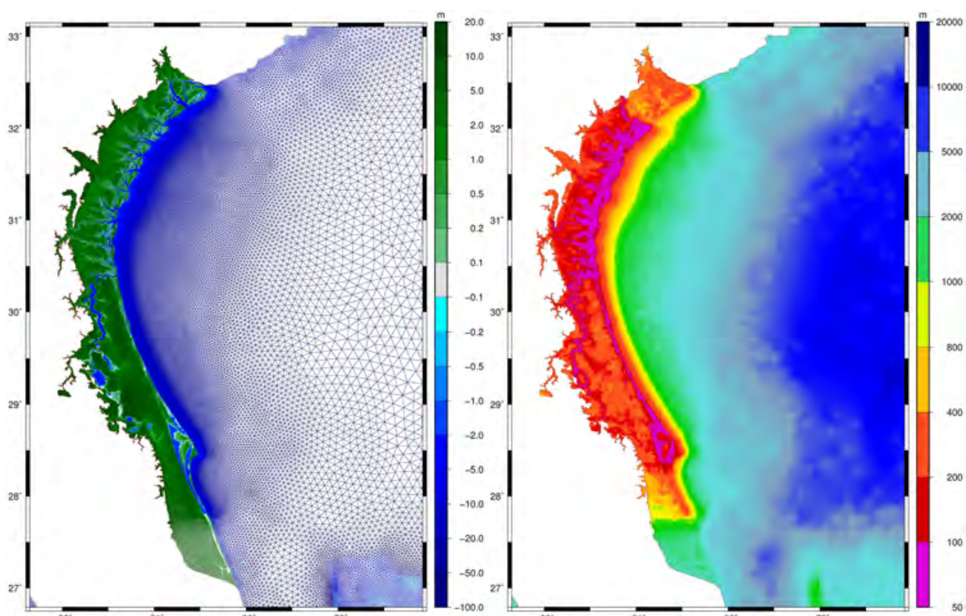

Figure 3.10 Bathymetry and topography in m (left), and resolution in m (right) in the GANEFL mesh.

3.3.4 East Coast Central Florida (ECCFL)

The East Coast Central Florida (ECCFL) mesh was developed with a goal to determine the revised Base Flood Elevations (BFEs) and flood inundation boundaries for 1 percent annual flood total water levels, and also update the coastal Flood Insurance Study (FIS) and FIRM Panels (Federal Emergency Management Agency, 2012). The relatively coarse resolution of the EC2001 mesh, which covers the U.S. Atlantic coast, Caribbean, and Gulf of Mexico, provided a reasonable mesh for regions away from the study area. The ECCFL mesh covers the counties from Brevard to Martin in Central Florida (Figure 3.11, left). The version 6 of this mesh has 1,406,543 vertices and 2,793,387 elements. The resolution varies from 30 to 50 m in the more complex terrain and developed areas, to 80 to 200 m nearshore, and to 1 to 5 km at the offshore boundary (Figure 3.11, right). Like in the GANEFL mesh, a resolution of 80 to 200 m extends 4.8 km offshore, with an element spacing of 4 km at the eastern shelf edge (BakerAECOM, 2013).

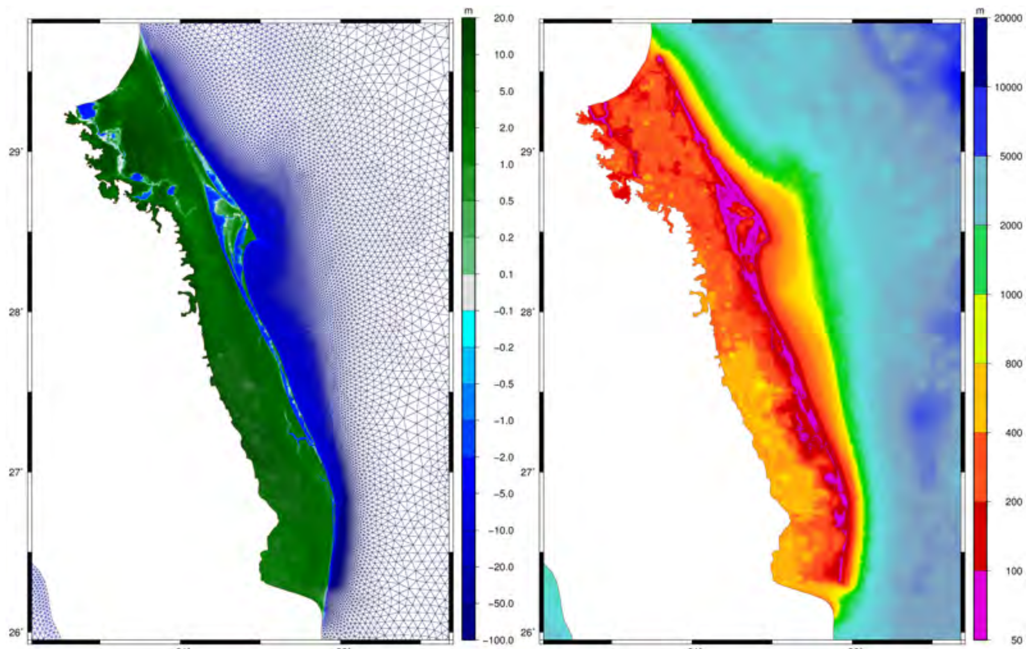

Figure 3.11 Bathymetry and topography in m (left), and resolution in m (right) in the ECCFL mesh.

3.3.5 South Florida (SFL)

The South Florida (SFL) mesh was developed as part of the South Florida Storm Surge Study (SFLSSS) (BakerAECOM, 2016) by FEMA. The mesh covers the FL counties from Monroe to Palm Beach (Figure 3.12, left). The bathymetric data came from various sources including USACE, St. Johns River Water Management District (SJRWMD), NOS, NOAA, etc (Bender, 2015). The version 11 of this mesh has 2,249,093 vertices and 4,480,230 elements. Because the FIRMs rely on modeled water levels, the highly populated areas of Palm Beach County and Broward County were given an element spacing of 60 to 150 m. The resolution is the highest among the five component FEMA meshes with an element spacing of approximately 75 m along the Atlantic coastline and throughout the Florida Keys. The resolution goes down to 10 to 25 m to describe the complex canal systems in Broward County, FL. Along the unpopulated Gulf of Mexico coastline in mainland Monroe County, the resolution averages 150 m. In the far inland regions of the mesh that will not realistically experience coastal flooding, including northeastern portions of Everglades National Park, an element spacing of 300 m was provided.

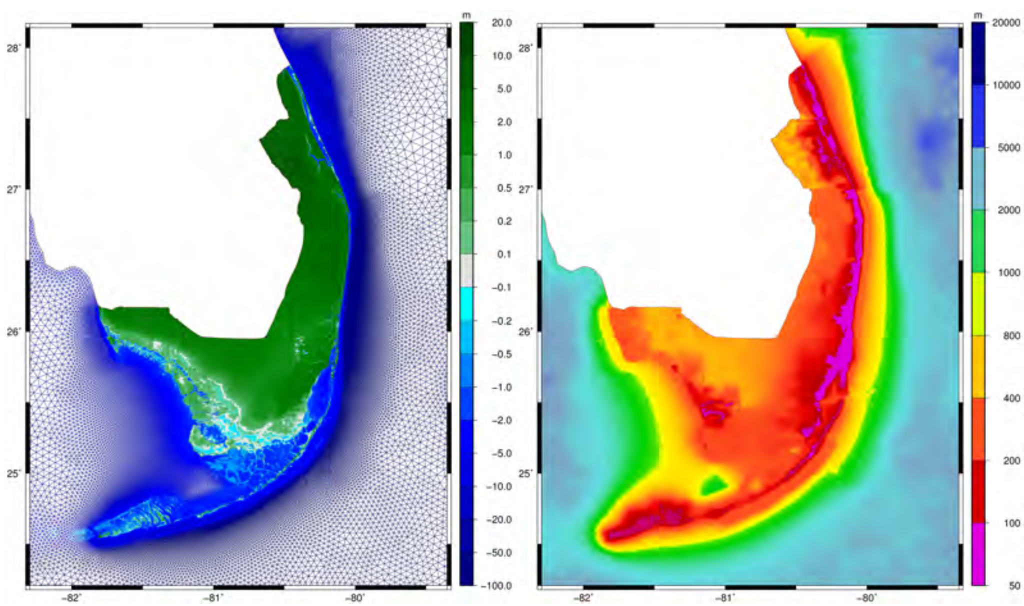

Figure 3.12 Bathymetry and topography in m (left), and resolution in m (right) in the SFL mesh.

3.3.6 Open-Water Mesh

The purpose of using high-resolution component meshes is to have a very clear description of regions where the well-validated HSOFS mesh does not have sufficient coverage. This includes inland areas with finer features like floodplains, smaller channels, levees, etc. It is therefore okay for the high-resolution meshes to have coarser element spacing in the offshore regions. This will also help in reducing the number of elements, which in-turn helps in cutting down simulation time. For this purpose, an open-water mesh was developed by removing floodplains from the HSOFS mesh, using the EC2001 mesh (Mukai et al., 2002) boundary and maximum water levels from a 30-day tidal run as guidelines. This mesh mostly has its boundary along the coastline but also includes large water-bodies like the Galveston and Trinity Bay in Texas, Lake Pontchartrain and Chandeleur Sound in Louisiana, Mobile Bay in Alabama, Tampa Bay in Florida, Ossabaw Sound in Georgia, Bulls Bay in South Carolina and Pamlico Sound in North Carolina. It has 616,113 nodes, which is about one-third the total size of the HSOFS mesh.

The mesh was tested with 5 storms (Harvey, Irma, Isaac, Matthew, and Sandy), each impacting different regions of the U.S. east and GoM coasts. The maximum of the maximum water levels from each storm, along with their respective tracks are shown in Figure 3.13. A qualitative analysis of results using open-water gauge measurements revealed the ability of this mesh to capture well the water levels at the open coastline. This mesh will therefore be used to merge with high-resolution meshes, to cut down their resolution in open water.

3.4 Mesh Development

As mentioned earlier, the idea is to use the five FEMA component meshes to describe the floodplains from FL to NC at high resolution, and to use the coarser open-water mesh for other regions of the model domain. We denote the new, combined mesh as FEMA-SAB. This section describes the decisions made while merging the component meshes, and how the FEMA-SAB mesh compares to the coarser HSOFS mesh from Chapter 2.

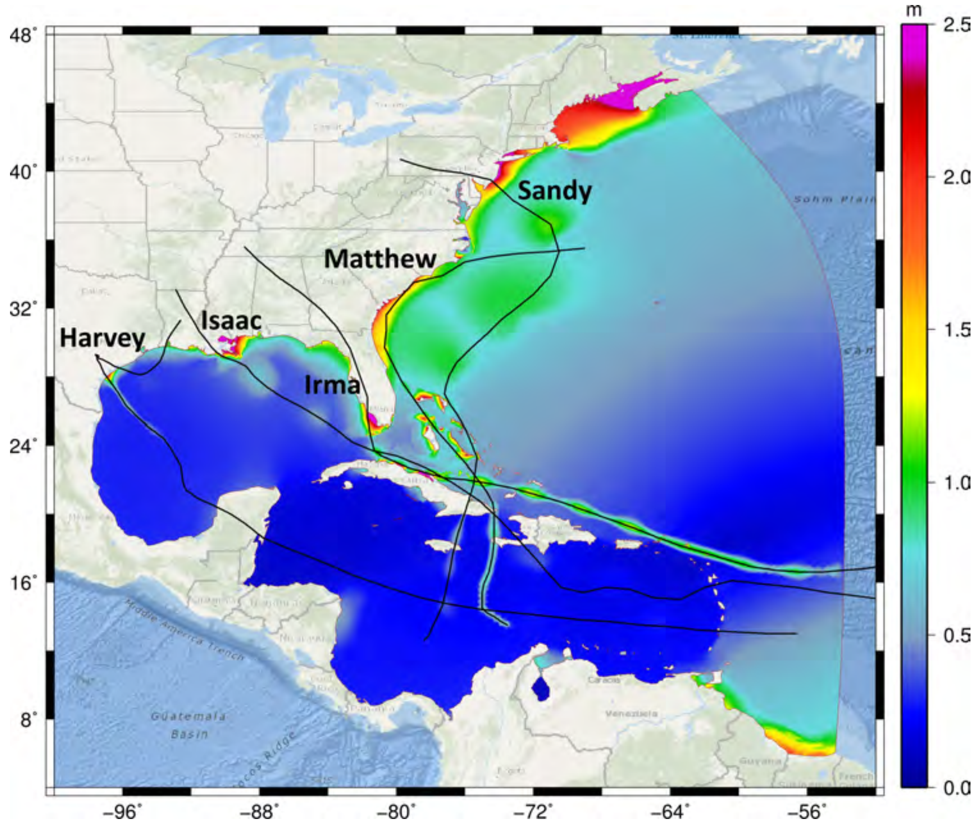

Figure 3.13 Maximum of the maximum water levels (m) from each storm simulation. The hurricane tracks are shown in black and the mesh-boundary in brown.

3.4.1 Datum Conversion

The FEMA component meshes have their topography and bathymetry referenced to the North American Vertical Datum of 1988 (NAVD88), whereas the HSOFS mesh and hence the open-water mesh have data referenced to Mean Sea Level (MSL). It was therefore important to have all the component meshes referenced to the same datum, before starting the merging process. This was done by doing a MSL to NAVD88 conversion on the open-water mesh. Normally this conversion process would be done using NOAA's VDatum tool (National Oceanic and Atmospheric Administration, 2018b), but it uses a translation grid with several key areas missing, including Pamlico Sound and Indian River Inlet. Therefore, a HSOFS conversion grid (Riverside Technology et al., 2015) with nodal elevations equal to MSL-to-NAVD88 conversion values, was used for this purpose. Once in NAVD88, the open-water mesh was merged with the five FEMA component meshes. Thus, the FEMA-SAB mesh has its nodal elevations referenced to NAVD88.

3.4.2 Reducing Total Number of Nodes

The FEMA regional meshes were created with a goal of accommodating the anticipated area of inundation resulting from extreme storm events relevant to each study area. For example, the GANEFL mesh has its inland boundary at the 12.2 m topographic contour. But for our study, this is unnecessary as the maximum inundation from the storms that we are going to run on the FEMA-SAB mesh (Matthew and Florence) will not exceed 5 m even from a conservative point of view. It is therefore important to remove all vertices with elevations greater than this value, as the extra vertices can increase the simulation time substantially. For example, for the GANEFL mesh, a total of 349,375 vertices were removed that had elevations over 5 m. The difference in the mesh boundary after cutting these vertices is shown in Figure 3.14. These vertices are not only located close to the inland boundary, but also close to the coastline. A similar reduction of mesh size was done for all the regional FEMA meshes.

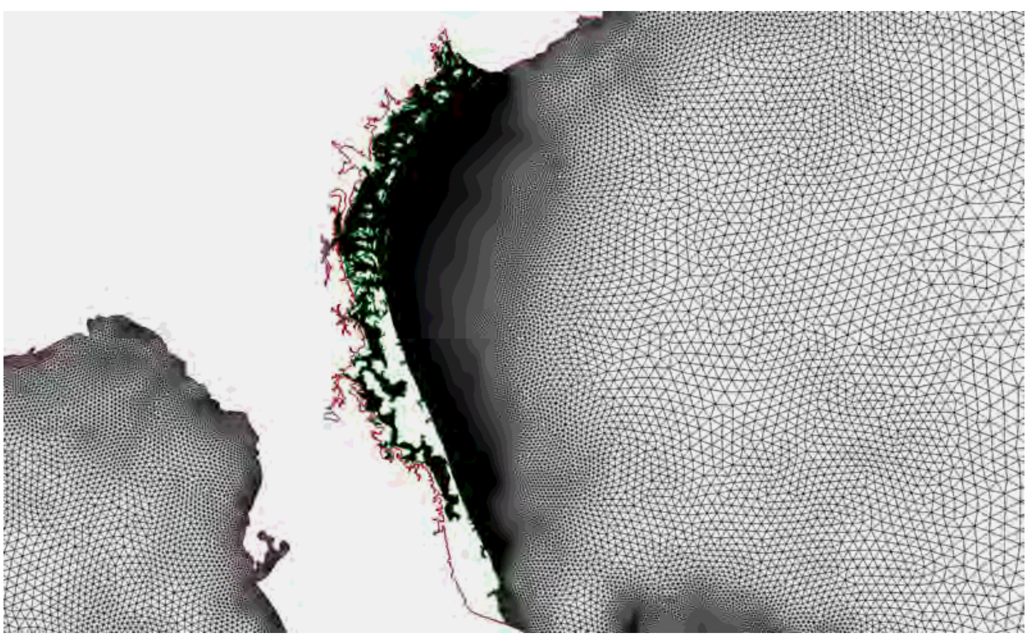

Figure 3.14 Difference in the GANEFL mesh-boundary after removing vertices with elevations over 5 m. The boundaries before and after the cut down is shown in brown and green, respectively.

3.4.3 Merging Component Meshes

Before combining the different component meshes to form the FEMA-SAB mesh, decisions were made regarding: (a) where the FEMA regional meshes merge on to the open-water mesh, (b) what to do at overlapping boundaries between regional FEMA meshes, (c) how to deal with resolution differences at merging boundaries, etc. These questions are answered here by explaining the process of merging the SFL mesh on to the open-water mesh as an example (Figure 3.15).

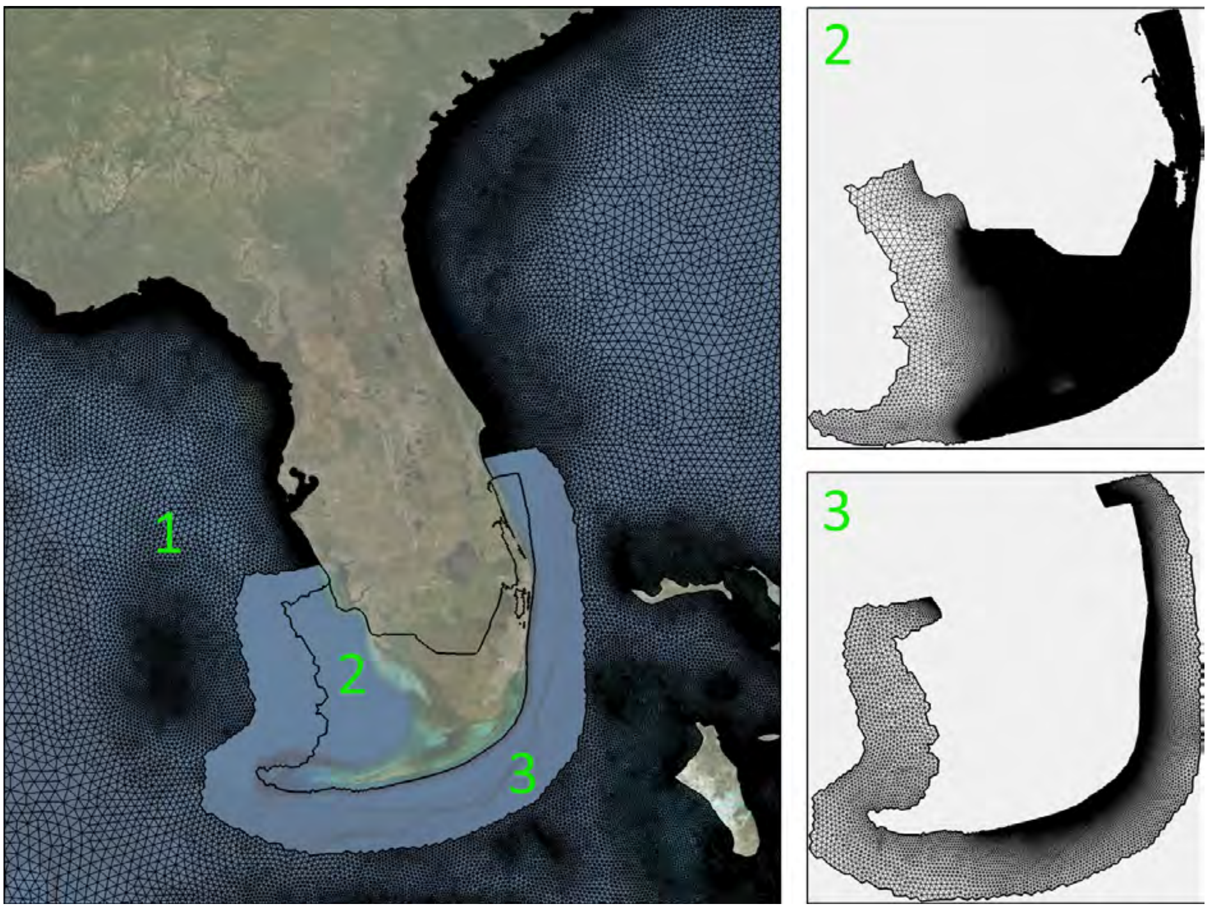

Figure 3.15 Merging the SFL and open-water meshes: (1) the open water mesh without the buffer and SFL regional mesh, (2) the SFL regional mesh cut at the 30 m bathymetric contour, and (3) the buffer mesh used to provide a smooth transition in element spacing between 1 and 2. The elements and boundaries are shown using black triangles and lines respectively.

The regional meshes are merged into the open-water mesh at the 30 m bathymetric contour. This is done to prevent any misalignment in bathymetric and topographic features between the regional and open-water mesh, close to the coastline. Improper nodal elevations can lead to model instabilities especially at locations where the topography and bathymetry changes rapidly, like at the shoreline. Moreover, the differences in bathymetry between meshes due to differences in resolution, usually occur inland near complex features like floodplains and small channels. By extending the regional mesh to the 30 m contour, any possible bathymetric variations are moved into deeper waters. Although an extension to further offshore would be better, this would add a lot of vertices from the regional mesh, thus increasing simulation times. Thus, choosing the 30 m contour for merging allows not to lose any bathymetric details from the regional mesh while taking as many elements as possible from the coarser open-water mesh. The first step in merging the SFL and open-water mesh was thus cutting the SFL mesh at the 30 m contour (Figure 3.15, 2).

At the inter-mesh boundaries, the regional mesh with better representation of the topography and bathymetry was used. To deal with differences in resolution at the inter-mesh boundaries, and at the boundary between the regional and open-water mesh, a buffer mesh was created that allows a smooth transition in element spacing. The width of this buffer zone thus depends on the resolution differences between the regional meshes and the open-water mesh. The second step was thus cutting the SFL mesh along with a space for buffer, out of the open water mesh (Figure 3.15, panel 1). We denote this mesh as OW-minus-SFL-minus-Buffer mesh. The buffer mesh is then created using the boundaries of the SFL and OW-minus-SFL-minus-Buffer mesh (Figure 3.15, panel 3). It is important that the boundaries of all the three meshes should match perfectly. The bathymetry and topography at nodes in the buffer mesh are interpolated from the regional mesh due to its higher resolution as compared to the open water mesh. The SFL, OW-minus-SFL-minus-Buffer, and Buffer meshes are finally merged together to complete the process. This process was then repeated for the other four regional meshes (ECCFL to NC).

Once all the regional meshes were merged into the open-water mesh, the combined mesh was then tested for possible issues, first using the model check in SMS. This tests for any disjoint or overlapping elements, voids in the mesh, numbering of node-strings, etc. There are also ways to look at mesh quality in terms of maximum slope, element area change, minimum and maximum interior angle, etc. Once the combined mesh passed all the model checks in SMS, it was then pushed through the MeshChecker application (ADCIRC, 2020a), which looks for errors in ADCIRC meshes including overlapping nodes/elements, boundary conditions, grid size, numbering, etc. Quality assurance and control were also performed by conducting a visual comparison between the elevations represented in the mesh and that in the original meshes using SMS.

3.4.4 FEMA-SAB Mesh and Comparison to HSOFS Mesh

The FEMA-SAB mesh was created with an aim of providing detailed coverage of the floodplains from FL to NC (Figure 3.16). It has a total of $5,584,241$ vertices and $11,066,018$ elements. Thus, it is roughly three times the size of the HSOFS mesh. This is because the HSOFS mesh was developed to provide widespread coverage of floodplains all along the entire U.S. coast, and thus its average coastal resolution was limited to 500 m. On the other hand, the FEMA-SAB has an element spacing of less than 100 m along the southeastern U.S. coastline, except in a few regions along the SC and NC coasts (Figure 3.17). The spacing is even less than 20 m in some of the smaller channels and floodplains.

The advantage of this added resolution in the FEMA-SAB mesh can be highlighted by zooming into three different locations along the U.S. southeast coast, each representing a different type of coastal feature (Figure 3.18). At the Saint Lucie Inlet in FL (Figure 3.18, bottom), the FEMA-SAB mesh has a resolution of 50 to 100 m. The narrow inlet and channels that travel inland from the shoreline are highly resolved to accommodate the large flows that needs to be transferred to the surrounding marshes and bays. The HSOFS mesh has elements at 300 to 500 m resolution, with just one element across the inlet, and in some of the adjoining channels. The bathymetry in this region is also different. The inlet has a width of 500 m in the FEMA-SAB mesh with a depth of 2.7 m at the center of the inlet. The HSOFS mesh has these values at 640 m and 1.3 m respectively. There are also differences in the depth of the back-bay, close to the beginning of the St. Lucie River. The FEMA-SAB mesh has a much deeper channel with a depth of 5.2 m, compared to 2.6 m in the HSOFS mesh.

Moving north, looking upstream of the Savannah River along the GA-SC border (Figure 3.18, center), the FEMA SAB mesh has a clear description of both of main channel, and its tributaries like the Little Back River, Middle River, Wilmington River,

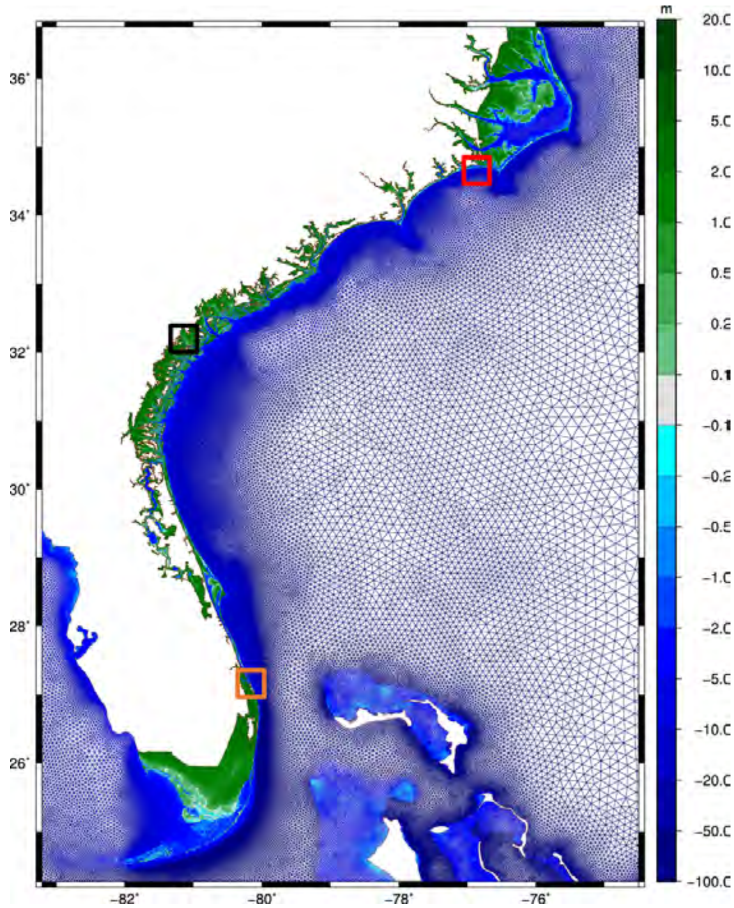

Figure 3.16 FEMA-SAB mesh bathymetry and topography (m relative to NAVD88) contoured on the mesh elements. Colored boxes indicate specific regions as shown in Figure 3.18.

etc. These tributaries are absent in the HSOFS mesh. The HSOFS mesh has the entire river described with just one element across, at a resolution of 350 to 520 m close to the Sound, and 275 m at the point where it ends upstream. The FEMA-SAB mesh has an element spacing of about 55 m at the river-entrance, and extends about 22 km further inland as compared to the main channel in the HSOFS mesh. The resolution at the most upstream location of the main channel is 78 m. This higher resolution in the FEMA-SAB mesh is important in increasing the accuracy for tidal signals, as propagation through narrow conveyances and attenuation plays an important role in capturing tidal dynamics (Kerr et al., 2013).

At a section of the Outer Banks in NC located south of the Bogue Sound (Figure 3.18, bottom), the HSOFS mesh has a higher resolution of 725 m at 13 km offshore,

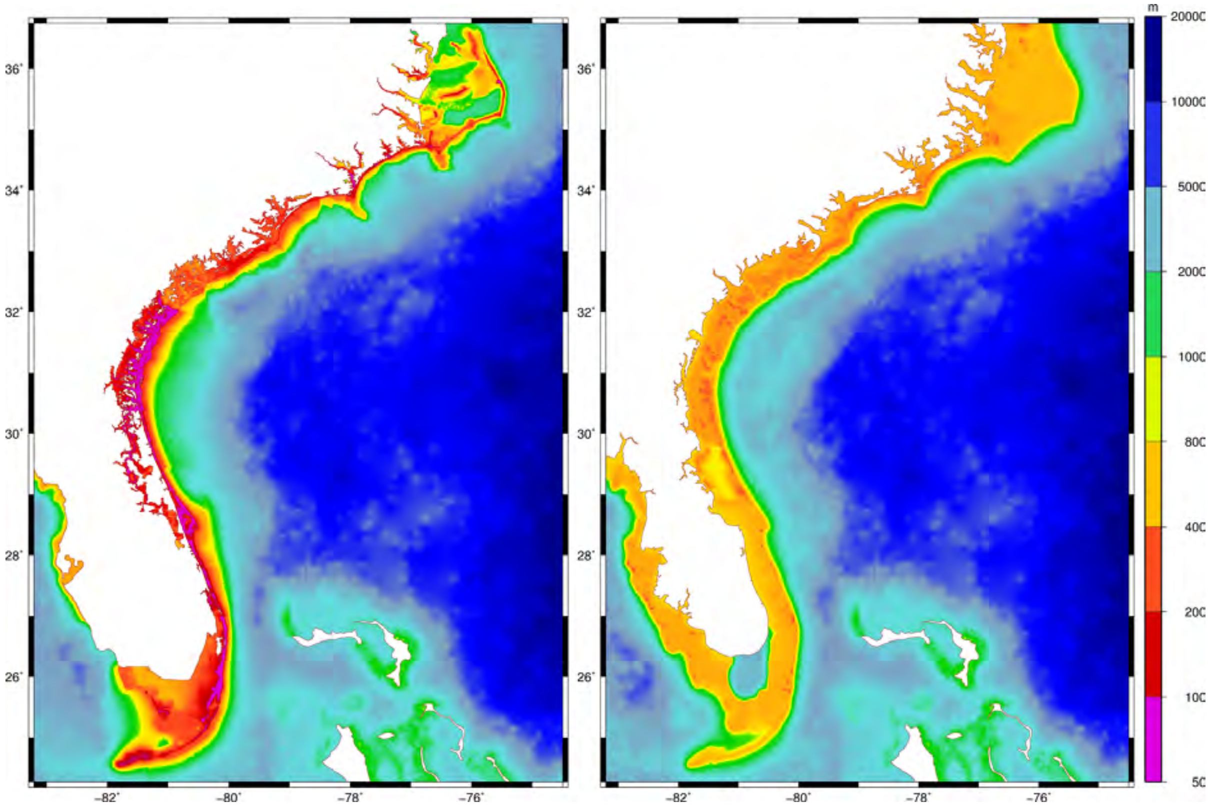

Figure 3.17 Element spacing (m) along the U.S. southeast coast in the (left) FEMA-SAB mesh and (right) HSOFS mesh.

compared to 1.7 km in the FEMA-SAB mesh. But at the coastline, the FEMA-SAB mesh transitions to much smaller elements, with a resolution of 120 m at the coastline, 120 to 165 m in the Outer Banks, and 6 to 170 m in the Bogue Sound. The HSOFS mesh has a uniform spacing of 425 to 450 m from the shoreline to the end of the Sound. It also has just one element across the Outer Banks at a 500 m resolution. There are also differences in the bathymetry and topography values. In the HSOFS mesh, the Bogue sound has a depth of 1.4 m everywhere, whereas the depths in the FEMA-SAB mesh vary from 1.4 m close to the Outer Banks to 4 m near the north boundary of the Sound. The HSOFS mesh also has a higher dune-elevation with value reaching as high as 8.4 m, compared to 6.4 m in the FEMA-SAB mesh.

Thus, although the FEMA-SAB mesh has a large number of vertices as compared to the HSOFS mesh, it does a good job of representing the complex bathymetric and topographic features, both nearshore and inland.

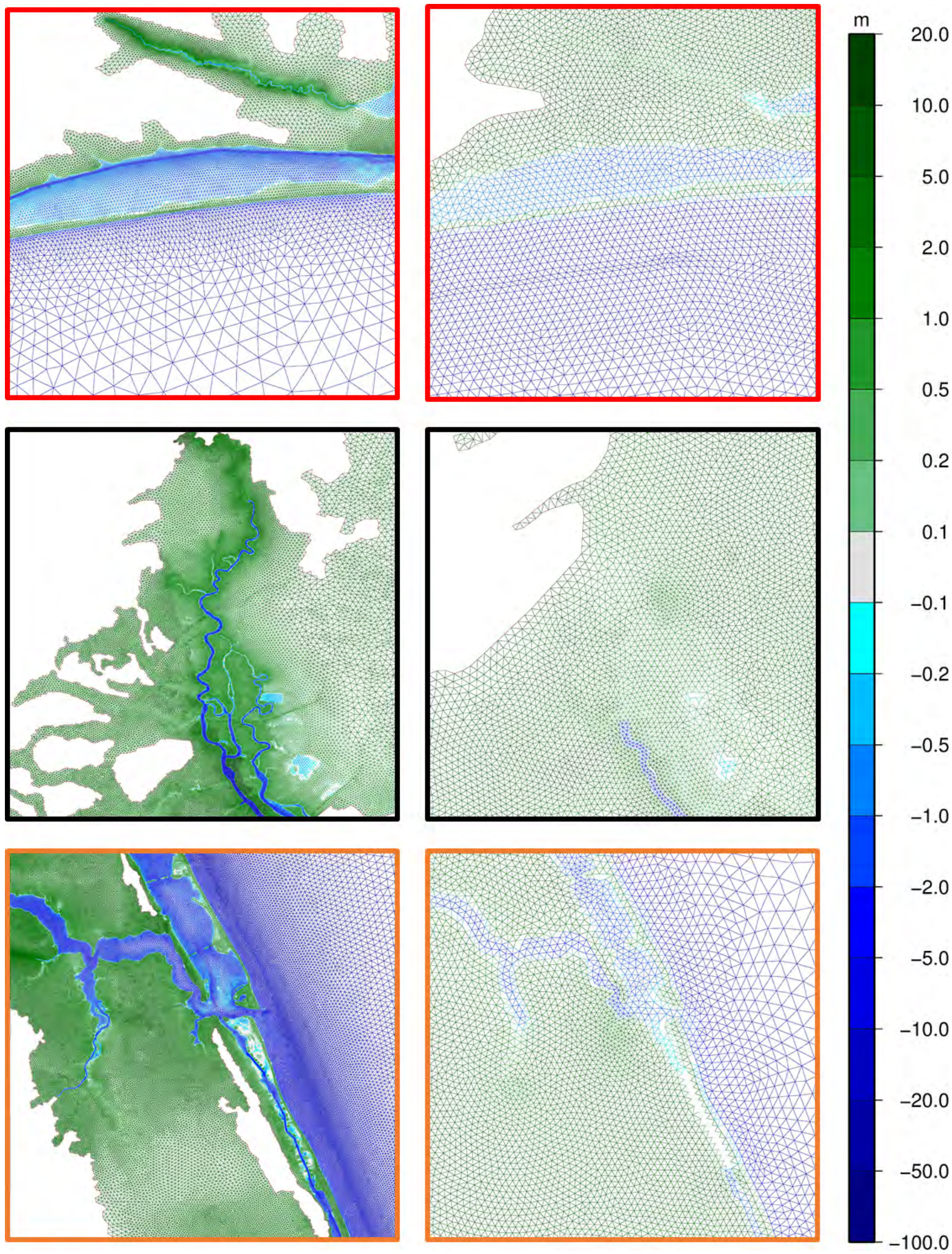

Figure 3.18 Bathymetry and topography (m) contoured on the mesh elements at locations represented by coloured grids in Figure 3.16. Columns correspond to: (left) FEMA-SAB mesh, and (right) HSOFS mesh. Rows correspond to: (top) Saint Lucie Inlet, FL, (center) Upstream Savannah River along the GA-SC border, and (bottom) Outer Banks, NC. The FEMA-SAB mesh bathymetry is relative to NAV888, whereas the HSOFS mesh values are referenced to LMSL).

3.5 Creating Nodal Attribute File

After the FEMA-SAB mesh passed the model checks, it was time to create other files that are required to run an ADCIRC simulation on it. The nodal attribute (`fort.13`) file (ADCIRC, 2020b) contains values of spatially-variable parameters, most of which alter wind and bottom drag using land use data, at each mesh vertex. The following 7 attributes are used for the FEMA-SAB mesh: eddy viscosity, primitive weighting in continuity equation (Tau0), Manning's n at sea floor (ManningsN), surface directional effective roughness length (z0Land), surface canopy coefficient (VCanopy), elemental slope limiter, and advection state. For attributes like eddy viscosity and Tau0, values were defined in classes that were most common among the regional meshes, based on bathymetric depth. For other attributes, values were mapped from the regional meshes wherever possible, or from the HSOFS mesh at locations where that attribute was missing in the corresponding regional mesh. Attributes for elemental slope limiter and advection state were added to stabilize the model.

The first step was creating a dummy `fort.13` with default values for all the attributes. The default values were 10 for eddy viscosity, 0.03 for Tau0, 0.02 for ManningsN, 0 for surface roughness, and 1 for VCanopy. The HSOFS mesh `fort.13` was then used to replace every attribute value in the dummy `fort.13`, everywhere in its extent. This created a fort.13 with HSOFS attribute values everywhere in its domain, and default values outside. The SouthFL mesh was then used to interpolate its attribute values only to vertices that fell in its high-resolution portion of the domain. This step was then repeated for each component FEMA mesh, until all the five FEMA component meshes had transferred their values to their corresponding vertices in the FEMA-SAB mesh `fort.13`. Every step that involved mapping attribute values from one mesh to another was done using FORTRAN, as it proved to be significantly faster than Python for interpolation purposes. Table 3.1 shows the attributes present in the component meshes. A description of all the nodal attributes in the FEMA-SAB mesh `fort.13` is given below.

Table 3.1 Attributes in the nodal attribute files of the various component meshes. The classes for eddy viscosity and Tau0 are also given.

Mesh	Eddy Viscosity	Tau0	ManningsN	z0Land	VCanopy	Geoid-Offset	Start-Dry	Initial river elevation
HSOFS		0.005,0.02,0.03	X	X	X		X	
SFL		0.005,0.02,0.03	X	X	X	X		
ECCFL	10,20	0.02,0.03	X	X	X	X		
GANEFL	5,10,20	0.02,0.03	X	X	X	X		
SC		0.005,0.02,0.03	X	X	X			
NC9	2,10	0.005,0.03	X	X	X			X
FEMA-SAB	20,50	0.005,0.02,0.03	X	X	X			

3.5.1 Horizontal Eddy Viscosity

Horizontal eddy viscosity is a term in the momentum equations to cover the turbulence closure problem, and represents the sub-mesh scale dissipation that was averaged out from the governing equations. This attribute can also be used to increase numerical stability. Eddy viscosity in ADCIRC can be applied in two ways. A spatially constant value can be applied using the ESLM parameter in the `fort.15` file, or a spatially varying eddy viscosity can be used using the nodal attribute file. The ECCFL, GANEFL, and NC9 meshes had spatially varying eddy viscosity with the values defined in classes (Table 3.1) that differed from mesh to mesh. The HSOFS, SFL and NC9 meshes had a constant eddy value of 50 $m^2\ s^{-1}$, 10 $m^2\ s^{-1}$, and 50 $m^2\ s^{-1}$, respectively. In order to have one eddy class for the entire FEMA-SAB mesh, tests were done to find out the most stable class out of the values and classes from the component meshes. An eddy class of 50 $m^2\ s^{-1}$ and 20 $m^2\ s^{-1}$ proved to be the most stable, and therefore was assigned for the entire FEMA-SAB mesh. This classification is based on the 0 m bathymetric contour, with the higher value for inland regions (Figure 3.19).

3.5.2 Primitive Weighting in Continuity Equation

The primitive weighting in continuity equation (Tau0) attribute influences the degree of numerical diffusion in ADCIRC's governing equations. Specifically, it influences the weighting factor that controls the relative contribution of the primitive and wave portions of the Generalized Wave-Continuity Equation (GWCE). This balance is such that a value of 0 is the pure wave equation, and a value greater than 1 behaves like a pure primitive continuity equation. Like eddy viscosity, Tau0 can be either specified in the `fort.15` (both as a flag telling ADCIRC how to operate, or as the actual value of Tau0), or as an attribute in the `fort.13`. For the FEMA-SAB mesh, the -3 flag in `fort.15` was used to vary Tau0 spatially and in time. Based on values in the component meshes (Table 3.1), classes of 0.005 s^{-1}, 0.02 s^{-1} and 0.03 s^{-1} proved to be most stable for the FEMA-SAB mesh. These classes were assigned to vertices based on their depths: 0.005 s^{-1} for depths greater than 10 m, 0.02 s^{-1} for depths of 0 to 10 m, and 0.03 s^{-1} for depths less than 0 m (Figure 3.20). The only exception to this was in South FL, where the 0.03 s^{-1} class had to be extended a little further offshore to improve model stability (like in the component SFL mesh).

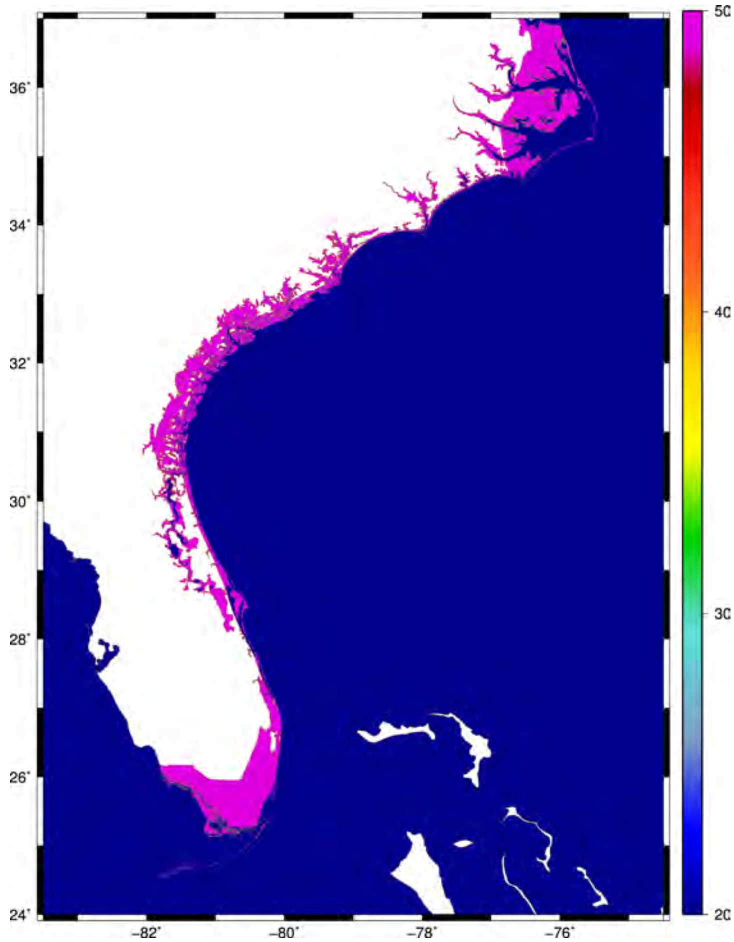

Figure 3.19 Variation of horizontal eddy viscosity ($m^2\ s^{-1}$) along the U.S. southeast coast in the FEMA-SAB mesh.

3.5.3 Manning's n at sea floor

The Manning's n at sea floor (ManningsN) is an isotropic scalar parameter that approximates resistance to flow from a variety of physical processes, including form drag and skin friction. During the ADCIRC run, the specified value of this attribute is converted into a quadratic friction coefficient before computing bottom drag stress. ManningsN values are typically derived from land-use data sets for that particular region. The typical values of this attribute are 0.02 m $s^{-1/3}$ for open water, 0.05 m $s^{-1/3}$ for scrub, 0.1 m $s^{-1/3}$ for estuarine forested wetland and developed medium intensity areas, 0.15 m $s^{-1/3}$ for developed high intensity areas, etc. As all component meshes had this attribute in its

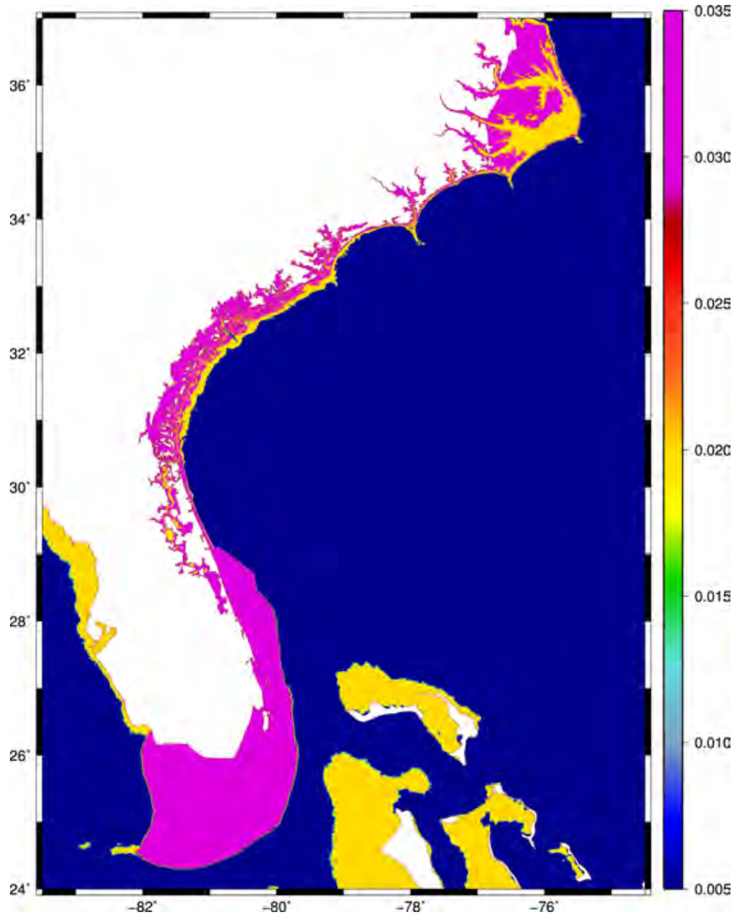

Figure 3.20 Variation of Tau0 (s^{-1}) along the U.S. southeast coast in the FEMA-SAB mesh.

`fort.13`, the value at a particular region in the FEMA-SAB mesh was interpolated from the corresponding component mesh (Figure 3.21). In the FEMA-SAB mesh, the highest value on the U.S. southeast coast occurs in the Everglades National Park, north of the Florida Keys where the ManningsN was 0.12 m $s^{-1/3}$.

3.5.4 Surface Directional Effective Roughness Length

The Surface Directional Effective Roughness Length (z0Land) attribute is a measure of the "roughness" of the land that can obstruct wind flow, and reduce the wind stress over rough terrain, urban areas, etc. The wind boundary layer depends on the roughness conditions upwind of a location. This upwind effect is especially important in the nearshore regions, where winds travel either offshore or onshore, and transitions to or from open

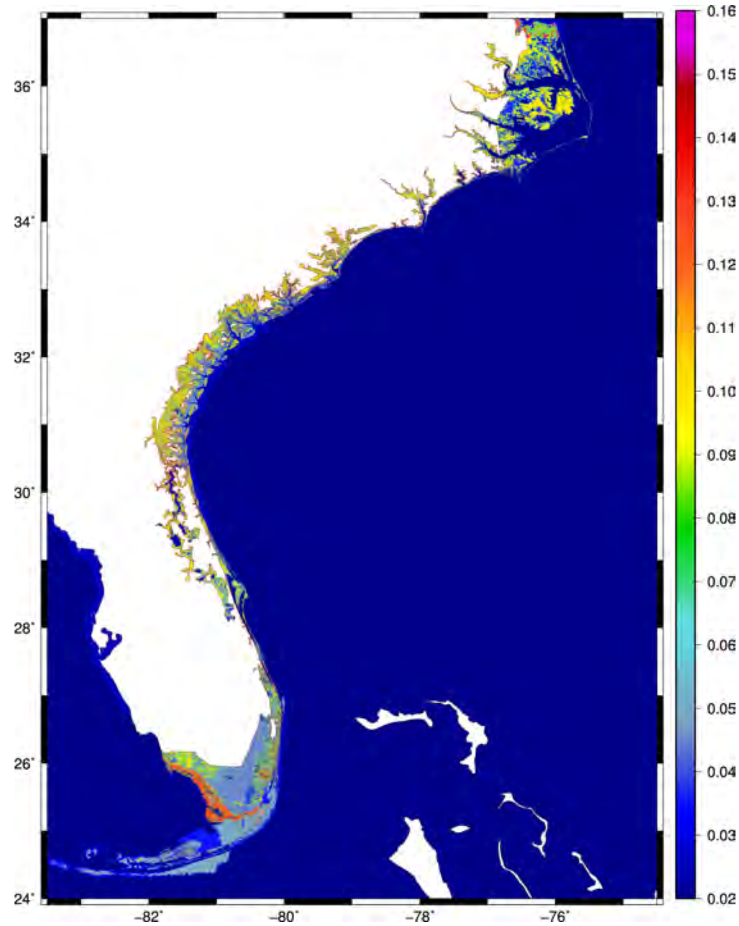

Figure 3.21 Variation of ManningsN (m $s^{-1/3}$) along the U.S. southeast coast in the FEMA-SAB mesh.

water conditions. It is critical to have accurate winds in these near-shore and low-lying overland regions that experience either draw-down or flooding (Federal Emergency Management Agency, 2007). To account for directionality in the upwind parameters, the roughness length is specified by 12 values at each mesh vertex, each representing a 30 degree "upwind" directional bin. Zero degrees represents due east (wind blowing west to east), and the values proceed counter clockwise. As an example, the value of this attribute is 0 for open water, and 0.72 for evergreen forest. Like ManningsN, the values of this attribute at a location in the FEMA-SAB mesh came from the corresponding component mesh `fort.13`. The attribute values for the 60 degree direction, is shown as an example (Figure 3.22).

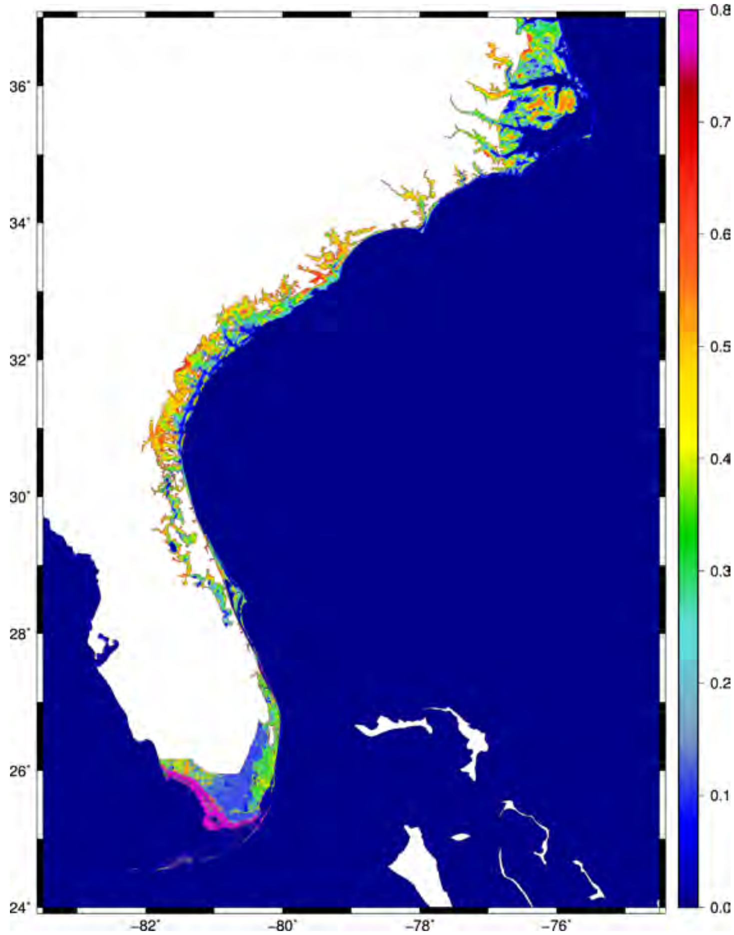

Figure 3.22 Variation of surface directional effective roughness length (m) along the U.S. southeast coast in the FEMA-SAB mesh, corresponding to the 60 degree direction.

3.5.5 Surface Canopy Coefficient

Heavily forested canopies can greatly reduce or remove the momentum flux transfer from the wind field to the water column (Reid et al., 1976). The Surface Canopy coefficient attribute (VCanopy) allows the user to account for vegetation canopy effects in the ADCIRC model. The user may turn off the wind stress in heavily forested areas where the canopy fully shields the water surface from the wind stress. The attribute is unitless, and value for the attribute is derived from land-use datasets, with the setting being binary: 0 for canopy, and 1 for everywhere else. For the FEMA-SAB mesh, the values of VCanopy at each mesh vertex were taken from the corresponding component `fort.13` (Figure 3.23).

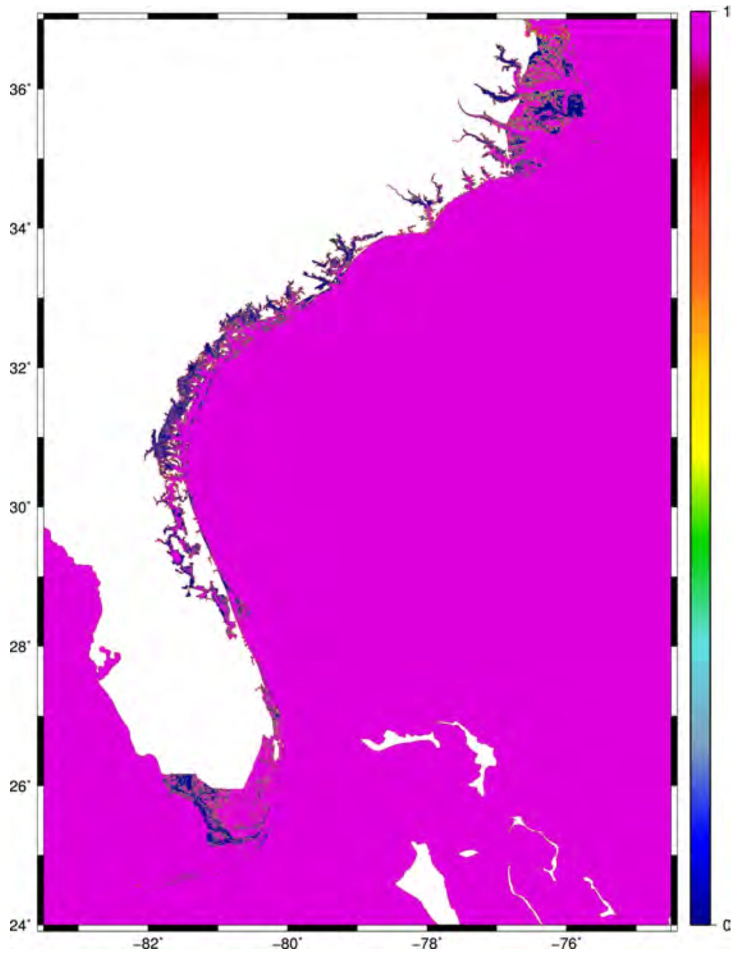

Figure 3.23 Variation of VCanopy (unitless) along the U.S. southeast coast in the FEMA-SAB mesh.

3.5.6 Elemental Slope Limiter

The elemental slope limiter attribute helps to selectively limit the maximum water surface elevation gradient that can occur across an element in the mesh. Thus, it helps in adding numerical stability. It is also capable of merely logging individual elements where a specified elemental slope is exceeded at some point during the simulation. When this attribute is active, the water surface elevation at that vertex is reset to the average of the water surface elevations of the surrounding vertices. If the gradient is not exceeded, the solution remains unchanged. As this attribute represent the elevation gradient across an element, it has units of m/m, or is unitless. For the FEMA-SAB mesh, the elemental slope limiter was used for vertices along the U.S. southeast coast with depths less than 10 m (Figure 3.24). This was done by assigning them an attribute value of 0.001, as suggested in the ADCIRC website (ADCIRC, 2020b). For other regions, a value of 99999 was used so that the slope limiter is never activated in those regions. The elemental slope limiter was also used in the SFLSSS to deal with instabilities in Broward County, FL (Engineering, 2018).

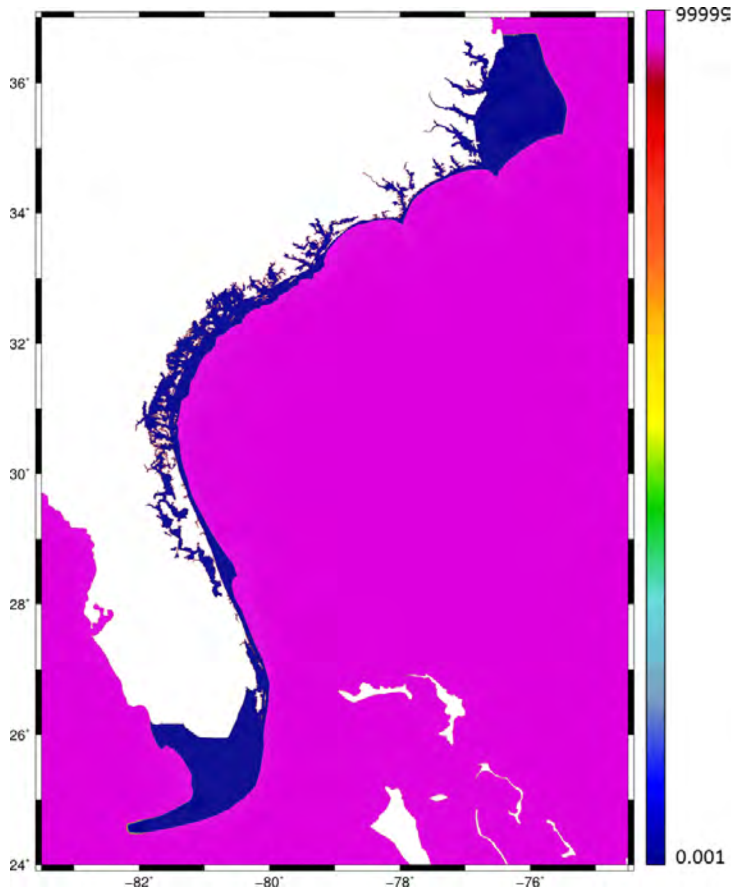

Figure 3.24 Variation of elemental slope limiter (unitless) along the U.S. southeast coast in the FEMA-SAB mesh.

3.5.7 Advection State

The NOLICA and NOLICAT parameters in `fort.15` helps in activating or deactivating the nonlinear advective terms in ADCIRC for the entire domain. The advection state attribute helps by allowing to disable advection on an element-by-element basis. If the bathymetric depth at any of the three nodes of a particular element is less than the corresponding nodal attribute value, the values of NOLICA and NOLICAT will be set to zero on that element, thus disabling advection. Like the elemental slope limiter, the advection state attribute was added to deal with instabilities that occurred while running the model with advection turned on. For the FEMA-SAB mesh, advection was disabled in the Caribbean and near the east boundary, far away from the U.S. southeast coast. These instabilities are associated with the HSOFS mesh, and can be seen in the the mesh development report (Riverside Technology et al., 2015), and also in our hindcast simulations of Hurricane Matthew (Thomas et al., 2019). Advection was also disabled in small locations along the SC coastline to deal with instabilities.

3.6 Hindcasts of Storms on the FEMA-SAB Mesh

Having developed the FEMA-SAB mesh and its nodal attribute file, the performance of the mesh was evaluated for two storms that impacted the U.S. southeast coast. In this section, details are provided about the atmospheric forcing used, as well as the input settings for the coupled ADCIRC+SWAN model.

3.6.1 Storms

The FEMA-SAB mesh is tested by running simulations of two storms: Matthew (2016) and Florence (2018). As seen in Chapter 2, Matthew was a Category-5 hurricane that caused widespread impacts along the U.S. southeast coast and made landfall with Category-1 intensity along the central coast of South Carolina during October 2016. Florence was a Category-4 hurricane that made landfall along the southeastern coast of North Carolina during September 2018 (Stewart et al., 2019) and caused significant storm surge flooding in eastern North Carolina. These two storms were selected as they impacted the U.S. southeast coast where the FEMA-SAB mesh has detailed coverage. But they vary in their storm parameters. Whereas Matthew was a shore-parallel storm from FL to NC, Florence had a shore-normal track (Figure 3.25). They also varied in the size, intensity of winds, duration, etc. Thus these two storms will be a good test in demonstrating the capability of the FEMA-SAB mesh for any storm that hits the southeastern U.S. coastline.

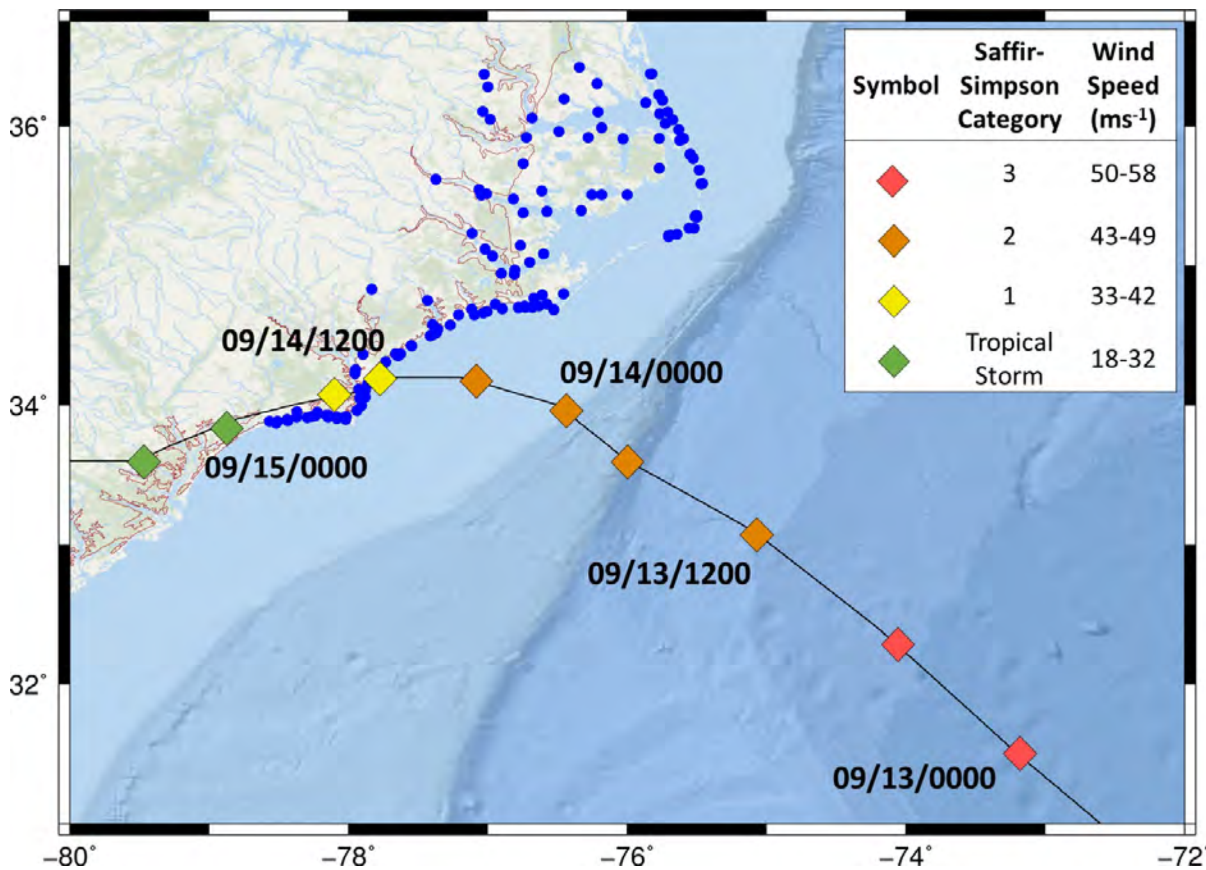

Figure 3.25 NHC best track for Florence (black line and diamonds), along with observation locations of water levels (blue circles) on the U.S. southeast coast. High-water marks are not shown. The storm center positions are shown every 6 hr and color-coded to categories on the Saffir-Simpson scale. The storm positions are labeled in dates/times relative to UTC.

3.6.2 Observations

For Matthew, the same set of observation data as in Chapter 2 is used to evaluate the predicted results. For Florence, observations were collected at National Ocean Service

(NOS) (NOAA, 2018a) and U.S. Geological Survey (USGS)- PERManent (PERM) (U.S. Geological Survey, 2020b), Rapidly-Deployed Gauges (DEPL) (USGS, 2018), and Storm Tide Sensors (STS) (USGS, 2018). Time series of water levels at 151 locations and 168 High-Water Marks (HWMs) were identified within the model extent in NC. For the analyses herein, those observations that did not operate during the peak of the storm or that had freshwater run-off or wave run-up were removed. This left a total of 120 time series (Figure 3.25) including 6 NOS, 6 USGS-PERM, 11 USGS-DEPL and 97 USGS-STS, and 85 HWMs to describe the water levels during Florence.

3.6.3 Atmospheric Forcing

For this study, we will use data-assimilated wind and pressure fields from Oceanweather Inc. (OWI), as they proved to be the most accurate representation of atmospheric forcing during Matthew (2). For Florence, the basin grid covers from 5°N to 47°N and from 99°W to 55°W with a spatial resolution of 0.25°, whereas the higher-resolution region field covers from 31°N to 37°N and from 82°W to 74°W with a spatial resolution of 0.05°, both covering a period from 0000 UTC 07 September 2018 until 0000 UTC 18 September 2018, at 15 min intervals. Thus the wind and pressure fields for Florence have the same resolution as that for Matthew, both in time and spatially.

3.6.4 ADCIRC+SWAN Settings

The settings used to run the coupled ADCIRC+SWAN model on the FEMA-SAB mesh for both Matthew and Florence, was mostly the same as that used for running Matthew on the HSOFS mesh in Chapter 2. The major difference is the ADCIRC time step. Whereas the HSOFS mesh could be run with a time step of 1 s, this was not possible for the FEMA-SAB mesh due to its smaller element spacing, especially in South FL. This is related to the Courant–Friedrichs–Lewy (CFL) condition that influences model stability and relates the model time step, element size, and shallow wave celerity. Therefore, a smaller time step of 0.5 s was used for running the FEMA-SAB mesh. The same value was used in SFL mesh development as well (BakerAECOM, 2016). Another difference was in the value of horizontal eddy viscosity. Whereas a spatially-constant horizontal eddy viscosity of 50 m^2 s^{-1} was used for the HSOFS-Mathew simulation, the FEMA-SAB simulations uses a spatially varying eddy viscosity defined in two classes of 50 and 20 in `fort.13`, as described earlier. The simulations on the FEMA-SAB mesh also employed a spatially-varying offset surface like in Chapter 2, for both Matthew and Florence.

3.7 Results and Discussion

This section will analyze water levels on the FEMA-SAB mesh during Matthew and Florence. Comparisons are made at observations all along the U.S. southeast coast for Matthew and in NC for Florence. Comparisons are also made to HSOFS results, especially at inland locations, to evaluate how the added resolution in the FEMA-SAB mesh improves the predictions. The same error metrics used in the previous chapter will be used to compare modeled results to measurement data, specifically, root-mean-squared error (E_{RMS}), mean normalized bias (B_{MN}), coefficient of determination (R^2) and best-fit slope (m).

3.7.1 Matthew (2016)

Water levels are analyzed first by looking at time series plots at the same 12 locations as in Chapter 2 (Figure 3.26). These gauges are located either close to the shoreline, or in the Pamlico Sound in NC (as for NCEM BLHN7), where the HSOFS mesh has adequate resolution to represent bathymetry and topography. Thus the predicted results from ADCIRC+SWAN using the FEMA-SAB mesh are similar to results from ADCIRC+SWAN using the HSOFS mesh. The only noticeable differences are at stations USGS-STS FLVOL03143 and NOS 8654467. At the USGS-STS FLVOL03143 station located between Orlando Beach and St. Augustine Beach, Florida, the observations indicate a peak of 2.02 m. Although the station remains dry during low tide after the storm peak has passed, the predictions on the FEMA-SAB mesh are a better match to the observed peak with a value of 2.12 m, compared to 1.84 m as predicted on the HSOFS mesh. At the NOS 8564467 gauge at the United States Coast Guard station on Hatteras Island, the observed peak was 1.82 m. In the FEMA-SAB mesh, the channel that leads to this station is represented by elements of 240 m, whereas the element spacing in this area is 525 m in the HSOFS mesh. This leads to a better predicted peak of 1.42 m, as compared to 1.15 m when using the coarser HSOFS results.

As demonstrated earlier, the main differences in resolution between the FEMA-SAB and HSOFS meshes occur far inland, away from the coastline. The predicted time series

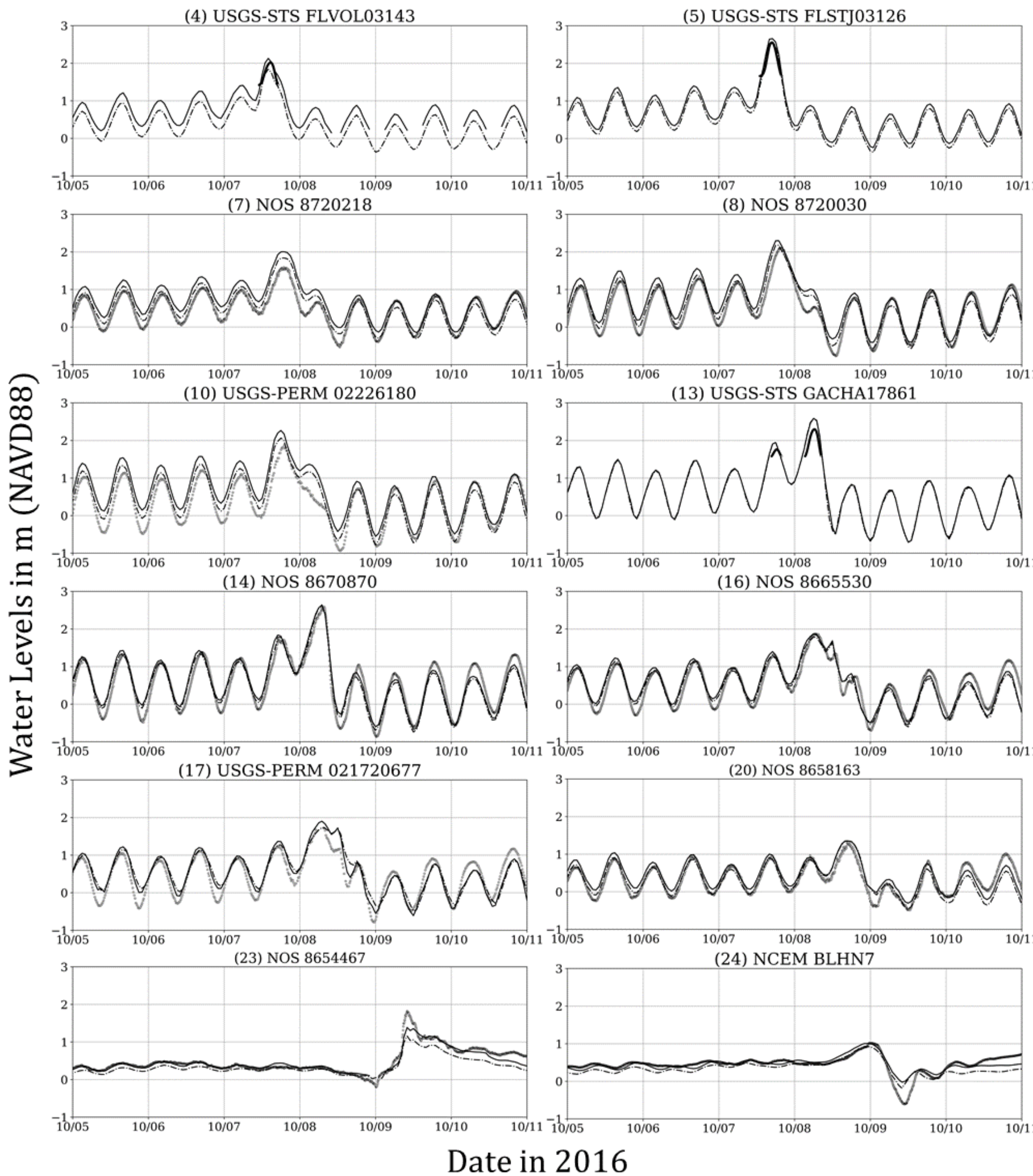

Figure 3.26 Time series of water levels (m relative to NAVD88) at the 12 locations shown in Chapter 2. Observed values are shown with gray circles, and predicted results using black lines with line types corresponding to: (solid) FEMA-SAB mesh, and (dashed-dotted) HSOFS mesh.

of water levels (Figure 3.28) are therefore compared at 10 stations from FL to NC (Figure 3.27), located in small channels or high in the rivers. This should highlight the role of

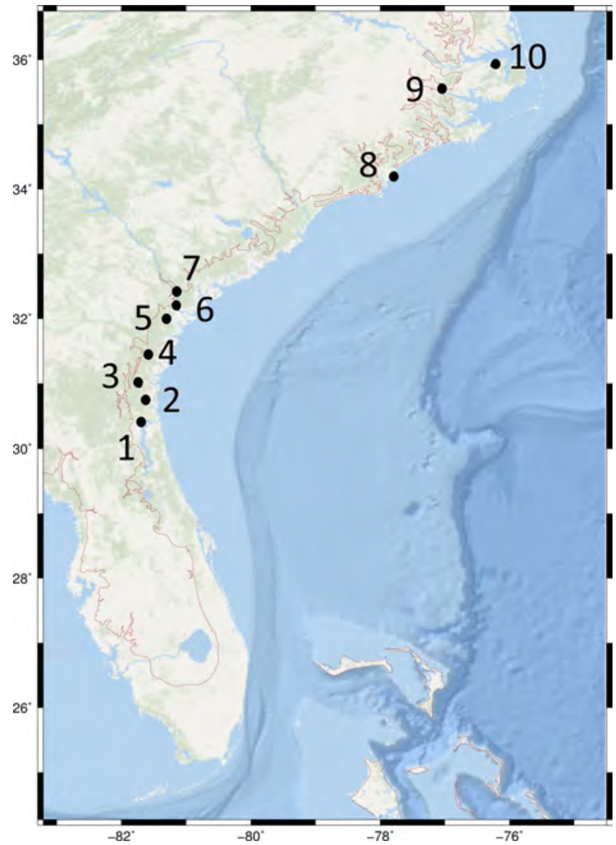

Figure 3.27 Locations of selected stations for comparison of water levels. The points are numbered from south to north.

added resolution in the FEMA-SAB mesh in improving flooding predictions. At the USGS-PERM 02246621 station located in the Trout River (tributary of the St. Johns River), FL, the resolution in the channel at this location in the FEMA-SAB mesh is 44 m. The HSOFS mesh does not resolve this channel, as its element spacing is 280 m in this region, and thus the station remains dry except during the storm peak. The prediction using the FEMA-SAB mesh do capture the tides and the storm surge, although it over-predicts the peak water levels especially before and during the storm. At the USGS-PERM 02231254 station located in the St. Mary's River along the FL-GA border, the trends in the results are the same. Although the ADCIRC-predicted peaks on both meshes are similar, the predictions using the HSOFS mesh do not capture tides. The HSOFS mesh does not have the river extending to this location due its coarser resolution of 342 m. The FEMA-SAB mesh has the river extending farther inland, with an element

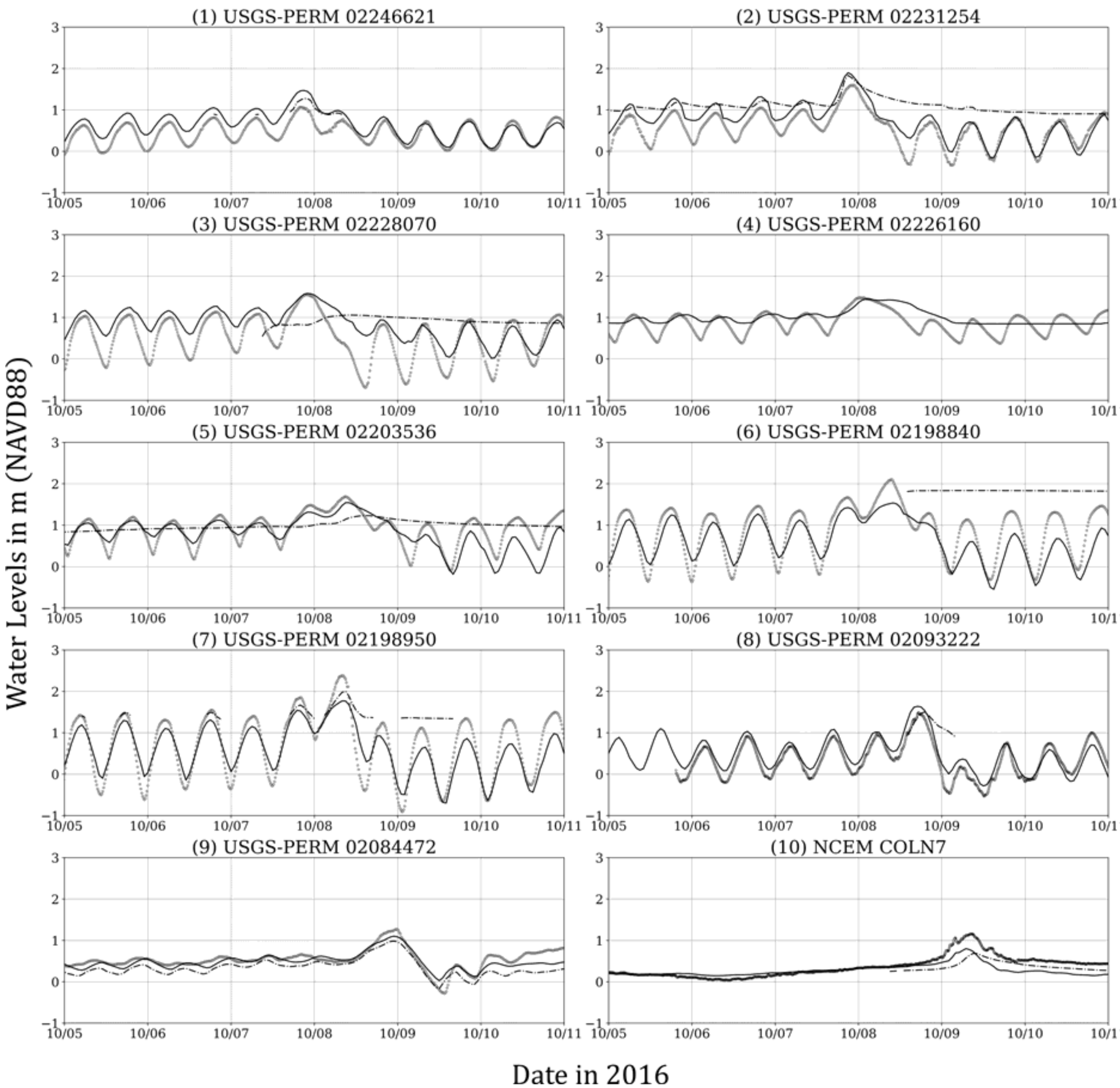

Figure 3.28 Time series of water levels (m relative to NAVD88) at the 10 locations shown in Figure 3.27. Observed values are shown with gray circles, and predicted results using black lines with line types corresponding to: (solid) FEMA-SAB mesh, and (dashed-dotted) HSOFS mesh.

spacing of 62 m at the station.

At the USGS-PERM station 02228070 situated in the Satilla River, Georgia, the predictions using the FEMA-SAB mesh are a good match to the observed peak of 1.5 m. The predictions using the HSOFS mesh indicate a constant value close to 1 m for most of the storm duration. This inaccurate prediction with the HSOFS mesh is attributed to its poor bathymetry, which has the channel extending to the station location. The resolutions in the FEMA-SAB and HSOFS meshes at this location are 50 m and 379 m, respectively. At the USGS-PERM 02226160 station located in the Altamaha River, Georgia, the element spacing varies from 60 m in the FEMA-SAB mesh to 397 m in the HSOFS mesh. This coarser resolution in the HSOFS prevents the main river from reaching the station location, and hence the water levels remain dry throughout the simulation. On the other hand, although the prediction using the FEMA-SAB mesh do not capture the tides accurately, it has a good match to the observed peak of 1.48 m with a value of 1.45 m. The station USGS-PERM 02203536 located in the Ogeechee River, Georgia is located in an element of size 61 m in the FEMA-SAB mesh. In the HSOFS mesh, the corresponding element size is 417 m. Moreover it has region indicated as topography with an average elevation of 0.8 m. This is reflected in the predictions using the FEMA-SAB mesh, which match fairly well to the observations, with a good representation of tides and storm surge. The predictions using the HSOFS mesh again have a constant value of 1 m.

As described in Section 3.2, along the Savannah River on the GA-SC border, the HSOFS mesh has a poor representation of bathymetry due its coarser resolution. The USGS-PERM stations 02198840 and 02198950 are located in some of smaller channels in this region. The average resolution at these station locations varies from approximately 52 m in the FEMA-SAB mesh to 535 m in the HSOFS mesh. The water levels stay dry for most of the simulation using the HSOFS mesh. The predictions on the FEMA-SAB match the observations fairly well, although the peak is under-predicted by 0.5 to 0.6 m. At the USGS-PERM 02093222 station, located in the Banks Channel in North Carolina, the FEMA-SAB mesh results has a good match to the observations although it over-predicts the peaks by 0.15 m. Although the HSOFS results capture the peak better, water levels are only predicted during the peak of the storm. The channel is absent in the HSOFS mesh and it has an element spacing of 302 m at this location. The corresponding resolution in the FEMA-SAB mesh is 155 m.

At the USGS-PERM 02084472 station located in the Pamlico River, North Carolina, the predictions on both meshes are similar, and match the observations quite well. The FEMA-SAB mesh results are more accurate with a better representation of tides before and after the storm. It also has a better match to the observed peak of 1.27 m with a value of 1.1 m, compared to 0.98 m in the HSOFS mesh results. In this region, the HSOFS mesh has a higher resolution of about 520 m compared to 760 m in the FEMA-SAB mesh. At the NCEM COLN7 station located in the Scuppernong River that evolves from the Albemarle Sound, the FEMA-SAB mesh has a resolution of 200 m compared to a much coarser resolution of 1300 m in the HSOFS mesh. The observations indicate a maximum water level of 1.15 m at the peak of the storm. The FEMA-SAB mesh results are a better match in terms of peaks and water levels before the storm. It has a predicted peak of 0.82 m compared to 0.67m in the HSOFS results. The HSOFS water levels also remain dry before the storm peak occurs.

3.7.1.1 Error Statistics

Like in Chapter 2, a total of 753 locations were used to evaluate model performance during Matthew along the U.S. southeast coast. These include the 289 hydrograph-derived peak water levels, and 464 USGS-observed HWMs. In Figure 3.29, the points are color-coded based on predicted error (predicted less observed) expressed as a percentage of observed value. Warm colors indicate over-prediction by the model, whereas the cool colors indicate under-prediction. Out of the 626 stations wetted by ADCIRC, and within the model extent, the errors in the modeled peaks were within 10 percent at 337 (54 percent) stations and within 25 percent at 509 (81 percent) stations. For the scatter plots, the R^2 value was 0.76 and the slope of the best-fit line was 1.02 (Table 3.2).

Table 3.2 Error statistics for the FEMA-SAB and HSOFS meshes, for both Matthew and Florence.

	FEMA-SAB		HSOFS	
Error	Matthew	Florence	Matthew	Florence
Stations	626	190	622	184
Best-Fit Slope	1.02	1.00	0.96	0.99
R^2	0.76	0.91	0.78	0.91
E_{RMS} (m)	0.28	0.20	0.28	0.21
B_{MN}	0.03	0.01	-0.03	-0.01

The model over-predicted the peaks by more than 25 percent in the FL part of the coastline, south of Juno Beach. These regions did not experience storm effects; the total

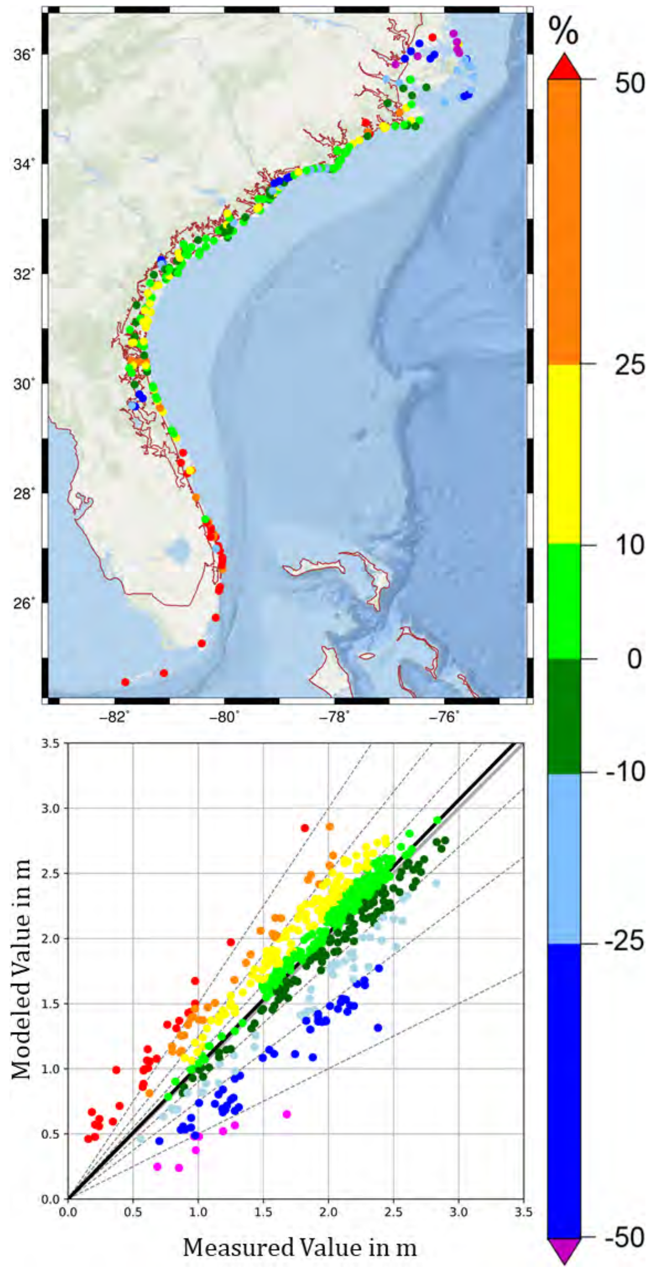

Figure 3.29 Locations (top row) and scatter plots (bottom row) of HWMs and peak hydrograph values during Matthew. Colors indicate error expressed as a percentage of observed value. Green points indicate errors within 10%; yellow and light blue indicate errors between 10% and 25%; orange and dark blue indicate errors between 25% and 50%; and red and purple indicate errors over 50%. The thick gray and black lines represent $y = x$ and best-fit lines, respectively. Statistical metrics are shown in Table 3.2.

water levels were always less than 1.0 m. An explanation for this over-prediction could be related to the attribute for sea surface height above geoid. The SFL and ECCFL component meshes use this attribute to create an initial offset of −0.155 m and −0.17 m. respectively. This attribute is not employed while running the FEMA-SAB mesh. The errors were also large on the sound side of the Outer Banks in NC, where the model under-predicted the peaks by more than 25 percent. The same trends were also seen for the HSOFS simulation (Chapter 2), although the resolution in the sound is much higher in the HSOFS mesh (Figure 3.1). In other regions, the errors were lesser, especially along the South Atlantic Bight. A positive value of B_{MN} indicated an over-prediction of the peaks overall. Although these error statistics are similar to the HSOFS results, the benefit of added resolution in the FEMA-SAB mesh occurs mainly at inland stations, as seen previously.

3.7.2 Florence (2018)

Florence was a Category-4 hurricane that made landfall (with Category-1 intensity) along the southeast coast of North Carolina during September 2018. The capability of the FEMA-SAB mesh in predicting water levels during Florence is first evaluated for time series of water levels at 10 locations in NC (Figure 3.30) that were impacted by the storm. The HSOFS predictions are also shown, to compare how the difference in resolution between the two meshes, translates to a difference in storm surge (Figure 3.31).

At the NOS 8654467 gauge located in Hatteras on the sound-side of the Outer Banks, the resolution in the FEMA-SAB mesh is 240 m, whereas that in the HSOFS mesh is 464 m. Regardless of these resolution differences, the bathymetry in the area is fairly the same in both meshes, and therefore the predictions of water levels on both meshes are similar. These predictions represent the storm impacts quite well, including the drawdown during the storm. The USGS-STS NCBEA11768 gauge located along Bath Creek, a tributary of the Pamlico River, falls in an element that has an average size of about 1030 m and 380 m in the FEMA-SAB and HSOFS mesh respectively. Although the FEMA-SAB mesh has a much larger element spacing (about three times) in this region, it has a better representation of bathymetry, with one of the element-vertex represented as part of the channel. In the HSOFS mesh, all three vertices represent topography. Thus, although both meshes have similar predictions during the storm, the FEMA-SAB mesh captures even the little tidal effects that occur way before the storm peak.

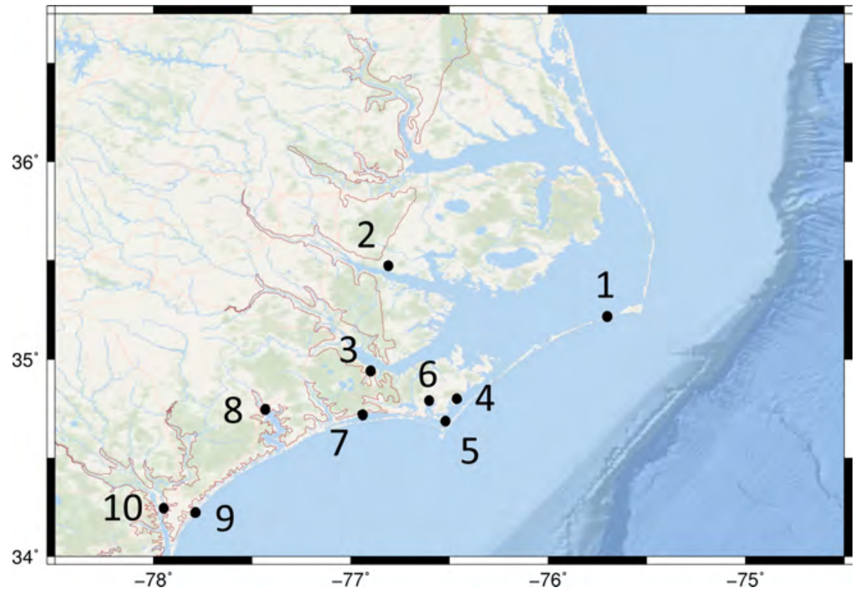

Figure 3.30 Locations of selected stations for comparison of water levels. The points are numbered from north to south.

The maximum storm surge inundation heights produced by Florence were 2.4 to 3.4 m above ground level along the shores of the Neuse River and its tributaries, where they empty into the Pamlico Sound. Although the sound has very little tidal influence, the easterly winds from Florence raised water levels on the western side of the sound and backed up the normal flow of the Neuse River, causing significant shoreline inundation in Craven, Pamlico and Carteret Counties (Stewart et al., 2019). The USGS-STS NC-CRA13628 gauge located in Slocum Creek in this area of the Neuse River, observed a peak surge of 3.1 m. For both meshes, the simulations under-predict this observed peak by 0.2 to 0.4 m. The FEMA-SAB mesh has the channel represented at a 280 m resolution, whereas it is missing in the HSOFS mesh with its resolution of 400 m in this region. Thus the HSOFS predictions do not capture the tidal effects before the storm.

At the USGS-STS NCCAR12128 gauge located along the Core Sound, FEMA-SAB mesh has a resolution of 290 m, whereas that in the HSOFS mesh is about 500 m. The FEMA-SAB also has a much deeper bathymetry at the center of the Sound, with a value of 3.8 m compared to 1.6 m in the HSOFS mesh. Although the predictions on both meshes under-predict the peak of the storm, the simulation with the FEMA-SAB mesh has a better match of 1.45m to the observed peak of 1.60 m. The corresponding value

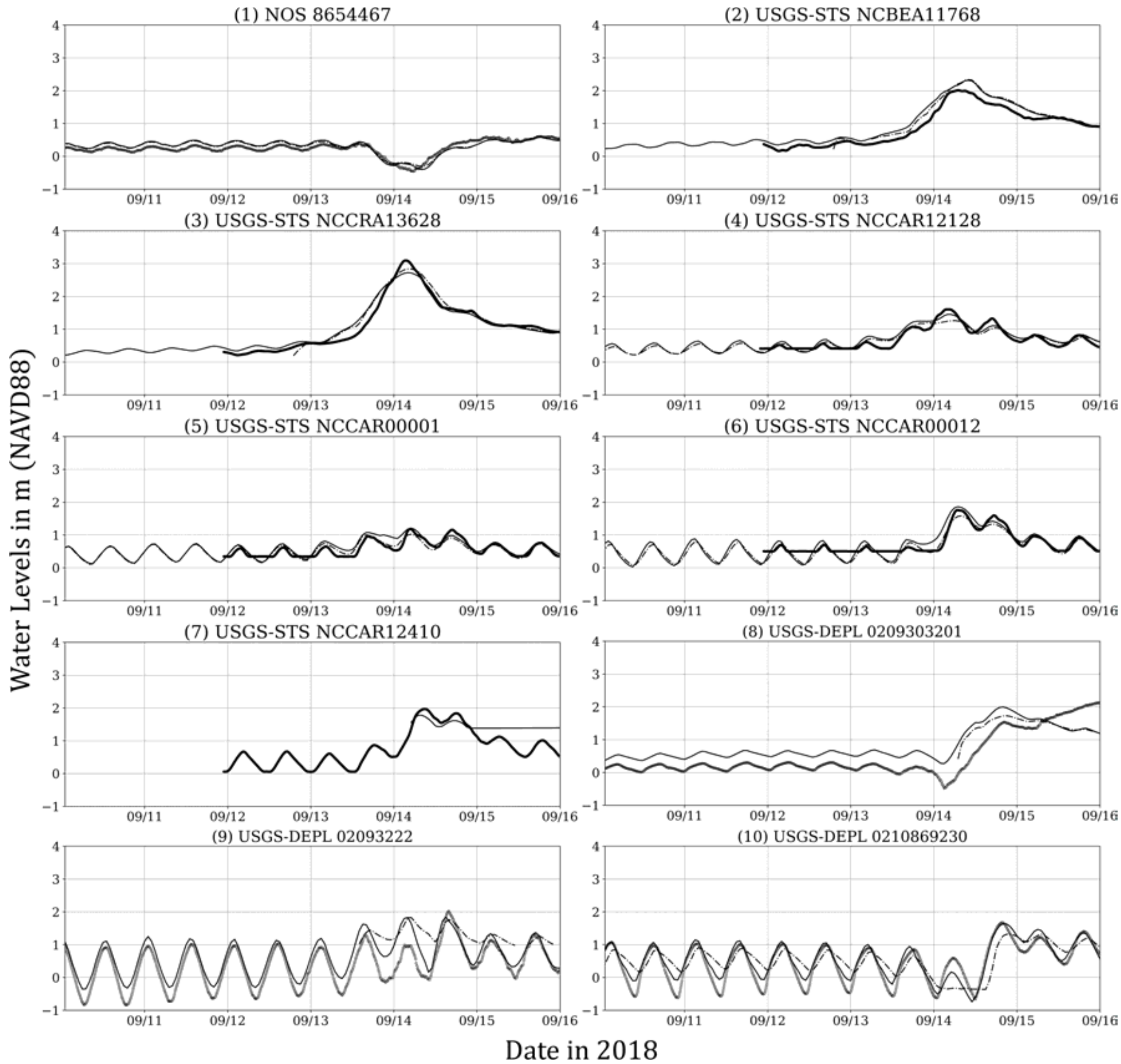

Figure 3.31 Time series of water levels (m relative to NAVD88) at the 10 locations shown in Figure 3.30. Observed values are shown with gray circles, and predicted results using black lines with line types corresponding to: (solid) FEMA-SAB mesh, and (dashed-dotted) HSOFS mesh.

from the HSOFS mesh is only 1.21 m. At the USGS-STS NCCAR00001 gauge located on Harkers Island, the simulation with the FEMA-SAB mesh has a perfect match to the observed peak of 1.2 m, although it slightly over- and under-predicts the water levels before and after the peak. The simulation with the HSOFS mesh under-predicts this peak value by 0.21 m. The resolution in this region is 121 m and 422 m in the FEMA-SAB and HSOFS meshes, respectively.

At the USGS-STS NCCAR00012 gauge located up the North River that originates from the Back Sound, the FEMA-SAB mesh has a resolution of 210 m compared to 380 m in the HSOFS mesh. Although the predictions from both meshes are similar, the FEMA-SAB mesh has a much better match to the observed peak value of 1.78 m with a predicted value of 1.86 m. The simulation with the HSOFS mesh under-predicts the peak by over 20 cm. The USGS-STS NCCAR12410 gauge is located along the Broad Creek that originates from the Bogue Sound. Although both meshes do not have the channel extending into the station, the FEMA-SAB mesh has the channel ending just 250 m shy of this location, with a resolution of about 140 m in this region. The HSOFS mesh has a much coarser resolution of 465 m with the channel ending far away. It therefore stays dry for the entire storm duration. The FEMA-SAB mesh on the other hand is able to record the peak of the storm, with a predicted value of 1.78 m as compared to the observed peak of 1.96 m.

At the USGS-DEPL 0209303201 gauge located along the New River in Jacksonville, the resolution in the FEMA-SAB mesh is 57 m. The HSOFS mesh on the other hand has this region represented at 395 m resolution, with the New River ending 2 km south of the station. It therefore stays dry for most of the storm duration, except during the peak. The simulation with the FEMA-SAB mesh over-predicts the water levels by 0.2 to 0.45 m throughout the storm including at the peak, where it over-predicts the maximum water levels by 0.42 m. The simulation with the HSOFS mesh over-predicts the observed peak value of 1.58 m by only 0.18 m. After the peak of the storm, both meshes predict similar water levels, although the observations indicate effects of river-runoff. At the USGS-DEPL 02093222 gauge along the Banks Channel, the trends in predicted water levels are similar. The simulation with the HSOFS mesh stays dry for the entire storm duration except at the peak, with both meshes under-predicting the observed peak value of 2.02 m. The simulation with the FEMA-SAB mesh also has a better peak prediction of 1.84 m compared to 1.75 m in the HSOFS results. These differences in the predictions are attributed to the differences in bathymetry and mesh-resolution. The HSOFS mesh has a coarser resolution of about 300 m, with this region indicated as topography. The FEMA-SAB mesh has a smaller element spacing of about 150 m with a proper presentation of the channel.

At the USGS-DEPL 0210869230 gauge located high up in the Cape Fear River, the

FEMA-SAB mesh has a resolution of 60 m with a bathymetry of about 10 m at the center of the channel. The HSOFS mesh has a much coarser resolution of 330m with the channel being only 1.4 m deep. The FEMA-SAB mesh also has 7 elements across the channel compared to just 1 element in the HSOFS mesh. These differences in resolution and bathymetry are reflected in the predicted results as well. The FEMA-SAB mesh results are a better match to water levels before the storm, both in terms of timing and magnitude of the peaks. It also has a better prediction of water levels during the storm, with a predicted peak value of 1.64 m, compared to 1.68 m in the observations. The HSOFS mesh predictions under-estimate this peak by 0.3 m.

3.7.2.1 Error Statistics

All stations that are wetted by ADCIRC are included while computing error statistics. Thus, the mesh to mesh comparisons may have different number of stations. As mentioned earlier, a total of 319 locations were used to evaluate model performance during Florence along the NC coast. In Figure 3.32, the points are color-coded based on predicted error (predicted less observed) expressed as a percentage of observed value. Warm colors indicate over-prediction by the model, whereas the cool colors indicate under-prediction. Out of the 190 locations suitable for peak-analysis and wetted by ADCIRC, the errors in the modeled peaks were within 10 percent at 125 (66 percent) stations and within 25 percent at 181 (95 percent) stations (Figure 3.32, top). For the scatter plots, the R^2 value was 0.91 and the slope of the best-fit line was 1.00 (Table 3.2). A positive value of B_{MN} indicated an over-prediction of the peaks overall. Thus the ADCIRC prediction on the FEMA-SAB mesh for Florence was a good match to the observations, almost everywhere within the model extent in NC.

A similar analysis was done for the Florence predictions on the HSOFS mesh as well. Out of the 184 locations wetted by ADCIRC, the errors in the modeled peaks were within 10 percent at 116 (63 percent) stations and within 25 percent at 176 (96 percent) stations (Figure 3.32, bottom). or the scatter plots, the R^2 value was 0.91 and the slope of the best-fit line was 0.99 (Table 3.2). A negative value of B_{MN} indicated an under-prediction of the peaks overall. Thus although the error statistics are similar, the FEMA-SAB results has a better value of best-fit slope m (closer to 1) and E_{RMS} (closer to 0), and it also floods a large number of stations. These extra stations are located upstream the major rivers and in the smaller channels, where the HSOFS mesh does not have enough

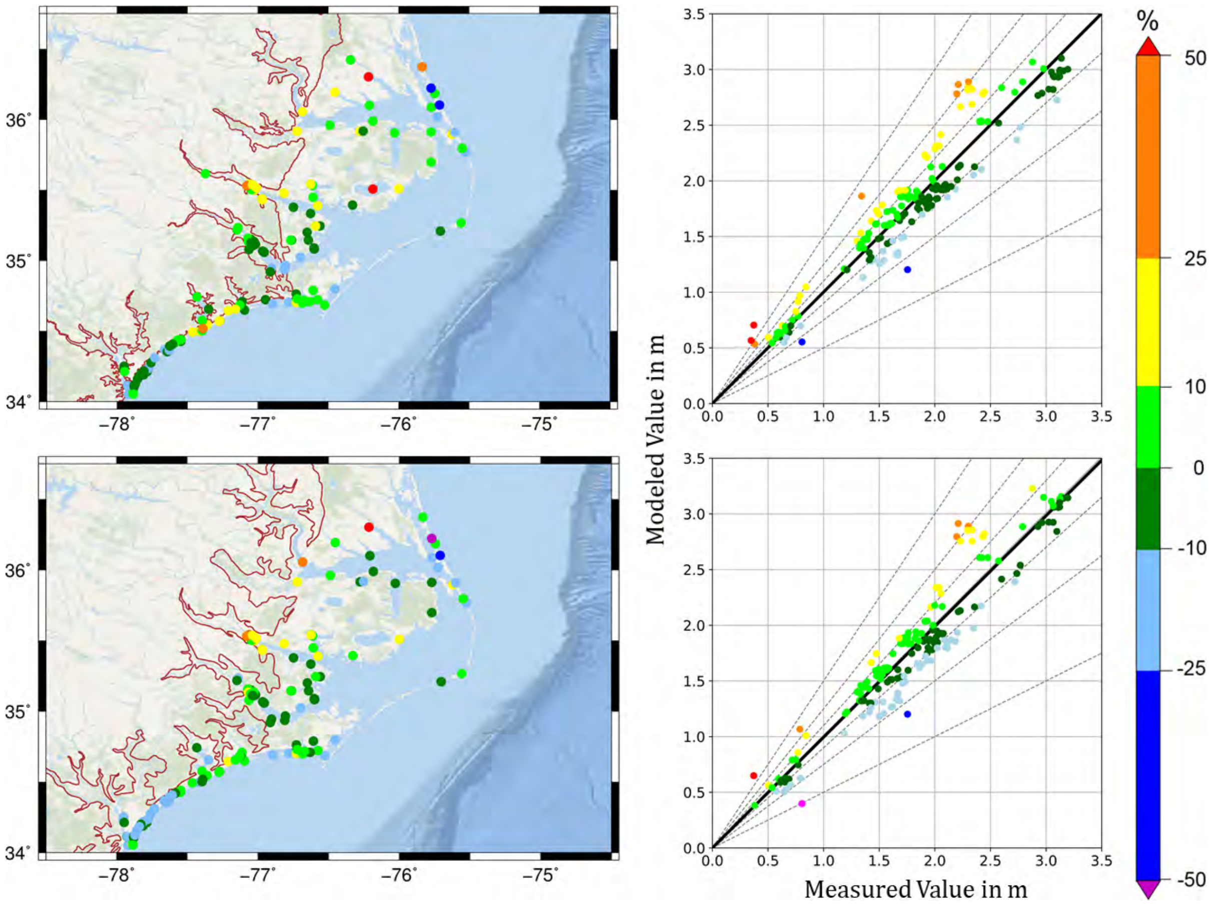

Figure 3.32 Locations (left column) and scatter plots (right column) of HWMs and peak hydrograph values during Matthew. Rows correspond to: (ltop) FEMA-SAB mesh; and (bottom) HSOFS mesh. Colors indicate error expressed as a percentage of observed value. Green points indicate errors within 10%; yellow and light blue indicate errors between 10% and 25%; orange and dark blue indicate errors between 25% and 50%; and red and purple indicate errors over 50%. In the location plots, the mesh-boundary is shown in brown. For the scatter plots, the thick gray and black lines represent $y = x$ and best-fit lines, respectively. Statistical metrics are shown in Table 3.2.

resolution.

3.8 Conclusions

A high-resolution mesh, describing the coastal floodplains from FL to NC, was developed by merging five FEMA regional meshes (South Florida, East Coast Central Florida, Georgia and Northeast Florida, South Carolina and North Carolina) to an open-water mesh. The combined mesh, referred to as the FEMA-SAB mesh, has a total of $5,584,241$ vertices and $11,066,018$ elements. The element spacing is less than 100 m along the southeastern U.S. coastline, except in a few regions along the SC and NC coasts.

The FEMA-SAB mesh was then tested by running ADCIRC+SWAN simulations of two storms that impacted the U.S. southeast coast in different ways. For both Matthew and Florence, a qualitative analysis of time-series plots of water levels at inland locations indicated that the FEMA-SAB mesh out-performed the HSOFS mesh in terms of better capturing tidal impacts and/or having a better match to the peak water levels. A similar trend was seen in the error statistics. For the shore-parallel storm Matthew, for a total 626 locations all along the U.S. southeast coast, the FEMA-SAB mesh had a R^2 value of 0.76, slope of the best-fit line of 1.02, E_{RMS} of 0.28, and B_{MN} of 0.03. For Florence, for a total of 120 location in NC, the R^2 value was 0.91, the slope of the best-fit line was 1.00, E_{RMS} was 0.20, and B_{MN} was 0.01. These error statistics for the FEMA-SAB predictions are either better or close to that for the HSOFS predictions, meanwhile flooding a larger number of points. Thus, although the FEMA-SAB mesh is roughly three times the size of the HSOFS mesh, its predictions are a better match to observations, especially inland.

Chapter 4

Using a Multi-Resolution Approach to Improve the Accuracy and Efficiency of Flooding Predictions

4.1 Overview

The use of unstructured meshes in ADCIRC enables a high-resolution representation of the geometry, bathymetry, and topography of the coastal region. But this does come at a heavy cost. Using a mesh that has high resolution everywhere, causes the simulations to take several hours of run-time, even on thousands of computational cores. This is especially true for meshes that describe a large extent of the coastline, like the FEMA-SAB mesh described in Chapter 3. In this chapter, we describe an approach that will provide resolution only when and where it is required.

When a storm is far out in the open ocean, predictions can be made with a mesh with an extensive coverage of the U.S. coastline but having a relatively coarse resolution that will not include extensive coastal features. As the storm approaches the coastline and the landfall location becomes more certain, the simulation will switch to a fine-resolution mesh that describes the coastal features in that region in high detail. Results will be mapped from the coarse to the fine mesh, and then the simulation will continue. This chapter begins with a description of the multi-resolution approach, including its application on a simple example test case. The technique is then applied to high-resolution hindcasts of two recent storms to impact the southeast coast of the United States. Finally, the benefits of the approach in terms of accuracy and efficiency are evaluated by comparing it to single simulations on coarse- and fine-resolution meshes.

4.2 Introduction

During tropical cyclones and other coastal storms, the greatest threat to life is storm surge, the rise of water above the normal predicted astronomical tide. In flat regions, this may lead to intrusion of the salt water 10 to 20 miles inland (Conner et al., 1957). The development and implementation of numerical models allows for the prediction of storm surge, so lives and property can be protected from future storms.

Numerical models must represent physical processes and geographical features that influence storm surge over a range of scales. Large-scale features that influence this surge include: the intensity, size, speed, and path of the storm; the general configuration of the coastline; bottom topography near the coast; and the stage of the astronomical tide (Harris, 1956; Reid et al., 1954). Small-scale features can affect the surge locally, such as convergence or divergence in bays and estuaries, local wind-setup, seiching, etc. Higher levels of resolution are required in ocean circulation models to represent: steep gradients in bathymetry like the continental shelf break (Westerink et al., 1992; Luettich et al., 1995; Blain et al., 1998; Hagen et al., 2000), wave propagation in shallow water regions (Hagen et al., 2001), and complex topography in overland regions (Westerink et al., 2008).

This complexity has led to the development of models that use unstructured meshes, so model resolution can be varied. ADvanced CIRCulation (ADCIRC) (Luettich et al., 1992; Luettich et al., 2004; Westerink et al., 2008) is a depth-integrated, shallow-water, finite-element model capable of simulating tidal circulation and storm-surge propagation over large computational domains. ADCIRC is used by FEMA in the development of flood insurance rate maps (Federal Emergency Management Agency, 2019), by the U.S. Army Corps of Engineers (USACE) for navigation and storm protection projects (U.S. Army Corps of Engineers, 2018) and also by the National Oceanic and Atmospheric Administration (NOAA) for tidal calibrations and incorporation into its vertical datum transformation software VDatum (E. Myers et al., 2007). ADCIRC uses unstructured meshes with triangular finite elements of varying sizes to represent complex coastal features, barrier islands and internal barriers. This also permits gradation of the mesh that increases feature detail when moving from the deeper ocean, onto the continental shelf, into estuaries and marshes, and over low-lying coastal floodplains.

These unstructured meshes can be large, composed of millions of elements, which is thus costly for computation. A recent study of flooding during Hurricane Ike (2008) along the Gulf of Mexico (Hope et al., 2013) used a mesh with 18 million elements to provide a detailed description of coastal floodplains of Alabama, Mississippi, Louisiana, and Texas. Element sizes varied from 20 km or larger in the Atlantic Ocean and Caribbean Sea, to as small as 20 m in channels and other hydraulic features. Although these models provide reliable and accurate results by virtue of their high-resolution description of coastal features, their simulations can be computationally expensive, requiring several hours even on thousands of computational cores (Dietrich et al., 2012). This is a challenge in forecasting applications when model predictions are required on the order of 1 hr or so, to aid emergency mangers in decision-making during a storm (Cheung et al., 2003).

Various techniques are used in the modeling community to provide fine resolution only when and where it is required, thus not dramatically increasing the cost of simulations. Adaptive Mesh Refinement (AMR) uses algorithms that dynamically refine the grids to obtain fine-scale solutions in the areas of interest. The mesh can be refined along the moving wave front for tsunami simulations (Berger et al., 2011), or refined to follow the storm for a coastal flooding simulation (Mandli et al., 2014). AMR can also be implemented by starting with a single mesh and then splitting up its elements as the simulation proceeds. This is done locally in regions that require additional resolution on account of local flow properties, using h (grid size) refinement, and/or p (polynomial order) refinement, in the case of hp finite element methods (Kubatko et al., 2006; Kubatko et al., 2009). However, while h refinement has been successful on structured grids (Mandli et al., 2014), it has not been achieved for large-domain storm surge simulations on unstructured meshes.

Nested meshes have been used for the investigation of tropical cyclones and mid-latitude disturbances and in coastal ocean applications (Ookochi, 1972; Mathur, 1974; Hovermale, 1976; Miyakoda et al., 1977; Oey et al., 1992). In ADCIRC, a one-way nesting technique called *Multistage* was tested for two small estuarine systems using an outer large-scale coarse mesh and an inner small-scale fine mesh (Taeb et al., 2019). Results indicated run-time reductions of 54% to more than 80%, with the solutions showing relatively small deviations from the conventional single-domain technique. The inclusion of a coarse representation of the estuary in the coarse mesh was seen to be critical in providing representative boundary conditions to the fine mesh. Also using ADCIRC, a related technique is subdomain modeling (Baugh et al., 2015), in which a single full-scale simulation is used as forcing to repeated simulations on subdomains with local changes. This technique has been extended to be adaptive (Altuntas et al., 2017), by adjusting boundaries in response to domain changes, to relieve users from determining the sizes and shapes of subdomain grids and provide greater performance gains. These techniques are similar in the sense that they perform a large-domain simulation to obtain boundary conditions to force a simulation on a local mesh. However, both techniques require the large-domain simulation to be completed before moving to the higher-resolution simulation.

This chapter describes a multi-resolution approach to increase the accuracy of flooding predictions and reduce the total computational cost of running unstructured-mesh, storm surge models like ADCIRC. *It is hypothesized that, by 'switching' from coarse- to fine-resolution meshes, with the resolution in the fine mesh concentrated only at specific coastal regions influenced by the storm at that point in time, both accuracy and computational gains can be achieved.* A mesh without extensive coastal detail is used when the storm is far away. As the storm approaches the region of interest, the coarse-resolution results are mapped onto a high-resolution mesh. The simulation then continues on the new mesh with highly-accurate results for that coastline. This approach is most promising for real-time forecast applications. In the following sections, we describe the mechanics of the multi-resolution approach, and then demonstrate the gains in accuracy and efficiency for representative storms.

4.3 Multi-Resolution Approach

4.3.1 Motivation

ADCIRC is employed for real-time forecasts via the ADCIRC Prediction System (APS, `https://adcircprediction.org`). A principal component is the ADCIRC Surge Guidance System (ASGS, (Fleming et al., 2008)), which automates the simulation of ADCIRC on high-performance computing clusters. During a tropical cyclone, the ASGS can: detect the forecast advisories issued by the National Hurricane Center (NHC), use a parametric vortex model to generate the atmospheric forcings, monitor the progress of multiple simulations, and post-process the model results. The forecast guidance is shared via the Coastal Emergency Risks Assessment (CERA, `https://cera.coastalrisk.live`). The APS has shared forecasts during the hurricane seasons of the past decade, and its guidance is accessed by thousands of people during storms.

The goal is to provide guidance about surge, waves, and flooding within 1-2 hours after each NHC forecast advisory. The main factors that affect this time are the ADCIRC mesh size, the time step size, the number of CPUs available, and the ability to restart from the end of a previous simulation (hot-start) (Fleming et al., 2008). To avoid longer hindcasts with each forecast advisory (as more storm information is available), the ASGS saves the state of the simulation at the nowcast point (end of hindcast). This saved state is then reloaded during the next advisory cycle to avoid having to start the simulation from the beginning. Thus, the system always builds on previous results. However, prior to the current study, these hot-starts had to be done on the same mesh. This required the use of high-resolution meshes during the entire storm, even when it was far from landfall.

As an example, consider Tropical Storm Bill (2015), which made landfall in southeast Texas. The storm developed quickly, and was designated as a tropical storm about 17 hr before its landfall (R. Berg, 2015). The ASGS started a simulation with tidal forcing on a high-resolution mesh describing the Texas coastline with 6.7 million elements. Even using 1120 cores on the world-class Stampede cluster at the Texas Advanced Computing Center, this initial simulation took 18 hr of wall-clock time. When it finished and the system was ready to produce a forecast, the storm had already moved inland, and the worst of the wave and surge impacts had passed.

The proposed approach will avoid this problem because tidal spin-up runs on such high-resolution meshes will not be required, thus saving hours of simulation time. The basic idea of the proposed multi-resolution approach can be outlined as follows. When a storm is in the open ocean, there is uncertainty where it will make landfall. At this time, predictions can be made with a mesh with an extensive coverage of the U.S. coastline but having a relatively coarse resolution that will not include extensive coastal features. As the storm approaches the coastline and the landfall location becomes more certain, the simulation will switch to a fine-resolution mesh that describes the coastal features in that region in high detail. Results will be mapped from the coarse to the fine mesh, and then the simulation will continue. This mapping will require a careful alignment between the two meshes, as well as automated scripts to interpolate variables such as water elevation and water velocity in a way that is conservative and stable. The approach, although similar to adaptive mesh refinement, does not have the difficulty of finding and populating the refined region with data during the simulation, because everything is pre-computed.

4.3.2 *Adcirpolate*

The general flow of the multi-resolution approach is given below:

1. Start with a simulation on the coarse mesh
2. Run the coarse simulation until the storm approaches the coastline
3. Map results from the coarse to the fine mesh
4. Continue the simulation on the fine mesh

The key step in this approach is the mapping of simulation data between meshes, so the forecasts can continue on a higher-resolution mesh. This mapping is done with a new technology called *Adcirpolate*, which is implemented via the Earth System Modeling Framework (ESMF, (Hill et al., 2004)). The mapping is done in two stages. First, an interpolation weight matrix is generated to describe how points in the source (coarse-resolution) mesh are related to points in the destination (fine-resolution) mesh. The values on the source mesh are then multiplied by the interpolation weight matrix to produce values for the fine mesh via a parallel sparse matrix multiplication. Interpolation is not possible to a point in the destination mesh that is not originally contained within the extents of the source mesh. It is possible for vertices to be dry in the source mesh but wet in the destination mesh, e.g. when a small channel is refined only on the higher-resolution mesh. In these cases, the vertices are tagged as wet in the destination mesh, and they start with water levels at zero in the ensuing simulation.

The data from the last time-step of an ADCIRC simulation is contained in a hot-start file (named `fort.67` or `fort.68` in the ADCIRC convention). This file includes information about surface elevation at the previous and current time-step, depth averaged velocities at the current time-step, wet/dry state of vertices and elements, etc. When the coarse simulation is complete, the fine mesh is localised into the same number of cores/directories as used for the coarse simulation. *Adcirpolate* then maps the hot-start information from the coarse mesh on to these sub-directories. Interpolation is done bi-linearly in region-destination points and extrapolation for remaining points with nearest source to destination. The wet/dry array of the fine mesh is populated by activating elements which have an intersection with another active element on the coarse mesh. The entire mapping process is done in parallel and on the same number of cores as used for the coarse and fine simulations. The mapped data in the fine sub-directories are then gathered on root and a global `fort.67/fort.68` file is written for the fine mesh. This global hot-start file is then used to continue simulation on the fine mesh.

4.3.3 Simple Example

Before the approach is applied on large meshes during real storms, its performance is first demonstrated on a simple example. We consider an idealized domain with an open coast, shallow embayment and a deep channel (Figure 4.1). The domain size is 100 m $\times$ 100 m, and a digital elevation model is used to describe the topography and bathymetry at a resolution of 0.5 m. The open coast has a constant offshore bathymetric depth of 10 m. The inlet has bathymetric depths that vary linearly to 5 m inside the back bay, which has dimensions of 40 $\times$ 30 m. The deep channel extends to a no-flow boundary at the top/north of the domain; the channel has a constant width of 10 m and bathymetric depth of 10 m.

Two meshes at varying levels of resolution were created using the Surface-water Modelling System (SMS, `https://www.aquaveo.com/software/sms-surface-water-modeling-system-introduction`). The coarser mesh has a total of 46 vertices with an average element spacing of about 20 m, whereas the finer mesh has a total of 142 vertices with an average element spacing of 10 m. Bathymetry and topography values were then interpolated onto the two meshes. The difference in resolution causes features to be represented differently between the two meshes (Figure 4.1, top-center and top-right). In the coarse mesh, the inlet to the back bay is missing, and the deep channel extends only part of its total length.

A semi-diurnal tide of amplitude 1.2 m was added to a surge signal of peak amplitude 2 m applied as forcing (Figure 4.2, top-left) on the bottom/south boundary of the two meshes. The total run duration was 54 hr. The simulation started on the coarse mesh,

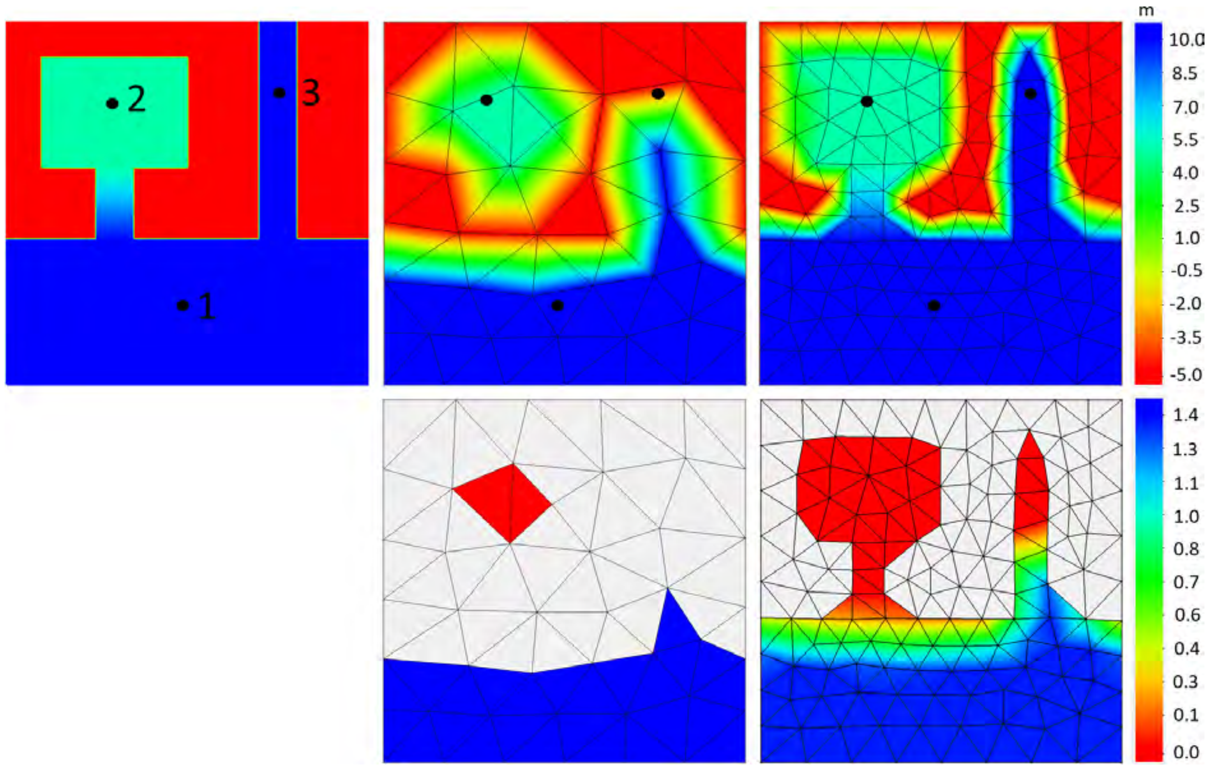

Figure 4.1 Panels showing (top row) bathymetry (m) and (bottom row) water levels (m) from the *Mixed* simulation on the example case. Columns correspond to: (left) the digital elevation model; (center) coarse mesh; and (right) fine mesh. The water levels shown are for: (bottom-center) at the end of the coarse part of *Mixed* before the switch, and (bottom-right) at the beginning of the fine part of *Mixed* after the switch. (The water levels in (bottom-center) are interpolated/extrapolated to become the water levels in (bottom-right).) Black dots indicate locations of the points where water levels are shown in Figure 4.2, and triangles indicate locations of mesh elements.

but after 24 hr, when the water level on the ocean boundary reached 1.4 m, it was switched to the fine mesh for the remainder of the run. Before switching, at the end of the simulation on the coarse mesh (Figure 4.1, bottom-center), the water levels were 1.4 m at the open coast, but the water levels were still zero in the back bay, and the rest of the mesh was dry. After switching, at the start of the simulation on the fine mesh (Figure 4.1, bottom-right), these water levels were mapped to the true coastline, extended into the inlet and deep channel, and expanded in the full back bay.

Water levels were analyzed at three stations: (1) open coast, (2) back bay, and (3) deep channel (Figure 4.1), and for three simulations: *Coarse*, *Fine*, and *Mixed*. At the

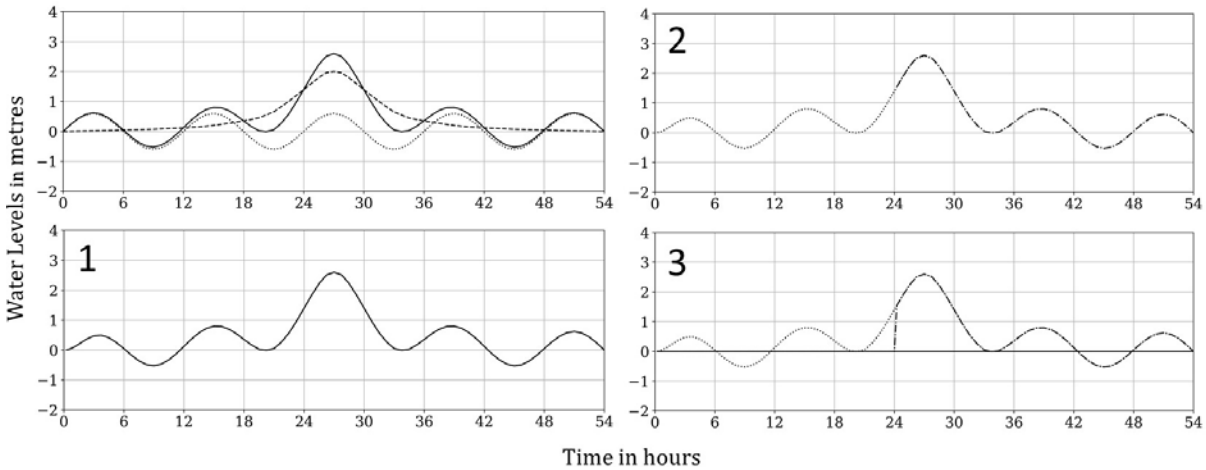

Figure 4.2 Boundary forcing (m) and water levels (m) for the simple example. On the top-left is the variation in input forcing with line types corresponding to (dotted) tides-only, (dashed) surge-only, and (solid) tides plus surge. The other three plots indicates time-series of water levels (m) at the three locations shown in Figure 4.1 with line types corresponding to: (solid) *Coarse*, (dotted) *Fine*, and (dashed-dotted) *Mixed*.

open coast (station 1), there was no difference between the simulations, because both meshes had a sufficient resolution in open water to represent the combined tide and surge forcing. At the back bay (station 2), the water levels are zero for all simulations on the coarse mesh (*Coarse* and first 24 hr of *Mixed*), and in the deep channel (station 3), the station was dry for the same simulations. However, very shortly after the switch, the water levels in *Mixed* were raised to match *Fine*. This was an increase of 1.4 m in just 0.25 hr, with no oscillations or instabilities in the computed solution. Thus, even when the *Coarse* simulation had locations that were dry or had zero water levels, the *Mixed* simulation was able to 'catch up' to the *Fine* results.

4.3.4 Goal and Objectives

In this manuscript, we describe and evaluate the implementation of this multi-resolution approach for simulations of coastal flooding along the U.S. coast. The goal of the proposed approach is to improve the efficiency (via a smaller wall-clock time) of storm surge predictions, while maintaining accuracy in complex coastal regions. The objectives can be summarized as:

1. Implement the approach for hindcasts of two recent storms that impacted different

regions of the U.S. Atlantic coastline in different ways.

2. Quantify the benefits in accuracy, via water level comparisons with single simulations on coarse- and fine-resolution meshes.

3. Quantify the benefits in efficiency, via run-time comparisons with single simulations on coarse- and fine-resolution meshes.

4.4 Methods

In this study, we hindcast for two storms, each having different parameters like track, intensity, flooding extent, etc. For each storm, we perform three simulations: (1) *Coarse*, (2) *Fine*, and (3) *Mixed*. The results from these simulations are then analyzed to quantity the benefits of the proposed approach. In this section, we describe the storms, the wind and pressure fields used as model forcing, the unstructured meshes used to represent geographic features, and how the results were analysed.

4.4.1 Historical Storms

The proposed approach is tested on two storms: Matthew (2016), and Florence (2018). Matthew was a Category-5 hurricane that caused widespread impacts all along the U.S. southeast coast, and made landfall with Category-1 intensity along the central coast of South Carolina during October 2016 (Stewart, 2017). Florence was a Category-4 hurricane that made landfall along the southeastern coast of North Carolina during September 2018 (Stewart et al., 2019), and caused significant storm surge flooding in eastern North Carolina. The impacts of these storms on water levels along the U.S. southeast coast has been discussed in detail in the previous chapters. These storms were selected because of their varied landfall locations, tracks, and other parameters. Matthew's track was shore-parallel from Florida to North Carolina, and Florence's tracks were shore-normal. They also had variations in parameters including track orientation to shoreline, intensity of winds, duration, size, etc. These storms also impacted regions described by the HSOFS and FEMA-SAB meshes at different levels of resolution. The proposed approach will be tested in these two cases to demonstrate its capability for any storm.

4.4.2 Simulation Settings

This chapter will consider hindcasts of the two storms by using data-assimilated surface pressure and wind velocities from Oceanweather Inc. (OWI), and using ADCIRC version 54.dev. The details regarding these wind fields have been described in the previous chapters for both Matthew and Florence, and therefore not presented here. The ADCRIC run-settings are the same as in Chapter 2 for the HSOFS or coarse-mesh simulations, and as in Chapter 3 for the FEMA-SAB or fine-mesh simulations. As the proposed approach is yet to be applied on the coupled ADCIRC+SWAN model, the simulations in this chapter will be done using just ADCIRC, and hence the predictions will not include wave effects.

4.4.3 Unstructured Meshes

ADCIRC uses unstructured, finite-element meshes to describe the coastal ocean. In this study, we use a coarse-resolution mesh with coverage of the entire U.S. coast, as well as a fine-resolution mesh with higher resolution along the U.S. southeast coast.

4.4.3.1 Coarse-Resolution Mesh

The proposed method will require a base mesh on which simulations will be performed for daily, non-storm conditions, as well as for storms as they develop far from shore. This base mesh will be coarse, but its simulations will be used as the source for mapping and continuing the forecast simulations on a fine-resolution mesh with coverage of coastal floodplains in the region near the expected storm landfall. The HSOFS mesh is the coarse-resolution base mesh due to its extensive coverage of nearshore regions and coastal floodplains along the entire U.S. coast from Texas through Maine.

4.4.3.2 Fine-Resolution Mesh

After a storm's track is certain, simulations will be continued on meshes with high-resolution coverage of the landfall region. The FEMA-SAB mesh is used as the high-resolution mesh in this study as it has detailed coverage of the coastal floodplains from FL to NC, which represent the impacted areas from Matthew and Florence.

4.4.4 Error Statistics

The agreement between the observations and predicted results is quantified using error metrics like root-mean-squared error (E_{RMS}), mean normalized bias (B_{MN}), coefficient of determination (R^2) and best-fit slope (m), like in the previous chapters. The efficiency of the approach is evaluated by comparing its wall-clock time to that of the *Fine* simulation. For the approach, a total of the times required for the coarse part of the simulation, *Adcirpolate*, and the fine part is taken for comparison. To avoid any inconsistencies with run-times due to different types of cores and/or hardware being used, each simulation is run three times on the same number of cores. The minimum of the three run-times is then taken as the final value for comparisons.

4.4.5 Validation of Fine Meshes

The accuracy of the multi-resolution approach will be evaluated by comparing its predicted water levels to that from the corresponding *Fine* simulation. The FEMA-SAB mesh is therefore validated for ADCIRC simulations of Matthew and Florence. Observations of water levels and high-water marks (HWMs) were collected (Thomas et al., 2019), covering FL to NC for Matthew and NC for Florence. Observations were omitted that did not record the storm peak or that showed elevated water levels after the storm due to freshwater run-off or wave run-up. Comparisons were made only at locations that were wetted by ADCIRC. Thus a total of 580 locations for Matthew and 190 locations for Florence were used in the analysis (Figure 4.3). For Matthew, the errors in modeled peaks were within 10 percent at 316 (55 percent) stations and within 25 percent at 479 (83 percent) stations. For the scatter plots, the $R^2 = 0.78$, and the slope of the best-fit line was $m = 0.93$ (Table 4.1). For Florence, the errors were within 10 percent at 93 (49 percent) stations and within 25 percent at 181 (95 percent) stations. The correlation and best-fit line slope were $R^2 = 0.91$ and $m = 0.95$, respectively. For both storms, the FEMA-SAB mesh had an E_{RMS} less than 0.3 m and a negative value of B_{MN}, indicating an under-prediction of the peaks overall.

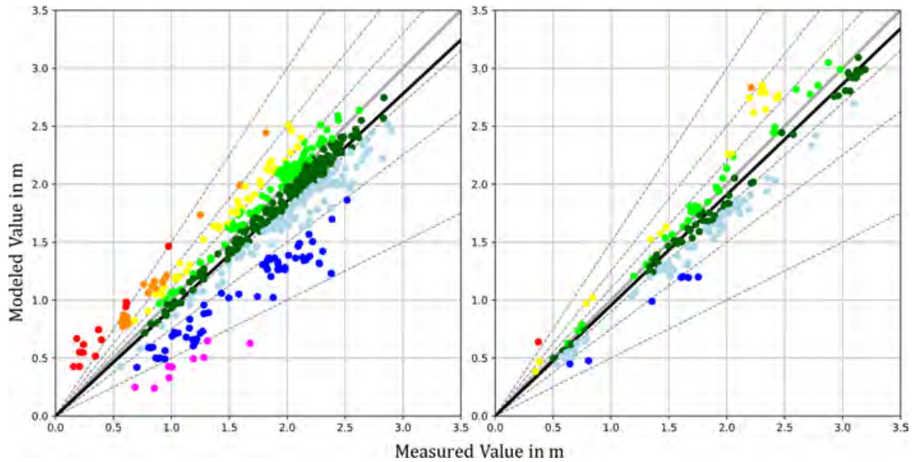

Figure 4.3 Scatter plots of HWMs and peak hydrograph values during Matthew (left) and Florence (right) on the FEMA-SAB mesh. The points are color-coded based on error (predicted less observed) expressed as percentage of the observed value. Warm colors indicate regions of over-prediction by ADCIRC, whereas cooler colors indicate regions of under-prediction. Green points indicate errors within 10%; yellow and light blue indicate errors between 10% and 25%; orange and dark blue indicate errors between 25% and 50%; and red and purple indicate errors over 50%. The thick gray and black lines represent $y = x$ and best-fit lines, respectively. Statistical metrics are shown in Table 4.1.

Table 4.1 Error Metrics for the *Fine* and *Mixed* Simulations

	Fine		*Mixed*	
Error	Matthew	Florence	Matthew	Florence
Stations	580	190	580	190
Best-Fit Slope	0.93	0.95	0.93	0.95
R^2	0.78	0.91	0.77	0.90
E_{RMS} (m)	0.29	0.22	0.29	0.23
B_{MN}	-0.07	-0.05	-0.06	-0.06

4.5 Results and Discussion

4.5.1 Storm Simulations and Switching Parameters

For each storm, three simulations are done: *Coarse*, *Mixed* and *Fine*. For the *Mixed* simulations, the HSOFS mesh is used when the storm is away from a coastline and its path is uncertain. As the landfall location becomes more certain, we switch to the high-resolution mesh for that region. The switching times for these simulations were determined from time series of water levels at locations along the coastline. The idea is to identify the time at which the total water levels become larger than the normal tidal levels. For example, for a storm like Matthew that approached the U.S. southeast coastline from the south, switching is done when tidal gauges in FL indicated an increase in normal tidal levels. When the *Mixed* simulation is complete, the maximum water levels are compared to that from the corresponding *Fine* simulation. An ideal switching time would result in near-zero differences in water levels overall (and thus a minimal loss in accuracy), and be as late as possible (and thus a maximum gain in efficiency). The run duration and the switching times for the *Mixed* simulations, for both storms are given in Table 4.2.

Table 4.2 Switching times for Matthew and Florence

		Run Duration (days)		
Storm	Simulation Date	Coarse	Fine	Total
Matthew	Oct 2-Oct 11, 2016	4.5	4.5	9
Florence	Sept 7-Sept 16, 2018	6	3	9

But prior to this primary coastal surge, water levels during a storm can increase several hours before landfall, e.g. the forerunner surge before Ike (Kennedy et al., 2011). Thus there is a need to explore parameters other than water levels, to be used as possible triggers for switching between meshes. Whenever a subtropical storm occurs, the NHC issues tropical cyclone advisories at-least every 6 hours. These contain information about the date/time and location of the center of the storm, direction and speed of the storm's forward motion, lowest atmospheric pressure, maximum sustained wind speeds with maximum gust speed, diameter of the storm's eye, the radii of the maximum wind in four quadrants (NE, SE, SW, and NW) in three categories($\geq$ 64 kt, $\geq$ 50 kt, and $\geq$ 34 kt), etc. If we can utilize any of these parameters to trigger switching, then the approach can easily be replicated during real-time forecasting. The use of radius of the 34-, 50-, and 64-kt isotachs is discussed herein. Although this section will only discuss the use of these radii during Florence, Table 4.3 gives these values for both storms.

On 0000 UTC 13 September 2018 (about 36 hours before landfall), the effects of Florence were not yet felt on the NC coastline, as indicated by normal tidal water levels

Table 4.3 Distance to wind isotachs (km) at switching

Storm	Distance to Isotach (km) 34 kt	50 kt	64 kt
Matthew	170.77	279.57	307.78
Florence	252.83	342.41	466.60

at real time gauges. At this time, the storm's eye was located about 477 km off the Hatteras Inlet (Figure 4.4). From a location where the effects of the storm was seen on water level hydrographs for the first time, distances are calculated to the 34-, 50-, and 64-kt isotachs. Although the radii of maximum winds for these isotachs can vary from storm to storm, these distances gives an approximate idea of when switching should be done to a fine resolution mesh, irrespective of the storm-size. While this study did not use these distances as criteria for switching, we document these values so that they may be used for future reference.

4.5.2 Accuracy Benefits

The accuracy of the *Mixed* simulation is evaluated relative to that from the *Fine* and *Coarse* simulations. For an ideal switching time, there should not be any loss in accuracy in the *Mixed* results, as compared to that from the *Fine* simulation. At the same time, its results should also have a much higher degree of accuracy as compared to that from the corresponding *Coarse* simulation.

4.5.2.1 Comparison to Validation Data

Before we analyze accuracy gains using the approach, it is important to demonstrate that there is no major loss in accuracy as compared to *Fine* results. The *Mixed* results are first validated against the same observations of water levels and HWMs as in Section 4.4.5. Then, these validation data are compared to that from the *Fine* mesh (Table 4.1). We analyze the maximum water levels for the entire hindcast, to evaluate the flooding magnitude and extent. To consider the maximum water levels for the *Mixed* hindcast, we consider the overall maxima of both its coarse and fine segments.

For Matthew, for the 580 total locations from FL to NC, the errors in modeled peaks from the *Mixed* hindcast were within 10 percent at 319 (55 percent) stations and within

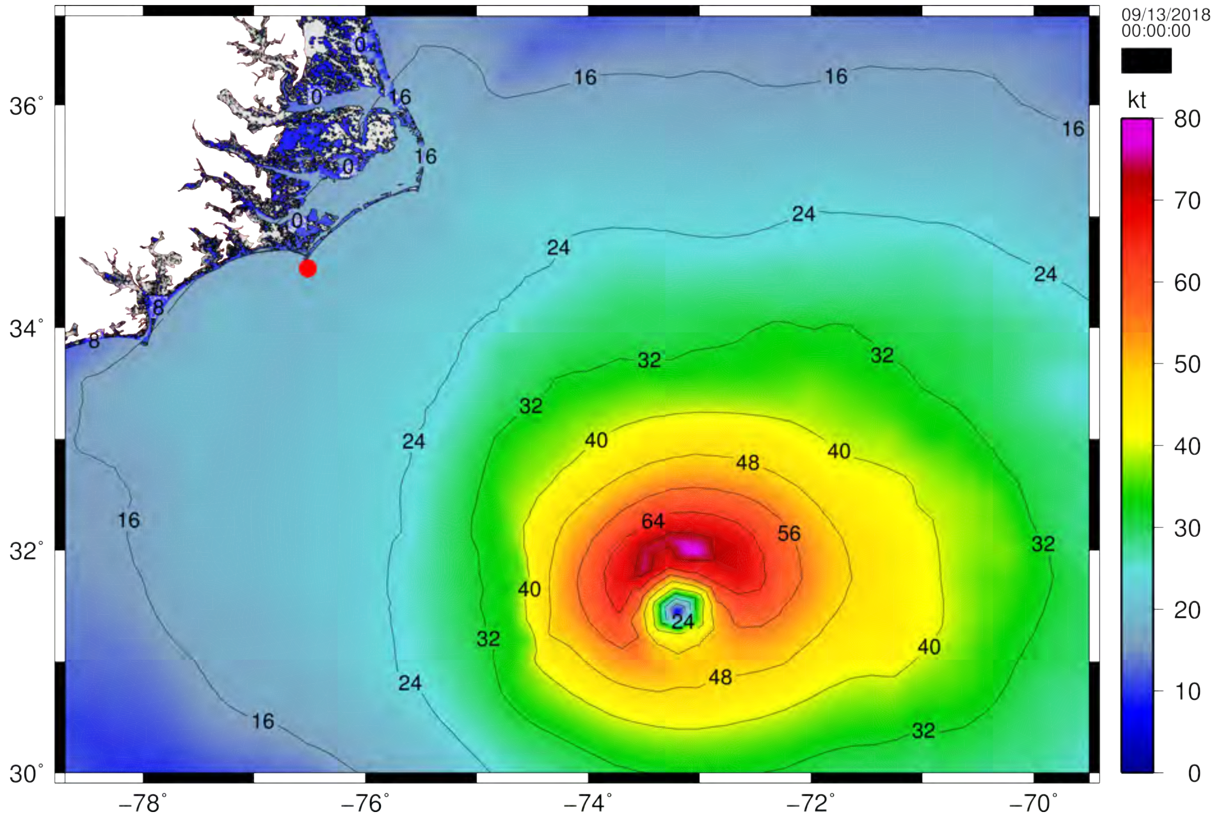

Figure 4.4 Contours of wind speeds (knots) during Florence along the NC coast. The time corresponds to 0000 UTC 13 September 2018 (36 hours before landfall), when switching between the coarse and fine meshes was done in the *Mixed* approach. Red dot indicates the point used to calculate distances to the maximum wind isotachs in Table 4.3

25 percent at 479 (83 percent) stations. For the scatter plots, the $R^2 = 0.77$, and the slope of the best-fit line was $m = 0.93$ (Table 4.1). For Florence, for the 180 locations in NC, the errors were within 10 percent at 93 (49 percent) stations and within 25 percent at 176 (93 percent) stations. The correlation and best-fit line slope were $R^2 = 0.90$ and $m = 0.95$, respectively. For both storms, the *Mixed* results had a E_{RMS} of less than 0.3 m and a negative value of B_{MN}, indicating an under-prediction of the peaks overall.

These *Mixed* results are now compared to the corresponding *Fine* validation data in Table 4.1. For both Matthew and Florence, the error metrics (R^2, slope of best-fit line, E_{RMS}, and B_{MN}) for the *Mixed* and *Fine* simulations match really well. The differences are in the second decimal (in R^2 and B_{MN} for Matthew, and in R^2, E_{RMS} and B_{MN} for Florence), and are negligible when accounting for the possible savings in total run-times

Table 4.4 Errors from simulations with coarse and mixed meshes, compared to a simulation on the fine mesh.

	Matthew		Florence	
Error	Coarse	Mixed	Coarse	Mixed
Stations	1,981,764	2,664,921	182,289	264,812
Best-Fit Slope	0.99	1.0	0.95	1.0
R^2	0.91	0.96	0.86	0.90
E_{RMS} (m)	0.22	0.13	0.22	0.18
B_{MN}	-0.01	0	-0.05	0

as compared to the corresponding *Fine* simulation. Thus the *Mixed* approach retains the accuracy of the *Fine* simulation, without having to run the fine mesh for the entire storm duration.

4.5.2.2 Comparison to ***Fine*** Maximum Water Levels

The accuracy of the *Coarse* and *Mixed* results are also analyzed by comparing them to the *Fine* solution. This subsection evaluates the gain in accuracy of the *Mixed* approach as compared to the *Coarse* simulation, by validating the modelled results from both against *Fine* results.

The same error metrics as in the previous sections are calculated for both the *Coarse* and *Mixed* simulations. However, instead of comparison to observations, the *Fine* maximum water levels is taken as the "truth" (Table 4.4). This allows for an evaluation of accuracy throughout the entire region, not only where the observations were collected. For this comparison, the *Coarse* results are mapped onto the fine mesh as a post-processing step, so comparisons are made at the same number of vertices. For the *Mixed* approach, a maximum of water levels from the coarse and fine parts of the simulation are taken. Results are compared only at vertices in the affected area of the storm (FL to NC for Matthew, NC for Florence), that are not in open-ocean (depths less than 10 m), and that were wetted in both simulations.

For both Matthew and Florence, the *Mixed* results have a B_{MN} equal to 0, whereas the *Coarse* results have a negative value indicating an overall under-prediction by the model. The *Mixed* solution also have a best-fit line slope equal to 1, indicating a good fit to the fine results. The E_{RMS} (closer to 0) and R^2 (closer to 1) are also better. But the most interesting difference lies in the number of stations that were used for comparison.

For both storms, the *Mixed* simulation has comparisons made at a much higher number of vertices (about 680K more vertices for Matthew and 82K for Florence), indicating much more wetting of vertices as compared to the *Coarse* simulation. The considerably larger number for Matthew is due to the larger region of analysis (FL to NC), as compared to just in NC for Florence. These extra vertices are located in the wetting-drying regions of the model like barrier islands, sounds, etc., and also high up in the rivers. Thus, in addition to the gain in accuracy, the *Mixed* approach also have a much larger flooding coverage, something that can be crucial during forecasting.

4.5.2.3 Global Comparisons of Flooding

Having quantified the increase in the number of vertices that were flooded in the *Mixed* simulation as compared to the *Coarse* results, this subsection examines where these vertices are located. This is done for Hurricane Florence as an example, via difference maps of maximum water levels between the *Coarse*, *Mixed*, and *Fine* simulations,. Comparisons are made at the fine mesh resolution by mapping the *Coarse* and *Mixed* results to the fine mesh. As an example, Figure 4.5a shows the difference in maximum water levels between the *Coarse* and *Fine* simulations. The values indicate how the maximum water levels at a location in the coarse mesh compare to the same location in the fine mesh, including locations where the coarse mesh was wet and fine mesh was dry. Locations where the coarse mesh was dry but fine mesh was wet are show in grey.

Compared to the *Coarse* results, the *Fine* water levels are higher in regions like the Albemarle Sound, Atlantic Intracoastal Waterway, Core Sound and up-stream all major rivers (Figure 4.5a). This is attributed to the higher resolution in the fine mesh that allows in a better representation of bathymetry, and in turn, a better hydraulic connectivity for water to flow into these complex regions. In the coarse mesh, the coarser resolution forces the water that cannot flow up into the rivers to pile up, resulting in larger water levels a little below upstream. There are almost zero differences in the open ocean, along the coast and in the Pamlico Sound.

The differences between the *Coarse* and *Mixed* results are very similar (Figure 4.5b), as switching has happened well before the storm impacted the NC coast. This is confirmed by almost-zero differences in water levels between the *Mixed* and *Fine* results, everywhere (Figure 4.5c). Small differences exists in the upper-left region of the domain far away from the storm's impact. These differences are contributed by the coarse

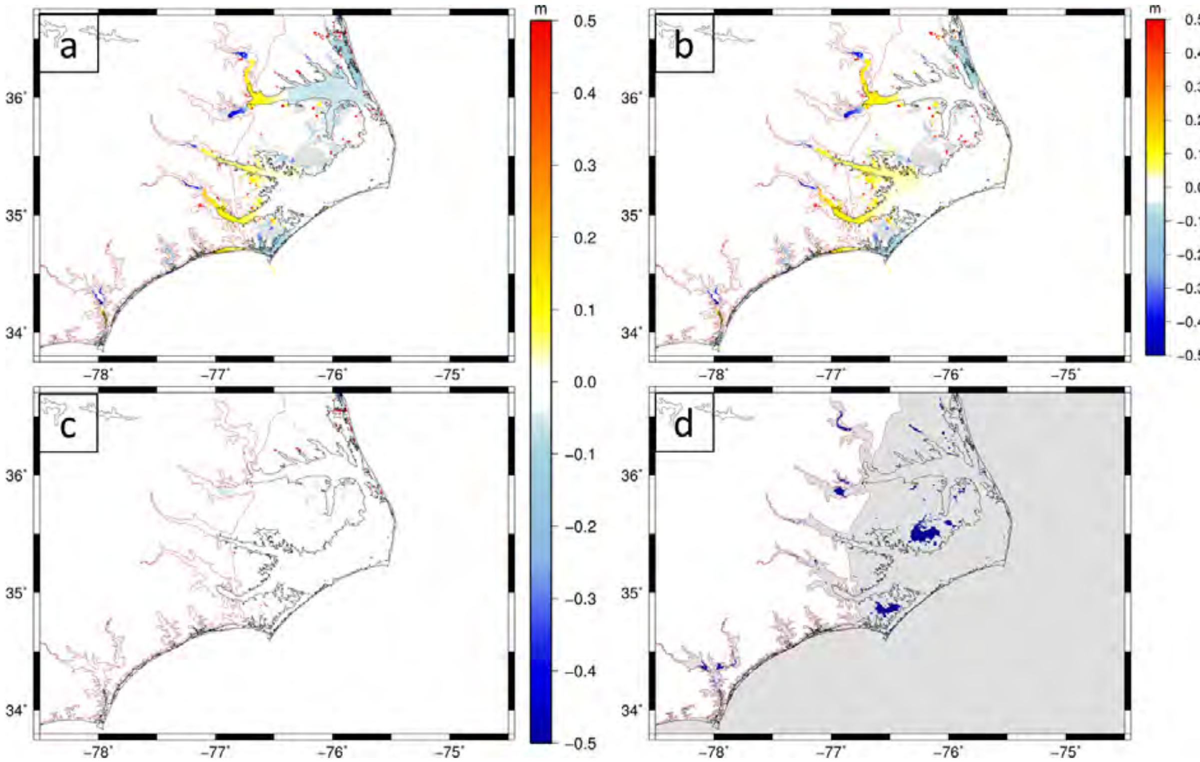

Figure 4.5 Difference in maximum water levels (m) between: (a) *Coarse* and *Fine*, (b) *Coarse* and *Mixed*, (c) *Mixed* and *Fine*, and (d) *Coarse* and *Mixed*, but only locations where the *Coarse* was dry and *Mixed* was wet. The coastline is shown in black and the fine-mesh boundary in brown.

part of the *Mixed* simulation due to the large difference in resolution between the coarse and fine mesh. The advantage of using the *Mixed* approach is evident at points that were dry during the *Coarse* simulation but were wetted in the *Fine* simulation (Figure 4.5d). These additional wetted vertices are located along the wetting-drying regions as well as upstream rivers, where the coarse mesh does not have sufficient resolution. Thus the *Mixed* approach allows for a more accurate flooding in terms of matching the *Fine* solution, as well as a much larger flooding extent as compared to the *Coarse* results.

These trends in the difference in flooding extent between the *Coarse*, *Mixed*, and *Fine* simulations are supported by the total volume of inundation (Table 4.5). For an element, this volume is equal to the area of the element multiplied by the average height of water in the three vertices. An element contributes to the total volume only if all the three vertices: (1) have a negative z value (topography), (2) lie in the affected area of

Table 4.5 Inundation Volume from maximum water levels

	Volume of Inundation x 10^9 (m^3)		
Storm	Coarse	Mixed	Fine
Matthew	3.66	5.21	5.27
Florence	0.98	1.60	1.64

the storm, and (3) were flooded during the simulation. For all storms, the *Mixed* and *Fine* simulations have comparable values, thus proving the effectiveness of the approach in matching the *Fine* simulation flooding extent. The *Coarse* simulation on the other hand, has a much lesser total volume as it floods lesser number of elements and lacks the flooding extents of both the *Mixed* and *Fine* simulations.

4.5.2.4 Comparisons at Inland Locations

Having compared the global trends in maximum water levels from the *Coarse*, *Mixed*, and *Fine* simulations during Florence, this subsection will analyze time series of water levels at a localized region, this time for Matthew. This should highlight the accuracy benefits of the approach as these are the regions where a higher resolution in the fine mesh should make a difference. For Matthew, water levels are compared at 3 locations along the Savannah River on the GA-SC border (Figure 4.6). Looking at the topo-bathy of this region in the coarse and fine meshes (Figure 4.6, left), it is clear that Stations 1 and 2 are located higher up the river where the coarse mesh does not have sufficient resolution. This is reflected in the model outputs as well (Figure 4.6, right). At Stations 1 and 2, the *Mixed* results do not capture a proper tidal signal before the switch, something that the fine mesh is able to do. But once the switching happens, the *Mixed* and *Fine* results match really well. At Station 3, both meshes have sufficient resolution, and hence the *Coarse* and *Mixed* results are a good match before and after the switch.

The difference in maximum water levels between the *Coarse* and *Mixed* simulations at this location shows the same trend as seen globally during Florence in the section above (Figure 4.7). The *Coarse* simulation results in increased flooding closer to the coastline due to water piling up, whereas the *Mixed* simulation allows more flooding into the estuaries, tidal and flood plains due to its better representation of topography and bathymetry. Thus the approach is beneficial in accurately predicting water levels at stations well inland where the coarse mesh does not have good topo-bathy representation.

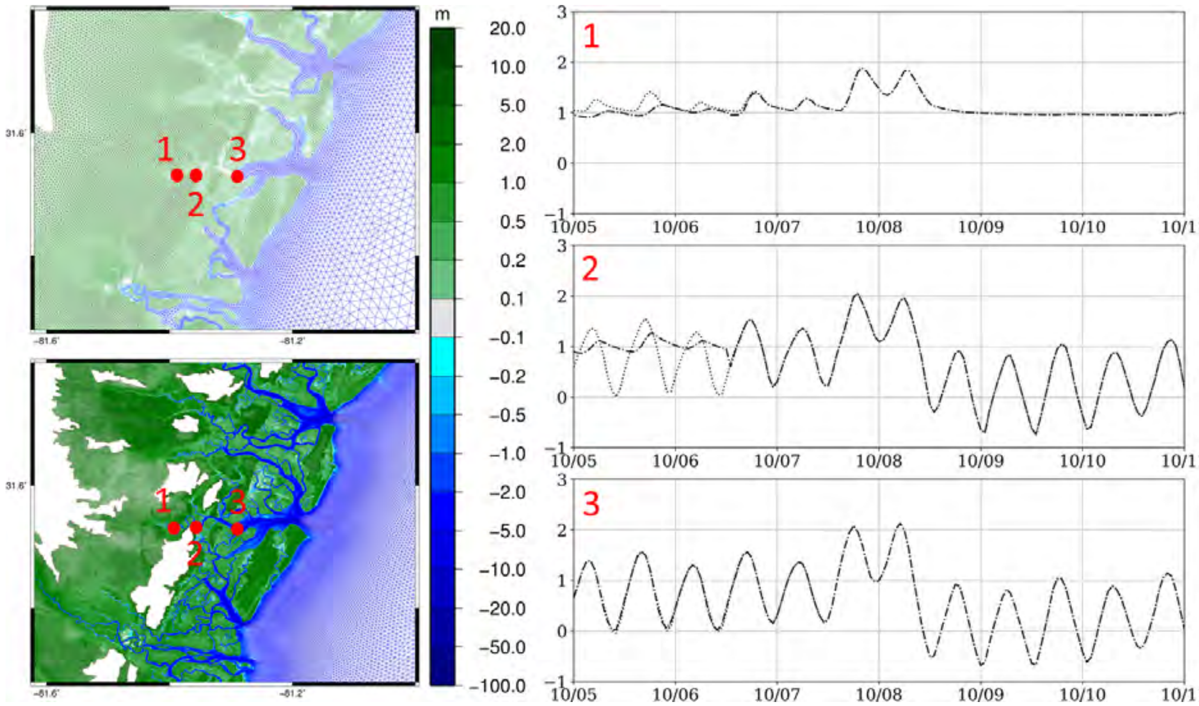

Figure 4.6 Columns correspond to: (left) Bathymetry and topography in the coarse (upper) and fine (bottom) meshes; and (right) Time Series of water levels (m) at the 3 locations indicated by red dots, with line types corresponding to: (solid) *Coarse*, (dotted) *Fine*, and (dashed-dotted) *Mixed*.

4.5.3 Performance Benefits

Having evaluated the accuracy benefits of the approach, this subsection looks at the gains in efficiency in terms of wall-clock time. For both storms, the total time required for the *Mixed* simulation is compared with that for the corresponding *Fine* simulation. For the *Mixed* approach, the total time required for the coarse part of the run, *Adcirpolate*, and fine part of the simulation is used for comparison. All simulations for Matthew and Florence were done on the Stampede2 computing cluster at the Texas Advanced Computing Center, on a total of 532 cores (including 10 writer cores). This helps in avoiding any inconsistency associated with the difference in the type of hardware or number of cores.

For both Matthew and Florence, the total simulation times for the *Mixed* and *Fine* simulations are given in Table 4.6. For Matthew, the full 9-day simulation on the FEMA-SAB mesh took 393 minutes, whereas the *Mixed* approach took a total of 243 minutes

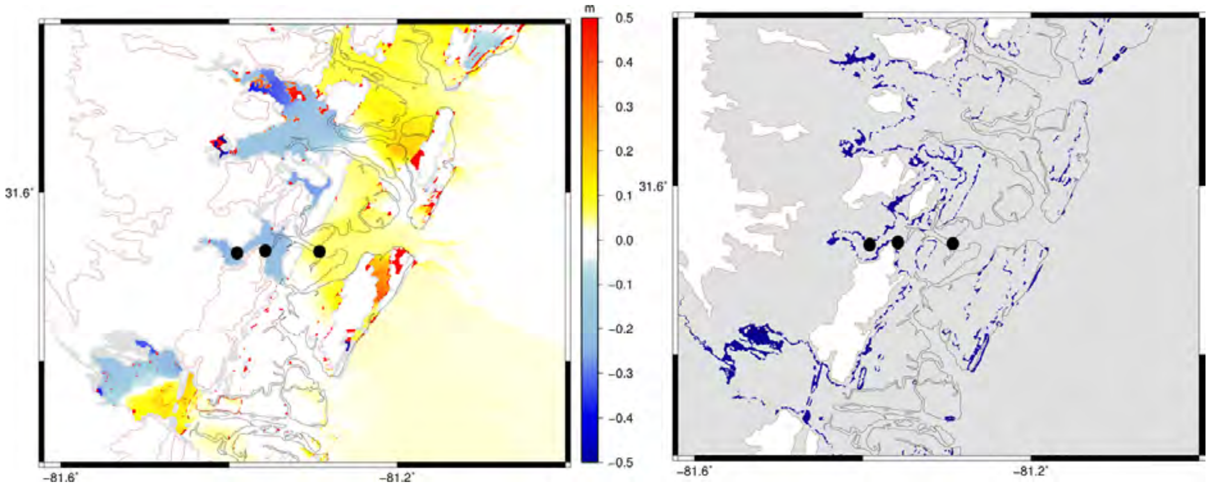

Figure 4.7 Columns correspond to: (left) Difference in maximum water levels (m) between *Coarse*; and *Mixed* and (right) Only locations where the *Coarse* was dry and *Mixed* was wet. The coastline is shown in black and the fine-mesh boundary in brown. Black dots indicates the locations of the three points in Figure 4.6

Table 4.6 Comparison in simulation wall-clock times between the *Mixed* and *Fine* simulations

	Run time in minutes				
	Mixed				Fine
Storm	Coarse	*Adcirpolate*	Fine	Total	
Matthew	29	12	202	243	393
Florence	37	12	129	178	380

only. The time to switch from the HSOFS to the FEMA-SAB mesh after 4.5 days in the the *Mixed* approach was 12 minutes. For Florence, the full 9-day simulation on the FEMA-SAB mesh took a total of 380 minutes, whereas the *Mixed* approach took a total of 178 minutes only. The time to switch from the coarse to fine mesh after 6 days in the *Mixed* simulation took the same 12 minutes, as the meshes and number of cores remained unchanged.

Compared to the *Mixed* approach, the *Fine* simulation requires an additional 2.5 hours for Matthew, and and an additional 3 hours for Florence. Thus the *Mixed* simulation has a time savings of 38% for Matthew and 53% for Florence. The lesser reduction in time for Matthew is attributed to the fact that it was a shore parallel storm that affected a large geographical extent, and lasted for several days. The *Mixed* approach therefore required the fine mesh to be used for a longer time, as compared to its application during a shore-normal storm like Florence. This reduction in simulation time by several hours, can be crucial, especially in forecasting applications where multiple scenarios can be tested to account for uncertainties in storm parameters.

4.6 Conclusions

ADCIRC simulations can be computationally costly. A simulation with a high-resolution mesh, describing a large extent of the coastline and for the entire duration of a storm, can take several hours even on thousands of computational cores. This is not ideal, especially during forecasting applications, where the emergency managers require predictions of flooding as quickly as possible. A multi-resolution approach that allows the use of high-resolution meshes only when it is required, was implemented in the ADCIRC modelling system. When the storm is far away, simulations can be done on a mesh with a coarse description of the coastline. As the storm approaches the coast, the system can switch to a high-resolution mesh that describes the coastline in great detail. Results are then mapped from the coarse to the fine mesh, and the simulation is continued on the fine mesh.

The approach was tested in the case of two storms that impacted the U.S. southeast coast in different ways. The benefits of the approach were evaluated in terms of accuracy and efficiency by comparisons to single-simulations on coarse- and fine- resolution meshes. For both Matthew and Florence, the *Mixed* approach retains the accuracy of the *Fine* results, but it floods a larger region as compared to the corresponding *Coarse* simulation. This extra flooding coverage is at regions like barrier islands, up-stream rivers, etc., where the coarse mesh does not have sufficient resolution to provide the required hydraulic connectivity for flooding to occur. But the main benefit of the approach comes in terms of wall-clock time. The multi-resolution approach enables a time savings of more than 2.5 hours (38%) in case of Matthew, and more than 3 hours (53%) during Florence, as compared to the corresponding *Fine* simulation. This efficiency gain is crucial as it allows for ensemble possibilities during forecasting to reduce the uncertainty associated with storm advisories, at the same time providing faster predictions that can help emergency managers in taking necessary precautions during a hurricane.

Chapter 5

Optimizing the Multi-Resolution Approach by Exploring Criteria for Switching Between Meshes

5.1 Overview

The multi-resolution approach described in the previous chapter is applied again to high-resolution hindcasts of Hurricane Matthew. The objective here will be to explore how best to apply the approach, given the best-available, post-storm information about the storm's track, size, intensity, speed, and other critical parameters. Rather than using just one switch from the coarse mesh to the fine mesh with the same coverage, multiple switches using fine-resolution meshes with smaller coverages will be done to achieve maximum gains in efficiency. We will explore questions about which combinations of coarse- and fine-resolution meshes should be used, which storm and surge parameters should be used to trigger switching between the fine-resolution meshes, and what gains in accuracy and efficiency can be achieved. First, this concept is tested on smaller meshes that are developed from HSOFS using state boundaries as guidelines. Then the same principle is applied on the finer FEMA-SAB mesh by creating component meshes, but this time using watershed boundaries as guidelines. These smaller meshes are used to switch from one mesh to another as Matthew moved from south-to-north along the U.S. southeast coast. The aim will be to achieve an optimal balance between accuracy and efficiency.

5.2 Motivation

The evolution of water levels during Hurricane Matthew has been well-described (Chapter 2). The shore-parallel storm moved from south-to-north, causing elevated water levels along the U.S. coast from Florida through North Carolina. But it did not affect this entire region at the same time. Instead, the effects moved with the storm. When Matthew was offshore of Florida, it caused elevated water levels and coastal flooding along the Florida coast, but it did not yet affect North Carolina. And conversely when Matthew was offshore of North Carolina, its effects had already receded in Florida. Thus, this storm will be a good test of the multi-resolution approach, as we will want to apply the highest spatial resolution only in regions as they are impacted by the storm.

As a possible example of its application, consider a division of the southeast U.S. Atlantic coast into three regions: the East-FL coast, the GA-SC coast, and the NC coast. The storm effects were recorded as water level observations along these extents (Figures 5.1 and 5.2). For East-FL, the NOS 8722670 station at Lake Worth Pier gives the first indication of Matthew's impacts on water levels along the U.S. coast. On 1500 UTC 06 October (T1), this gauge recorded 0.53 m above NAVD88, which is a little greater than its normal high-tide level. The storm-effects along the east-FL coast lasted until about 1900 UTC 08 October (T4) as seen at the NOS 8720030 gauge at Fernandina Beach.

For GA-SC, the storm's impact on water levels along this coastline can be first observed on 0800 UTC 07 October (T2) at the USGS-PERM 02228295 at Cumberland Sound, Georgia. On 1200 UTC 09 October (T5), the water levels returned to normal at the USGS-PERM 02110777 located along the Intracoastal Waterway at Nixons Crossroads, SC. For NC, the storm's impact was first recorded around 0200 UTC 08 October (T3) as visible from observations at USGS-STS NCBRU00014, and lasted until about 2000 UTC 10 October (T6) as seen at NOS 8652587 station at Oregon Inlet Marina. These divisions (East-FL, GA-SC, NC) are arbitrary, but they illustrate how this coastline can be segmented by using the water-level response at real gauges.

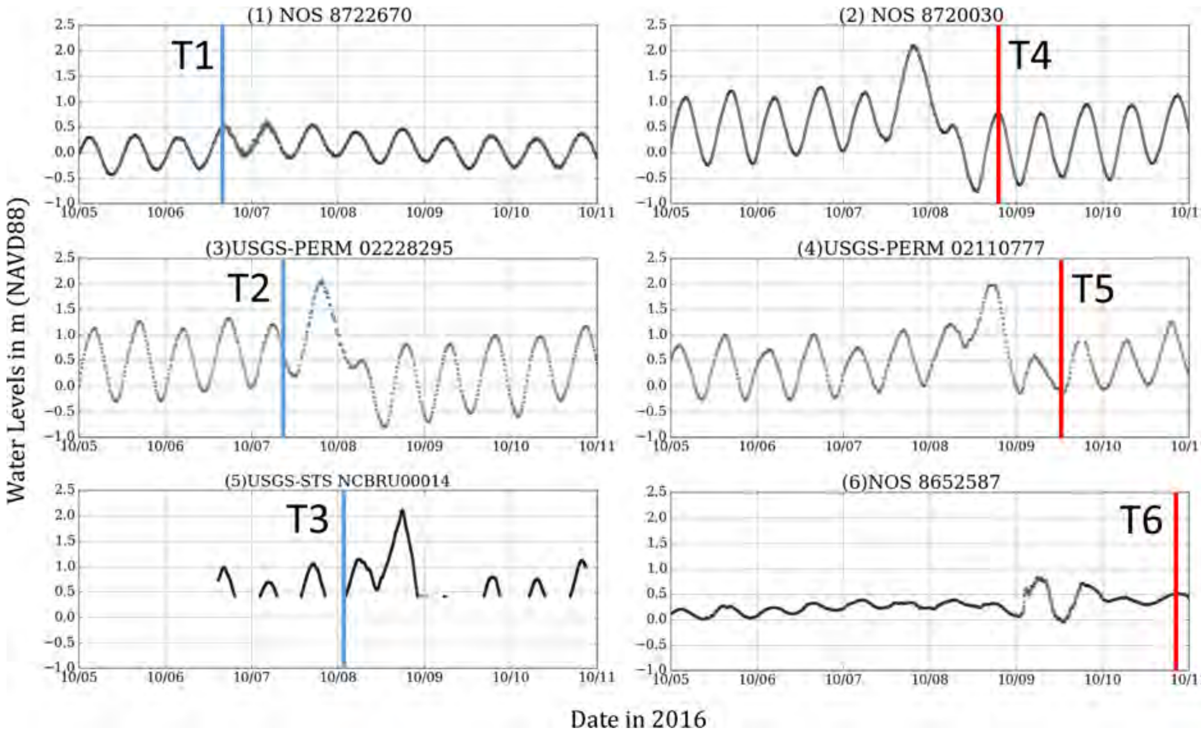

Figure 5.1 Time series of water levels (m relative to NAVD88) at 6 locations along the US coastline (south to north) during Matthew. Rows correspond to: (top) stations on East-Florida coastline; (center) stations along the GA-SC coastline; and (bottom) stations along the NC coastline. Columns correspond to: (left) station where the impact of the storm was first recorded; and (right) station where the impact was last recorded on that particular coastline. Observed values are shown with gray circles. Blue and red lines indicate the starting and ending time of storm's impact on water levels along that particular coastline respectively.

5.3 Research Hypotheses and Objectives

Thus, the impacts of Matthew were felt at different regions of the U.S. southeast coast at different days/times. To predict these impacts, we can use one switch between the coarser HSOFS mesh and the high-resolution FEMA-SAB mesh with excellent coastal detail along the entire region, like in Chapter 4. However, this would be costlier due to lengthy run-times, even on thousands of computational cores. And it would be unnecessary for a storm like Florence, which impacted a relatively-smaller region. For these and other storms, resolution should be provided only when and where it is required. *It is hypothesized that, by applying smaller high-resolution meshes that describe specific regions of the U.S. southeast coast as they are affected by Matthew, the predictions can*

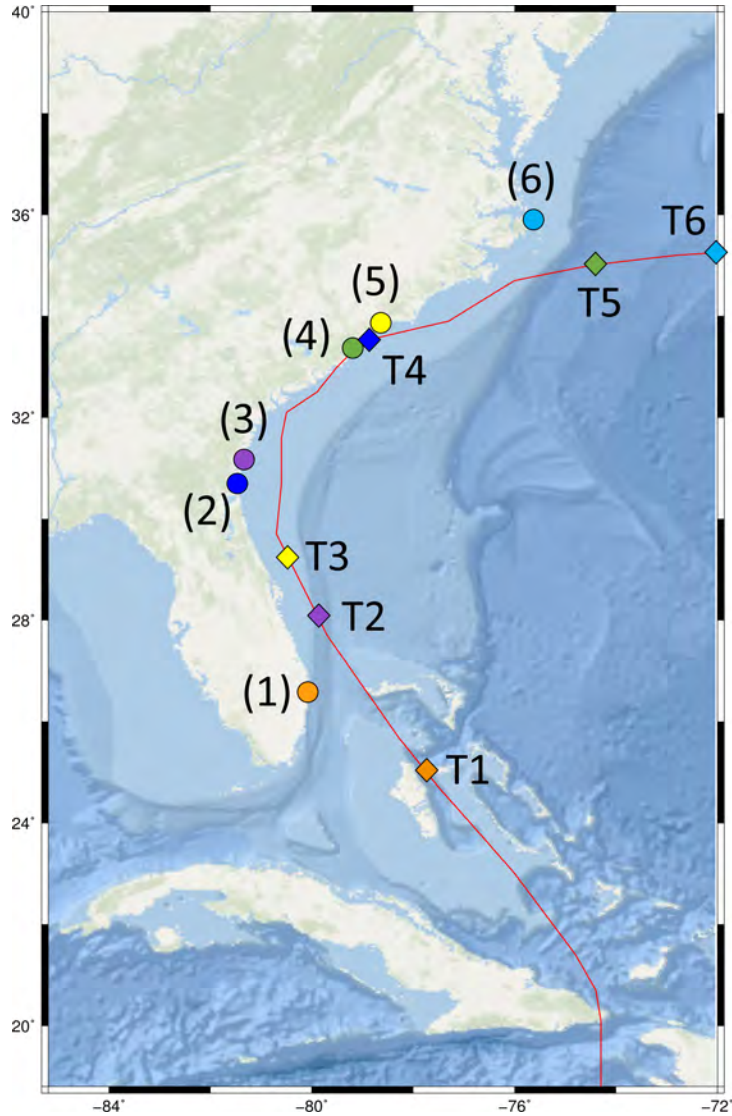

Figure 5.2 Locations of eye of the Matthew (diamonds) along with corresponding observation station (circles) on the U.S. southeast coast that recorded its impact at that point in time. The stations and times are same as in Figure 5.1. The NHC best track for Matthew is shown by red lines.

be further improved in both accuracy and efficiency.

When a storm is in the open ocean, simulations can be performed on a coarse-resolution mesh that doesn't have much coastal detail. As a storm approaches a specific coastline, we can switch to a high-resolution mesh that has its resolution concentrated on that region. The question here is when should the mesh-switching occur? Several parameters could be used in this regard: for example, the distance of the storm-eye from the coast/shelf, size of the storm, observation of wind speeds and/or wave heights, etc. *It is hypothesized that, by using information available during the storm, the optimal times for switching meshes can be identified.*

To investigate the hypotheses articulated above, this research will have the following objectives:

1. Identify the optimal number of segments along the U.S. southeast coast, to represent the variation in water levels during Matthew without excessive switching between meshes.

2. Evaluate the storm information available during the storm, including both storm parameters (track, size, intensity, etc.) and ocean response (waves and water levels at real-time gauges), as possible triggers for switching between meshes.

3. Quantify the benefits in accuracy and efficiency of the multi-resolution approach, via comparisons with a single simulation on the FEMA-SAB mesh.

5.4 Methods

This chapter discusses the use of smaller component meshes made out of a large-domain mesh, to be used based on where the storm's impact area is at that point in time. This is demonstrated through the example of Hurricane Matthew, as it provided enough opportunity to switch from one mesh to another, while the storm travelled along the U.S. southeast coast from FL to NC. This section describes how smaller fine-resolution meshes were created from the HSOFS and FEMA-SAB meshes, the storm parameters taken as criteria for switching between meshes, the different simulations that will be done, and the error metrics that are used to analyze the results.

5.4.1 Creating Smaller Fine-Resolution Meshes

5.4.1.1 HSOFS Mesh at State Boundaries

As a first test of the approach, the HSOFS mesh is divided into smaller pieces based on state boundaries. Section 5.2 described how the observed water levels indicated the beginning and ending of Matthew's impact, along the three mesh extents of East-FL, GA-SC and NC. The total duration of storm's impact on a particular gauge was indicated by the period of increased water levels from normal tidal elevations. This was done conservatively, by picking times when the water levels at these boundary points indicted even a small increase from normal tidal levels. Based on this, Figure 4.5 indicates how the proposed approach can be applied during Matthew. The steps are outlined below. The times (T1 to T5) and stations (1 to 6) are as shown in Figures 5.1 and 5.2.

1. When the storm is far out in the Atlantic (Figure 5.3a), the storm impacts are not felt along the U.S. coastline. The simulation will therefore use the relatively-coarse HSOFS mesh.

2. At time T1 as the storm approaches the Florida coastline (Figure 5.3b), there is a slight increase in water levels from tidal heights at Station 1. But impacts are not felt along the GA-SC or the NC coasts. Therefore, at this point we will switch to the high-resolution east-Florida mesh.

3. As the storm moves north (Figure 5.3b), impacts start to appear on the Georgia-South Carolina coastline as well, as recorded by Station 3 at time T2 (17 hours later). Since the storm impacts are felt along the east-Florida and GA-SC coasts but not along the NC coast at this time, we will add only the GA-SC part of the high-resolution mesh on to the east-FL mesh.

4. At time T3 (18 hours later) when the eye of the storm is close to Daytona Beach, Florida (Figure 5.3d), the impacts of the storm starts to appear on gauges along the North Carolina coast as well. As the storm's impact are felt through out the US southeast coast region, we will switch to the full high-resolution mesh that has coverage from Florida to North Carolina.

5. As the eye of the storm moves north (Figure 5.3e), its impacts are no longer felt on the Florida coast as indicated by water level observations at Station 2. We will therefore switch to a mesh with high-resolution only from GA to NC, and the simulation will continue for a period of about 17 hours during which this extent of the coast experienced storm effects.

6. At time T5 (17 hours later) when the eye of the storm is located offshore the NC coast, observations at Station 4 indicates absence of storm's effects. Since we

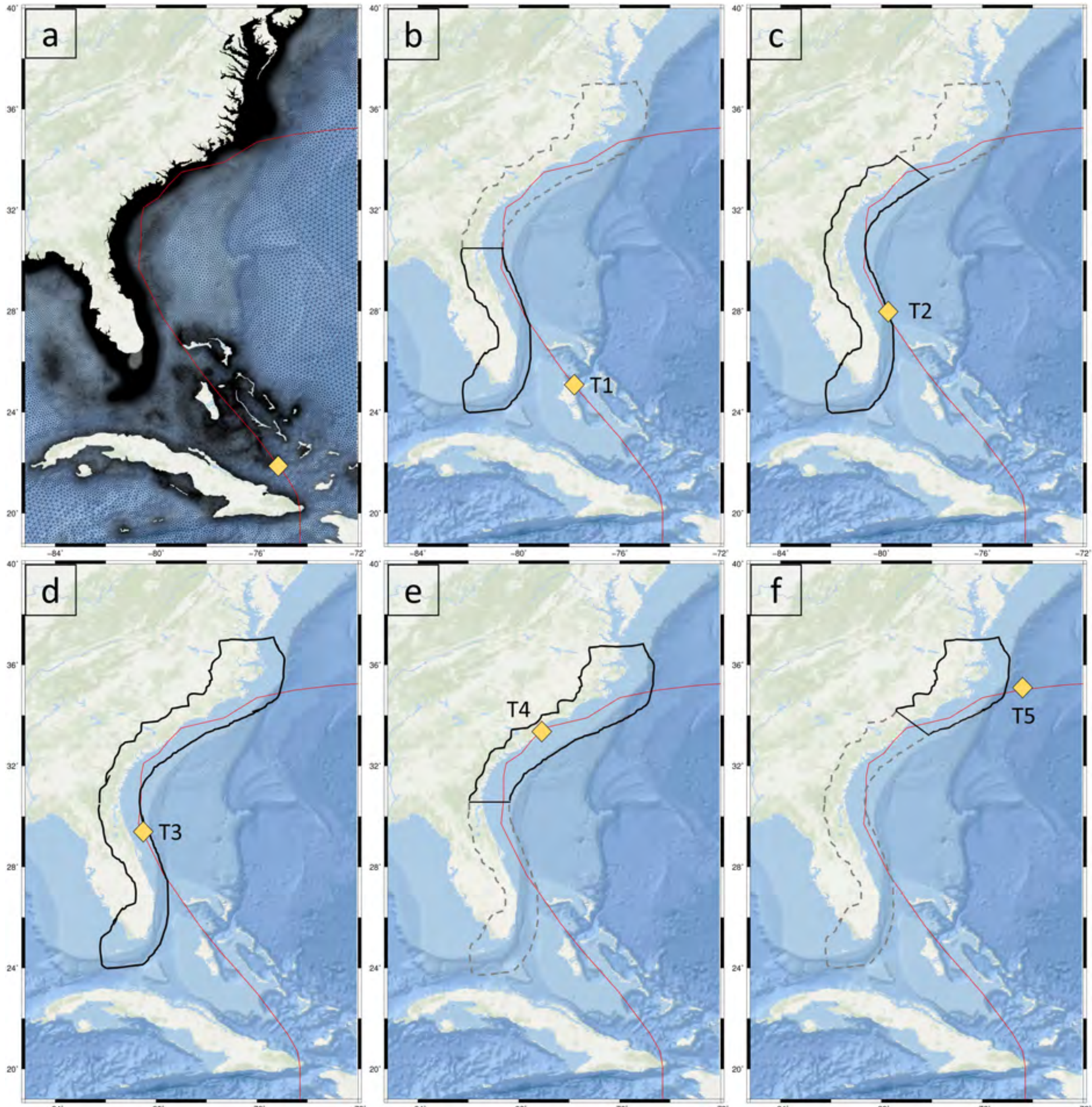

Figure 5.3 Application of the approach during Matthew. Black triangles(a) indicate the elements of the HSOFS mesh. Solid black lines (b to f) indicate the part of the single high resolution mesh (black dashed lines) to be used at that particular point in time. Times T1 to T5 are the same as in Figures 5.1 and 5.2. The NHC best track for Matthew is shown by red lines and the storm-eye by diamonds.

require high-resolution only in North Carolina at this point, we will switch to the high-resolution NC mesh. The simulation on this mesh will continue till time T6 (about 32 hours later), when the storm effects were last recorded in NC, as seen from water levels at Station 6.

Based on this logic, five meshes were created from the HSOFS mesh. They represent five different regions (FL, FL+GA+SC, FL+GA+SC+NC, GA+SC+NC, NC) along the U.S. southeast coast. Subscripts are used to indicate the region along the coast represented by that particular mesh. For example, HSOFS_{FL} indicates the HSOFS component mesh representing the Florida coastline. The number of vertices and days of simulation on each are given in Table 5.1. Like in the previous chapters, all Matthew simulations start at 0000 UTC 02 October 2016. These meshes are then used one by one, to represent Matthew's impact, as it moved from south to north along the U.S. southeast coast, affecting different regions of the coast at different points in time.

Table 5.1 Applying the approach using HSOFS component meshes

Mesh	Vertices	Days
HSOFS	1,813,443	4.5
HSOFS_{FL}	804,964	0.75
$\text{HSOFS}_{\text{FL+GA+SC}}$	942,427	0.75
$\text{HSOFS}_{\text{FL+GA+SC+NC}}$	1,057,880	0.75
HSOFS_{NC}	784,911	1.5

5.4.1.2 FEMA-SAB Mesh at Watershed Boundaries

The watershed boundary dataset (WBD) (U.S. Geological Survey, 2020a) represents the areal extent of surface water drainage to a point, accounting for all land and surface areas. The hydrologic units represent regions that drain to a portion of the stream network. More specifically, they define the areal extent of surface water drainage to an outlet point on a dendritic stream network, or to multiple outlet points where the stream network is not dendritic. Watershed boundaries are identified solely based on science-based hydrologic principles, thus not favouring any administrative boundaries, nor any particular program or agency. The drainage areas are nested within each other so that a large drainage area, like the Upper Mississippi River, will be composed of numerous smaller drainage areas, such as the Wisconsin River. Each of these smaller areas can further be subdivided into smaller and smaller drainage areas. The WBD uses six different levels in this hierarchy, with the smallest averaging about 30,000 acres. The WBD is made up of polygons nested into six levels of data respectively defined by regions, sub-regions, basins, sub-basins, watersheds, and sub-watersheds.

Out of the 21 "regions" of the USGS hydrologic unit system, the U.S. southeast coast falls under the South Atlantic-Gulf region represented by the two digit code 03. This covers an area of $724,330$ km^2 that represents the drainage within the United States that ultimately discharges into: a) the Atlantic Ocean within and between the states of Virginia and Florida; b) the Gulf of Mexico within and between the states of Florida and Louisiana; and c) the associated waters (Water Resource Region, 2020). This is then subdivided into 18 "sub-regions" numbered 0301 to 0318. For our study, the boundaries of the "sub-regions" 0301 to 0309 (north to south) are used to cut the FEMA-SAB mesh into smaller meshes (Figure 5.4). In this chapter, subscripts are used to indicate the watershed boundary region represented by that particular mesh. For example, $\text{WSB}_{307+306+305}$ indicates the FEMA-SAB sub-mesh with high-resolution in the watershed regions from 0307 to 0305, from boundary points 3 to 6 (Figure 5.5).

5.4.2 Criteria for Switching

For a storm hindcast, various parameters can be used as triggers for switching from one mesh to another. This includes post-storm information about the storm's track, size, intensity, speed, and other critical parameters, as well as observations of water levels and wave heights that were collected after the storm. But during a forecast, we are limited with the information in the NHC tropical cyclone advisories issued at-least every 6 hours. These contain information about the date/time and location of the center of the storm, direction and speed of the storm's forward motion, maximum sustained wind speeds, diameter of the storm's eye, the radii of the maximum wind in four quadrants (NE, SE, SW, and NW) in three categories(≥ 64 kt, ≥ 50 kt, and ≥ 34 kt), etc. For an ideal switch between the HSOFS and the full FEMA-SAB mesh, a possible application of using the radii of maximum winds were described in Chapter 4 for both Matthew and Florence. Moreover, water levels and wave heights at real-time gauges are also available during a storm, to be used as possible triggers during forecasting.

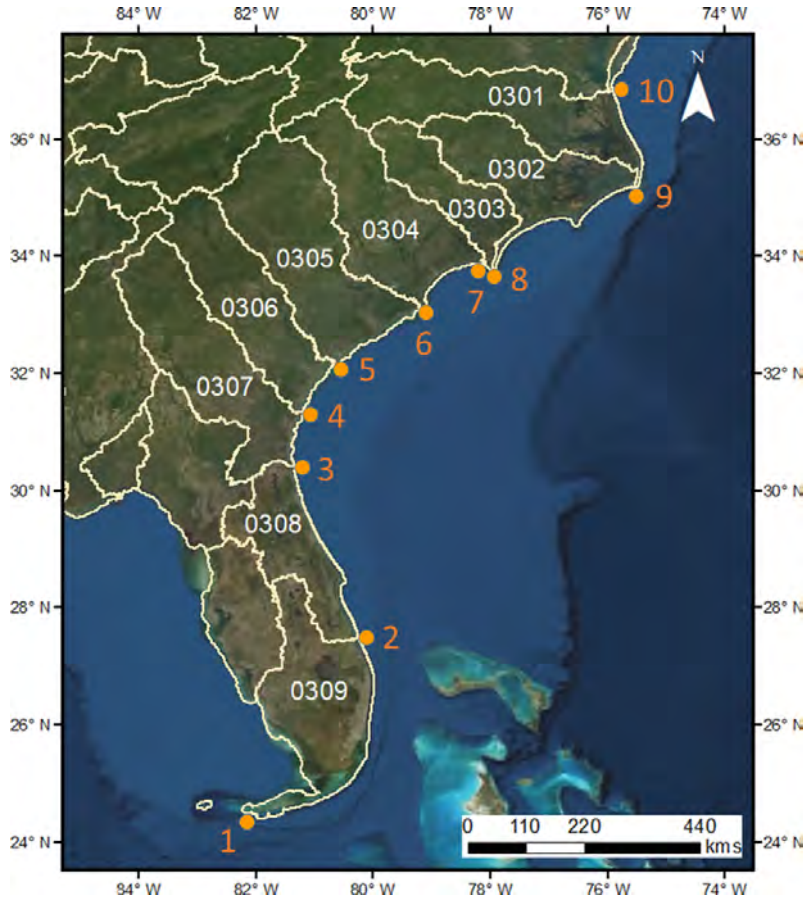

Figure 5.4 Watershed boundaries for the U.S. southeast coast. Orange dots indicate points that will be used to trigger switching between the meshes.

But these real-time gauges are not available everywhere along the coastline. Also, they are not reliable as they could be damaged during a storm leaving us with no information to switch from one mesh to another. A solution to this is to use forecast water levels rather than information at real time gauges. These are available at any point in the domain, and can be used to indicate the need of switching to a high-resolution mesh for a region, at a particular point in time. An increase in the total water levels from the usual tidal height at a location, will indicate the presence of storm nearby, and thus the need of using a high-resolution mesh to capture storm effects better. Thus water levels will be used as the main trigger in this chapter.

First, this will be tested with the sub-meshes created from the HSOFS mesh using state-line boundaries. Then, the same principle will be applied on smaller meshes created

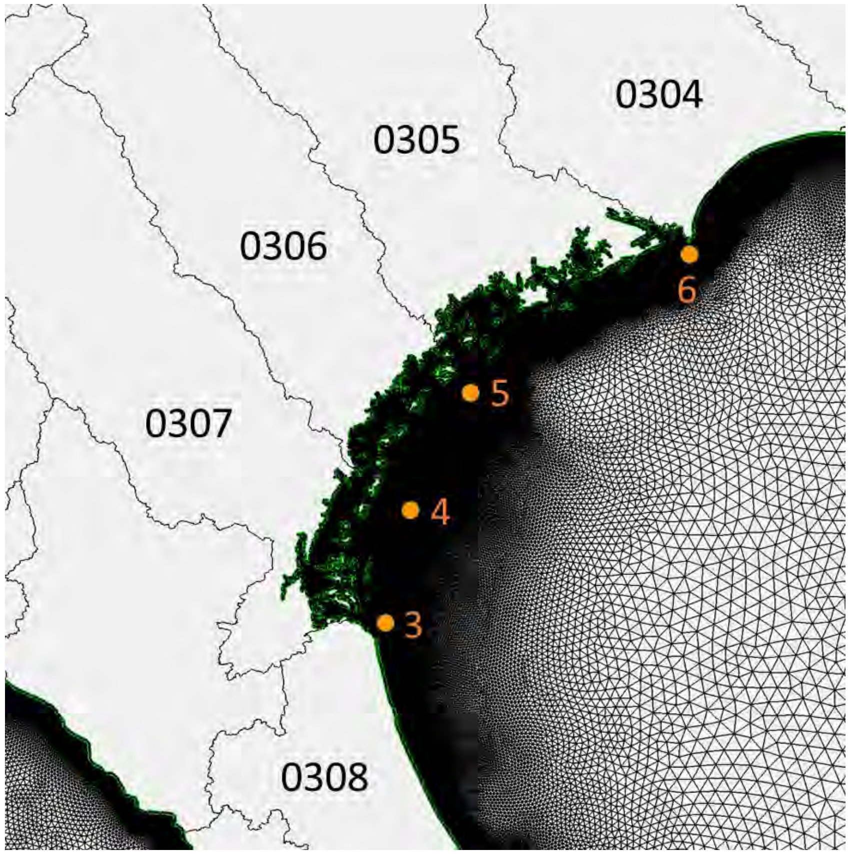

Figure 5.5 High-resolution coverage of the $WSB_{307+306+305}$ mesh. The mesh-elements are shown as black triangles, the mesh-boundary in green, and the orange dots indicates watershed boundary points as in Figure 5.4.

out of the FEMA-SAB mesh using watershed boundaries as guidelines. Water levels will be checked at boundaries of each FEMA-SAB sub-mesh (Figure 5.4) to identify how long each region was impacted by the storm (Figure 5.6). For example, the rise in water levels from normal tidal heights at point 5 will indicate when the sub-mesh 0305 was first impacted by Matthew. These impacts would have lasted until the water levels at point 6 returned to normal tidal heights. To deal with processes like forerunner surge that could raise water levels several hours before the actual storm (Kennedy et al., 2011), values of wind speeds and wave heights will be also considered (Figure 5.7 and 5.8).

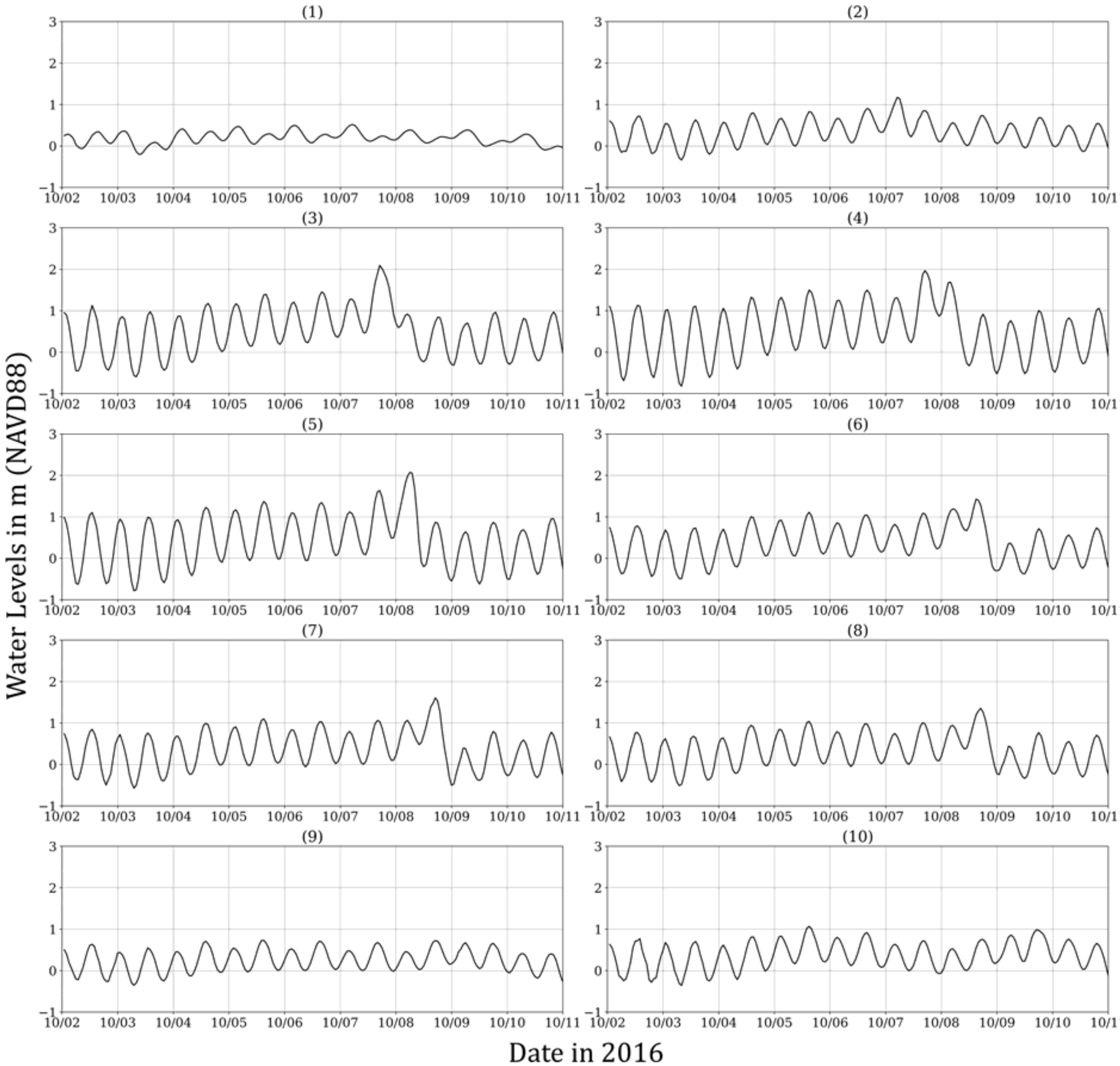

Figure 5.6 Time series of water levels (m relative to NAVD88) at the 10 locations shown in Figure 5.4.

5.4.3 Simulations

This chapter will consider four ADCIRC simulations of Hurricane Matthew using the multi-resolution approach. But compared to the simulations done in the previous chapter, multiple smaller high-resolution meshes will be used instead of a single high-resolution mesh, to cut down the wall-clock time. Out of these four simulations, the first will

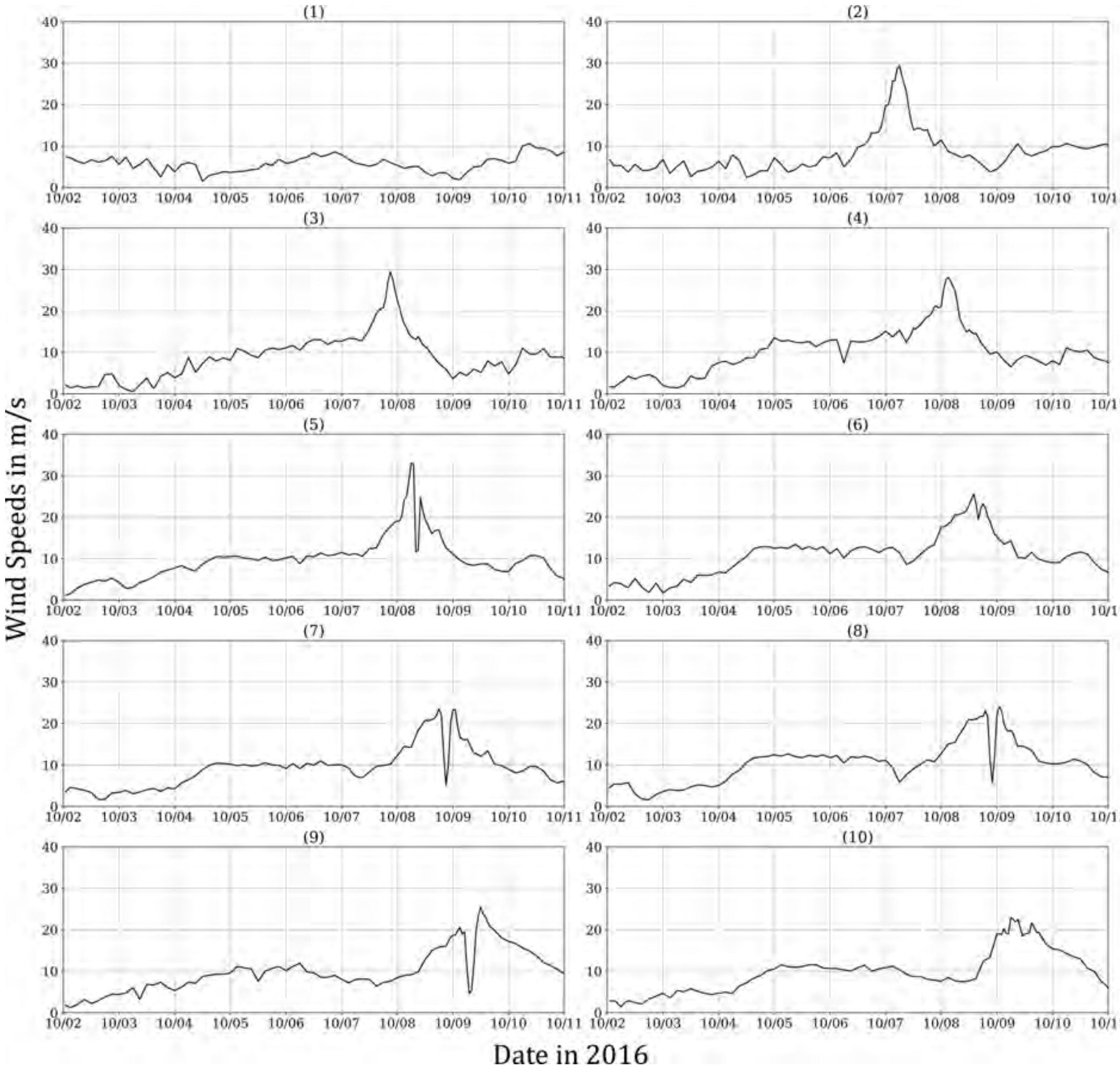

Figure 5.7 Time series of wind speeds (m/s) at the 10 locations shown in Figure 5.4.

use sub-meshes created out of the HSOFS mesh using state boundaries. This will act as a proof of concept that reduction in simulation times can be achieved without a compromise in the accuracy. The last 3 simulations will be done using the FEMA-SAB sub-meshes created using watershed boundaries as guidelines. The first will target maximum accuracy without concentrating too much on the efficiency. The second will be an optimum simulation in terms of accuracy and simulation time. The last will target maximum efficiency by compromising on the accuracy a little bit. These three simulation

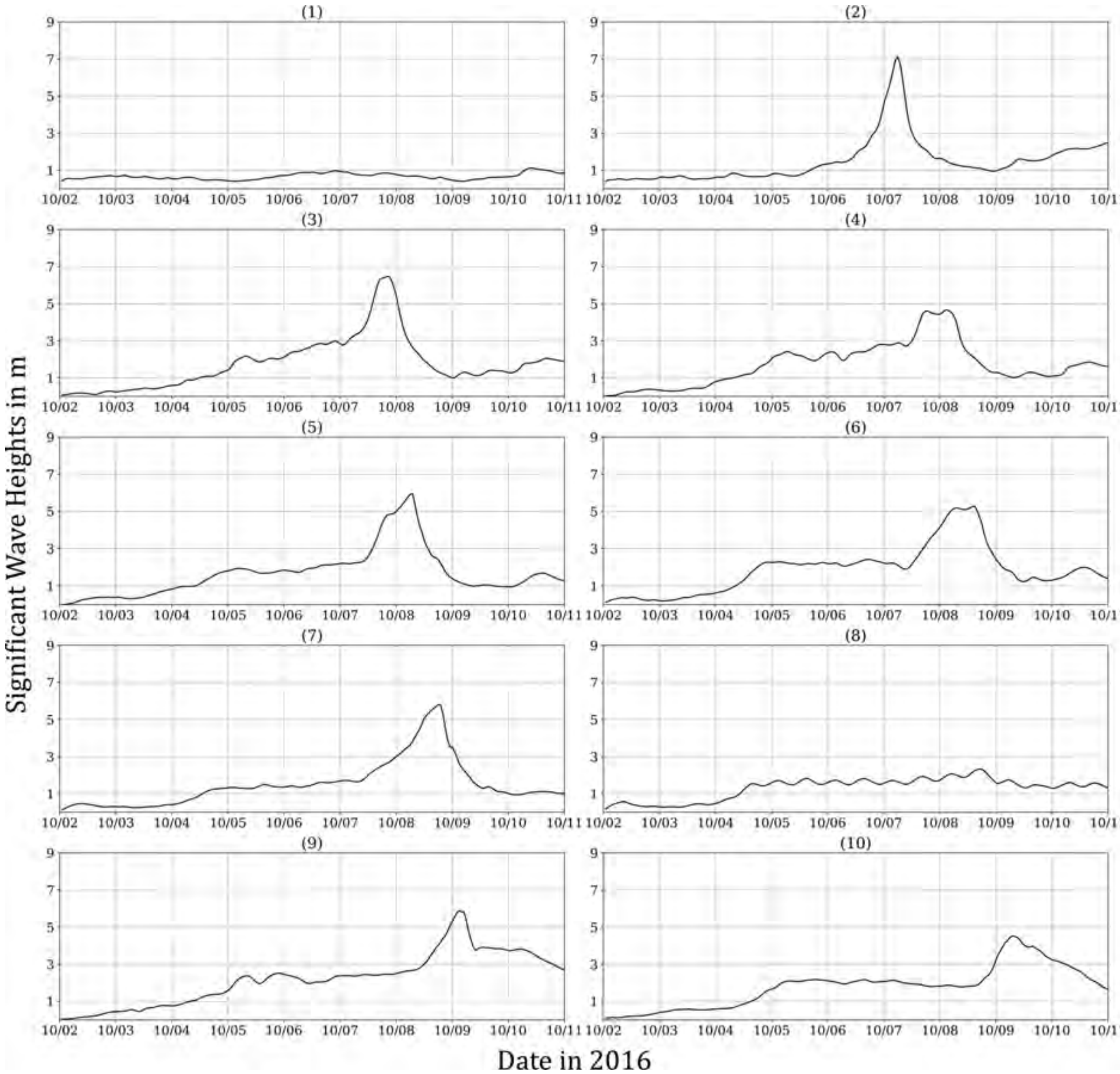

Figure 5.8 Time series of significant wave heights (m) at the 10 locations shown in Figure 5.4.

will be referred to as $FEMA\text{-}SAB_{ACC}$, $FEMA\text{-}SAB_{OPT}$ and $FEMA\text{-}SAB_{EFF}$ herein. More details of the simulations will be given in the next section.

5.4.4 Error Metrics

The modeled results will be evaluated for both accuracy and efficiency. For accuracy comparisons, the error metrics used will be the same as in the previous chapters, including root-mean-squared error (E_{RMS}), mean normalized bias (B_{MN}), coefficient of determination (R^2) and best-fit slope (m). Instead of comparing the results from the approach to observations, the *Fine* maximum water levels will be taken as the truth. The efficiency gains will be quantified through the use of actual speedup S_{actual}:

$$S_{\text{actual}} = \frac{T_{\text{fine}}}{T_{\text{mixed}}}$$

and theoretical speedup $S_{\text{theoretical}}$:

$$S_{\text{theoretical}} = \frac{NT}{\sum_{i=1}^{n} N_i T_i}$$

where T_{fine} is the total wall-clock time for the *Fine* simulation in days, T_{mixed} is the total wall-clock time for the approach including the times for switching in days, N is the number of vertices in the *Fine* mesh, T is the total days of *Fine* simulation, n is the number of component meshes used in the approach, and N_i and T_i are the number of vertices and days of simulation for the component meshes.

5.5 Results and Discussion

5.5.1 Simulation using the HSOFS sub-meshes

As mentioned in Section 5.4.1.1, when Matthew was far out in the open-ocean, the HSOFS mesh was used for simulations as the path of the storm was uncertain, and since the HSOFS mesh has a good representation of the U.S. coastline from Texas to Maine. As the track became more certain, switching was done to the HSOFS_{FL} mesh that has resolution only in Florida. Resolution was then added or removed as the storm moved north, depending on the storm's impact region at a point in time (Table 5.2). This simulation will be referred to as $HSOFS_{Test}$ herein.

To evaluate the accuracy of the approach, the maximum water levels are compared to that from a simulation that uses the HSOFS mesh for the entire 9 days for the storm (*Fine* simulation). For the approach, the maximum water levels were calculated by taking a maximum of the maximum water levels from each simulation on the component meshes, at each HSOFS vertex. The maximum water levels (Figure 5.9, left) look different from that obtained from simulations on the FEMA-SAB sub-meshes as presented in the

Table 5.2 Applying the approach using HSOFS component meshes

			Time in minutes	
Mesh	Vertices	Days	ADCIRC	*Adcirpolate*
HSOFS	1,813,443	4.5	34	
				2
HSOFS_{FL}	804,964	0.75	3	
				2
$\text{HSOFS}_{\text{FL+GA+SC}}$	942,427	0.75	3	
				3
$\text{HSOFS}_{\text{FL+GA+SC+NC}}$	1,057,880	0.75	4	
				2
$\text{HSOFS}_{\text{GA+SC+NC}}$	886,565	0.75	3	
				2
HSOFS_{NC}	784,911	1.5	6	

next sub-section, as these simulations did not employ a spatially varying offset surface, and they used GAHM winds instead of OWI. But compared to *Fine* predictions, the differences in maximum water levels are zero almost everywhere except at a few points along the Bight, where the results are under-predicted by 0 to 0.15 m (Figure 5.9, right). These near-zero differences everywhere along the coast indicates that each component mesh was subjected to the storm for the sufficient amount of time.

The accuracy can be further evaluated by calculating error metrics for the approach, using the *Fine* maximum water-levels as “truth” (Table 5.3). This allows an evaluation of accuracy throughout the entire domain, not only where observations were collected. Results are compared only at vertices in the region from FL to NC that are not in open-ocean (depths less than 10 m), and that were wetted in both simulations. For a total of 169,444 vertices that satisfied the above criteria, the values of E_{RMS} (close to 0), best-fit slope m (equal to 1), R^2 (equal to 1), and B_{MN} (close to 0) all indicate a good fit to the fine results. The overall negative value of B_{MN} indicates a slight under-prediction by the model, and are due to the few points along the Bight where there were differences as mentioned earlier.

The *Fine* simulation took a total of 67 minutes to run 9 days of storm on the full HSOFS mesh. The combined simulation with the component meshes took a total of

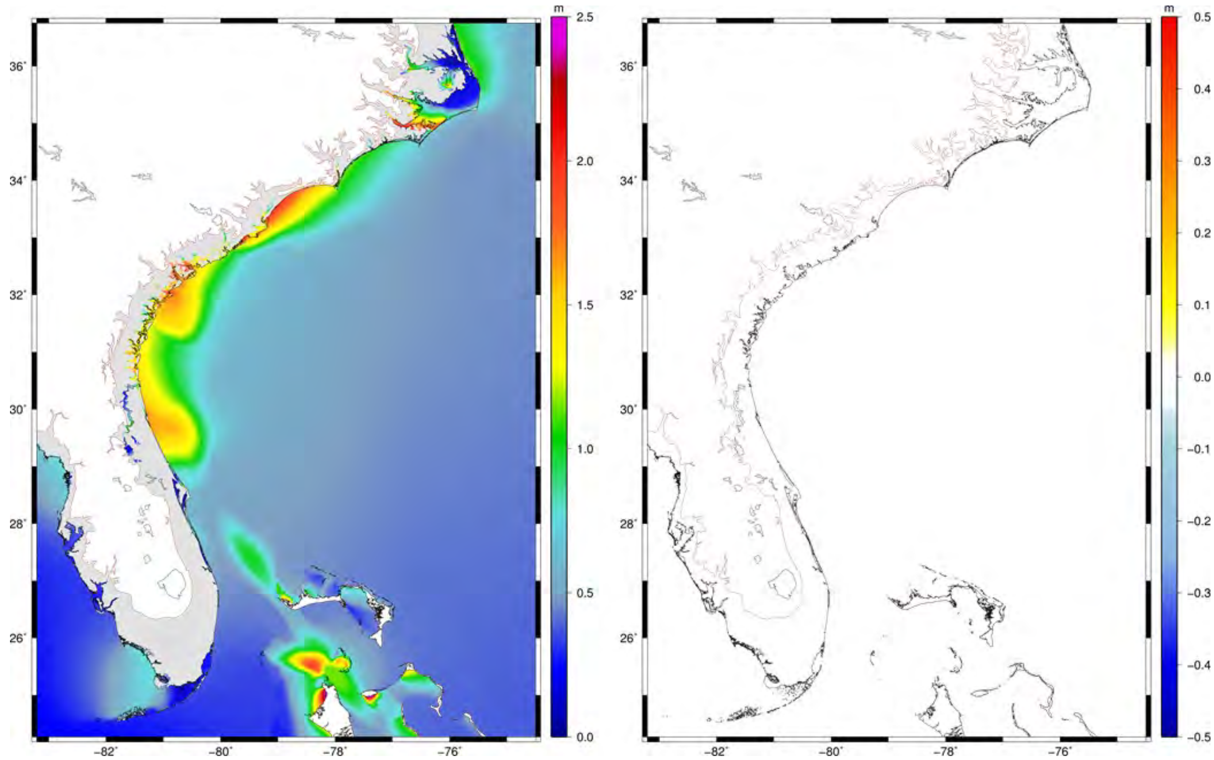

Figure 5.9 Panels of: (left) Maximum water levels (m, NAVD88) for the HSOFS *Fine* simulation; and (right) difference in maximum water levels (m) between the $HSOFS_{Test}$ and *Fine* simulations. The coastline is shown in black and the mesh-boundary in brown.

Table 5.3 Modelled errors from the $HSOFS_{Test}$ approach compared to a *Fine* simulation ("truth").

Error	$HSOFS_{Test}$
Stations	169,444
Best-Fit Slope	1.0
R^2	1.0
E_{RMS} (m)	0.01
B_{MN}	-0.001

64 minutes, including the time for switching between the various component meshes (Table 5.2). The S_{actual} and $S_{\text{theoretical}}$ were 1.05 and 1.35, respectively. This difference between the actual and theoretical speedup is caused by the time for switching between meshes, which came to a total of 11 minutes. Thus, although the savings in wall-clock time was only 3 minutes (4.5 percent) (Table 5.4), this acts as a proof of concept for the

fact that, instead of using one single high-resolution mesh for the entire U.S. southeast coast, multiple component meshes can be used, depending on where the storm is at that point in time without a loss in accuracy. The component meshes, which acted as fine resolution meshes for the different extents here, were all developed from the HSOFS mesh. However, moving forward, they will be developed from the FEMA-SAB mesh, and therefore be much larger. A considerable gain in efficiency should be expected.

Table 5.4 Total wall-clock time (min) for all four simulations described in this chapter.

	Time in minutes		
Simulation	*Fine*	Approach	Save in time (%)
$HSOFS_{Test}$	67	64	4.5
$FEMA\text{-}SAB_{ACC}$	393	279	29.01
$FEMA\text{-}SAB_{OPT}$	393	203	48.35
$FEMA\text{-}SAB_{EFF}$	393	152	61.32

5.5.2 Simulations using the FEMA-SAB sub-meshes

As mentioned earlier, three simulations were done using the FEMA-SAB sub-meshes: $FEMA\text{-}SAB_{ACC}$, targeting maximum accuracy; $FEMA\text{-}SAB_{OPT}$, an optimum simulation in terms of accuracy and simulation time; and $FEMA\text{-}SAB_{EFF}$, targeting maximum efficiency by compromising on the accuracy.

5.5.2.1 $FEMA\text{-}SAB_{ACC}$

The $FEMA\text{-}SAB_{ACC}$ simulation is aimed at getting maximum accuracy out of the approach, by switching between multiple combinations of the FEMA-SAB sub-meshes, based on what region along the U.S. southeast coast was impacted by Matthew at a particular point in time. There are no restrictions on the number of sub-meshes used in a single simulation. Although it will be good to have zero errors everywhere compared to maximum water levels from the *Fine* simulation, smaller differences are acceptable as the use of the full FEMA-SAB mesh is avoided throughout the storm duration. Looking at time-series of water levels at watershed boundary points, a combination of meshes (Table 5.5) was chosen in such a way that at any point in the simulation, the mesh being used has enough coverage to fully represent Matthew's impact. During the simulation, regions were added or removed as water levels at boundary points became greater- or lesser-than 1.1 times the tidal maxima, in most cases (Table 5.6).

Table 5.5 The combination of meshes used in the *FEMA-SAB*$_{ACC}$ simulation. The starting time of this simulation is 0000 UTC 02 October, and the Days column counts forward from this starting time. Component meshes were added/subtracted when their water levels became greater/less than 1.1 times their tidal maxima.

			Time in minutes	
Mesh	Vertices	Days	ADCIRC	*Adcirpolate*
HSOFS	1,813,443	3	19	
				8
$WSB_{309+308}$	3,813,463	1.5	48	
				16
$WSB_{309+308+307+306}$	5,013,281	0.75	33	
				13
$WSB_{309+308+307+306+305+304}$	5,263,482	0.75	36	
				14
FEMA-SAB	5,584,241	0.75	36	
				8
$WSB_{307+306+305+304+303+302+301}$	3,229,413	0.75	19	
				5
$WSB_{304+303+302+301}$	1,853,662	1.5	24	
Total		9	215	64

Table 5.6 Water level (m), Wind speed (m/s), and Significant wave height (m) at the boundary points between the various component meshes during switching in the *FEMA-SAB*$_{ACC}$ simulation. The boundary points are the same as in Figure 5.4.

Mesh	Time of switching	Boundary Point	Parameters at switching: Water Level	Wind Speed	Significant Wave Height
HSOFS					
	0000 UTC 05 October	1	0.26	3.66	0.43
$\mathrm{WSB}_{309+308}$					
	1200 UTC 06 October	3	0.53	13.09	2.72
$\mathrm{WSB}_{309+308+307+306}$					
	0600 UTC 07 October	5	0.96	11.22	2.24
$\mathrm{WSB}_{309+308+307+306+305+304}$					
	0000 UTC 08 October	7	0.22	12.24	2.99
FEMA-SAB					
	1800 UTC 08 October	3	0.85	7.27	1.32
$\mathrm{WSB}_{307+306+305+304+303+302+301}$					
	1200 UTC 09 October	6	-0.38	10.09	1.24
$\mathrm{WSB}_{304+303+302+301}$					

Compared to water levels from the *Fine* simulation (Figure 5.10), the *FEMA-SAB*$_{ACC}$ predictions are a very good match. The differences are zero along most of the U.S. southeast coast. Very small differences of magnitude less than 0.15 m occur inland in regions north of the Keys, downstream Indian River in FL, and the Albemarle Sound in North Carolina. These differences are further evaluated by comparing maximum water levels from the approach to the *Fine* solution ("truth") (Table 5.7). Results are compared only at vertices in the region from FL to NC, that are not in open-ocean (depths less than 10 m), and that were wetted in both simulations. For a total of 2,665,697 vertices that satisfied the above criteria, the values of E_{RMS} (close to 0), m (equal to 1), R^2 (close to 1), and B_{MN} (close to 0) all indicate a good fit to the fine results. The slight negative value of B_{MN} indicates an overall under-prediction by the model.

Table 5.7 Modelled errors from the *FEMA-SAB* simulations compared to a *Fine* simulation ("truth").

Error	*FEMA-SAB*$_{ACC}$	*FEMA-SAB*$_{OPT}$	*FEMA-SAB*$_{EFF}$
Stations	2,665,697	2,618,907	2,571,024
Best-Fit Slope	1.00	0.96	0.95
R^2	0.98	0.96	0.94
E_{RMS} (m)	0.08	0.15	0.18
B_{MN}	-0.003	-0.050	-0.070

The *FEMA-SAB*$_{ACC}$ simulation took a total of 279 minutes to run 9 days of Matthew on the various component meshes (Table 5.5). This includes the 64 minutes (23 percent) for switching between meshes. Compared to the *Fine* simulation that took 393 minutes to run 9 days of storm on the full FEMA-SAB mesh, this is a savings in wall-clock time by about 2 hr (29 percent) (Table 5.4). The values of S_{actual} and $S_{\text{theoretical}}$ were 1.41 and 1.78, respectively. The difference between these two values is attributed to the time taken to switch between the various component meshes.

5.5.2.2 *FEMA-SAB*$_{OPT}$

This simulation is aimed at an optimum prediction of water levels, and the combination of meshes was chosen accordingly (Table 5.10). Compared to the *Fine* simulation, the differences in predictions should not be too large, and there should be a considerable cut

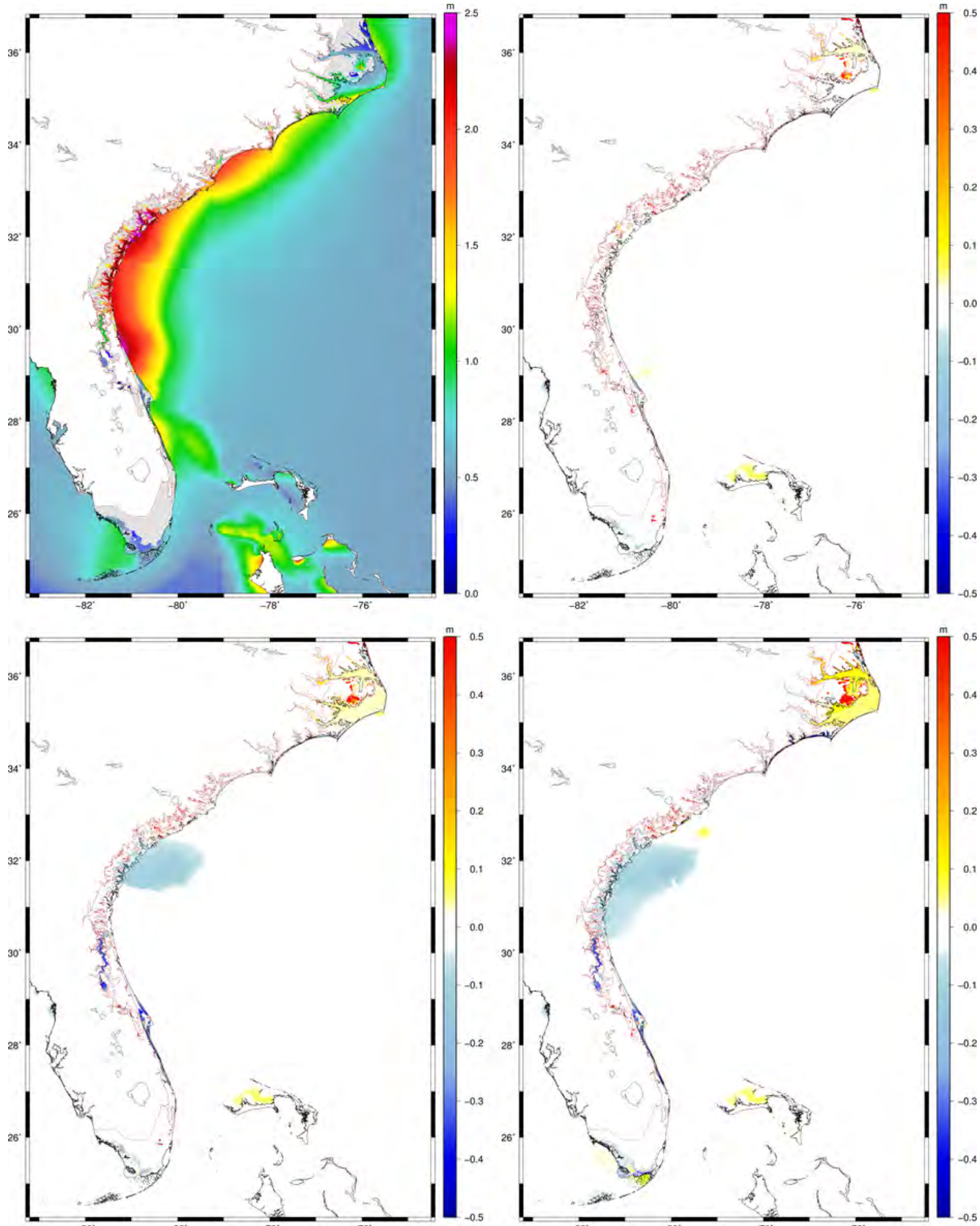

Figure 5.10 Maximum water levels (m, NAVD88) from the *Fine* simulation (top-left), and differences in maximum water levels (m) as compared to the *Fine* results for: (top-right) $FEMA\text{-}SAB_{ACC}$; (bottom-left) $FEMA\text{-}SAB_{OPT}$; and (bottom-right) $FEMA\text{-}SAB_{EFF}$ simulations. The coastline is shown in black and the mesh-boundary in brown.

down in the the wall-clock time. Compared to the *FEMA-SAB*$_{ACC}$ simulation, the goal here is to achieve an increase in efficiency by using smaller component meshes. But this will lead to larger accuracy errors, because we will not represent the coastal regions with the finest mesh resolution for as much time. For most switches, the trigger for adding or removing resolution was based on water level comparison to 1.2 times the tidal maxima, at watershed boundaries.

Table 5.8 The combination of meshes used in the *FEMA-SAB*$_{OPT}$ simulation. The starting time of this simulation is 0000 UTC 02 October, and the Days column counts forward from this starting time. Component meshes were added/subtracted when their water levels became greater/less than 1.2 times their tidal maxima.

			Time in minutes	
Mesh	Vertices	Days	ADCIRC	*Adcirpolate*
HSOFS	1,813,443	3	19	
				7
WSB_{309}	2,803,323	2	41	
				17
$\mathrm{WSB}_{309+308+307+306+305}$	5,181,167	1	45	
				8
$\mathrm{WSB}_{307+306+305+304}$	2,910,982	0.25	6	
				6
$\mathrm{WSB}_{306+305+304}$	2,246,580	0.25	5	
				7
$\mathrm{WSB}_{306+305+304+303+302+301}$	2,565,008	0.5	11	
				5
$\mathrm{WSB}_{302+301}$	1,681,994	2	26	
Total		9	153	50

Table 5.9 Water level (m), Wind speed (m/s), and Significant wave height (m) at the boundary points between the various component meshes during switching in the *FEMA-SAB*$_{OPT}$ simulation. The boundary points are the same as in Figure 5.4.

Mesh	Time of switching	Boundary Point	Parameters at switching: Water Level	Wind Speed	Significant Wave Height
HSOFS					
	0000 UTC 05 October	1	0.26	3.66	0.43
WSB_{309}					
	0000 UTC 07 October	2	0.45	19.80	4.56
$WSB_{309+308+307+306+305}$					
	0000 UTC 08 October	3	0.70	22.56	5.45
		6	0.36	17.71	4.14
$WSB_{307+306+305+304}$					
	0600 UTC 08 October	4	1.27	24.74	4.35
$WSB_{306+305+304}$					
	1200 UTC 08 October	7	0.71	20.78	5.07
$WSB_{306+305+304+303+302+301}$					
	0000 UTC 09 October	8	-0.23	21.20	1.58
$WSB_{302+301}$					

Compared to the *Fine* simulation (Figure 5.10), differences in maximum water levels were seen along the Florida coastline north of the Keys, along the Indian and St. Johns Rivers in Florida, along the South Atlantic Bight in Georgia, and in North Carolina. These differences are attributed to these regions not having the finest mesh resolution for sufficient amount of time. For example, in the St. Johns River, Florida, the model under-predicted the peaks by 0.15 to 0.35 m. In the approach, this region (WSB_{308}) was used only for the period from 0000 UTC 07 October to 0000 UTC 08 October. Whereas predictions of water levels at locations inside the river indicated storm effects extending beyond 0000 UTC 11 October. Smaller differences of 0.03 m was seen in the middle of the Pamlico Sound in North Carolina, where the model over-predicted the peaks. Along the coastline, differences were seen offshore WSB_{308} where the peaks were under-predicted by about 0.15m.

These differences are evaluated by computing error metrics as before, taking the *Fine* results as the "truth" (Table 5.7). For a total of 2,618,907 points compared, the B_{MN} was equal to -0.05 indicating an overall under-prediction by the model. The best-fit line slope, R^2, E_{RMS} were 0.96, 0.96, and 0.15 m respectively. Thus the predictions are a fair match to the *Fine* results, although we did not consider all of the storm impacts at the watershed boundary points, to decide the combination meshes and simulation times for each. Compared to the *FEMA-SAB$_{ACC}$* simulation, the errors have increased: the overall E_{RMS} has increased by 0.07 m, and about 50,000 lesser points are used for comparison to *Fine* solution.

The benefit of the approach is now evaluated in terms of efficiency. The *Fine* simulation required 393 minutes to run 9 days of Matthew on the full FEMA-SAB mesh. Compared to this, the *FEMA-SAB$_{OPT}$* simulation required a total of 203 minutes (Table 5.8). Thus, the S_{actual} was 1.94. This includes the 50 minutes (25 percent) for switching between the various component meshes. The value of $S_{\text{theoretical}}$ was 2.27. Thus the *FEMA-SAB$_{OPT}$* resulted in a savings in time of over 3 hr (48 percent), compared to the *Fine* simulation (Table 5.4).

5.5.2.3 *FEMA-SAB$_{EFF}$*

This simulation was aimed for maximum efficiency of the multi-resolution approach by compromising on the accuracy. To avoid large simulation times by any of the component-mesh simulations, it was decided not to use a combination of more than three sub-meshes at any point in the simulation. The criteria for adding or removing resolution is based on the value of 1.4 times the tidal maxima at most locations. As efficiency in terms of wall-clock times was the major objective from this simulation, each mesh will be used only for the peak of the storm, and thus not for the entire duration where it felt impacts of the storm (Table 5.10). Thus a loss in accuracy at different regions along the U.S. southeast coast is expected.

Table 5.10 The combination of meshes used in the *FEMA-SAB*$_{EFF}$ simulation. The starting time of this simulation is 0000 UTC 02 October, and the Days column counts forward from this starting time. Component meshes were added/subtracted when their water levels became greater/less than 1.4 times their tidal maxima.

			Time in minutes	
Mesh	Vertices	Days	ADCIRC	*Adcirpolate*
HSOFS	1,813,443	4.5	29	
				6
WSB$_{309}$	2,803,323	0.5	11	
				9
WSB$_{308}$	2,471,130	0.5	10	
				11
WSB$_{308+307+306}$	3,670,946	0.5	15	
				6
WSB$_{306+305}$	2,164,263	0.5	9	
				5
WSB$_{305+304+303}$	1,808,744	0.25	4	
				4
WSB$_{304+303}$	1,632,726	0.25	4	
				4
WSB$_{302+301}$	1,681,994	2	25	
Total		9	107	45

Table 5.11 Water level (m), Wind speed (m/s), and Significant wave height (m) at the boundary points between the various component meshes during switching in the *FEMA-SAB*$_{EFF}$ simulation. The boundary points are the same as in Figure 5.4.

Mesh	Time of switching	Boundary Point	Parameters at switching: Water Level	Wind Speed	Significant Wave Height
HSOFS					
	1200 UTC 06 October	1	0.08	8.36	0.90
WSB_{309}					
	0000 UTC 07 October	2	0.45	19.80	4.56
WSB_{308}					
	1200 UTC 07 October	3	0.63	15.60	4.18
$WSB_{308+307+306}$					
	0000 UTC 08 October	4	0.93	21.09	4.43
		5	0.69	19.07	4.99
$WSB_{306+305}$					
	1200 UTC 08 October	5	-0.20	19.46	3.44
		6	0.78	23.0	5.12
$WSB_{305+304+303}$					
	1800 UTC 08 October	6	1.02	23.25	4.31
$WSB_{304+303}$					
	0000 UTC 09 October	8	-0.23	22.0	1.58
$WSB_{302+301}$					

The simulation starts on 0000 UTC 02 October with the relatively coarse HSOFS mesh, as the center of the storm is away from the U.S. southeast coast at this time. At station 1, there are no major storm effects on water levels, as it stays below 0.5 m through the storm duration (Figure 5.6). At station 2, which is located at the boundary of WSB_{309} and WSB_{308}, the peak of the storm is felt on 0600 UTC 07 October. Therefore, we switch from the HSOFS to the WSB_{309} mesh on 1200 UTC 06 October, 18 hr before the storm peak. A combination of WSB_{309} and WSB_{308} is avoided as it would result in large simulation times owing to its large number of elements (3,813,463), and due to the fact that the maximum water level at station 2 is only about 1.25 m. The simulation is then continued using different combinations of meshes as suggested by the value of water levels at various watershed boundary locations (Table 5.6).

The maximum water levels from the approach are compared to that from the *Fine* simulation. As expected, there were differences along the coast and inland at various regions on the U.S. southeast coast (Figure 5.10). Differences were seen north of the Keys and along the Indian and St. Johns River in Florida, along the coastlines of Georgia and South Carolina, and inland in North Carolina. Although the location of most of these differences are similar to that in $FEMA\text{-}SAB_{EFF}$, the magnitude of error is higher owing to each region having the finest-resolution mesh for a lesser duration of the storm.

Along the coast, errors occur along the shoreline of Georgia and South Carolina, where the model under-predicted the peaks by a maximum of 0.16 m. In NC, the model predictions from the approach over-predicted the maximum water levels in regions like the Pamlico and Albemarle Sound. This falls in (WSB_{302}) and (WSB_{301}) which were employed for the 2 days from from 0000 UTC 09 October to 0000 UTC 11 October. Observations and predictions in this region indicate peak of the storm occurring before and on 0000 UTC 09 October thus missing some of the storm effects, including the draw-down that happens after the peak. This under-prediction of the draw-down causes the over-prediction in these regions. In the north-east portion of the Pamlico Sound close to the Pamlico River, water levels were over-predicted by 0.1 m.

Comparing to *Fine* results (Table 5.7), for a total of 2,571,024 points analyzed, the results from the approach have a B_{MN} equal to -0.07 indicating an overall under-prediction by the model. The best-fit line slope, R^2, E_{RMS} were 0.95, 0.94, and 0.18 m, respectively. Although these values are not ideal, they are not too bad either for the large amount of points compared. And as mentioned earlier, some errors are expected as the combination of meshes were selected just to capture the major peaks at different locations along the coast. Compared to the *FEMA-SAB*$_{ACC}$ simulation, the errors have increased significantly. The overall E_{RMS} has increased by 0.10 m, the values of R^2 and best-fit line slope have gone worse, and about 95,000 lesser points are used for comparison to *Fine* solution.

Compared to the *Fine* simulation that required 393 minutes to run 9 days of storm on the full FEMA-SAB mesh, the *FEMA-SAB*$_{EFF}$ simulation required a total of 152 minutes including the time for switching between the various component meshes (Table 5.10). The S_{actual} and $S_{\text{theoretical}}$ were equal to 2.59 and 2.80 respectively. This difference between the actual and theoretical speedup is caused by the time for switching between meshes, which came to a total of 45 minutes (29.6 percent) (Table 5.4). But compared to the *Fine* simulation, the savings in time was about 4 hr (61 percent). This huge savings in the simulation time is particularly useful during forecasting, to give out predictions faster, or to run ensemble simulations to manage the uncertainty in the storm parameters in the NHC advisories.

5.6 Conclusions

The multi-resolution approach was applied for hindcast simulations of Hurricane Matthew as it affected the U.S. southeast coast. But rather than using just one high-resolution for the entire region, multiple smaller higher-resolution meshes that were created out of the full-domain mesh are used to maximize gains in efficiency. The concept was first applied using sub-meshes created out of the HSOFS mesh using state-line boundaries as guidelines. Time series of water levels at the boundary points were used as trigger for switching from one mesh to another. Although this approach did not result in a considerable savings in time (only 3 minutes), the maximum water levels from the approach were a close match to that from the corresponding *Fine* simulation, thereby acting as a proof of concept.

The approach was then applied to three simulations of Matthew with sub-meshes created out the FEMA-SAB mesh using watershed boundaries as guidelines. The first simulation was targeted for maximum accuracy without concentrating too much on the efficiency (*FEMA-SAB*$_{ACC}$). Even a small increase in water levels at boundary points of the component meshes was used as triggers for switching. Its errors in predictions were minimal, it flooded the maximum number of points, and it had the best error statistics as compared to *Fine* results. But it had a savings in wall-clock time by only about 2 hr (29 percent). The second was an optimum simulation in terms of accuracy and simulation time (*FEMA-SAB*$_{OPT}$). Compared to *FEMA-SAB*$_{ACC}$, switching between meshes was done only when total water levels at the boundary points indicated a major increase in water levels from tidal heights. This simulation resulted in larger errors of water levels and flood extent, flooded lesser number of points, and had worse error statistics as compared to *Fine* results. However, the compromise in accuracy was reflected in its better efficiency, with a savings in wall-clock time of over 3 hr (48 percent).

The last simulation targeted maximum efficiency by compromising on the accuracy further (*FEMA-SAB*$_{EFF}$). Only the major peaks in water levels were used as triggers, and not more than 3 combination of sub-meshes were used at any point in the simulation. This resulted in the largest errors out of the three simulations. Compared to the *FEMA-SAB*$_{OPT}$ simulation, the errors in maximum water levels were larger at multiple locations along the U.S. southeast coast. It also flooded the least amount of points and had the worst error statistics out of the three simulations. But the efficiency in terms of wall-clock time was maximum, taking 4 hr (61 percent) lesser time as compared to the *Fine* simulation. This is a significant save in time, and can be crucial, especially during forecasting applications for faster guidance.

These three simulations act as a proof that different levels of accuracy and efficiency can be achieved out of the multi-resolution approach, by using different combinations of smaller high-resolution meshes that represent different regions along the U.S. southeast coast. They also demonstrate how predicted time-series of water levels at different locations along the coast can be used to trigger switching and achieve various levels of accuracy. By targeting only the major peaks in the total water levels, maximum efficiency can be achieved, although this would compromise on accuracy at different locations. To deal with phenomena like a fore-runner surge, predicted values of wind speeds and significant wave heights can also be used to identify proximity of the storm to the coastline. Moreover, a careful choice of the combination of meshes to be used in the approach, is necessary to avoid larger simulation times. Repeated switching between different component meshes will contribute to a large difference between S_{actual} and $S_{\text{theoretical}}$.

Chapter 6

Concluding Remarks

Storm surge and coastal flooding can cause significant loss of life and damage to property and landscapes. ADCIRC, a state-of-the-art model for coastal flooding, uses unstructured meshes to represent the coastal region with varying resolution, from several thousands of kilometers in the open ocean to hundreds of meters along the coast to tens of metres in the channels and small hydraulic features. Although predictions using this model are reliable and accurate due to its detailed representation of the coast, its simulations can take several hours even on thousands of computational cores. This is a challenge during forecasting, where predictions are required as soon as possible, so that emergency managers can take necessary precautions.

This dissertation contributes to the field of storm surge modeling in the following ways: (a) quantification of the contributions of non-linear interactions between surge and tides to the total water levels during a hurricane, (b) improving the understanding of the influence of storm timing and forward speed to the associated flooding, (c) development and validation of a high-resolution mesh for the entire U.S. southeast coast, and (d) application of a multi-resolution approach to improve the accuracy and efficiency of flooding predictions. Important findings in each of these areas are summarized in the following paragraphs.

Hurricane Matthew was a powerful storm that impacted the southeastern U.S. during October 2016, moving mostly parallel to the coastline from Florida through North Carolina. Compared to the parametric vortex model based on best track information from the National Hurricane Center, data-assimilated wind fields proved to be the most accurate representation of Matthew's impacts. This atmospheric forcing was then used along with a relatively-coarse HSOFS mesh with an average coastal resolution of 500 m, to run the coupled ADCIRC+SWAN model in simulating Matthew's effects on water levels. Water level comparisons at 241 locations on the U.S. southeast coast resulted in an overall E_{RMS} of less than 30 cm and a B_{MN} of near zero. There was also good correlation between modeled and measured peak water levels. For 622 HWMs, the R^2 value was 0.78 and the slope of the best-fit line was 0.96. These values are comparable to results from studies using meshes with much higher resolution. The contribution of non-linear interactions between tides and surge on the total water levels along the southeast U.S. Atlantic coast during Matthew was then explored. These interactions were found to have a constructive effect on the total water levels during a low tide and a destructive effect during a high tide. This study was the first to consider these interactions for a long coastline during a shore-parallel storm. The magnitudes of these interactions varied at different regions with respect to the coast, with small values on the ocean side and large values on the estuary side. In the estuaries, these interactions were larger than 1 m, larger than in previous studies.

The timing and forward speed of a storm can also have significant effects on flooding. With regards to timing, the effects can vary based on how the storm coincides with different stages of the tidal cycle. These effects are more important for a shore-parallel storm that travel over a large section of the coast, thus interacting with several tidal cycles. Slower storms having more time to impact coastal regions, were found to produce more flooding in the bays and estuaries. Faster storms move quickly across the coast producing more flooding along the coast and lesser surge in the bays and estuaries. This study was the first to consider these interactions for a long coastline during a shore-parallel storm. Although these findings were specific to Hurricane Matthew, it shows the importance of considering these factors in flood risk studies, and how they can change the magnitude of flooding during storms.

Although the overall error statistics for predictions using the relatively-coarse mesh were good, there were plenty of locations, especially inland away from the coastline, where the predictions did not match observations well. These were attributed to the poor representation of topographic and bathymetric features owing to large element spacing. Thus, a high-resolution model of the U.S. southeast coast was developed by merging five FEMA regional meshes onto an open-water mesh. The combined mesh has $5,584,241$ vertices and $11,066,018$ elements, and its resolution is less than 100 m along the U.S. southeastern coastline, except in a few regions along the SC and NC coasts. The mesh was then validated for Hurricanes Matthew and Florence: two storms with different characteristics like intensity, track, etc. For Matthew, for a total of 626 stations from FL to NC, E_{RMS} was 0.28 m, R^2 value was 0.76, the slope of the best-fit line was 1.02, and B_{MN} was 0.03. For Florence, for a total of 190 stations in NC, these values were 0.2, 0.91, 1.00, and 0.01 respectively. There error statistics are either comparable to or better than that for the HSOFS predictions, meanwhile flooding a greater number of stations. Moreover, a qualitative analysis of time-series plots of water levels at inland locations indicated the FEMA-SAB mesh out-performing the HSOFS mesh in terms of better capturing tidal impacts and/or having a better match to the peak water levels.

But using large meshes like FEMA-SAB during forecasting is challenging as simulations take several hours even on thousands of computational cores. Thus, a multi-resolution approach was developed that allows switching from a coarse- to a fine-resolution mesh during a simulation. A coarse-resolution mesh is used when the storm is far away, thus enabling a savings in time. As the storm approaches a particular coastal, we can switch to a high-resolution mesh for that region. Results are mapped from the coarse to the fine mesh, and then the simulation can continue. The use of a higher-resolution mesh close to the landfall, allows a higher accuracy of predictions. Although techniques like adaptive mesh refinement exist in the literature, the multi-resolution approach is novel as it does not have the difficult of finding and populating the high-resolution regions with data during the simulation, as everything is pre-computed.

The approach was applied during Hurricanes Matthew and Florence, and results were evaluated for both accuracy and efficiency by comparisons to single simulations on coarse- and fine-resolution meshes. Results from the approach exhibited the same level of accuracy as that of a full simulation on the fine-resolution mesh, but it enabled flooding of a much larger region as compared to the corresponding simulation on the coarse-resolution mesh. This extra flooding coverage is due to its higher resolution in regions like barrier islands, up-stream rivers, etc. where the coarse mesh does not have sufficient resolution to provide the required hydraulic connectivity for flooding. But the main benefit of the approach is in its wall-clock time. The multi-resolution approach enables a time savings of more than 2.5 hours (38%) in case of Matthew, and more than 3 hours (53%) during Florence, as compared to a full simulation on the fine-resolution mesh. These efficiency gains can be crucial during forecasting to provide faster predictions that can help decision makers in taking necessary precaution during a hurricane.

Instead of using just one switch between the coarse HSOFS mesh and the fine FEMA-SAB mesh, multiple smaller higher resolution meshes can be used to further improve efficiency gains from the approach. A set of smaller meshes were therefore developed from the FEMA-SAB mesh using watershed boundaries as guidelines. The approach was then applied in the case of Hurricane Matthew using these smaller high-resolution meshes as the storm moved from south to north across the U.S. southeast coast, impacting different regions at different points in time. Questions about which combinations of coarse- and fine-resolution meshes should be used, which storm and surge parameters should be used to trigger switching between the fine-resolution meshes, and what gains in accuracy and efficiency can be achieved, are answered through three different simulations each aimed at a different level of accuracy and efficiency. Time series of water levels at boundary points of these meshes were used as triggers to switch from one mesh to another. The need to use a particular mesh was indicated by the rise in water levels from tidal maxima. To deal with processes like fore-runner surge, wind speeds and significant wave heights can also be used to indicate presence of a storm nearby. For the multi-resolution simulation with maximum accuracy, the results were a close match to a full simulation on the fine-resolution mesh, meanwhile having an efficiency gain of 2 hr (29 percent). For the simulation aimed at maximum efficiency, the errors were the largest, but it had a significant cut down in wall clock time of 4 hr (61 percent). Thus, different levels of accuracy and efficiency can be achieved out of the multi-resolution approach, by using different combinations of smaller high-resolution meshes that represent different regions along the U.S. southeast coast.

This study does have scope for improvements. For simulations on the FEMA-SAB mesh, the elemental slope limiter and advection state attributes were used to deal with model instabilities in different regions of the domain. The elemental slope limiter attribute works by limiting the water surface elevation gradient that can occur across an element, and was used for all of the inland regions from Florida to North Carolina. The advection state attribute disables advection at selected elements, and was used at localized regions along the South Carolina coast and near the southeast boundary of the domain away from our region for interest. Although the validation data were satisfactory, these restrictive nodal attributes would have slightly modified the solution. Future work will deal with stabilizing the FEMA-SAB mesh without the use of these attributes in the `fort.13` file.

The multi-resolution approach was validated for Hurricanes Matthew and Florence that impacted the U.S. southeast coast. Future research will explore application of the technique to other coastlines for storms that had different parameters like track, intensity, size, etc. Another limitation is regarding the format of hot-start file used. Currently, the approach works only for hot-start files in binary format (`fort.67` or `fort.68`). Future improvements will add netCDF capabilities. Moreover, the technique needs to be extended to the SWAN nearshore wave model so that all the runs can be re-done using the coupled ADCIRC+SWAN model, adding wave effects. This will require developing ways to move the wave solution between computational cores, and onto finer meshes. The approach finally needs to be extended into the ADCIRC Surge Guidance System (ASGS) so that the entire process of interpolating from one mesh to another is fully automated, and available as a straight-forward option for the user.

Although this work was specific to the U.S. southeast coast, findings from this study can be applied to storms that impacted other coastlines. As hurricanes, tsunamis, Nor'easters and winter storms continue to pose increased threat to more and more coastal communities, faster and more accurate forecasting will prove to be critical for emergency mangers in taking necessary precautions before, during, and after these natural hazards. The multi-resolution approach presented in this thesis can support their decision-making process by enabling storm surge forecasting with both ensemble and high-resolution capabilities.

BIBLIOGRAPHY

ADCIRC (2020a). *ADCIRC Utility Programs*. `https://adcirc.org/home/related-software/adcirc-utility-programs/`. [Retrieved 11 May 2020].

— (2020b). *Nodal Attributes File (fort.13)*. `https://adcirc.org/home/documentation/users-manual-v53/input-file-descriptions/nodal-attributes-file-fort-13/`. [Retrieved 23 April 2020].

Adcroft, A. & Marshall, D. (1998). "How slippery are piecewise-constant coastlines in numerical ocean models?" *Tellus A* **50**.1, pp. 95–108.

Altuntas, A. & Baugh, J. (2017). "Adaptive subdomain modeling: A multi-analysis technique for ocean circulation models". *Ocean Modelling* **115**, pp. 86–104.

Antonov, J. I., Levitus, S. & Boyer, T. P. (2005). "Thermosteric sea level rise, 1955–2003". *Geophysical Research Letters* **32**, p. L12602.

Asher, T. G., Luettich, R. A. & Fleming, J. G. (2018). *Ocean Modelling*. In preparation.

Bacopoulos, P. & Hagen, S. C. (2017). "The intertidal zones of the South Atlantic Bight and their local and regional influence on astronomical tides". *Ocean Modelling* **119**, pp. 13–34.

BakerAECOM (2013). *Hydrodynamic and Wave Model Development*. Tech. rep. Task Order 114 - East Central Florida Flood Insurance Study. BakerAECOM.

— (2016). *Hydrodynamic and Wave Model Development*. Tech. rep. ISD1:Section7. BakerAECOM.

Baugh, J., Altuntas, A., Dyer, T. & Simon, J. (2015). "An exact reanalysis technique for storm surge and tides in a geographic region of interest". *Coastal Engineering* **97**, pp. 60–77.

Bender, C. (2013). *Georgia and Northeast Florida Coastal Storm Surge and Mapping Study*. `https://fsbpa.com/2013TechPresentations/Bender.pdf`. [Retrieved 23 April 2020].

— (2014). *East Coast Central Florida Coastal Storm Surge and Mapping Study*. `http://www.floods.org/Files/Conf2014_ppts/E7_Bender.pdf`. [Retrieved 23 April 2020].

Bender, C. (2015). *South Florida Coastal Storm Surge and Mapping Study*. http://www.floods.org/Files/Conf2015_ppts/A7_Bender.pdf. [Retrieved 23 April 2020].

Berg, N. J. (2013). "On the influence of storm parameters on extreme surge events at the Dutch coast". MA thesis. Civil Engineering and Management, University of Twente.

Berg, R. (2015). *Tropical Cyclone Report, Tropical Storm Bill, 16 - 18 June 2015*. Tech. rep. National Hurricane Center.

Berger, M. J., George, D. L., Leveque, R. J. & Mandli, K. T. (2011). "The GeoClaw software for depth-averaged flows with adaptive refinement". *Advances in Water Resources* **34**, pp. 1195–1206.

Bernier, N. B. & Thompson, K. R. (2007). "Tide-surge interaction off the east coast of Canada and northeastern United States". *Journal of Geophysical Research* **112** (C6), p. C06008.

Bhaskaran, P. K., Nayak, S., Bonthu, S. R., Murthy, P. L. N. & Sen, D. (2013). "Performance and validation of a coupled parallel ADCIRC-SWAN model for THANE cyclone in the Bay of Bengal". *Environmental Fluid Mechanics* **13**, pp. 601–623.

Blain, C. A., Westerink, J. J. & Luettich, R. A. (1994). "The influence of domain size on the response characteristics of a hurricane storm surge model". *Journal of Geophysical Research* **99**, pp. 467–479.

— (1998). "Grid Convergence studies for the prediction of hurricane storm surge". *International Journal for Numerical Methods in Fluids* **26**, pp. 369–401.

Blanton, B. O. & Luettich, R. A. (2008a). *North Carolina Coastal Flood Analysis System: Model Grid Generation*. Tech. rep. TR-08-05. Renaissance Computing Institute.

— (2010). *North Carolina Floodplain Mapping Program, Coastal Flood Insurance Study: Water Level Validation Study*. Tech. rep. TR-10-06. Renaissance Computing Institute.

Blanton, B. O., Luettich, R. A., Hanson, J. L., Vickery, P., Slover, K. & Langan, T. (2012). *North Carolina Floodplain Mapping Program, Coastal Flood Insurance Study: Production Simulations and Statistical Analyses*. Tech. rep. TR-12-03. Renaissance Computing Institute.

Blanton, B. O. & Vickery, P. J. (2008b). *North Carolina Coastal Flood Analysis System: Hurricane Parameter Development*. Tech. rep. TR-08-06. Renaissance Computing Institute.

Blanton, B. O., Werner, F. E., Seim, H. E., Luettich, R. A., Lynch, D. R., Smith, K. W., Voulgaris, G., Bingham, F. M. & Way, F. (2004). "Barotropic tides in the South Atlantic Bight". *Journal of Geophysical Research* **109**, pp. 1–17.

Booij, N., Ris, R. C. & Holthuijsen, L. H. (1999). "A third-generation wave model for coastal regions, Part I, Model description and validation". *Journal of Geophysical Research* **104**, pp. 7649–7666.

Bretschneider, C. L., Krock, H. J., Nakazaki, E. & Casciano, F. M. (1986). *Roughness of typical Hawaiian terrain for tsunami runup calculations: A users manual*. Tech. rep. University of Hawaii.

Bunya, S., Dietrich, J. C., Westerink, J. J., Ebersole, B. A., Smith, J. M., Atkinson, J. H., Jensen, R. E., Resio, D. T., Luettich, R. A., Dawson, C. N., Cardone, V. J., Cox, A. T., Powell, M. D., Westerink, H. J. & Roberts, H. J. (2010). "A High-Resolution Coupled Riverine Flow, Tide, Wind, Wind Wave and Storm Surge Model for Southern Louisiana and Mississippi: Part I – Model Development and Validation". *Monthly Weather Review* **138** (2), pp. 345–377.

Cardone, V. J., Cox, A. T., Greenwood, J. A. & Thompson, E. F. (1994). *Upgrade of Tropical Cyclone Surface Wind Field Model*. Tech. rep. Miscellaneous Paper CERC-94-14. U.S. Army Corps of Engineers.

Chan, H. F. & Walker, G. O. (1979). "Empirical Studies of the Peak Surge due to Tropical Storms at Hong Kong*". *Journal of the Oceanographical Society of Japan* **35** (2), pp. 110–117.

Chen, C., Liu, H. & Beardsley, R. C. (2003). "An unstructured grid, finite-volume, three-dimensional, primitive equations ocean model: Application to coastal ocean and estuaries". *J. Atmos. Oceanic Technol.* **20** (1), pp. 159–186.

Cheung, K. F., Phadke, A. C., Wei, Y., Rojas, R., Douyere, Y. J. M., Martino, C. D., Houston, S. H., Liu, P. L. F., Lynett, P. J., Dodd, N., Liao, S. & Nakazaki, E. (2003). "Modeling of storm-induced coastal flooding for emergency management". *Ocean Engineering* **30** (11), pp. 1353–1386.

Conner, W. C., Kraft, R. H. & Harris, D. L. (1957). "Empirical Methods for Forecasting the Maximum Storm Tide due to Hurricanes and Other Tropical Storms". *Monthly Weather Review* **85** (4), pp. 113–116.

Creel, L. (2003). *Ripple effects: Population and coastal regions*. Tech. rep. Population Reference Bureau.

Cyriac, R., Dietrich, J. C., Fleming, J. G., Blanton, B. O., Kaiser, C., Dawson, C. N. & Luettich, R. A. (2018). "Variability in Coastal Flooding Predictions due to Forecast Errors during Hurricane Arthur (2014)". *Coastal Engineering* **137**, pp. 59–78.

Danilov, S. (2013). "Ocean modeling on unstructured meshes". *Ocean Modelling* **69**, pp. 195–210.

Danilov, S., Kivman, G. & Schroter, J. (2004). "A finite element ocean model: principles and evaluation". *Ocean Modelling* **6**, pp. 125–150.

Dawson, C. N., Westerink, J. J., Feyen, J. C. & Pothina, D. (2006). "Continuous, Discontinuous and Coupled Discontinuous-Continuous Galerkin Finite Element Methods for the Shallow Water Equations". *International Journal for Numerical Methods in Fluids* **52**, pp. 63–88.

Dietrich, J. C., Dawson, C. N., Proft, J., Howard, M. T., Wells, G., Fleming, J. G., Luettich, R. A., Westerink, J. J., Cobell, Z. & Vitse, M. (2013a). "Real-time forecasting and visualization of hurricane waves and storm surge using SWAN+ADCIRC and FigureGen". *Computational Challenges in the Geosciences*. Ed. by Dawson, C. N. & Gerritsen, M., pp. 49–70.

Dietrich, J. C., Muhammad, A., Curcic, M., Fathi, A., Dawson, C. N., Chen, S. S. & Luettich, R. A. (2018). "Sensitivity of Storm Surge Predictions to Atmospheric Forcing During Hurricane Isaac". *Journal of Waterway, Port, Coastal and Ocean Engineering* **144** (1).

Dietrich, J. C., Tanaka, S., Westerink, J. J., Dawson, C. N., Luettich, R. A., Zijlema, M., Holthuijsen, L. H., Smith, J. M., Westerink, L. G. & Westerink, H. J. (2012). "Performance of the Unstructured-Mesh, SWAN+ADCIRC Model in Computing Hurricane Waves and Surge". *Journal of Scientific Computing* **52** (2), pp. 468–497.

Dietrich, J. C., Westerink, J. J., Kennedy, A. B., Smith, J. M., Jensen, R. E., Zijlema, M., Holthuijsen, L. H., Dawson, C. N., Luettich, R. A., Powell, M. D., Cardone, V. J., Cox, A. T., Stone, G. W., Pourtaheri, H., Hope, M. E., Tanaka, S., Westerink, L. G., Westerink, H. J. & Cobell, Z. (2011a). "Hurricane Gustav (2008) Waves and Storm Surge: Hindcast, Validation and Synoptic Analysis in Southern Louisiana". *Monthly Weather Review* **139** (8), pp. 2488–2522.

Dietrich, J. C., Zijlema, M., Allier, P. E., Holthuijsen, L. H., Booij, N., Meixner, J. D., Proft, J. K., Dawson, C. N., Bender, C. J., Naimaster, A., Smith, J. M. & Westerink, J. J. (2013b). "Limiters for Spectral Propagation Velocities in SWAN". *Ocean Modelling* **70**, pp. 85–102.

Dietrich, J. C., Zijlema, M., Westerink, J. J., Holthuijsen, L. H., Dawson, C. N., Luettich, R. A., Jensen, R. E., Smith, J. M., Stelling, G. S. & Stone, G. W. (2011b). "Modeling Hurricane Waves and Storm Surge using Integrally-Coupled, Scalable Computations". *Coastal Engineering* **58**, pp. 45–65.

Dresser, C. & Inc., M. (1985). *Study to Revise and Update FEMA's Storm Surge Model*. Tech. rep. Washington, DC: Federal Emergency Management Agency.

Dupont, F., Straub, D. & Lin, C. A. (2004). "Influence of a step-like coastline on the basin scale vorticity budget of mid-latitude gyre models". *Tellus A* **55**, pp. 255–272.

Engineering, T. (2018). *ADCIRC Storm Event Modeling for the Broward County Flood Study*. Tech. rep. Taylor Engineering.

Ezer, T., Atkinson, L. P., Corlett, W. B. & Blanco, J. L. (2013). "Gulf Stream's induced sea level rise and variability along the U.S. mid-Atlantic coast". *Journal of Geophysical Research* **118**, pp. 685–697.

Federal Emergency Management Agency (2007). *Mississippi coastal analysis project: Grid development report (Task 4)*. Tech. rep.

— (2012). *Discovery Meeting: East Coast Central Florida (ECCFL) Coastal Study*. Tech. rep.

— (2019). *Guidance for flood risk analysis and mapping: Determination of wave characteristics*. Tech. rep.

Feng, X., Olabarrieta, M. & Valle-Levinson, A. (2016). "Storm-induced semidiurnal perturbations to surges on the US Eastern Seaboard". *Continental Shelf Research* **114**, pp. 54–71.

FIT (2018). `https://www.fit.edu/`. [Retrieved 10 March 2018].

Fix, G. J. (1975). "Finite Element Models for Ocean Circulation Problems". *SIAM Journal on Applied Mathematics* **29**, pp. 371–387.

Fleming, J., Fulcher, C., Luettich, R. A., Estrade, B., Allen, G. & Winer, H. (2008). "A Real Time Storm Surge Forecasting System Using ADCIRC". *Estuarine and Coastal Modeling (2007)*, pp. 893–912.

Fringer, O., Gerritsen, M. & Street, R. (2006). "An unstructured-grid, finite-volume, nonhydrostatic, parallel coastal ocean simulator". *Ocean Modelling* **14**.3, pp. 139–173.

Gao, J., Luettich, R. A. & Fleming, J. G. (2017). “Development and Evaluation of a Generalized Asymmetric Tropical Cyclone Vortex Model in ADCIRC”. In Preparation.

Garratt, J. R. (1977). “Review of drag coefficients over oceans and continents”. *Monthly Weather Review* **105**, pp. 915–929.

Hagen, S. C., Westerink, J. J. & Kolar, R. L. (2000). “One-dimensional finite element grids based on a localized truncation error analysis”. *International Journal for Numerical Methods in Fluids* **32**, pp. 241–261.

Hagen, S. C., Westerink, J. J., Kolar, R. L. & Horstmann, O. (2001). “Two-dimensional, unstructured mesh generation for tidal models”. *International Journal for Numerical Methods in Fluids* **35**, pp. 669–686.

Haidvogel, D. B. & Beckmann, A. (1999). *Numerical Ocean Circulation Modeling*. London: Imperial College Press, p. 344.

Harris, D. L. (1956). *Some problems involved in the study of storm surges*. Tech. rep. National Hurricane Research Project Report No. 4. Washington D.C.: U.S. Department of Commerce and Weather Bureau.

— (1963). *Characteristics of the hurricane storm surge*. Tech. rep. Technical Paper No. 48. Washington D.C.: U.S. Department of Commerce and Weather Bureau.

Hasselmann, S., Hasselmann, K., Allender, J. H. & Barnett, T. P. (1985). “Computations and parameterizations of the nonlinear energy transfer in a gravity wave spectrum, Part II: Parameterizations of the nonlinear transfer for application in wave models”. *Journal of Physical Oceanography* **15** (11), pp. 1378–1391.

Hill, C., DeLuca, C., Balaji, V., Suarez, M. & da Silva, A. (2004). “Architecture of the Earth System Modeling Framework”. *Computing in Science and Engineering* **6** (1).

Ho, F. P. & Myers, V. A. (1975). *Joint Probability Method of Tide Freequency Analysis applied to Apalachicola Bay and St. George Sound, Florida*. Tech. rep. NOAA Technical Report NWS 18. National Oceanic and Atmospheric Administration.

Holland, R. W. (1980). “An Analytic Model of the Wind and Pressure Profiles in Hurricanes”. *Monthly Weather Review* **108**, pp. 1212–1218.

Hoover, R. A. (1957). “Empirical relationships of the central pressures in hurricanes to the maximum surge and storm tide.” *Monthly Weather Review* **85**, pp. 167–174.

Hope, M. E., Westerink, J. J., Kennedy, A. B., Kerr, P. C., Dietrich, J. C., Dawson, C. N., Bender, C. J., Smith, J. M., Jensen, R. E., Zijlema, M., Holthuijsen, L. H., Luettich Jr, R. A., Powell, M. D., Cardone, V. J., Cox, A. T., Pourtaheri, H., Roberts, H. J., Atkinson, J. H., Tanaka, S., Westerink, H. J. & Westerink, L. G. (2013). "Hindcast and Validation of Hurricane Ike (2008) Waves, Forerunner, and Storm Surge". *Journal of Geophysical Research: Oceans* **118**, pp. 4424–4460.

Horsburgh, K. J. & Wilson, C. (2007). "Tide-surge interaction and its role in the distribution of surge residuals in the North Sea". *Journal of Geophysical Research* **112**, pp. 1–13.

Hovermale, J. B. (1976). *The movable fine mesh (MFM)-A new operational forecast model*. Tech. rep. National Weather Service.

Hu, K., Chen, Q. & Kimball, K. S. (2012). "Consistency in hurricane surface wind forecasting: An improved parametric model". *Natural Hazards* **61**, pp. 1029–1050.

Hu, K., Chen, Q. & Wang, H. (2015). "A numerical study of vegetation impact on reducing storm surge by wetlands in a semi-enclosed estuary". *Coastal Engineering* **95**, pp. 66–76.

Idier, D., Dumas, F. & Muller, H. (2012). "Tide-surge interaction in the English Channel". *Natural Hazards and Earth System Sciences* **12**, pp. 3709–3718.

Irish, J. L., Resio, D. T. & Ratcliff, J. J. (2008). "The Influence of Storm Size on Hurricane Surge". *Journal of Physical Oceanography* **38** (9), pp. 2003–2013.

Iskandarani, M. & Haidvogel, D. B. (1995). "A staggered spectral element model with application to the oceanic shallow water equation". *International Journal for Numeric Methods in Fluids* **20**, pp. 393–414.

Jelesnianski, C. P. (1972). *SPLASH: Special Program to List Amplitudes of Surges from Hurricanes*. Tech. rep. Silver Spring, Maryland: U.S. Dep. of Commer., Natl. Oceanic and Atmos. Admin., Natl. Weather Serv.

Jelesnianski, C. P., Chen, J. & Shafer, W. A. (1992). *SLOSH: Sea, Lake, and Overland Surges from Hurricanes*. Tech. rep. Silver Spring, Maryland: U.S. Dep. of Commer., Natl. Oceanic and Atmos. Admin., Natl. Weather Serv.

Kennedy, A. B., Gravois, U., Zachry, B. C., Westerink, J. J., Hope, M. E., Dietrich, J. C., Powell, M. D., Cox, A. T., Luettich, R. A. & Dean, R. G. (2011). "Origin of the Hurricane Ike Forerunner Surge". *Geophysical Research Letters* **38(8)**.

Kerr, P. C., Donahue, A. S., Westerink, J. J., Luettich, R. A., Zheng, L. Y., Weisburg, R. H., Huang, Y., Wang, H. V., Teng, Y., Forrest, D. R., Roland, A., Haase, A. T., Kramer, A. W., Taylor, A. A., Rhome, J. R., Feyen, J. C., Signell, R. P., Hanson, J. L., Hope, M. E., Estes, R. M., Dominguez, R. A., Dunbar, R. P., Semeraro, L. N., Westerink, H. J., Kennedy, A. B., Smith, J. M., Powell, M. D., Cardone, V. J. & Cox, A. T. (2013). "U.S. IOOS coastal and ocean modeling testbed: Inter-model evaluation of tides, waves, and hurricane surge in the Gulf of Mexico". *Journal of Geophysical Research: Oceans* **118**, pp. 5129–5172.

Kinnmark, I. (1986). "The Shallow Water Wave Equations: Formulation, Analysis and Application". *Lecture Notes in Engineering*. Ed. by Brebbia, C. A. & Orszag, S. A. Vol. 15. Springer-Verlag, pp. 12–26.

Kolar, R. L., Westerink, J. J., Cantekin, M. E. & Blain, C. A. (1994). "Aspects of nonlinear simulations using shallow water models based on the wave continuity equations". *Computers and Fluids* **23** (3), pp. 1–24.

Kubatko, E. J., Bunya, S., Dawson, C. & Westerink, J. J. (2009). "Dynamic p-adaptive Runge–Kutta discontinuous Galerkin methods for the shallow water equations". *Computer Methods in Applied Mechanics and Engineering* **198** (21–26), pp. 1766–1774.

Kubatko, E. J., Westerink, J. J. & Dawson, C. N. (2006). "hp Discontinuous Galerkin methods for advection dominated problems in shallow water flow". *Computer Methods in Applied Mechanics and Engineering* **196** (1–3), pp. 437–451.

Labeur, R. J. & Pietrzak, J. D. (2005). "A fully three dimensional unstructured grid non-hydrostatic finite element coastal model". *Ocean Modelling* **10**, pp. 51–67.

Levitus, S., Antonov, J. I., Boyer, T. P. & Stephens, C. (2000). "Warming of the World Ocean". *Science* **287** (5461), pp. 2225–2229.

Lin, N., Emmanuel, K., Oppenheimer, M. & Vanmarcke, E. (2012). "Physically based assessment of hurricane surge threat under climate change". *Nature Climate Change* **2**, pp. 462–467.

Luettich, R. A. & Westerink, J. J. (1995). "Continental shelf scale convergence studies with a barotropic tidal model". *Coastal and Estuarine Studies*. Ed. by Lynch, D. R. & Davies, A. M., pp. 349–372.

— (2004). *Formulation and Numerical Implementation of the 2D/3D ADCIRC Finite Element Model Version 44.XX*. `http://adcirc.org/adcirc_theory_2004_12_08.pdf`.

Luettich, R. A., Westerink, J. J. & Scheffner, N. W. (1992). *ADCIRC: An Advanced Three-Dimensional circulation model for shelves coasts and estuaries, report 1: Theory and methodology of ADCIRC-2DDI and ADCIRC- 3DL*. Tech. rep. United States Army Corps of Engineers.

Lynch, D. R. & Gray, W. G. (1979). "A wave equation model for finite element tidal computations". *Computers and Fluids* **7**, pp. 207–228.

Lynch, D. R., Ip, J. T. C., Naimie, C. E. & Werner, F. E. (1996). "Comprehensive coastal circulation model with application to the Gulf of Maine". *Continental Shelf Research* **16**, pp. 875–906.

Lynch, D. R. & Werner, F. E. (1987). "Three-dimensional hydrodynamics on finite elements. Part I: Linearized harmonic model". *International Journal for Numerical Methods in Fluids* **7**, pp. 871–909.

Madsen, O. S., Poon, Y. K. & Graber, H. C. (1988). "Spectral wave attenuation by bottom friction: theory". *Proceedings 21st International Conference on Coastal Engineering*, pp. 492–504.

Mandli, K. T. & Dawson, C. N. (2014). "Adaptive mesh refinement for storm surge". *Ocean Modelling* **75**, pp. 36–50.

Mathur, M. B. (1974). "A multiple-grid primitive equation model to simualte the development of an asymmetric hurricane (Isbell,1964)". *Journal of Atmospheric Sciences* **31**, pp. 371–393.

Mattocks, C. & Forbes, C. (2008). "A real-time, event-triggered storm surge forecasting system for the state of North Carolina". *Ocean Modelling* **25**, pp. 95–119.

Mattocks, C., Forbes, C. & Ran, L. (2006). *Design and Implementation of a Real-Time Storm Surge and Flood Forecasting Capability for the State of North Carolina*. Tech. rep. University of North Carolina.

Miyakoda, K. & Rosati, A. (1977). "One-way nested grid models: The interface conditions and the numerical accuracy". *Monthly Weather Review* **105**, pp. 1092–1107.

Mukai, A., Westerink, J. J., Luettich, R. A. & Mark, D. J. (2002). *A Tidal Constituent Database for the Western North Atlantic Ocean, Gulf of Mexico and Caribbean Sea*. Tech. rep. ERDC/CHL TR-02-24. Vicksburg MS: U.S. Army Engineer Research and Development Center.

Myers, E., Hess, K., Yang, Z., Xu, J., Wong, A., Doyle, D., Woolard, J., White, S., S Gill, B. L. nd & Hovis, G. (2007). “VDatum and strategies for national coverage”. *Proceedings of the IEEE OCEANS Conference.*

Myers, P. G. & Weaver, A. J. (1995). “A diagnostic barotropic finite-element ocean circulation model”. *Journal of Atmospheric and Oceanic Technology* **12**, pp. 511–526.

Naimaster, A., Bender, C. & Miller, W. (2013). “Advanced Estimation of Coastal Storm Surge: Application of SWAN+ADCIRC in Georgia/Northeast Florida Storm Surge Study”. *Proceedings from the ATC and SEI Conference on Advances in Hurricane Engineering*. Miami, Florida.

National Oceanic and Atmospheric Administration (2018a). *Sea Level Trends*. `https://tidesandcurrents.noaa.gov/sltrends/sltrends.html`. [Retrieved 09 March 2018].

— (2018b). *Vertical Datum Transformation*. `https://vdatum.noaa.gov/`. [Retrieved 09 March 2018].

NCEM (2018). *Flood Inundation Mapping and Alert Network*. `https://fiman.nc.gov/`. [Retrieved 10 March 2018].

Nechaev, D., Schroter, J. & Yaremchuk, M. (2003). “A diagnostic stabilized finite-element ocean circulation model”. *Ocean Modelling* **5**, pp. 37–63.

NERRS (2018). *National Estuarine Research Reserve System*. `http://cdmo.baruch.sc.edu/`. [Retrieved 10 March 2018].

Niedoroda, A. W., Resio, D. T., Toro, G., Divoky, D. & Reed, C. (2010). “Analysis of the coastal Mississippi storm surge hazard”. *Ocean Engineering* **37** (1), pp. 82–90.

NOAA (2017). *National Data Buoy Center*. `http://www.ndbc.noaa.gov`.

— (2018a). *National Ocean Service*. `https://oceanservice.noaa.gov/`. [Retrieved 10 March 2018].

— (2018b). *NOAA’s Integrated Coral Observing Network*. `http://ecoforecast.coral.noaa.gov/`. [Retrieved 10 March 2018].

NOAA & U.S. Census Bureau (2013). *NOAA Coastal Population Report: Population trends from 1970 to 2020.* Tech. rep.

NPS (2018). *NPS's Everglades National Park*. `http://ecoforecast.coral.noaa.gov/`. [Retrieved 10 March 2018].

Oey, L. Y. & Chen, P. (1992). "A nested-grid ocean model: With application to the simulation of meanders and eddies in the Norvegian coastal current". *Journal of Geophysical Research* **97** (C1), pp. 20063–20086.

Ookochi, Y. (1972). "A computational scheme of the nesting fine mesh in the primitive equation model". *Japan Meteorological Agency* **50** (1), pp. 37–48.

Peng, M., Xie, L. & Pietrafesa, L. J. (2004). "A numerical study of storm surge and inundation in the Croatan-Albemarle-Pamlico Estuary System". *Estuarine, Coastal and Shelf Science* **59**, pp. 121–137.

— (2006). "A numerical study on hurricane-induced storm surge and inundation in Charleston Harbor, South Carolina". *Journal of Geophysical Research* **111**, pp. 81–101.

Platzman, G. W. (1981). "Some response characteristics of finite element tidal models." *Journal of Computational Physics* **40**, pp. 36–63.

Pore, N. A. (1964). "The relation of wind and pressure to extra tropical storm surges at Atlantic City". *Journal of Applied Meteorology* **3** (2), pp. 155–163.

Poulose, J., Rao, A. D. & Bhaskaran, P. K. (2017). "Role of continental shelf on non-linear interaction of storm surges, tides and waves: An idealized study representing the west coast of India". *Estuarine, Coastal and Shelf Science*, pp. 1–14.

Prandle, D. & Wolf, J. (1978). "Surge-Tide Interaction in the Southern North Sea". *Hydrodynamics of Estuaries and Fjords* **23**, pp. 161–185.

Proudman, J. (1953). *Dynamical Oceanography*. New York: John Wiley and Sons, p. 409.

— (1955). "The propagation of tide and surge in an estuary". *Proceedings of the Royal Society of London*. Vol. A231, pp. 8–24.

— (1957). "Oscillations of tide and surge in an estuary of finite length". *Journal of Fluid Mechanics* **2**, pp. 371–382.

Provost, C. L. & Vincent, P. (1986). "Some tests of precision for a finite element model of ocean tides". *Journal of Computational Physics* **65**, pp. 273–291.

Rego, J. L. & Li, C. (2009). "On the importance of the forward speed of hurricanes in storm surge forecasting: A numerical study". *Geophysical Research Letters* **36** (7), p. L07609.

— (2010). "Nonlinear terms in storm surge predictions: Effect of tide and shelf geometry with case study from Hurricane Rita". *Journal of Geophysical Research* **115**, p. C06020.

Reid, R. O. & Whitaker, R. E. (1976). "Wind-Driven Flow of Water Influenced by a Canopy". *Journal of the Waterways, Harbors and Coastal Engineering Division* **102**, pp. 61–77.

Reid, R. O. & Wilson, B. W. (1954). *Compendium of Results of Storm Tide and Wave Analysis for Full Hurricane Conditions at Freeport, Texas*. Tech. rep. A. and M. Project 91. Texas A. and M. Research Foundation,

Riverside Technology & AECOM (2015). *Mesh Development, Tidal Validation, and Hindcast Skill Assessment of an ADCIRC Model for the Hurricane Storm Surge Operational Forecast System on the US Gulf-Atlantic Coast*. Tech. rep.

Roberts, K. J., Pringle, W. J. & Westerink, J. J. (2019). "OceanMesh2D 1.0: MATLAB-based software for two-dimensional unstructured mesh generation in coastal ocean modeling". *Geoscientific Model Development* **12** (5), pp. 1847–1868.

Rossiter, J. R. (1961). "Interaction between tide and surge in the Thames". *Geophysical Journal of the Royal Astronomical Society* **6**, pp. 29–53.

Scheffner, N. W. & Carson, F. C. (2001). *Coast of South Carolina Storm Surge Study*. Tech. rep. TR-01-11. U.S. Army Corps of Engineers.

Schloemer, R. W. (1954). *Analysis and synthesis of hurricane wind patterns over Lake Okechobee, FL*. Tech. rep. 31. Govt. Printing Office.

SCO (2018). *The Coastal Data Information Program*. `http://cdip.ucsd.edu/`. [Retrieved 10 March 2018].

Sebastian, A. G., Proft, J. M., Dietrich, J. C., Du, W., Bedient, P. B. & Dawson, C. N. (2014). "Characterizing Hurricane Storm Surge Behavior in Galveston Bay using the SWAN+ADCIRC Model". *Coastal Engineering* **88**, pp. 171–181.

Skamarock, W. C., Klemp, J. B., Dudjia, J., Gill, D. O., Barker, D. M., Duda, M. G., Huang, X. Y., Wang, W. & Powers, J. G. (2008). *A description of the Advanced Research WRF Version 3*. Tech. rep. NCAR.

Stewart, S. R. (2017). *Tropical Cyclone Report for Hurricane Matthew, 28 September - 9 October 2016*. Tech. rep. National Hurricane Center.

Stewart, S. R. & Berg, R. (2019). *Tropical Cyclone Report for Hurricane Florence, 31 August-17Septemeber 2018*. Tech. rep. National Hurricane Center.

Suh, S. W., Lee, H. Y., Kim, H. J. & Fleming, J. G. (2015). "An efficient early warning system for typhoon storm surge based on time-varying advisories by coupled ADCIRC and SWAN". *Ocean Dynamics* **65** (5), pp. 617–646.

Suhayda, J. N. & Young, M. H. (1988). "Storm surge simulation using new FEMA model". *Mathematical and Computational Modelling* **11**, pp. 87–95.

Szpilka, C., Dresback, K., Kolar, R., Feyen, J. & Wang, J. (2016). "Improvements for the Western North Atlantic, Caribbean and Gulf of Mexico ADCIRC Tidal Database (EC2015)". *Journal of Marine Science and Engineering* **4** (4), p. 72.

Taeb, P. & Weaver, R. J. (2019). "An operational coastal forecasting tool for performing ensemble modeling". *Estuarine, Coastal and Shelf Science* **217**, pp. 237–249.

Tanaka, S., Bunya, S., Westerink, J. J., Dawson, C. N. & Luettich, R. A. (2011). "Scalability of an Unstructured Grid Continuous Galerkin Based Hurricane Storm Surge Model". *Journal of Scientific Computing* **46**, pp. 329–358.

Tancreto, A. E. (1958). "A method for forecasting the maximum surge at Boston due to extra tropical storms". *Monthly Weather Review* **86** (6), pp. 197–200.

Tang, Y. M., Grimshaw, R., Sanderson, B. & Holland, G. (1996). "A Numerical Study of Storm Surges and Tides, with Application to the North Queensland Coast". *Journal of Physical Oceanography* **26**, pp. 2700–2711.

Thomas, A., Dietrich, J. C., Asher, T. G., Blanton, B. O., Cox, A. T., Dawson, C. N., Fleming, J. G. & Luettich, R. A. (2019). "Influence of Storm Timing and Forward Speed on Tide-Surge Interactions during Hurricane Matthew". *Ocean Modelling* **137**, pp. 1–19.

Thompson, E. F. & Cardone, V. J. (1996). "Practical Modeling of Hurricane Surface Wind Fields". *Journal of Waterway, Port, Coastal, and Ocean Engineering* **122** (4), pp. 195–205.

Tibbetts, J. (2002). "Coastal cities: living on the edge". *Environ Health Perspect.* **110** (11), pp. 674–681.

U.S. Army Corps of Engineers (2018). *North Atlantic Coast Comprehensive Study Report*. http://www.nad.usace.army.mil/CompStudy/. [Retrieved 13 March 2018].

U.S. Geological Survey (2018). *Elevation*. https://nationalmap.gov/elevation.html. [Retrieved 09 March 2018].

— (2020a). https://www.usgs.gov/core-science-systems/ngp/ngtoc/watershed-boundary-dataset. [Retrieved 17 May 2020].

— (2020b). *USGS Current Water Data for the Nation*. https://waterdata.usgs.gov/nwis/rt. [Retrieved 23 May 2020].

UN Atlas of the Oceans (2018). *Human Settlements on the Coast*. http://www.oceansatlas.org/subtopic/en/c/114/. [Retrieved 04 October 2018].

UNC (2018). *Coastal Studies Institute*. http://coastalstudiesinstitute.org/. [Retrieved 10 March 2018].

UNCW (2018). *Coastal Ocean Research and Monitoring Program*. http://cormp.org/. [Retrieved 10 March 2018].

United Research Services (2009). *South Carolina Storm Surge Project Deliverable 1: Grid Development Report Development*. Tech. rep.

USACE (2018). http://www.usace.army.mil/. [Retrieved 10 March 2018].

USGS (2018). *USGS Flood Event Viewer*. https://water.usgs.gov/floods/FEV/. [Retrieved 10 March 2018].

Valle–Levinson, A., Olabarrieta, M. & Valle, A. (2013). “Semidiurnal perturbations to the surge of Hurricane Sandy”. *Geophysical Research Letters* **40**, pp. 2211–2217.

Water Environment Consultants (2016). *Phase II Storm Surge Analysis: Post 45 Project, Charleston, SC*. Tech. rep.

Water Resource Region (2020). https://en.wikipedia.org/wiki/Water_resource_region. [Retrieved 17 May 2020].

Weisburg, R. H. & Zheng, L. (2006). “Hurricane Storm Surge Simulations for Tampa Bay”. *Estuaries and Coasts* **29** (6), pp. 899–913.

Westerink, J. J., Luettich Jr, R. A., Feyen, J. C., Atkinson, J. H., Dawson, C. N., Roberts, H. J., Powell, M. D., Dunion, J. P., Kubatko, E. J. & Pourtaheri, H. (2008). “A

Basin to Channel Scale Unstructured Grid Hurricane Storm Surge Model Applied to Southern Louisiana". *Monthly Weather Review* **136** (3), pp. 833–864.

Westerink, J. J., Luettich, R. A. & Muccino, J. C. (1994). "Modeling tides in the western North Atlantic using unstructured graded grids". *Tellus A* **46A**, pp. 178–199.

Westerink, J. J., Luettich, R. A. & Scheffner, N. W. (1993). *ADCIRC: An Advanced Three-Dimensional Circulation Model for Shelves Coasts and Estuaries, Report 3: Development of a Tidal Constituent Database for the Western North Atlantic and Gulf of Mexico*. Tech. rep. DRP-92-6. Vicksburg, MS: U.S. Army Corps of Engineers.

Westerink, J. J., Muccino, J. C. & Luettich, R. A. (1992). "Resolution requirements for a tidal model of the Western North Atlantic and Gulf of Mexico". *Computational Methods in Water Resources*. Ed. by al., T. F. R. et, pp. 669–674.

White, L., Deleersnijder, E. & Legat, V. (2008). "A three-dimensional unstructured mesh finite element shallow-water model, with application to the flows around an island and in a wind-driven, elongated basin". *Ocean Modelling* **22**, pp. 26–47.

Williamson, D. L. (2007). "The evolution of dynamical cores for global atmospheric models". *Journal of the Meteorological Society of Japan* **85B**, pp. 241–269.

Willis, J. K., Roemmich, D. & Cornuelle, B. (2004). "Interannual variability in upper ocean heat content, temperature,and thermosteric expansion on global scales". *Journal of Geophysical Research* **109**, p. C12036.

Wolf, J. (1978). "Interaction of tide and surge in a semi-infinite uniform channel, with application to surge propagation down the east coast of Britain". *Applied Mathematical Modeling* **2**, pp. 245–253.

— (1981). "Surge-tide interaction in the North Sea and River Thames". *Floods due to High Winds and Tides* (4), pp. 75–94.

Xie, L., Bao, S., Pietrafesa, L. J., Foley, K. & Fuentes, M. (2006). "A Real-Time Hurricane Surface Wind Forecasting Model: Formulation and Verification". *Monthly Weather Review* **134**, pp. 1355–1370.

Zhang, W., Shi, F., Hong, H., Shang, S. & Kirby, J. T. (2010). "Tide-surge Interaction Intensified by the Taiwan Strait". *Journal of Geophysical Research* **115**, p. C06012.

Zhang, Y. & Baptista, A. M. (2008). "Selfe: A semi-implicit Eulerian–Lagrangian finite-element model for cross-scale ocean circulation". *Ocean Modelling* **21** (3), pp. 71–96.

Zhang, Y., Baptista, A. M. & Myers, E. P. (2004). "A cross-scale model for 3D baroclinic circulation in estuary–plume–shelf systems: I. Formulation and skill assessment". *Continental Shelf Research* **24**.18. Recent Developments in Physical Oceanographic Modelling: Part I, pp. 2187–2214.

Zhang, Y., Ye, F., Stanev, E. V. & Grashorn, S. (2016). "Seamless cross-scale modeling with SCHISM". *Ocean Modelling* **102**, pp. 64–81.

Zijlema, M. (2010). "Computation of wind-wave spectra in coastal waters with SWAN on unstructured grids". *Coastal Engineering* **57**, pp. 267–277.